X68-84903
CR-94173

Final Report

FEASIBILITY STUDY AND MODEL DEVELOPMENT FOR A FERROFLUID VISCOUS DAMPER

(8 November 1966 -- 8 March 1967)

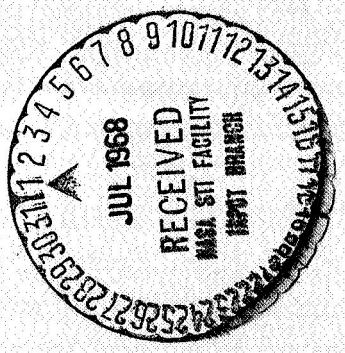

Contract No.: NAS5-9431
AVSSD-0222-67-CR

Prepared by

AVCO MISSILES, SPACE, AND ELECTRONICS GROUP
SPACE SYSTEMS DIVISION
201 Lowell Street
Wilmington, Massachusetts 01887

for

GODDARD SPACE FLIGHT CENTER
Greenbelt, Maryland

RQ-7-52143

This document consists of 234 pages,
102 copies, Series A

Final Report

FEASIBILITY STUDY AND MODEL DEVELOPMENT FOR A FERROFLUID VISCOUS DAMPER

(8 November 1966 -- 8 March 1967)

N 68 30485

Contract No.: NAS5-9431
AVSSD-0222-67-CR

Prepared by

AVCO MISSILES, SPACE, AND ELECTRONICS GROUP
SPACE SYSTEMS DIVISION
201 Lowell Street
Wilmington, Massachusetts 01887

for

GODDARD SPACE FLIGHT CENTER
Greenbelt, Maryland

ABSTRACT

This is the final report on a four-month program to study the feasibility of the ferrofluid viscous damper concept for application on the Radio Astronomy Explorer (RAE) satellite.

The ferrofluid viscous damper is an energy dissipative damping mechanism used to couple together the damper boom and central body of an RAE type of satellite. Relative angular motion of the damper boom with respect to the satellite central body will result in energy dissipation in the damper, with velocity sensitive damping forces applied to the system.

This type of damper provides, for the first time, a lightweight viscous device that will result in better control characteristics for the RAE satellite than is available from dampers in current use.

The damper consists of a small quantity of magnetic fluid (ferrofluid) hermetically sealed in a vane that is mounted on the central body of the satellite. The ferrofluid is acted on by a permanent magnet mounted on the damper boom. Relative motion between the damper boom and the central body will cause motion of the ferrofluid under influence of the magnet, with resulting fluid shear and application of viscous damping forces to the system.

Work reported in this document includes investigation of ferrofluids most suitable for the RAE application. A reference fluid was selected and a quantity was made and evaluated. Studies were also made of the basic viscous damping mechanism and possible suspension techniques.

The investigation established the feasibility of the concept and resulted in the design and fabrication of a model to demonstrate the principle of operation. The damper can be made with an overall weight of 0.84 pound, including not only the basic damper assembly but also the caging mechanism used to protect the damper during the launch phase of the mission.

As a result of this study, development of a prototype ferrofluid damper is recommended.

Unclassified report

CONTENTS

CONTENTS (Cont'd)

CONTENTS (Cont'd)

CONTENTS (Concl'd)

ILLUSTRATIONS

ILLUSTRATIONS (Cont'd)

ILLUSTRATIONS (Cont'd)

ILLUSTRATIONS (Concl'd)

TABLES

TABLES (Concl'd)

I. INTRODUCTION

A. PROGRAM OBJECTIVES

The objectives of this program were as follows:

1. To conduct a study program to consider the feasibility of the magnetic fluid viscous damper concept for the Radio Astronomy Explorer (RAE) satellite.

2. To design and fabricate a model of the magnetic fluid viscous damper to demonstrate the principle of operation.

B. PROGRAM ORGANIZATION AND SCHEDULE

This program originated from the Radio Astronomy Explorer Satellite office of the NASA Goddard Space Flight Center. Mr. R. G. Barclay is the NASA Goddard Space Flight Center Technical Director. The Project Director at Avco Space Systems Division is Mr. R. E. Coulombre. Other principal participants in the program and their areas of contribution are Dr. R. Rosensweig and Dr. R. Kaiser, ferrofluid development; and Mr. H. d'Auriol and Mr. L. Schnee, electromechanical design and development.

This is the final report for NASA Contract NAS 5-9431. The study program reported here was started 8 November 1966 and completed 8 March 1967.

C. TECHNICAL SUMMARY

A study has been completed showing the feasibility of the magnetic fluid viscous damper for application on the RAE satellite. A model of the damper has been fabricated to demonstrate the concept. Investigation of both silicon and hydrocarbon ferrofluid mediums for the damper application has led to development of an alpha methyl naphthalene ferrofluid using Wright 400 magnetite particles and an oleic acid surfactant.

The material has a 13 percent magnetic solid concentration by volume. This concentration was maximized to provide maximum ferrofluid saturation magnetization (and hence minimum magnet weight) without exceeding the specification viscosity range of approximately 5 to 1. Saturation magnetization for the alpha methyl naphthalene ferrofluid was raised to 735 gauss, resulting in a change in viscosity of 5.06 to 1 over the 0° F to 70° F specification temperature range. Ferrofluid viscosity at 70° F is 79 centistokes.

Efforts to develop a silicone ferrofluid have not yet produced a sample material that will meet all the requirements of this program effectively. A great many sample silicone ferrofluids were investigated and a number of weakly magnetic fluids were

prepared and tested in the laboratory. Attempts to increase the magnetic moment resulted in undesirable gelling characteristics during the ferrofluid grinding process.

A new damping concept was conceived which makes it possible to use low viscosity hydrocarbon ferrofluids. The new concept uses orifice flow characteristics to amplify fluid damping forces. The concept was reduced to practice using an alpha methyl naphthalene hydrocarbon ferrofluid, and a model was designed and fabricated to demonstrate performance.

In addition to ferrofluid development work, study effort was applied to investigate the design feasibility of the basic damper, including the suspension mechanism, caging mechanism, and fluid dynamics. Each area of study is discussed in detail in the body of the report. In each case the results show the feasibility of the concept and suggest further development of the demonstration model into a prototype unit.

II. THE FERROFLUID VISCOUS DAMPER

A. RAE DAMPING REQUIREMENT

A damper, or energy dissipation device, is required on the RAE satellite to reduce the oscillatory motions induced in the satellite by its gravity gradient stabilization system and by disturbance torques. The damping concept used is described below.

The RAE satellite uses a passive, three axis, gravity gradient stabilization system to align the satellite with respect to the local vertical. This system keeps all axes aligned in the proper directions. Large, 750 foot booms are extended from the satellite to achieve gravity gradient stabilization. As the satellite rotates about the earth, the booms torque the satellite toward the local vertical. Libration oscillations, in the plane of the orbit, result from this torquing. The satellite also oscillates about all axes because of disturbance torques. It is necessary to damp the satellite libration and disturbance oscillations in order to obtain pointing accuracy.

Damping is achieved by flexibly coupling a boom to the satellite through a dissipative element. The damper boom and its coupling system must have a natural frequency of oscillation which differs from that of the satellite, in order for relative motion to take place. Energy can then be taken out of the system at a rate proportional to the relative angular velocities of the boom and satellite and to the damping constant of the dissipative element. Given the proper natural frequencies and a damping coefficient within the specified bounds, the satellite motion can be held within required limits.

Two functions must be performed by the damper assembly:

1. It must dissipate energy at a satisfactory rate.

2. It must provide a spring restraint between the damper boom and the satellite.

Energy can be dissipated by several methods; those most often used are hysteresis damping and viscous fluid damping . The rate of energy dissipation of a hysteresis damper can depend greatly on the initial offset angle of the device. A viscous damper has been shown to be much less sensitive to initial conditions and to be capable of providing adequate energy dissipation over a wider range of conditions (see Section II. D).

In a typical viscous damper used to damp oscillatory motion, a viscous fluid is forced to rotate within its container by a rotary piston attached to the moving portion of the device. A rotary seal is required to keep the fluid in the container. The seal has to be hermetic against a relative pressure of 15 psi if the damper is used in a space application.

The seal, the friction required to rotate the piston, and indeed the piston itself would be eliminated if the force were transmitted to the fluid without contacting it. Such a force can be transmitted to a magnetic fluid.

B. FERROFLUID VISCOUS DAMPER CONCEPT

The Avco ferrofluid viscous damper makes use of a magnetic fluid and assembly to transmit forces without coulomb friction and without a rotary seal. A schematic of the damper is shown in Figure 1. A hollow hermetically sealed damper vane attached to the satellite structure is partially filled with ferrofluid. The ferrofluid is a colloidal dispersion of magnetic solid particles in an inert carrier liquid. It has a magnetic moment proportional to the concentration of magnetic solids in the carrier liquid. The viscosity is a function of the carrier fluid viscosity and the concentration of magnetic solids. The ferrofluid magnetic moment and viscosity are selected to optimize the damping characteristics and the dimensions of the vane and magnet assembly.

The magnet assembly is rigidly mounted to the magnet support structure. The pole faces of the magnet are parallel to the larger faces of the vane, and provide a magnetic field normal to the direction of motion of the magnet. The magnetic field forces the ferrofluid to move with the magnet, thereby developing viscous shear forces against the damper vane in the direction of magnet motion.

The magnet support structure is suspended on flexural pivot springs having angular freedom about the suspension axis. The bottom of the structure is attached to the damper boom. Therefore the satellite and the damper boom are connected only by the frictionless pivot springs.

In summary, the Avco ferrofluid viscous damper provides energy dissipation in the form of viscous damping. There is no coulomb friction, because the magnet assembly attached to the damper boom is able to move the viscous ferrofluid with respect to the damper vane without physical contact. The flexible coupling between the satellite and the damping boom is accomplished by flexural pivot supports attached to the magnet support and the satellite interface structure.

C. MODEL DEVELOPMENT

The design and development effort carried out on the ferrofluid viscous damper resulted in fabrication of the model shown in Figures 2 and 3.

The viscous damping concept (vane/orifice/wide-angle magnet)selected for the model resulted from analysis and tradeoff studies that will be discussed later in this report. The concept is shown schematically in Figure 4. It consists of a cavity in the shape of a 150 degree sector, separated into two parts by a baffle 0.2 inch thick, with a connecting orifice 0.021 inch in diameter. A photograph of the actual sector, or vane, is shown in Figure 5.

The magnet shown in Figure 4 covers an arc of 80 degrees. Magnetic fluid in the vane also covers an arc of approximately 80 degrees, as shown in the figure. As the magnet is moved along the vane, it holds the ferrofluid fixed in its magnetic field, causing flow through the orifice. It is this orifice flow which develops the damping forces required.

Ferrofluid is hermetically sealed in the vane cavity, and the cavity is then evacuated to a pressure of approximately 1 mm of mercury. Sealing is accomplished while the vane is evacuated, by sealing the two pinch tubes protruding from the vane, as shown in Figure 5. A back tube is provided for equalization of pressure as the fluid moves back and forth in the vane Vane wall thickness is minimized, nominally 0.020 inch, to keep the magnet air gap as short as possible.

The magnet assembly used consists of barrium ferrite ceramic magnets and a back iron path of magnetically soft ingot iron (see Figure 6). One of the individual magnets used in the magnet assembly is shown in Figure 7. The magnets are machined out of a circular ferrite disk and magnetized face to face. They are then fastened to the back iron. The magnet assembly has a field strength of 2300 oersteds.

The housing assembly, suspension system, and caging system are shown assembled in Figure 8 with the magnet assembly attached, and in Figure 9 with the support yoke added.

Exploded views of the mechanism without the magnet and vane are shown in Figures 10 and 11. As shown, the lower housing (which supports the magnet and the boom deployment package) is suspended from the upper support yoke by a set of four rotary flexure pivots. The pivots are shown disassembled from the mechanism in Figure 10 and partially assembled in Figure 11. Figure 11 shows the support yoke, cantilever spring, and cantilever spring mounting bracket assembled at the top of the picture. Caging stops are shown in Figure 11 assembled at the sides of the housing. The caging spring, boom deployment system interface rods, and boom deployment system mounting plate are also shown assembled on the housing.

The complete ferrofluid viscous damper is pictured in its mounting stand in Figures 12 and 13. The latch at the bottom of the stand is used to engage and release the caging mechanism for demonstration purposes.

In the caged position the housing is forced against the two caging stops. These stops limit the load seen by the suspension and prevent damage to the flexural pivots during the boost environment, After the satellite is placed in orbit, the caging mechanism is released and the housing and magnet assemblies are supported by the flexural pivots, permitting normal operation of the system.

The damper can be removed from the mounting stand and fixed on top of the stand to demonstrate damping, as shown in Figure 14.

The fixture used for testing the damping mechanism is shown in Figure 15. The vane and magnet assembly are removed from the support structure and are mounted in the test fixture for evaluation.

The test fixture shown will permit measurement of the damping constant with relative ease.

The model has a damping constant of 7 ft-lb-sec and a spring constant of 0.12 in.-lb/radian. Details of testing leading to this design are included in Section IV.A.1.b of this report.

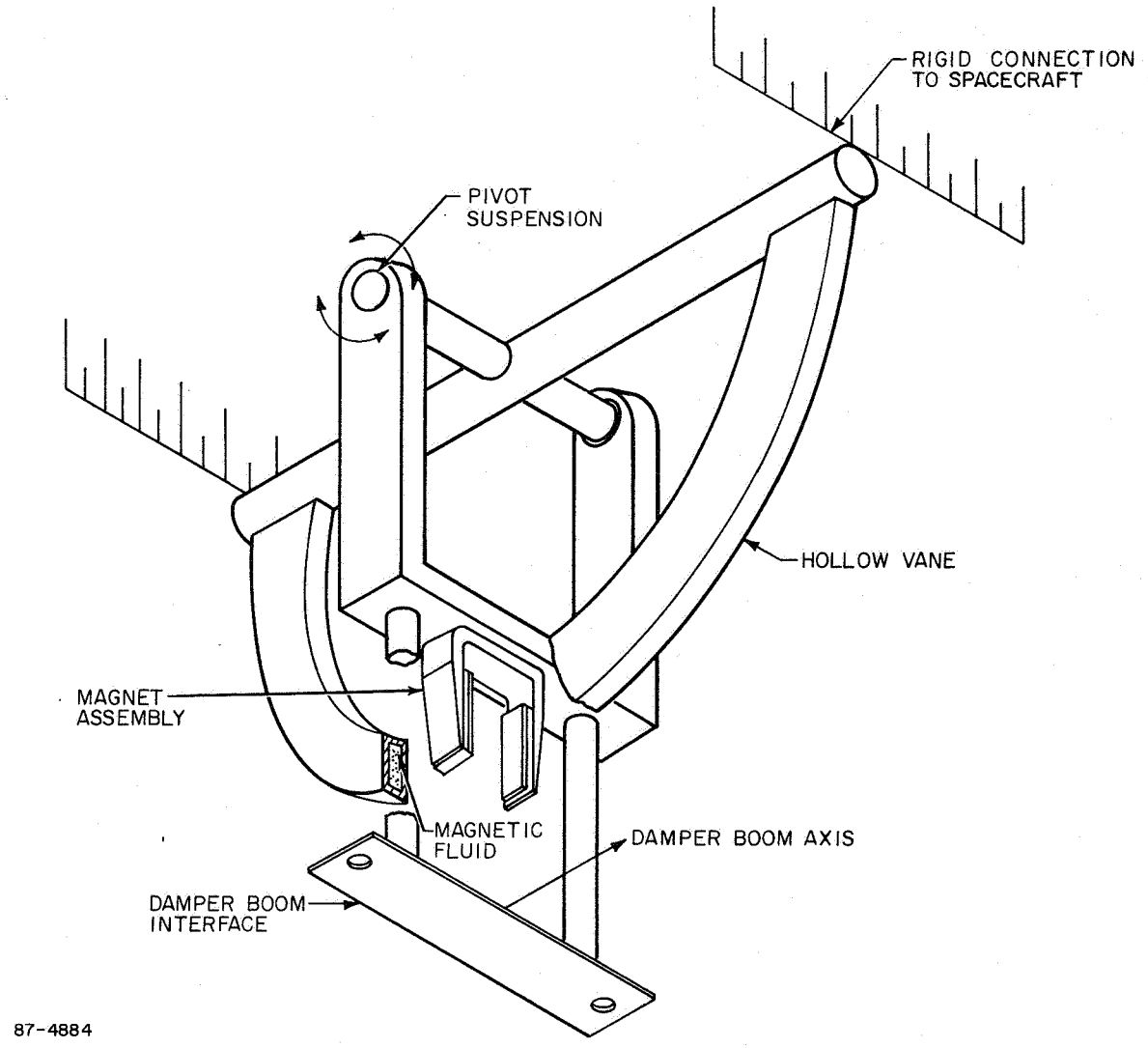

Figure 1 MAGNETIC FLUID VISCOUS DAMPER

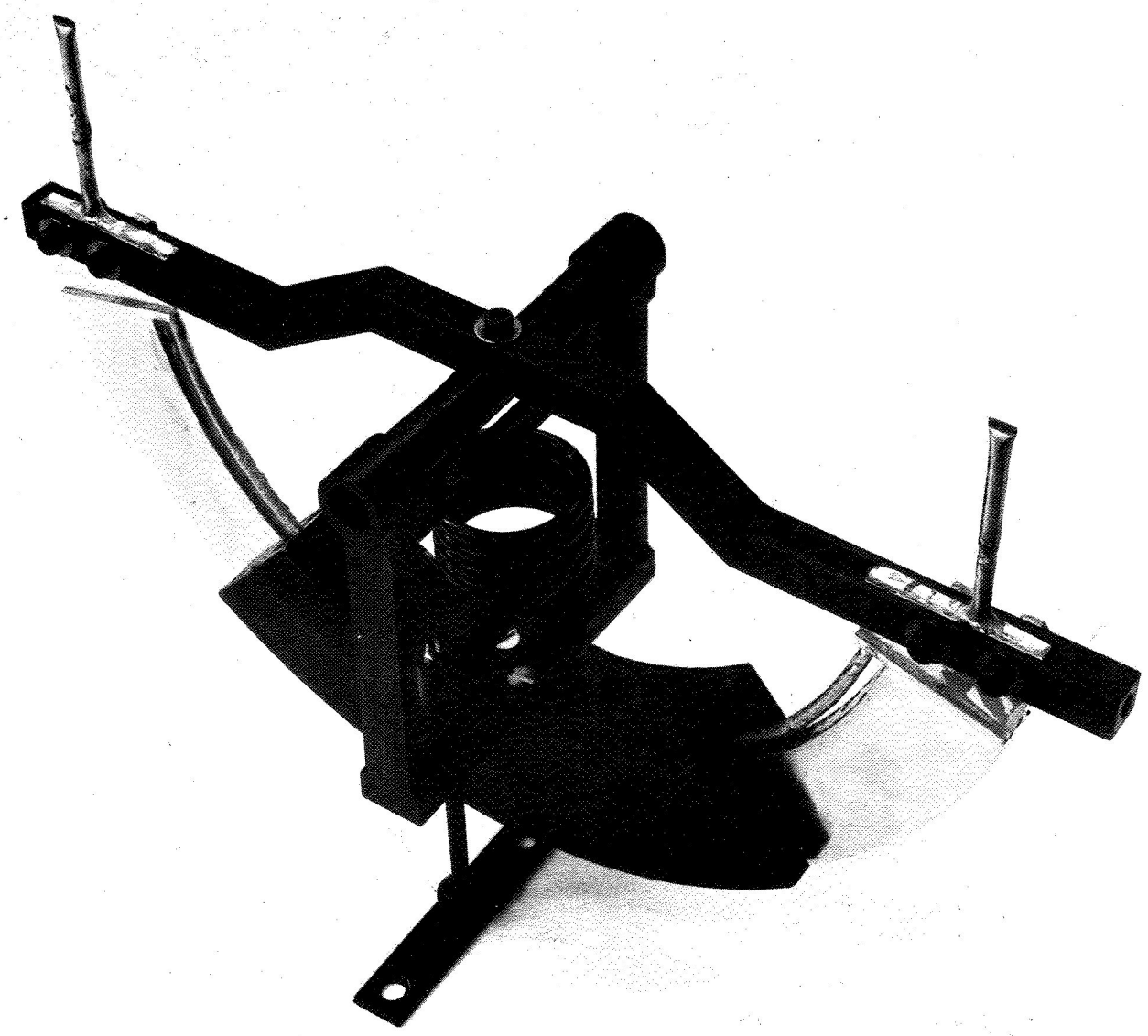

15877J

Figure 2 FERROFLUID VISCOUS DAMPER MODEL, 3/4 VIEW

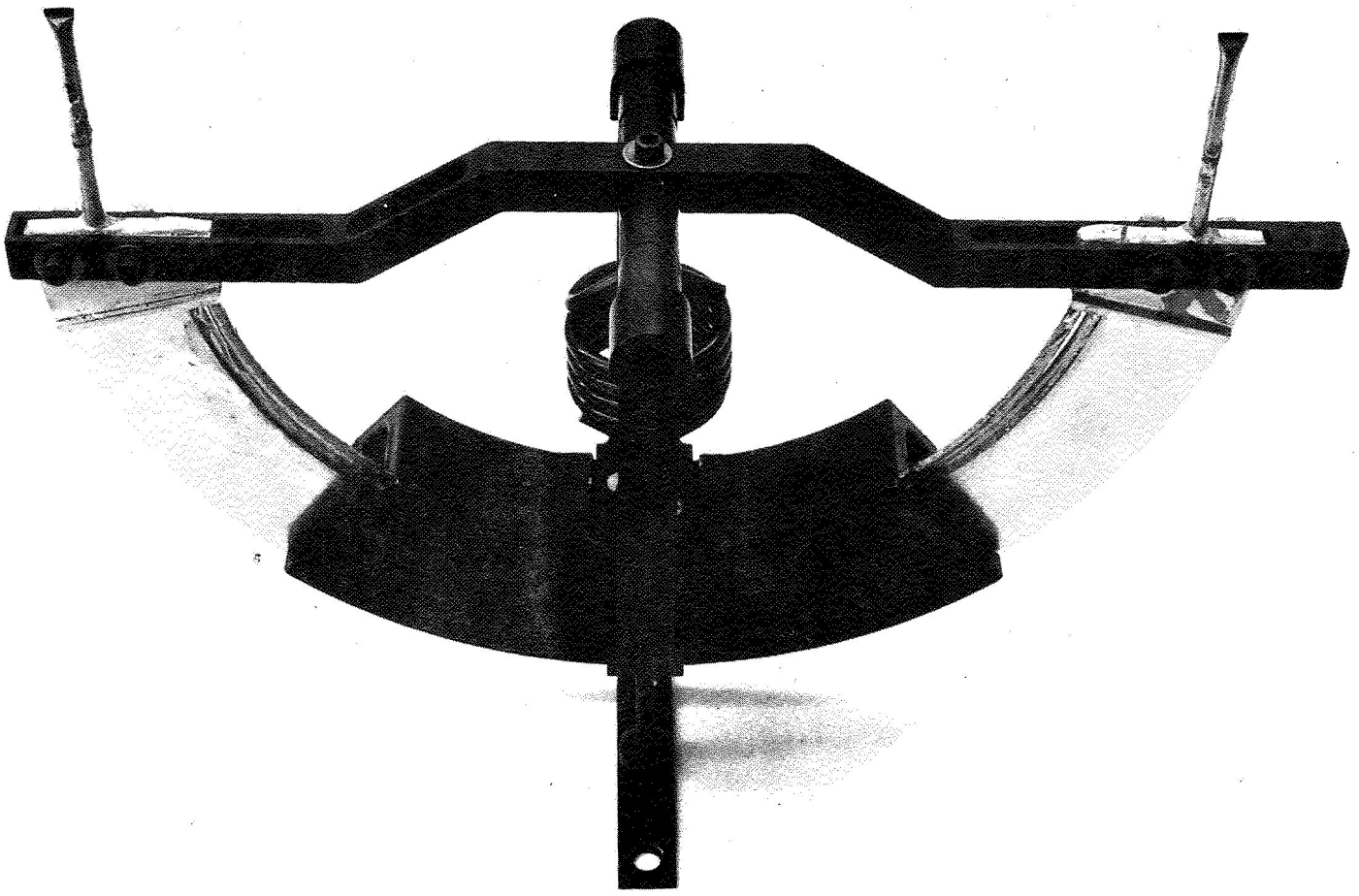

15877P

Figure 3 FERROFLUID VISCOUS DAMPER MODEL, SIDE VIEW

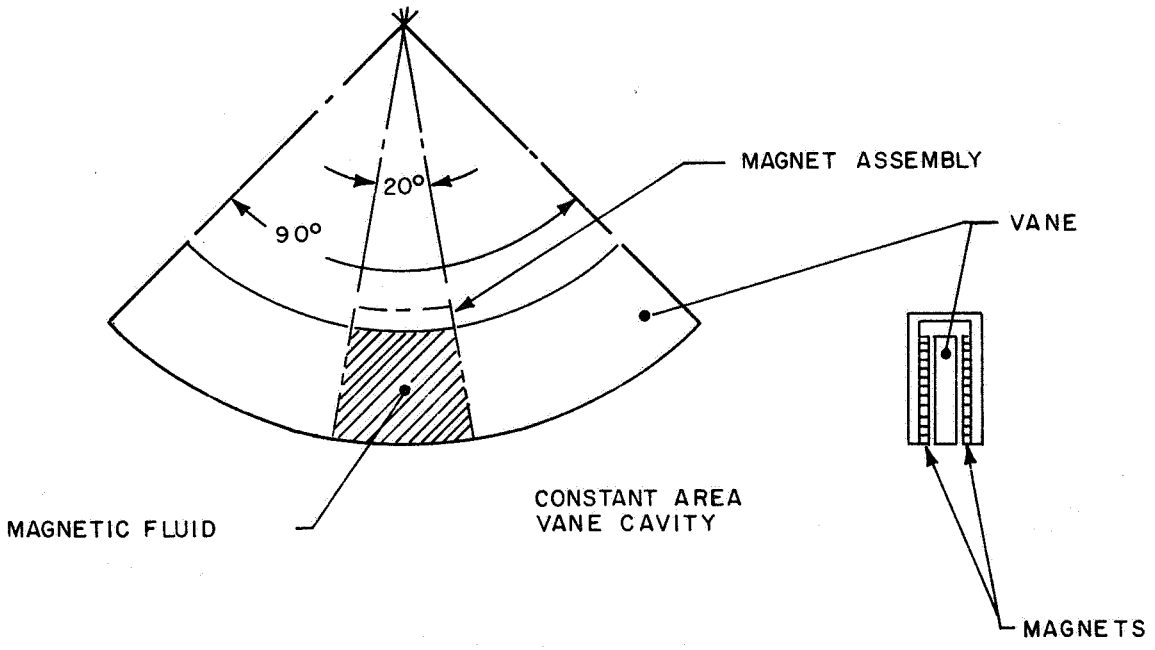

Figure 4 DAMPING CONCEPT

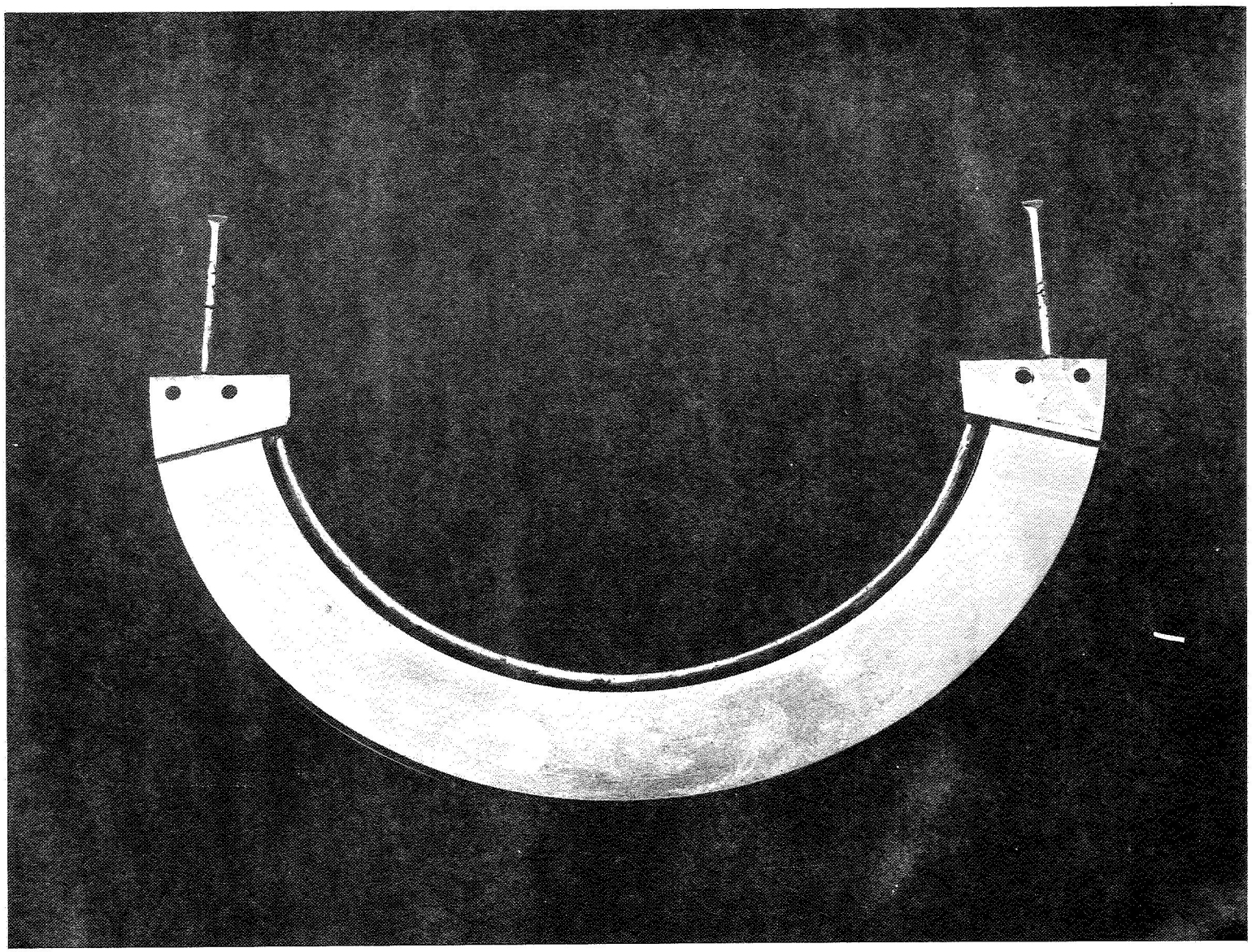

15877M

Figure 5 DAMPER VANE

15877D

Figure 6 MAGNETIC ASSEMBLY

15877G

Figure 7 CERAMIC MAGNET

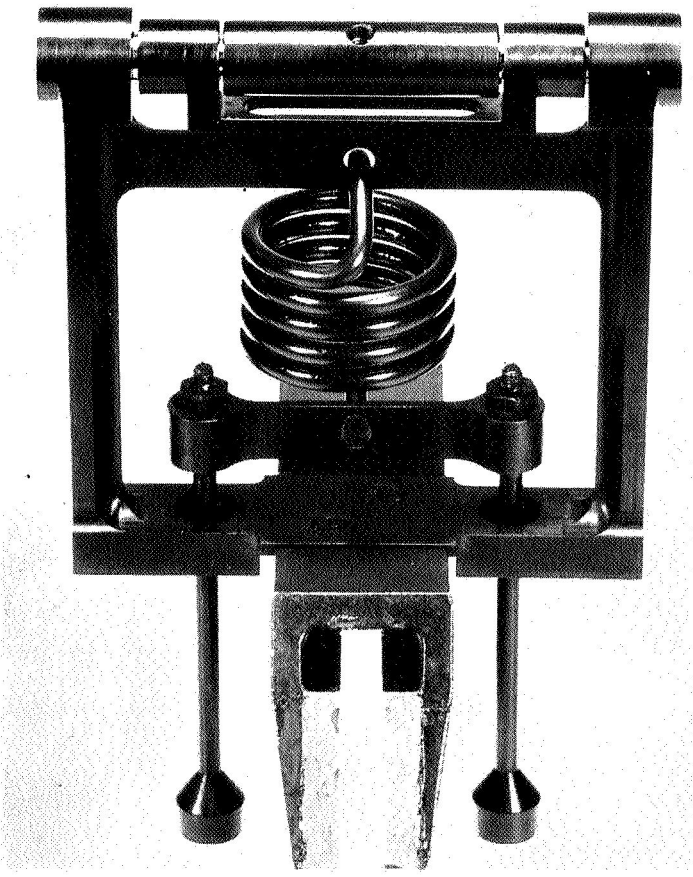

15817F

Figure 8 SUSPENSION AND CAGING MECHANISM WITH MAGNET

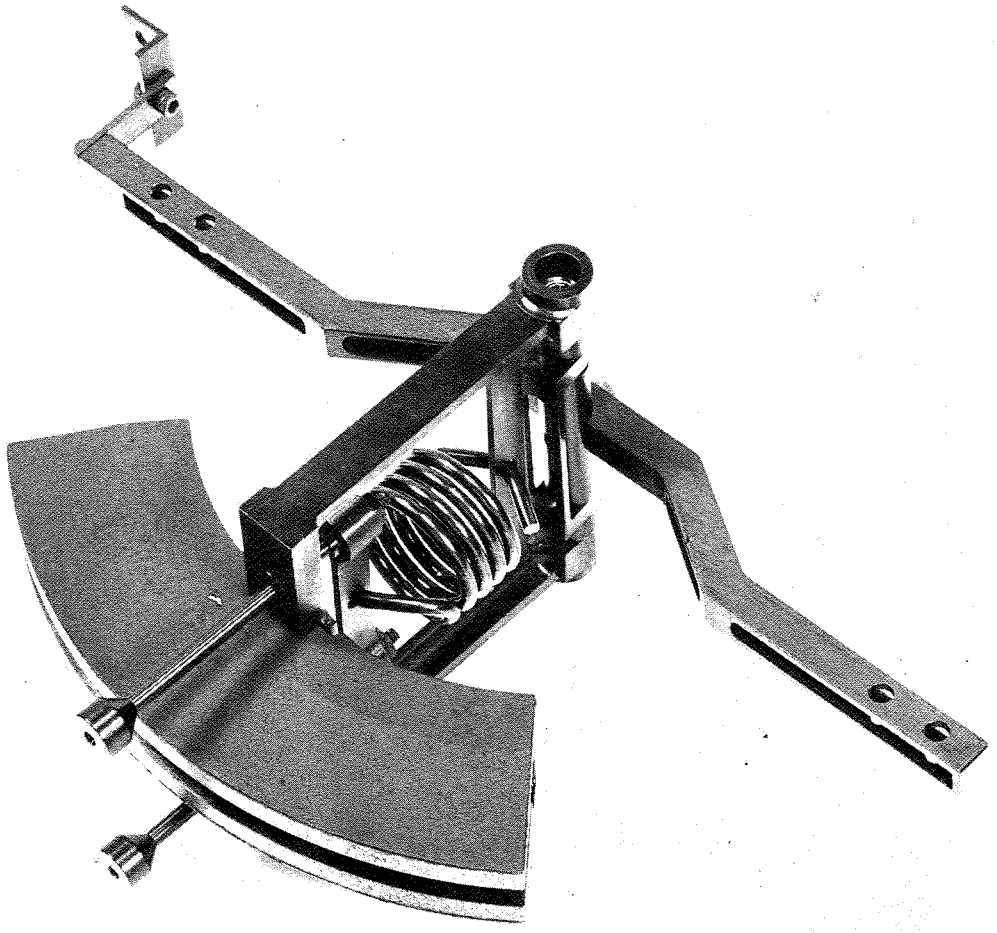

15817A

Figure 9 SUSPENSION AND CAGING MECHANISM WITH SUPPORT YOKE.

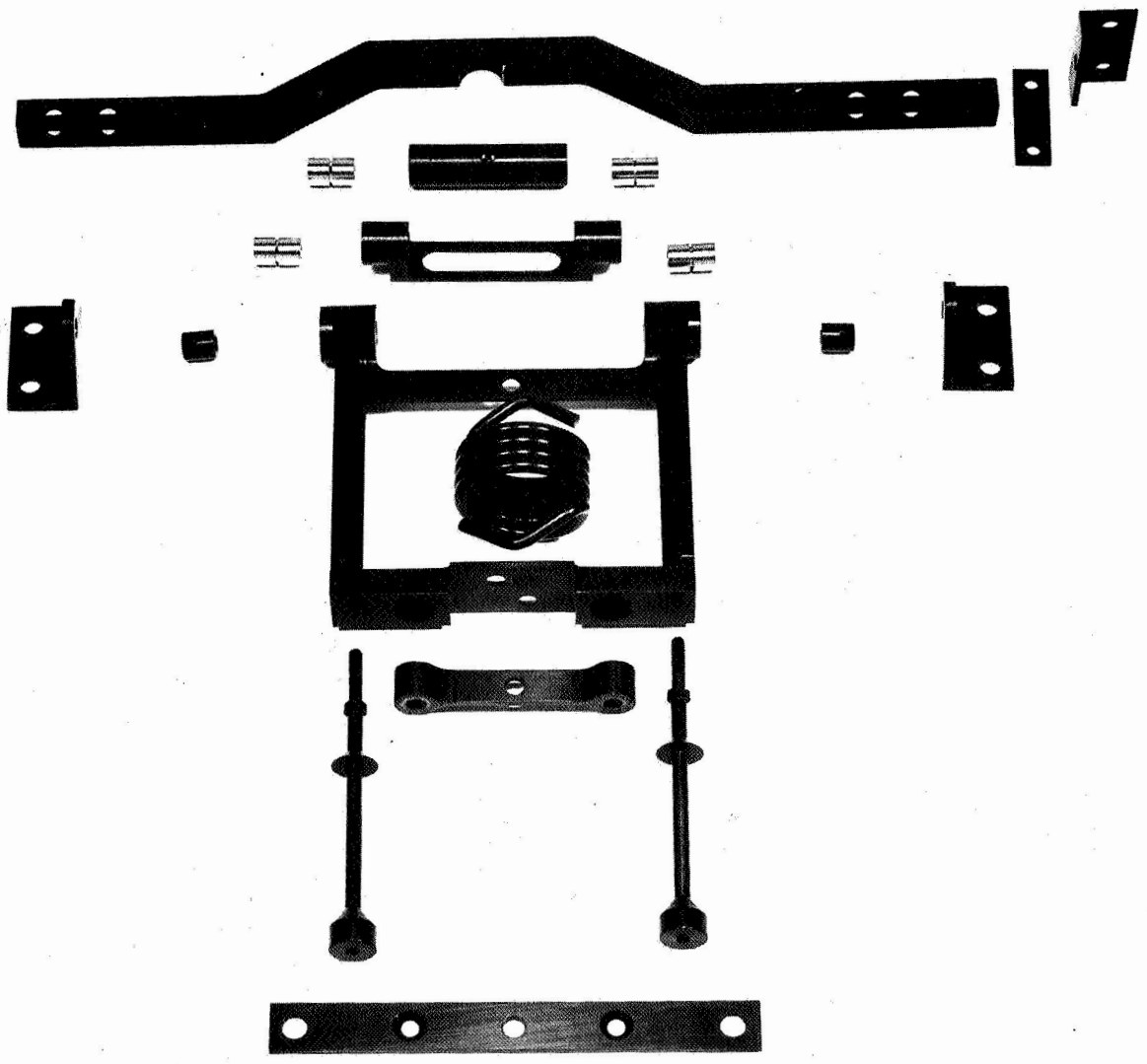

15817C

Figure 10 EXPLODED VIEW OF SUSPENSION AND CAGING MECHANISM

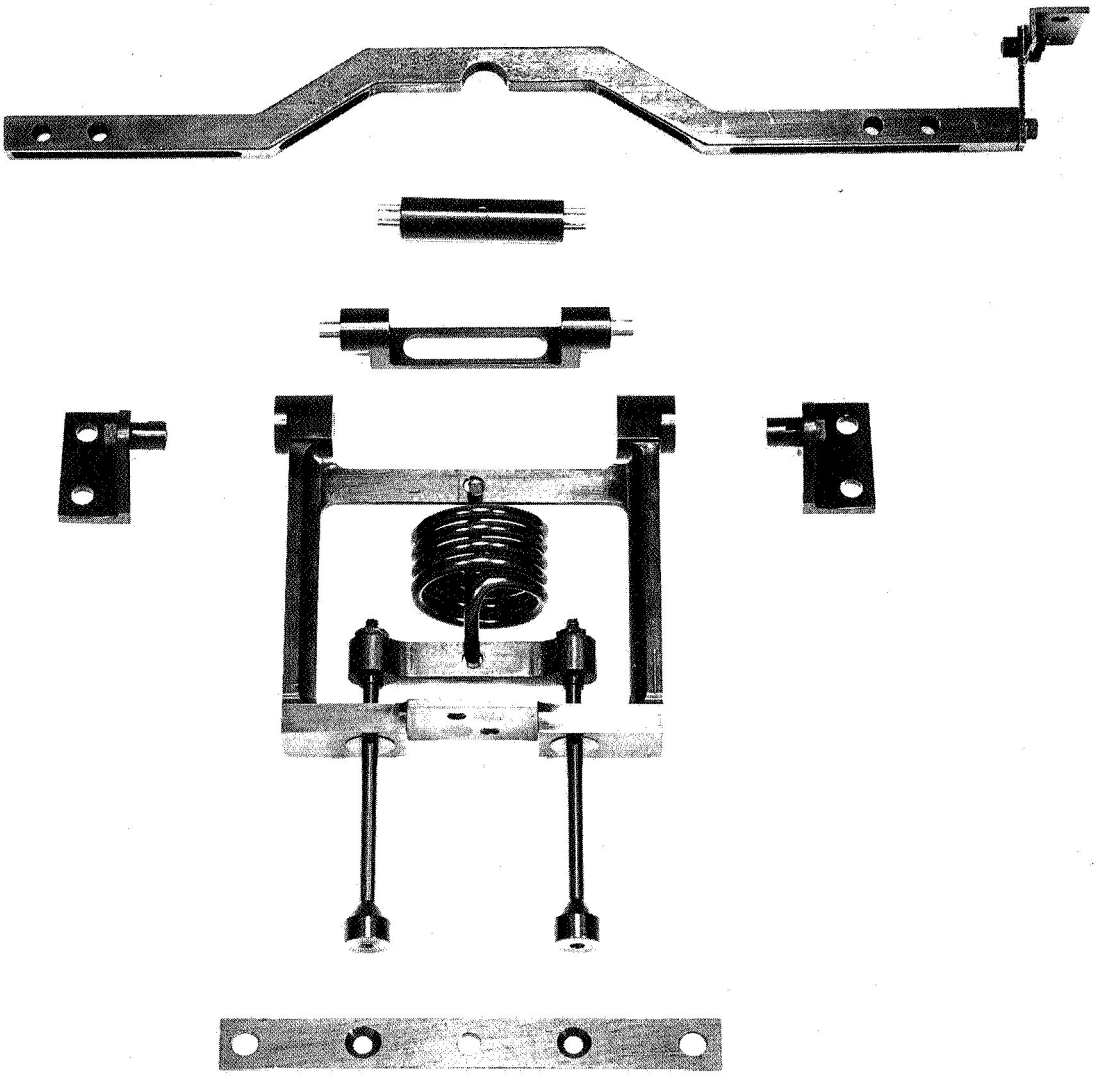

15817D

Figure 11 PARTIAL ASSEMBLY OF SUSPENSION AND CAGING MECHANISM

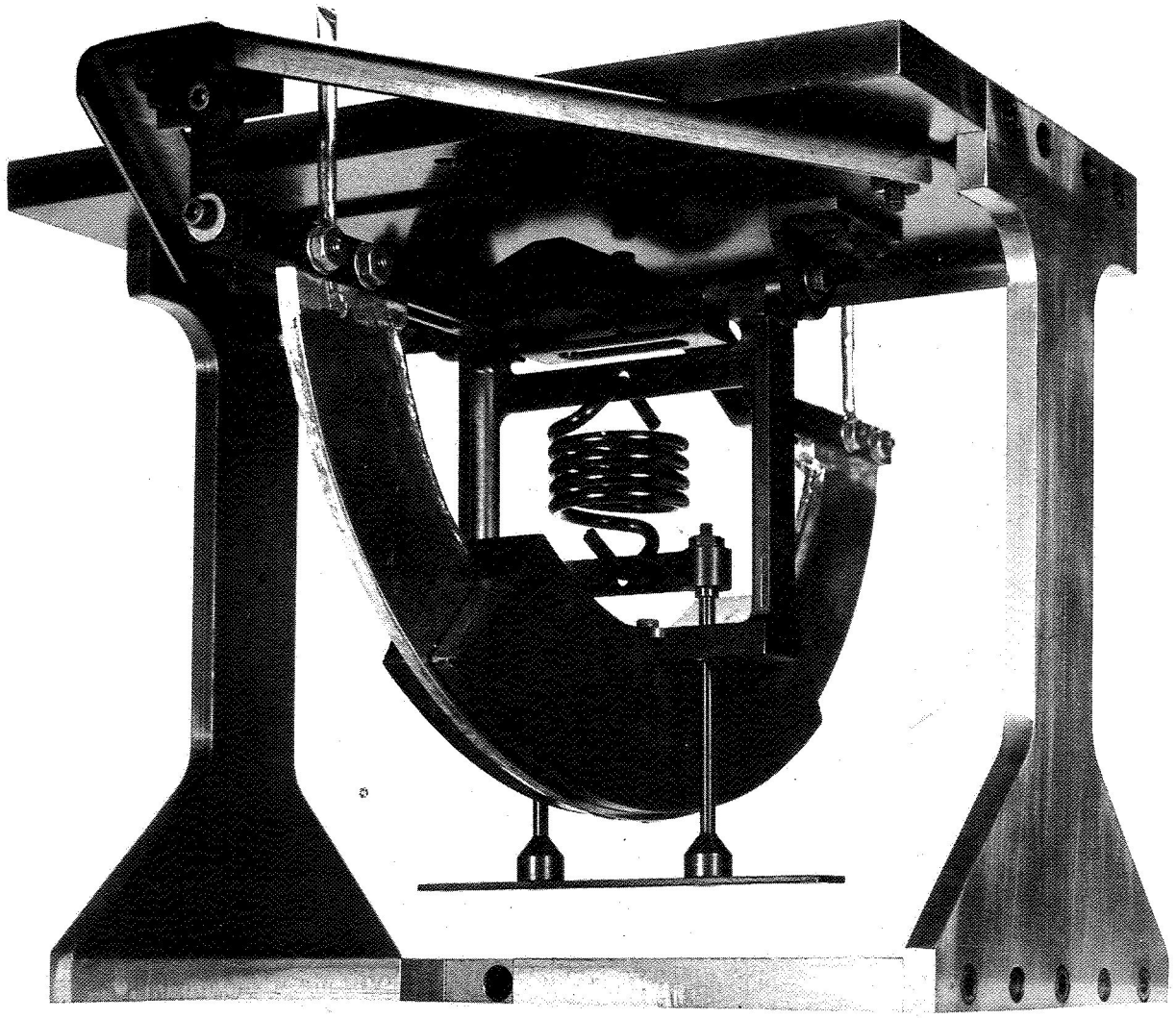

15892B

Figure 12 FERROFLUID VISCOUS DAMPER MODEL IN MOUNTING STAND: VIEW 1

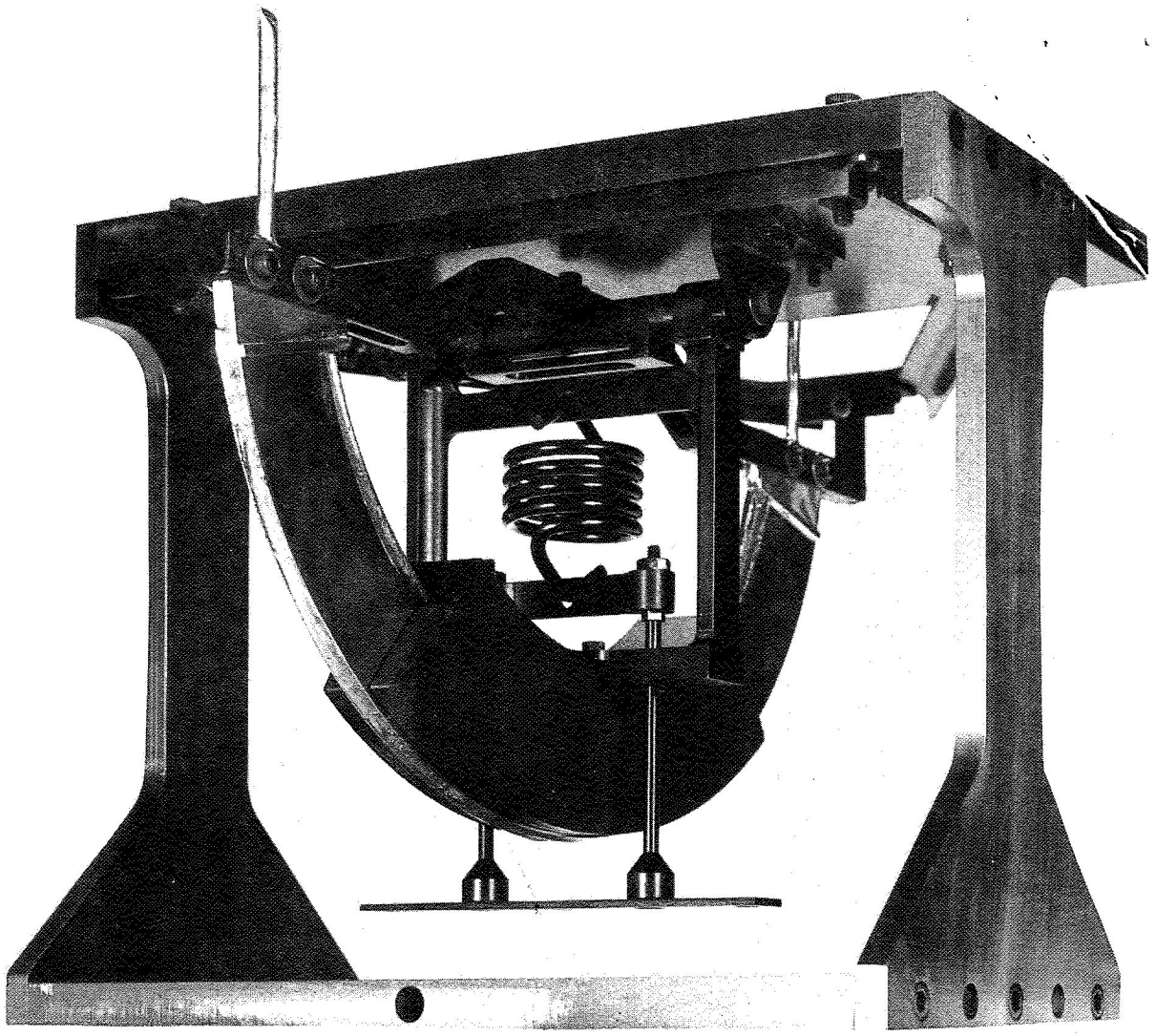

15892A

Figure 13 FERROFLUID VISCOUS DAMPER MODEL IN MOUNTING STAND: VIEW 2

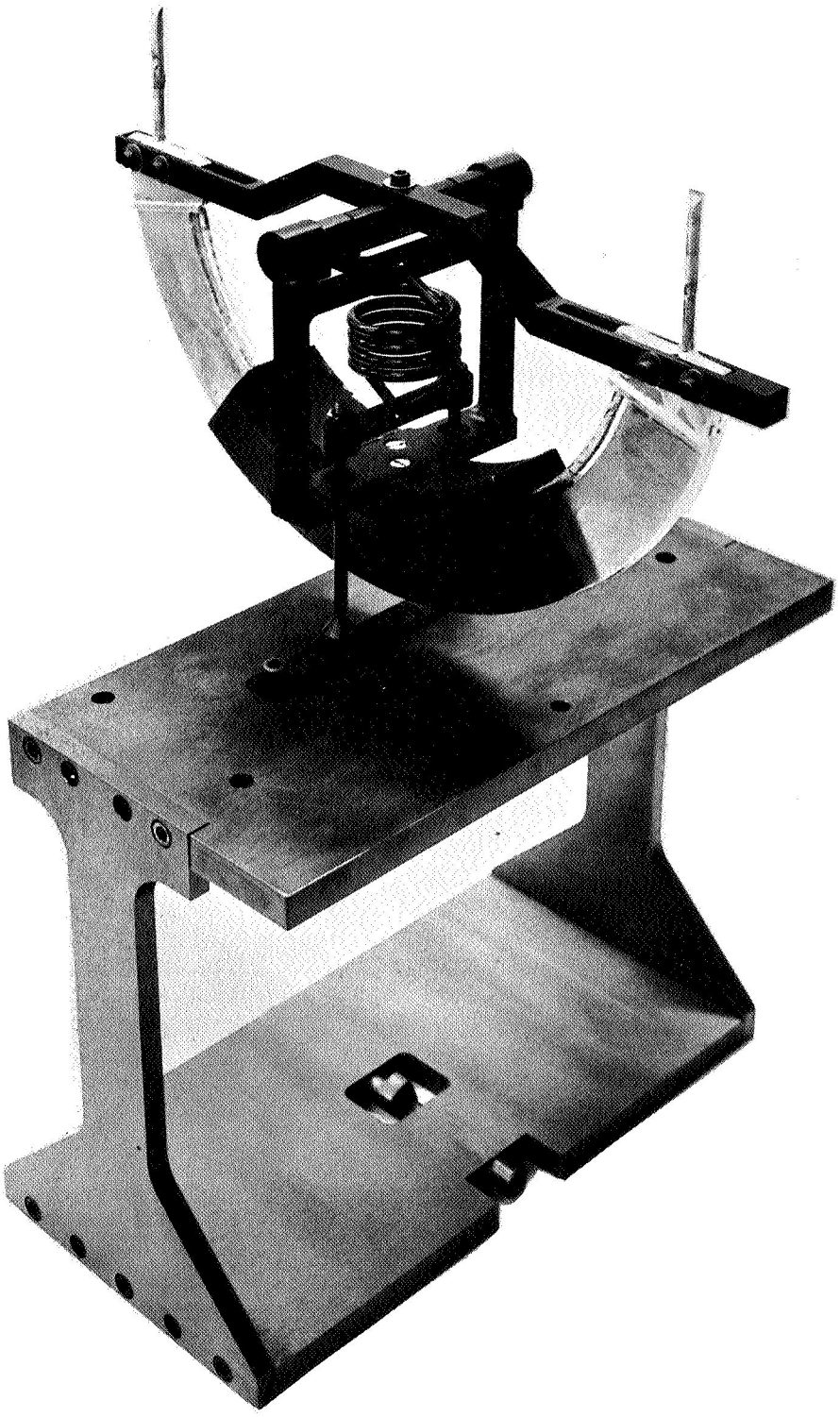

15877E

Figure 14 FERROFLUID VISCOUS DAMPER MODEL ON TOP OF MOUNTING STAND

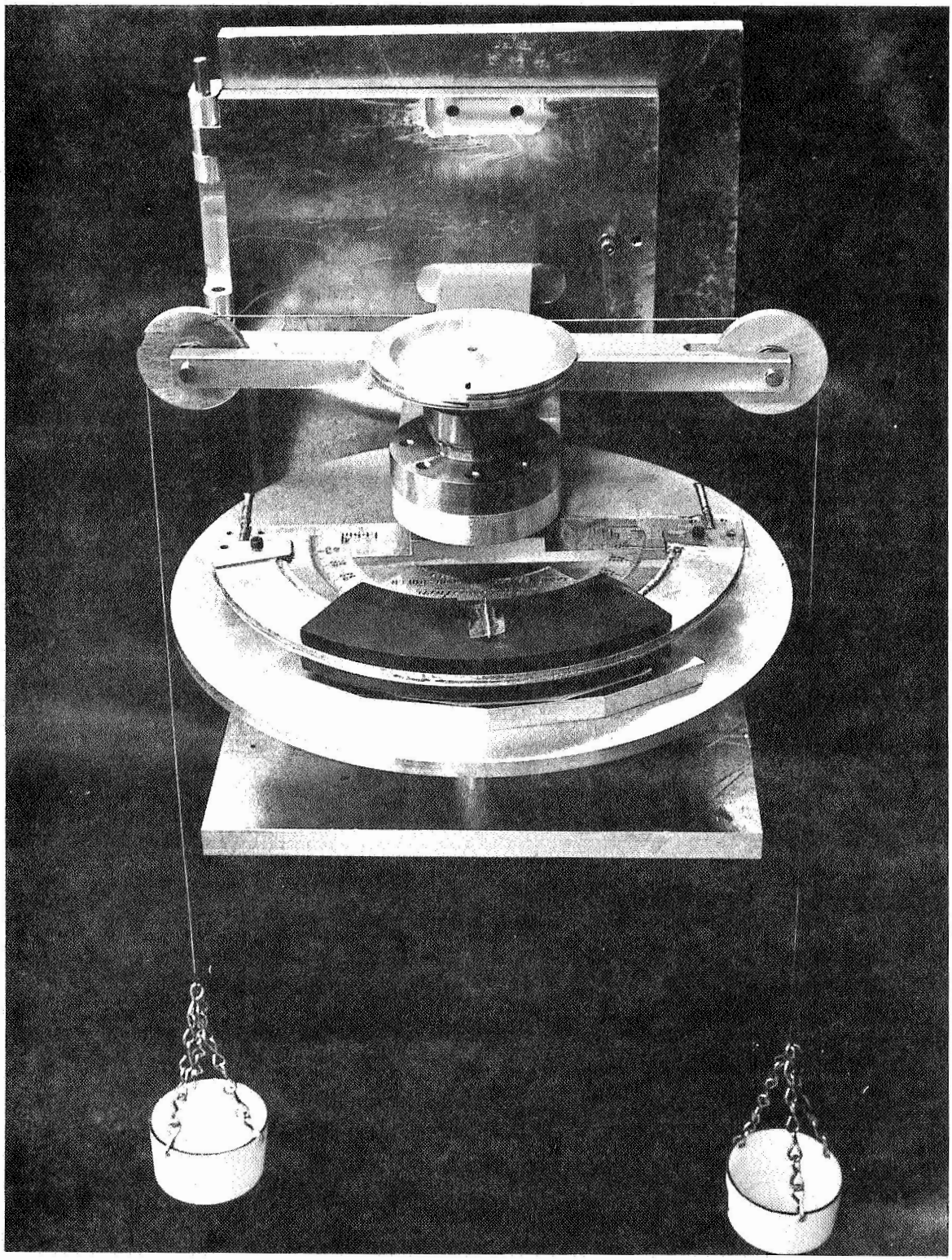

15877N

Figure 15 DAMPER MODEL VANE AND MAGNET IN TEST FIXTURE

D. SYSTEM CONSIDERATIONS

Study work completed by Avco under a previous NASA contract resulted in analysis of the RAE satellite system performance with hysteresis and viscous damping. The performance of the system was explored for a variety of initial conditions at the point of gravity gradient acquisition, as noted below:

	Initial Conditions
Case 1 (Nominal Case)	Pitch - 7°
	Yaw - 15°
	Roll - 4°
Case 2	Pitch - 0°
	Yaw - 90°
	Roll - 0°
Case 3	Pitch - 15°
	Yaw - 0°
	Roll - 0°
Case 4	Pitch - 25°
	Yaw - 0°
	Roll - 0°

Case 1 represents a normal grouping of satellite error angles at the time of gravity gradient system acquisition. Case 2 represents a very severe yaw initial condition, and Cases 3 and 4 cover increasing values of pitch initial error with zero yaw and roll errors.

Results of digital computer runs for these initial conditions are given in Tables I and II.

Tables I and II indicate that a viscous damper of the type described in this report will provide substantially better performance than a hysteresis damper. These tables have been compiled on the basis of conditions existing after 10 orbits.

Figures 16 and 17 illustrate the relative amount of energy dissipated by the viscous and hysteresis dampers over 10 orbits. The curves show that the viscous damper will generally dissipate more energy and hence damp the system more quickly than can be expected with the hysteresis damper. This difference is caused by the characteristic of the viscous damper that results in application of damping forces to the system in proportion to velocity.

TABLE I

HYSTERESIS DAMPER EFFECT ON RAE CONTROL SYSTEM PERFORMANCE

Case	Initial Conditions	Final Oscillation Angle (degrees)			Final In-Plane Tip Deflection(feet)	Final Out-Of-Plane Tip Deflection (feet)	Damper Contact With Stops	Final Damper Boom Angle (degrees)
		Pitch	Yaw	Roll				
1	P 7 Y 15 R 4	2.0	22.5	0.5	10.0	8.0	5	1.0
2	P 0 Y 90 R 0	8.0	90.0	8.0	50.0	40.0	31	36.0
3	P 15 Y 0 R 0	0	17.0	4.25	45	6.5	0	5.0
4	P 25 Y 0 R 0	2.0	17.0	0.5	15.0	10.0	8	0.75

TABLE II

VISCOUS DAMPER EFFECT ON RAE CONTROL SYSTEM PERFORMANCE

(C_D = 10 ft-lb-sec)

Case	Initial Conditions	Final Oscillation Angle (degrees)			Final In-Plane Tip Deflection(feet)	Final Out-of-Plane Tip Deflection (feet)	Damper Contact With Stops	Final Damper Boom Angle (degrees)
		Pitch	Yaw	Roll				
1	P 7 Y 15 R 4	0.5	0.0	0.5	5	0	0	0.5
2	P 0 Y 90 R 0	3.0	25.0	1.0	35	30	16	8.0
3	P 15 Y 0 R 0	0.5	1.8	0.25	60	6	1	1.0
4	P 25 Y 0 R 0	0.5	8.0	1.5	70	3	0	3.5

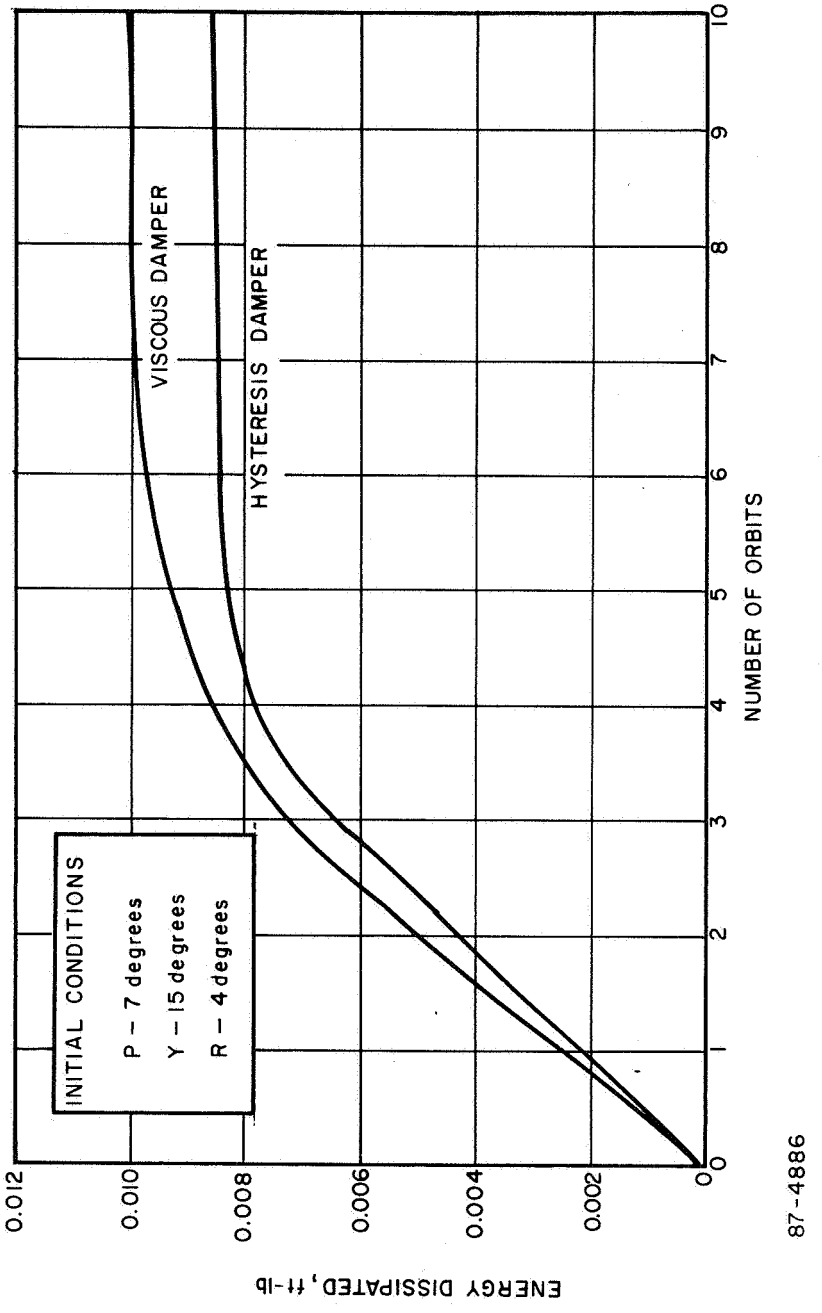

Figure 16 ENERGY DISSIPATED VERSUS TIME; P = 70, Y = 15°, R = 4°

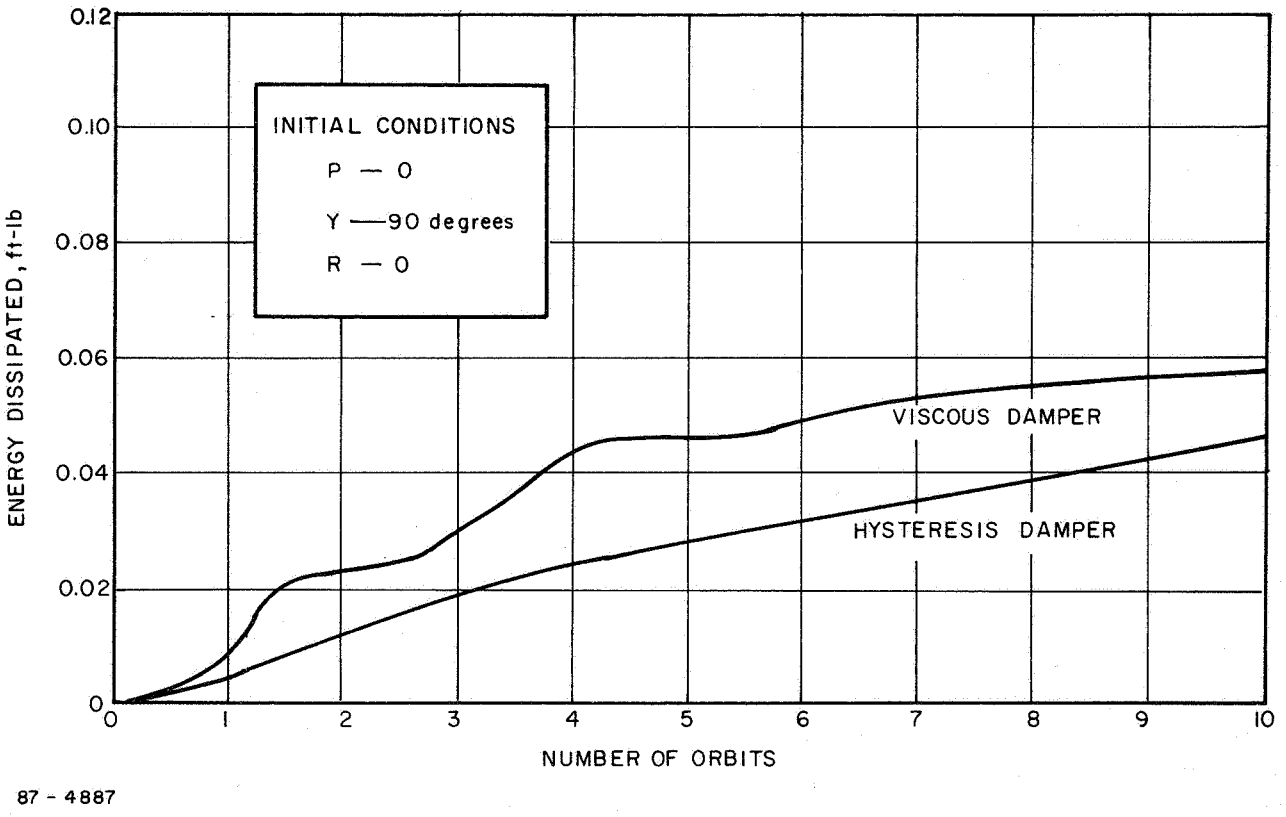

Figure 17 ENERGY DISSIPATED VERSUS TIME; P = 0°, Y = 90°, R = 0°

III. FERROFLUID DEVELOPMENT

A. PRELIMINARY SEARCH AND ANALYTICAL WORK

1. History and Background

The original Avco/SSD interest in magnetic fluids stems from the work of Resler and Rosensweig (Reference 1) who, under company-sponsored studies, developed principles relating to direct conversion of heat energy, using a ferromagnetic medium as the working substance. A thermodynamic cycle was devised that permitted the conversion efficiency to approach the Carnot limit, a limit which no heat engine can surpass. Analysis also revealed that a fluid form of the magnetic medium would constitute the ideal working substance, whereby regenerative heat transfer could be accomplished. In turn, this would permit the miniaturization of equipment.

All known materials that are strongly magnetic, like iron -- i.e., the ferromagnetic metals, alloys, and compounds -- are solids. While theoreticians do not rule out the possibility of true ferromagnetic liquids, none were known either then or at present (molten iron, for example, is not ferromagnetic). However, there seemed to be a good chance of making a stable suspension of a finely divided ferromagnetic solid in a "carrier" liquid and, accordingly, a laboratory effort was initiated.

After an extensive study, it was found that colloidal dispersions of magnetic particles could be produced by grinding ferromagnetic powders (such as ferrites) with steel balls in a tumbling mill for several weeks, following the lead of S. Papell, a NASA engineer.[2] The grinding was done in the presence of a liquid carrier, such as kerosene, within which was dissolved a dispersing agent that formed a repellent coating on each particle. The magnetic fluids are called ferrofluids and contain ferromagnetic particles of less than domain size.

Initial results in selecting, synthesizing, and characterizing these fluids were reported by Rosensweig, Nestor, and Timmins.[3] Their paper was devoted to the physical chemistry and magnetostatic aspects which contribute toward obtaining concentrated, magnetizable fluid dispersions of controlled viscosity and Curie point which may be stabilized to prevent agglomeration and settling. The working fluid which was synthesized retained its characteristics indefinitely. When heated in an applied field and cooled outside the field, it was induced into steady motion, thus demonstrating a new means of closed cycle, direct energy conversion for the first time.

These fluids should not be confused with the magnetic clutch fluid of Rabinow introduced during the late 1940's as the basis of clutches, dashpots, brakes,

and a method of casting. This fluid, a mixture of relatively large (micron size) particles in oil, has a viscosity that is highly field dependent, because the particles tend to chain together and, in fact, solidify under applied fields of moderate strength. In contrast, the ferrofluids are especially tailored to retain the fluid property under all applied fields and field gradients.

2. Ferrofluid Description

A ferrofluid is a colloidal dispersion of magnetic solid particles in an inert liquid. These solids are stabilized by a surface active third component forming a protective sheath around each particle.

The ferrofluids remain stable because the ferrite particles are very small and the energy they gain through thermal agitation and random impact with fluid molecules (Brownian motion) is larger than the energy associated with gravitational and magnetic fields. Hence the particles do not separate from the fluid under the influence of gravitational and magnetic fields. This process is successful in part because energy due to Brownian motion is particle size independent, while energy due to field effects is particle size dependent. Thus, the smaller the particle size, the more stable the ferrofluid suspension. Computations show that magnetic particles 25-100A in diameter should be stable on this basis.

In addition to gravitational and magnetic forces, particles in this size range are also subject to secondary valence forces of attraction. These forces are the result of the attraction of a fluctuating electric dipole for a neighboring induced dipole. According to Lifschitz, [4] the energy of attraction between two interacting particles decreases as a power function of the distance of separation of the particles. The exponent of this function varies between three and five, depending on the size and separation of the particles[4]. These attractive forces predominate over thermal forces only upon close approach of the particles (less than one particle diameter separation). This would lead to flocculation of the particles and separation of the liquid and solid phases. In order to avoid flocculation, it becomes essential to prevent such a close approach.

This is accomplished by incorporating a stabilizing agent into the solution, which results in the formation of a sheath of apparently bound fluid around each particle, physically preventing the surfaces of the individual particles from coming into contact. These stabilizing agents have a requisite chemical structure that will depend on both the nature of the solid to be dispersed and the dispersing medium. The stabilizing agent must contain a group that can interact strongly with the particle surface so that adsorption occurs. At the same time, the rest of the molecule must be compatible with the liquid medium. In fact, this part of the molecule should try to reproduce

all the properties of the medium except for being attached to the particle surface. As an example, magnetite dispersions in kerosene have been successfully prepared by grinding in the presence of oleic acid.

3. Characterization of Physical Properties

Most of the physical properties of the ferrofluids depend upon the properties of the carrier fluid alone (boiling point, flammability, etc.). Some important properties, however, depend on the individual components (liquid carrier, dispersed solid, and surfactant) and on the state of subdivision.

a. Magnetic Properties

The magnetic properties of the fluid are specifically due to the presence of the magnetic particles in suspension, each particle contributing to the overall magnetic effects. As the radius of a spherical domain is on the order of 150A for the common magnetic oxides considered in this work, the particles in a ferrofluid are essentially subdomain in size. The magnetic response of a ferrofluid increases with increasing solids concentration, as follows:

$$M = M_s \epsilon \tag{1}$$

where

M = saturation magnetization of the ferrofluid, in gauss

M_s = saturation magnetization of the suspended solid, in gauss

ϵ = volume fraction of solids in suspension.

b. Viscosity of a Ferrofluid

The utility and novelty of the ferrofluids is due to the fact that it has been possible to confer magnetic properties on a liquid medium. The resistance to flow of these liquids is of paramount interest. Theoretical predictions are available for determining the viscosity of a liquid containing suspended solids. The viscosity of the ferrofluids has been successfully characterized by the following equation:

$$\frac{1}{\epsilon}\left[\frac{\eta_s - \eta_o}{\eta_s}\right] = 2.5\left(\frac{\phi}{\epsilon}\right) - \left[\frac{2.5\ \phi_c - 1}{\phi_c^{\,2}}\right]\left(\frac{\phi}{\epsilon}\right)^2 \epsilon \tag{2}$$

where

η_s = absolute viscosity of the ferrofluid, in cp

η_o = absolute viscosity of the carrier fluid, in cp

ϕ = volumetric concentration of coated particles = solid particles + stabilizing sheath

ϵ = volume fraction of solids in suspension

ϕ_c = critical concentration of suspended matter at which the suspension becomes rigid

For practical purposes it has been found that

$$f(\phi_c) = \frac{2.5\ \phi_c - 1}{\phi_c^2} = 1.56 \tag{3}$$

By substitution into Equation 2 and transposition of terms, the following simplified equation for the viscosity of a ferrofluid is obtained:

$$\eta_s = \frac{\eta_o}{(1 - 1.25\ \phi)^2} \tag{4}$$

The ratio of ϕ to ϵ depends on the size distribution of the particles in suspension and on the thickness of the stabilizing layer, δ. For the case of equal size spheres of radius r, it becomes

$$\frac{\phi}{\epsilon} = \left[1 + \frac{\delta}{r}\right]^3 \tag{5}$$

These suspensions are Newtonian at low solids concentrations, but non-Newtonian at higher concentration. While the transition depends upon the individual system under consideration, it has been shown by Dintenfass[5] that this usually occurs at around 20 percent by volume solids in non-aqueous media.

c. Temperature Variation of Viscosity

According to Equation 4, η_s at any given temperature is a function of the viscosity of the base fluid and effective volume fraction solids (ϕ). The base fluids used in these studies are simple, unassociated liquids that normally follow Andrade's rule:

$$\eta_o = A\, e^{E/RT} \qquad (6)$$

where A and E are characteristic constants, R is the gas constant, and T is the absolute temperature.

In turn, ϕ is a function of the average particle size, the thickness of stabilizing layer δ, and the volume fraction solids ϵ. Particle size and ϵ can be considered not to depend on temperature, except for second order effects due to changes in density. The thickness δ is a complex function of temperature which depends on the variation of the adsorption of molecules on the particle surface and thermal agitation of these molecules. Previous experience has shown that δ increases with decreasing temperature (see Equation 6) so that the temperature coefficient of viscosity of a suspension is higher than the temperature coefficient of the carrier fluid.

4. Desired Properties of a Ferrofluid for Viscous Damper Applications

In order to be applicable in the viscous damper for the RAE satellite, the following preliminary requirements were placed on the properties of the ferrofluid:

a. The saturation magnetization is to be at least 150 gauss.

b. The nominal viscosity of the fluid at room temperature (30° C) is to be in the range from 10 cp to 500,000 cp.

c. The fluid is to be Newtonian in flow characteristics.

d. The fluid will be exposed to an operating temperature range from 0° F to 70° F. In this range, there will be less than a 5 to 1 variation in viscosity.

e. The fluid will be able to survive temperatures as low as -60° F and heating to 160° F during storage periods.

5. Choice of Components

a. Magnetic Solid

Previous experience in the preparation of hydrocarbon base ferrofluids has shown that synthetic magnetite is a satisfactory material. It is available in powdered form, it is a brittle solid material that can be ground to the required particle size, and the resulting particles do not lose their magnetic properties with time, even in the presence of air.

In the experimentation, two grades of magnetite were used. One powder is a synthetic magnetite manufactured by the C. F. Williams Company, Mineral and Pigments Division of Chas. Pfizer and Company, Inc. The pertinent properties of this powder are presented in Table III. The other powder is Wright Industries, Inc. (Brooklyn, New York), Magnetic Pigment 4000. This is a synthetic magnetite that is more finely divided (specific surface area: 23 m^2/gram) and therefore grinds more rapidly.

TABLE III

PROPERTIES OF MAGNETIC SOLID (MAGNETITE) BEFORE GRINDING

Manufacturer	Chas. Pfizer and Company, Inc.
Manufacturer's Code	IRN 100
Chemical Composition	$FeO.Fe_2O_3$
Particle Shape	Acicular
Average Particle Length	0.55 μ
Average Particle Width	0.08 μ
Specific Surface Area (B. E. T.)	12.5 m^2/gram
Specific Gravity	5.0 gram/cm^2
Saturation Magnetization	5660 gauss
Curie Point	570°C

b. Carrier Fluid

Many of the physical characteristics of the ferrofluid are determined by the physical properties of the carrier fluid. Basic requirements placed on the carrier fluid include the following:

1) The carrier fluid has to be liquid between 0°F and 70°F, the temperature range at which the magnetic damper has to perform.

2) The carrier fluid preferably should be liquid between -60°F and 160°F. If not, any phase changes that occur between -60°F and 160°F should not affect performance of the damper between 0°F and 70°F.

3) The viscosity variation of the carrier fluid between 0°F and 70°F has to be such that the damping coefficient variation is less than 5.0 to 1 in this temperature range.

Other desirable characteristics include the following:

1) The carrier fluid should be nonvolatile at room temperature, so that there will be no evaporation losses of carrier fluid during handling that would change the concentration of magnetic solids in the ferrofluid and thereby alter its physical properties.

2) The carrier fluid should be noncorrosive.

3) The carrier fluid should be nontoxic.

Examination of the physical properties of various candidate carrier fluids indicated that certain types of silicone oils would be the most satisfactory dispersion media, since as a class they exhibit an unusually low variation of viscosity with temperature and remain liquid over an extremely wide temperature range.

The silicone oils are semiorganic polymers whose structure can be represented by

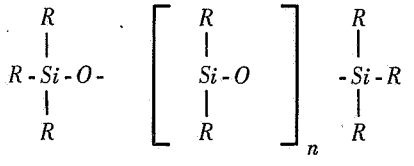

where R may be the same or different organic groups (methyl, phenyl, etc.). The properties of these oils may be varied through the use of many types of organic substituents and through variations in the length of the molecule.

The relevant physical properties of different commerically available silicone fluids are listed in Table IV.

The silicone oils, as a class, that show the lowest change of viscosity with temperature are the dimethyl silicones. Of all the low viscosity fluids (less than 1000 cp) examined, these oils appear to possess the best combination of physical properties.

TABLE IV

TYPICAL PROPERTIES OF COMMERCIAL SILICONES CONSIDERED AS CARRIER FLUIDS

Fluid Type	Nominal Viscosity at 77° F (cst)	Specific Gravity at 77° F	Boiling Point (°F)	Pour Point (ASTM D1298) (°F)	Viscosity Temperature Coefficient (*)	Principal Component	Commercial Designation	Manufacturer**
Dimethyl Silicone	0.65	0.761	211 at 760 mm	-90	0.31	Dimer	DC 200	D/C
Dimethyl Silicone	1.0	0.818	305 at 760 mm	-148	0.37	Trimer	DC 200	D/C
Dimethyl Silicone	2.0	0.873	446 at 760 mm	-148	0.48	Pentamer	DC 200	D/C
Dimethyl Silicone	3.0	0.900	158 to 212 at 0.5 mm	-148	0.51	Hexamer/ Heptamer	DC 200	D/C
Dimethyl Silicone	10.0	0.934	Nonvolatile	-148	0.56	Polymer	DC 200 L45	D/C, UCC
Dimethyl Silicone	50.0	0.960	Nonvolatile	-94	0.59	Polymer	DC 200 L45	D/C, UCC
Dimethyl Silicone	1000	0.971	Nonvolatile	-58	0.61	Polymer	DC 200 L45	D/C, UCC
Dimethyl Silicone	12,500	0.975	Nonvolatile	-51	0.61	Polymer	DC 200, L45	D/C, UCC
Methyl-Phenyl Silicone	100,000	0.971	Nonvolatile	-28	0.61	Polymer	DC 200, L45	D/C, UCC
Methyl-Phenyl Silicone	50	0.99	Nonvolatile	Below -70	0.63	Polymer	DC 510	D/C
	1000	1.00	Nonvolatile	-70	0.60	Polymer	DC 510	D/C
	100,000		Nonvolatile	-70	0.65	Polymer	DC 510	D/C
High Phenyl Methyl Silicone	500	1.10	Nonvolatile	-8	0.87	Polymer	DC 710	D/C
Aryl-Alkyl Silicone	12,000	1.08	Nonvolatile	+15	0.97	Polymer	L43	UCC

*Viscosity Temperature Coefficient = $K = 1 - \frac{\text{Viscosity at } 210°F}{\text{Viscosity at } 100°F}$

Note: $K < 0.67$ is equivalent to $\frac{\text{Viscosity at } 70°F}{\text{Viscosity at } 0°F} < 3$

**D/C = Dow Corning Chemical Co., Inc.

UCC = Union Carbide Corp.

The low molecular weight dimethyl siloxanes, while exhibiting the lowest variation of viscosity with temperature, are fairly volatile. For example, DC 200 fluid, 0.65 cst grade, exhibits only a 2.5-fold viscosity change between 0°F and 70°F, but boils at 211°F and has a vapor pressure of over 1 mm at room temperature, which makes it too volatile for use.

The intermediate molecular weight polydimethyl siloxanes (3 cst to 1000 cst, nominal viscosity) exhibit all the properties desired of a carrier solvent -- Newtonian flow, low viscosity-temperature variation, low pour point, and low volatility -- while also being chemically inert and nontoxic. The highest molecular weight dimethyl siloxanes have pour points which detract from their applicability in the proposed damper.

If a base material with a viscosity of more than 1000 cst is desired, the Dow Corning 510 fluids which are available in grades ranging from 50 cst to 100,000 cst appear to be best suited, since they are still serviceable at -70°F. The temperature-viscosity curve of these oils is not as flat as that of the dimethyl silicone oils, but they still exhibit less than a 3.5-fold variation in viscosity from 0°F to 70°F.

Other silicone oils considered were a high phenyl methyl silicone oil (Dow Corning 710 fluid) and an aryl-alkyl silicone oil (Union Carbide Corporation L-43). Both these products were unsuited for the present application, because they exhibit a large temperature variation of viscosity and a high pour point.

A stable colloidal dispersion of magnetite in a nonvolatile dimethyl silicone oil or phenyl methyl silicone oil would exhibit the combination of physical properties most suited to the magnetic damper application.

Past experience in the synthesis of ferrofluids was essentially limited to the preparation of colloidal dispersions in aliphatic hydrocarbon media. It was also known that stabilizing agents suited to the synthesis of hydrocarbon base ferrofluids did not work in other media such as silicones. A completely different class of stabilizing agents would be required for the dimethyl silicone base systems. There was no definite assurance that a satisfactory combination of materials would be found within the scope of the program that would result in the development of a completely satisfactory silicone base ferrofluid. Consideration was therefore also given to the preparation of a hydrocarbon base ferrofluid that would best perform in the magnetic damper.

Different hydrocarbons considered and some of their relevant physical properties are listed in Table V. None of these fluids exhibit all the physical properties desired: Fluids that have a low viscosity-temperature variation are usually volatile, and nonvolatile fluids have either a high freezing point or a large change of viscosity with temperature.

TABLE V

TYPICAL PROPERTIES OF HYDROCARBONS CONSIDERED AS CARRIER FLUIDS

Compound	Formula	Freezing Point (°F)	Boiling Point at 760 mm (°F)	Boiling Point at 1 mm (°F)	Viscosity at 10°C (Cst)	Viscosity Temperature Coefficient (*)	Specific Gravity	Comments
N. Decane	$C_{10}H_{22}$	-21	346	62	1.25	0.45	0.726	Too volatile
N. Dodecane	$C_{12}H_{24}$	+15	421	118	1.98	0.50	0.751	Freezing point too high
Tetralin	$C_{10}H_{12}$	-24	405	100	2.0	0.52	0.97	Possible
Cis-decalin	$C_{10}H_{18}$	-46	382	72	2.7	0.60	0.89	Too volatile
M-Xylene	C_8H_{10}	-54	291	20	0.705	0.38	0.86	Too volatile
1.3 Diethyl Benzene	$C_{10}H_{14}$	-119	358	69	1.2	---	0.86	Too volatile
Alpha Methyl Naphthalene	$C_{11}H_{10}$	-23	472	148	3.2	0.64	1.01	Possible
Ethyl Naphthalene	$C_{12}H_{12}$	+7	497	169	---	---	1.00	Freezing point too high

*Viscosity Temperature Coefficient = $1 - \frac{\text{Viscosity at } 210° \text{ F}}{\text{Viscosity at } 100° \text{ F}}$, see Table IV.

Of all the organic fluids listed, alpha methyl napthalene and tetralin offered the best compromise of physical properties. Tetralin possesses better viscosity-temperature characteristics, but it is more volatile then alpha methyl naphthalene. Since the viscosity characteristics of alpha methyl naphthalene were marginally acceptable, this compound was chosen in preference to tetralin in order to avoid difficulties caused by fluid loss by evaporation, namely, changes in overall physical properties and surface skin formation in particular.

c. Surfactants

Previous experience[2] has shown that oleic acid and Tenlo 70* are satisfactory stabilizing agents in hydrocarbon systems, and that ferrofluids obtained by grinding magnetite in mixtures of kerosene and oleic acid or kerosene and Tenlo 70 are stable over a wide range of conditions. Oleic acid was the stabilizer of choice for hydrocarbon systems for this application, since the properties of the oleic acid hydrocarbon mixtures were better known.

As mentioned, experience has shown that stabilizing agents that prove to be satisfactory for kerosene base suspensions are not satisfactory for silicone oil base suspensions. This is not surprising, since hydrocarbons are quite different from the silicones in internal structure. This is evidenced by the fact that the Hildebrand solubility parameter for hydrocarbons ranges between 7.5 and 8.0, while it is only about 4.0 for polymeric dimethyl silicone oils.

A completely different class of stabilizing agents is required for the dimethyl silicone base systems than for the hydrocarbon base systems. By analogy with oleic acid, a stabilising agent should have the following properties:

1) Solubility in the silicone oil under consideration.

2) A polar group which can adhere to the particle surface.

3) A silicophilic principal backbone that would have a structure similar to that of the dispersing silicone oil, with an overall molecular length equivalent to that of oleic acid. Table VI lists the silicone surfactants obtained for the screening tests.

* Trademark Nopco Chemical Company. Tenlo 70 is a commercial hydroxyamine.

TABLE VI

SILICONE SURFACTANTS OBTAINED FOR SCREENING TESTS

Manufacturer*	Code Number	Chemical Composition When Known
UCC	A110	Gamma-aminopropyltriethoxisilane
UCC	L 75	Non-ionic organosilicone surfactant
UCC	L 77	Non-ionic organosilicone surfactant
UCC	L 78	Non-ionic organosilicone surfactant
UCC	L 79	Cationic quarternary organosilicone surfactant
UCC	Y 4163	Methyl silicone ester
UCC	Y 5062 Y 6165	Amine modified silicone, 0.4% NH_2 100% silicone
UCC	Y 5078	Amine modified silicone, 6% NH_2, in isopropanol (65% silicone)
UCC	Y 5455	Amine modified silicone, 2% NH_2, 100% silicone
D/C	Z 6020	N (Trimethoxysilylpropyl) ethylenediamine
D/C	XZ-8-2502	Cationic silicone with amine silane backbone
G.E.	SF 1115	Dicarboxylic acid 10 silicone units long
G.E.	426-297-294	Dicarboxylic acid 10 silicone units long
G.E.	SF 1076	Carboxyl groups distributed along a silicone chain
G.E.	399-104-1114	Amine terminated fluid 20 silicone units long

* UCC = Union Carbide Corp.
D/C = Dow Corning Chemical Co., Inc.
G.E. = General Electric Co.

B. EXPERIMENTAL SCREENING AND PROCESSING TESTS

1. Dispersion Studies with Silicone Oils

Since a long period is required to detect any reasonable effects when a solvent/powder/surfactant mixture is ground in a mill, a screening method has been developed that eliminates evidently unfavorable combinations quickly and simply prior to the time-consuming grinding step.

The technique used to screen additives is simple. It consists of adding the surfactant to a given amount of solids in a fixed volume of liquid in the laboratory and shaking the mixture for a fixed period in a systematic fashion on an Eberbach reciprocating shaker. The tubes are then placed in a vertical position on a table, and the time of settling of the suspension is observed. A correlation has been observed between the effect of a surfactant on the rate of settling of magnetite powder in kerosene in the tube, and the formation of a stable ferromagnetic dispersion when the mixture of magnetite, kerosene, and surfactant under consideration is ground in a ball mill. Surfactants which result in the longest settling times prove to be the most successful grinding aids. The same principle is assumed to be true for other liquid systems, in particular the silicone fluids under present consideration.

The results of different dispersion studies carried out in 3 centistoke dimethyl silicone oils are presented in Table VII. By far the best results have been obtained with Union Carbide experimental silicones Y5062 and Y6165. According to the manufacturer, they are essentially the same compound: amine functional silicone surfactants with a nominal NH_2 concentration of 0.4 percent. Y6165 is the successor to Y5062, which is no longer available. They are labeled differently because of a minor processing change. Other surfactants did not give the same degree of dispersion. It should be noted that the oleic acid dispersant yielded poor results in these tests.

2. Grinding Studies with Silicone Oils

Grinding tests in different silicone fluids have been performed based on the results of the above dispersion tests.

A first run was started in a Svegari Attritor ball mill set at 505 rpm, with the following ingredients:

TABLE VII

SEDIMENTATION TESTS IN DIMETHYL SILICONE FLUID (THREE CENTISTOKES)

60 ml DC 200 - 3 cs fluid
1.00 gr Magnetite IRN 100
0.15 cc Surfactant (3 drops)

Surfactant*	Settling Time**
Blank	3 min
UCC L 75	10 min
UCC L 77	3 min
UCC L 78	10 min
UCC L 79	5 min
UCC Y4163	10 min
UCC Y5062	over 1 hour
UCC Y5078	15 min
UCC 5078 + 3 drops water	2 min
UCC 5078	15 min
UCC Y5455	15 min
UCC Y5062	over 1 hour
UCC Y6165	over 1 hour
G.E. SF1115	10 min
G.E. 426-297-294	5 min
G.E. SF1076	2 min (coagulation)
G.E. 399-104-1114	15 min
D/C Z6020	5 min
D/C XZ82502	10 min
Oleic Acid	10 min

*UCC = Union Carbide Corp.
D/C = Dow Corning Chemical Co., Inc.
G.E. = General Electric Co.
**For freshly prepared solution shaken on Eberbach reciprocating shaker at 280 cycles/min.

Dimethyl silicone oil (3 centistokes) D/C 200	240 cc
Magnetic Powder	40 gr
UCC Y5067 Surfactant	20 cc

After a day of grinding, a tea colored supernatant was obtained. After three days, a weakly magnetic supernatant was obtained. Due to the limited capacity of the attritor, the contents were transferred with additional fresh material into a regular mill, and the grind was continued as grind G52 listed in Table VIII. This table presents the results of various attempts to prepare ferrofluids by grinding magnetite in different dimethyl silicone oils in the presence of amine functional surfactants. In addition to the Y5062 and Y6165 surfactants, a related UCC experimental surfactant, Y5455, was tried even though it did not perform as well in the dispersion tests. This surfactant contains 2 percent NH_2 in its structure.

In all cases, after initially encouraging results, the grinds did not result in the formation of satisfactory ferrofluids. The initial stages of grinding resulted in very dilute suspensions of colloidal magnetite. With continued grinding, intractable gels were formed that did not respond to the addition of either excess solvent or excess surfactant or to further grinding.

In one case (G52), where the initial solids concentration was low, the grinding experiment was stopped after 393 hours of grinding. A definitely magnetic colloid dispersion was obtained which, however, had a saturation magnetization of only 25 gauss. This magnetization was too weak to use. Attempts to concentrate this fluid did not meet with much success, since a twofold reduction in volume of the fluid, which corresponds to an increase of saturation magnetization to only about 50 gauss, resulted in the formation of a viscous, gel-like material. This was the only time a dimethyl silicone fluid was prepared, however, in spite of the preliminary encouraging screening test results.

At this time, no satisfactory dimethyl silicone base ferrofluid has been prepared by direct grinding.

3. Preparation of Other Ferrofluids

Since difficulties were encountered in the preparation of silicone base ferrofluids, several hydrocarbon base ferrofluids were prepared for testing and development of various damper models.

Since the magnetic strength of a ferrofluid is proportional to the volume concentration of magnetic solids, fluids of increased magnetic strengths are obtained by partial removal of the carrier. The primary hydrocarbon fluids formed by grinding can be modified either by vacuum evaporation

TABLE VIII

LIST OF GRINDING RUNS WITH SILICONE CARRIER FLUIDS

Initial Formulation										
			Carrier		Surfactant		Magnetic Solid			
Run No.	Total Hours of Grind	Mill Size	Type	Volume (cc)	Type	Volume (cc)	Type	Volume (cc)	Additions During Run	Comments
A15	500	Attritor	D/C 200/3	240	Y 5062	20	IRN 100	8	70 cc of carrier, 19 cc of surfactant	Transferred to 652 after 500 hr
G52	393	4.7 pint	D/C 200/3	640	Y 5062	39	IRN 100	8	Added 330 cc of carrier to contents	M = 24.7 gauss
G54	816	1.6 gel	D/C 200/3	1250	Y 5062	50	Wright 4000	40	500 cc of D C 200/0.65 cst at 694 hr	Formed gel which liquid addition did not break
G56	1945	4.7 pint	UCC L45/10	625	Y 5062	50	IRN 100	20	Added 100 cc of carrier at 970 hr. 100 cc at 1129 hr. 100 cc of D/C 200/0.65 cst at 1779 hr	Formed gel which liquid addition did not break
G57	634	4.7 pint	D/C 200/0.65	625	Y 6165	50	IRN 100	20	100 cc of carrier at 489 hr	Formed gel which liquid addition did not break
G59	536	4.7 pint	D/C 200/0.65	625	Y 6165	10	IRN 100	20	10 cc of Y 6165 at 214 hr; 50 cc of carrier at 374 hr	Formed gel by liquid addition
G60	652	4.7 pint	D/C 200/0.65	625	Y 5455	50	IRN 100	20	100 cc of carrier at 490 hr	Formed gel
A17	400	Attritor	D/C 200/0.65	240	Y 6165	10	Wright 4000	8	200 cc of carrier at 300 hr	Mill down for repairs at 400 hr gel formation at this time

or by a flocculation-redispersion technique to produce ferrofluids with a wide range of properties.

It has been found that an excess of a polar solvent that is miscible with the carrier fluid, such as acetone or ethyl alcohol, results in flocculation, the particles separating from the liquid phase after the supernatant liquid is decanted. It has also been found that the solids redisperse spontaneously in fresh solvent or in fresh solvent to which a small amount of stabilizing agent has been added. It is thus possible to modify the ferrofluids by this alternate technique. By adding less carrier fluid to the flocculated material, it is possible to concentrate the system. By changing the carrier fluid solvent, interchange occurs. Different ferrofluids prepared and modified for the damper development program are listed in Table IX. These fluids are hydrocarbon base materials (including alpha methyl naphthalene), for two silicone base fluids. And L43 silicone oil base ferrofluid has been made by adding this material to a hydrocarbon base ferrofluid and evaporating the hydrocarbon under vacuum. This silicone oil is designed to be compatible with hydrocarbons, so that surfactants suited to kerosene systems are also compatible with this liquid. Unfortunately, the temperature-viscosity characteristics and pour point do not meet the project requirements.

A ferrofluid has been prepared in the 0.65 cst D/C 200 fluid, hexamethylene disiloxane. This methyl siloxane material differs from its polymeric homologues in that there are three methyl groups per silicon atom as compared with only two for the higher molecular weight compounds (hence, higher viscosity). This compound is apparently more closely related to the hydrocarbons in material structure than the higher molecular weight homologues, since addition of this fluid to flocculated oleic acid coated magnetite results in repertization and formation of a stable ferrofluid. The ferrofluid prepared in this manner can not be used in the program, because of the high volatility of this low boiling compound upon exposure to air at room temperature. There is a tendency for the ferrofluid to form a surface skin due to the evaporation of the carrier liquid.

C. EVALUATION OF FLUID VISCOSITY AND MAGNETIC PROPERTIES

The viscosity of each fluid listed in Table IX was measured. The viscosity measurements were performed in Fenske reverse flow capillary viscometers, which are especially suited for determinations on opaque liquids. These viscometers are bathed in a controlled constant temperature bath whose temperature can be varied over a wide range.

TABLE IX

LIST OF FLUIDS PREPARED FOR RAE PROGRAM BY GRINDING IN HYDROCARBON MEDIA

Primary Fluid Preparation							Modification Procedure	Properties Of Fluid Prepared			
Fluid No.	Preparative Grind No.	Carrier Fluid	Surfactant	Magnetic Powder (Magnetite)	Surfactant/ Magnetite Ratio (cc/gr)	Hours		Carrier Fluid	Saturation Magnetization	Density (gr/cm^3)	Kinematic Viscosity at 86°F (cst)
I	G15	Heptane	Oleic Acid	IRN 100	0.50	672	Evaporate to dryness, redisperse in decane	Decane	292	0.96	
II	G21	Kerosene	Oleic Acid	IRN 100	0.35	2726	Vacuum evaporate	Kerosene	602	1.482	37
III	G44	Kerosene	Tenlo 70	IRN 100	0.50	1475	No modification	Kerosene	212	0.953	2.45
IV	G44	Kerosene	Tenlo 70	IRN 100	0.50	1475	Vacuum evaporate, pass through 1.5 μ millipore filter	Kerosene	533	1.315	39.8
V	G40	Decane	Oleic acid	IRN 100	0.50	2000	Vacuum evaporate	Decane	538	1.345	55.6
VI	G40	Decane	Oleic acid	IRN 100	0.50	2000	Filter fluid VI with millipore 0.22 μ filter	Decane	518		
VII	G44	Kerosene	Tenlo 70	IRN 100	0.50	1475	Add L43 silicone fluid, remove kerosene by vacuum evaporation	L43 (90%), Kerosene (10%)	162	1.146	1100
VIII	G44	Kerosene	Tenlo 70	IRN 100	0.50	1475	Flocculate with ethanol, redisperse in D/C 200 0.65 cst fluid	D/C 200/0.65 Silicone	670	1.531	7.50
IX	G26	Kerosene	Oleic acid	Wright 4000	0.50	2629	Flocculate with ethanol, redisperse in alpha methyl naphthalene	Alpha methyl naphthalene	810		116
X	G26	Kerosene	Oleic acid	Wright 4000	0.50	2629	Dilution of fluid IX with alpha methyl naphthalene	Alpha methyl naphthalene	735	1.668	54.1

The saturation magnetization and density of the fluids were also measured, to obtain the volume concentration of solids in suspension. A search coil technique that employed a ballistic galvanometer in conjunction with a 10,000 gauss electromagnet was used to obtain the magnetization measurements. Density measurements were made by weighing calibrated pycnometers on an analytical chainomatic balance.

The results of the various measurements made are presented in Tables IX and X. Figure 18 also presents the viscosity of different alpha methyl naphthalene base ferrofluids as a function of magnetization and temperature. The variation of viscosity with temperature depends on the magnetic strength of the fluid (i.e., the solids concentration). The ratio of the kinematic viscosity at 70° F to the kinematic viscosity at 0° F versus magnetization is presented in Figure 19.

The magnetization curve (magnetization as a function of the applied field) for fluid X is presented in Figure 20.

TABLE X

VISCOSITY-TEMPERATURE CHARACTERISTICS OF ALPHA METHYL NAPHTHALENE BASE FERROFLUID

	Base Fluid	Fluid 1	Fluid 2
Room Temperature Magnetization M, in gauss, at H = 10,000 oersteds	0	735	810
Volume Fraction Magnetic solids $\epsilon_m = \frac{M}{5660}$	0	0.130	0.143
Experimental Kinematic Viscosity, centistokes at T = 0°C (32°F)	5.77	181	404
at T = 30°C (86°F)	2.62	54.1	116
at T = 70°C (158°F)	1.30	17.6	32.5
Kinematic viscosity at 0°F, cst (extrapolated), ν_o	9.3	400	950
Kinematic viscosity at 70°F, cst (interpolated), ν_{70}	3.3	79	167
ν_o / ν_{70}	2.8	5.1	5.7
Density at Room Temperature, gr/cm^3	1.0	1.668	1.734
Absolute Viscosity at 70°F, centipoise	3.3	131	290

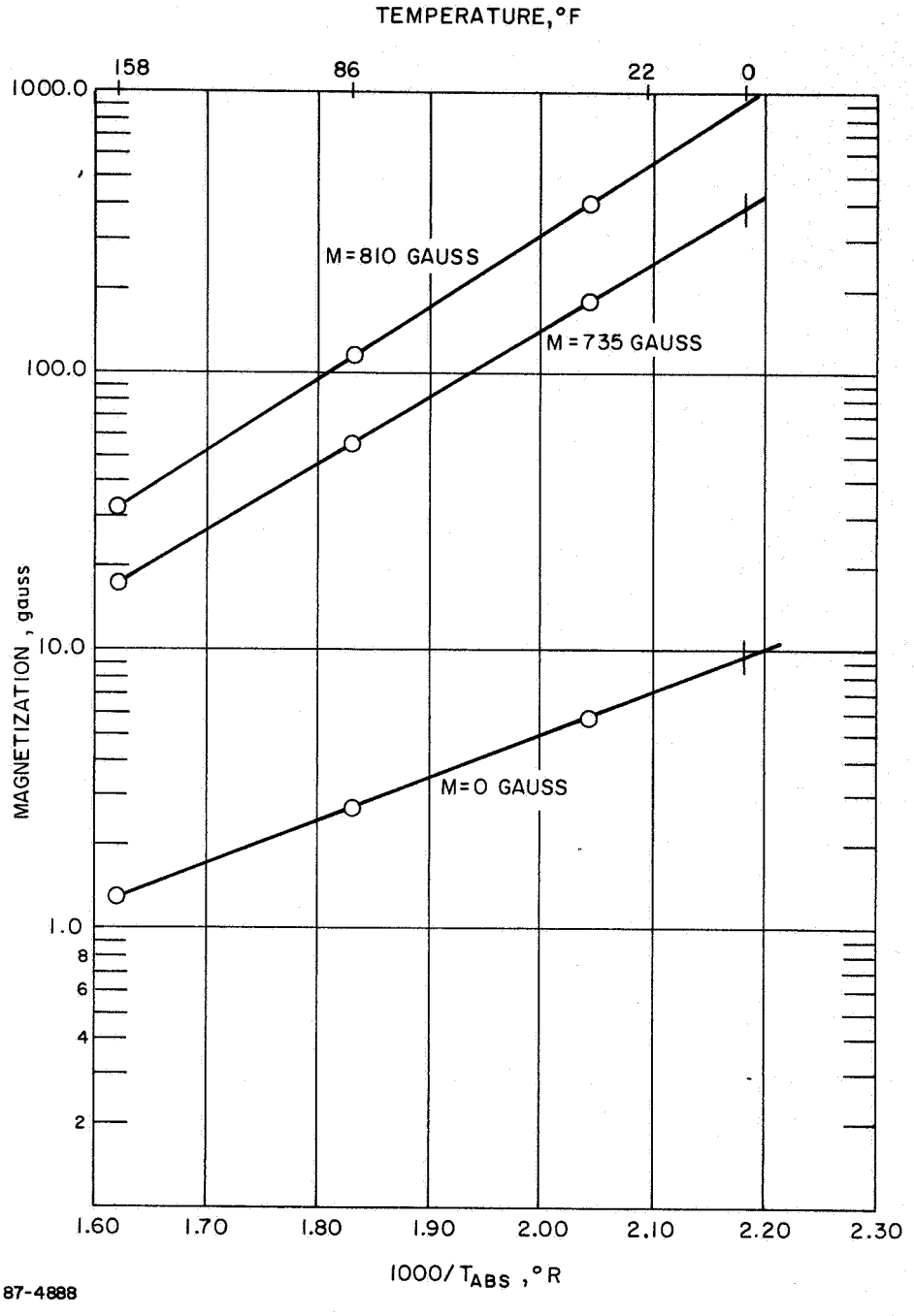

Figure 18 KINEMATIC VISCOSITY OF ALPHA METHYL NAPHTHALENE BASE FERROFLUIDS

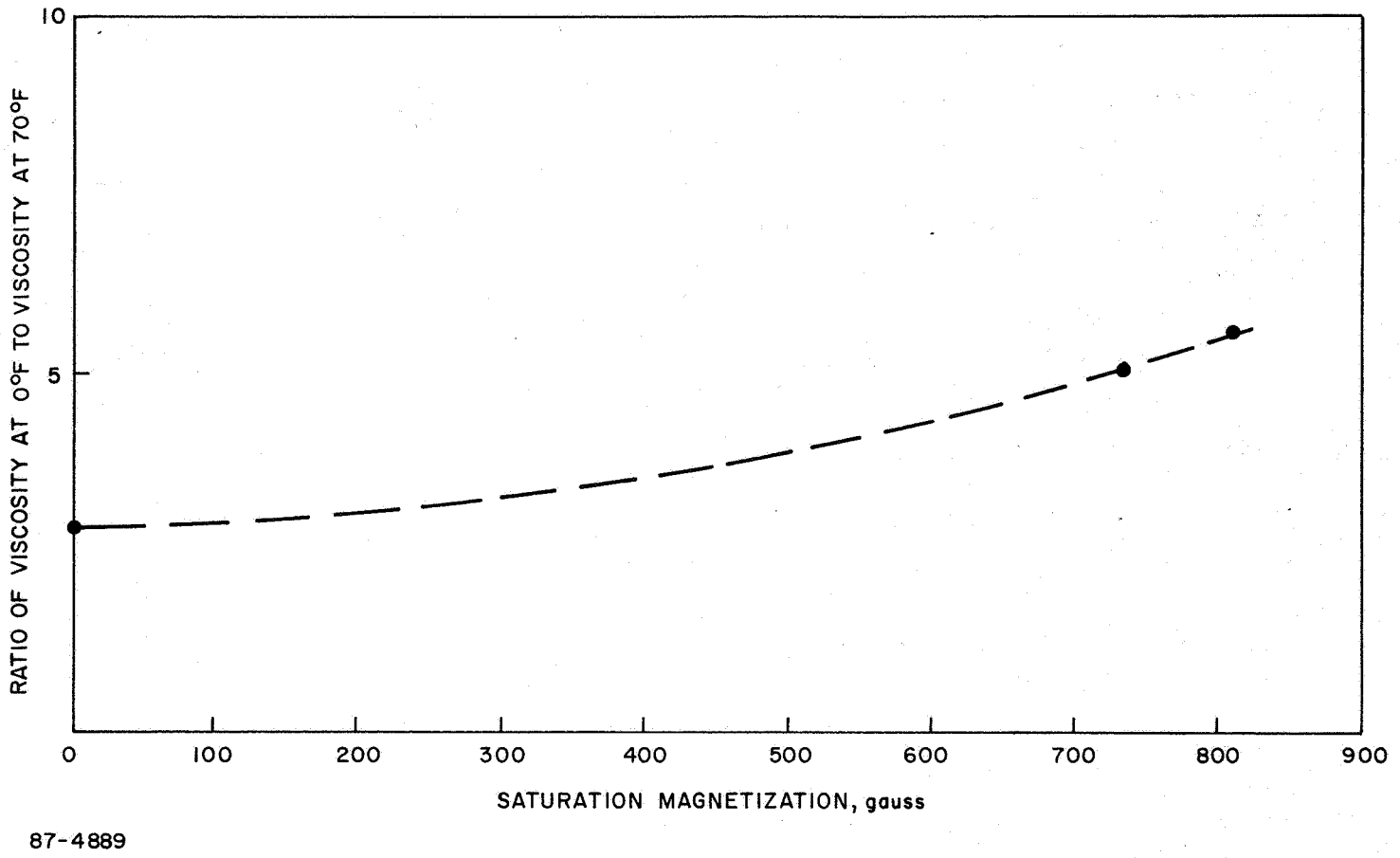

Figure 19 EFFECT OF MAGNETIC STRENGTH ON TEMPERATURE VARIATION OF VISCOSITY OF ALPHA METHYL NAPHTHALENE BASE FERROFLUID

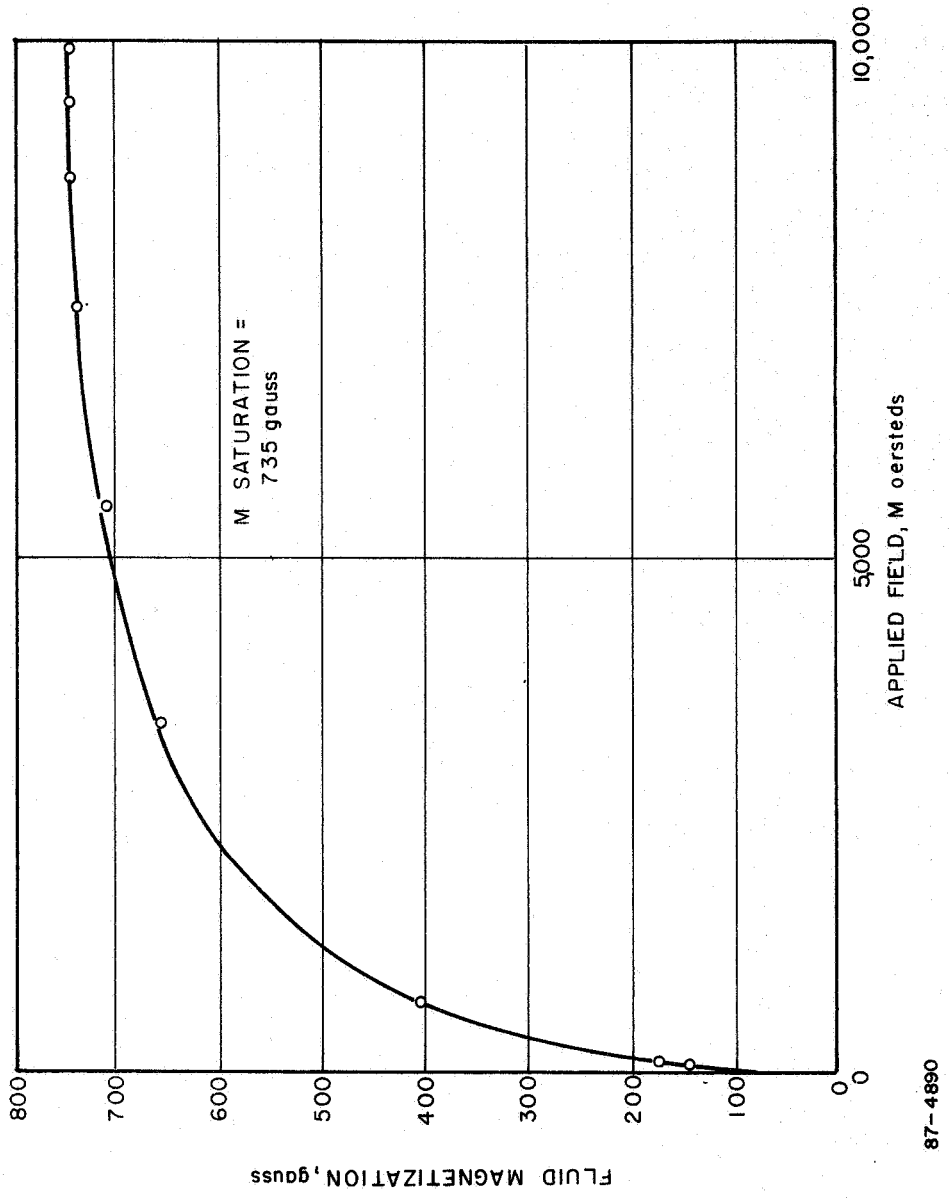

Figure 20 MAGNETIZATION CURVE OF FLUID X (ALPHA METHYL NAPHTHALENE BASE)

D. MAGNETIC FLUID REFERENCE DESIGN

Success in developing a damping mechanism that will provide necessary forces with low viscosity ferrofluid (see Section IV. A) has opened the full spectrum of low viscosity hydrocarbon ferrofluids to consideration for this application. Early difficulties in developing a silicone ferrofluid with high viscosity led to more forceful consideration of available hydrocarbon based materials for use with the vane orifice wide-angle magnet damper concept.

Alpha methyl naphthalene provides us with a material that has the basic characteristics necessary for the damper, including thermal-viscosity characteristics within necessary limits. Since a change in viscosity of 5 to 1 will provide good system performance over the design temperature range, the saturation magnetization level of the ferrofluid has been increased to 735 gauss to provide both the highest possible saturation magnetization and a viscosity change of 5 to 1. A fluid with this characteristic results in a small magnet size and weight.

Specific characteristics of the alpha methyl naphthalene developed are shown in Table XI. Forty cubic centimeters of this fluid was produced for experimentation and use in the final damper assembly.

TABLE XI

MAGNETIC FLUID REFERENCE DESIGN

I.	COMPOSITION	
	Carrier: Alpha methyl naphthalene	
	Magnetic Solid: Wright 4000 Magnetite	
	Stabilizing Agent: Oleic Acid	
	Magnetic Solids Concentration: 13% by Volume	
	Stabilizing Agent Concentration: 32% by Volume	
II.	VISCOSITY	
	At 70° F	79 Centistokes
	At 0° F	400 Centistokes
III.	MAGNETIZATION (At 10, 000 oersteds)	735 gauss
IV.	SPECIFIC GRAVITY	1.668 gm/cm^2

E. REFERENCE DESIGN EVALUATION

1. Thermal Stability

The operational temperature range of a ferrofluid is limited by the pour point or freezing point of the carrier at low temperatures and by either

a. The boiling point of the carrier liquid at system pressure.

b. The temperature at which significant desorption of the stabilizing agent occurs, due to either increased thermal motion or a reversal of the reaction holding the surfactant molecule to the particle surface. This action results in destruction of the stabilizing sheath around the individual particles, with ensuing flocculation at high temperatures.

The thermal requirements placed on the fluid were that it would be operational from 0°F to 70°F and that it could survive exposure to temperatures as low as -60°F and as high as +160°F.

Thermodynamic criteria placed on the carrier fluid as a result were the following:

a. Freezing or pour point to be at least - 20°F, or 20°F below the lower limit of the operational range.

b. Freezing of fluid not to result in an irreversible change in the properties of the ferrofluid.

c. Vapor pressure to be less than 1 mm Hg absolute at 60°C (140°F), to minimize fluid losses by evaporation during handling.

As evidenced in Table V, alpha methyl naphthalene meets these criteria.

a. High Temperature Stability

Thermal stability tests were carried out by heating samples of the alpha methyl naphthalene ferrofluid to a given temperature for a predetermined period. The samples were then examined for signs of deterioration.

A 2 cc sample of ferrofluid was placed in a standard 15 X 180 mm test tube. A water cooled cold finger condenser was inserted into the throat of the test tube to prevent loss of carrier fluid by evaporation. The test tube was heated in a constant temperature bath whose temperature could be controlled to within 1°C. By using Dow Corning 710 Silicone Fluid as the heat transfer medium, the bath could be operated from room temperature to over 400°F.

A first sample of the alpha methyl naphthalene fluid was subjected to the heating cycle described in Table XII. If there were no observable changes in the properties of the fluid after exposure to temperature, the temperature was then increased in an 18° F increment to the next level. If there were observable changes, the test was stopped. No noticeable changes in texture, apparent fluidity, or response to magnetic fields were observed in the first sample until it was exposed to a temperature of 320° F for 24 hours. The material gelled in this period and there was noticeable loss of fluid. The solids did not redisperse spontaneously when fresh carrier fluid (alpha methyl naphthalene) was added, indicating that an irreversible change in structure had occurred.

A second sample without a previous heating history survived heating to 320° F for 48 hours but thickened and gelled after 64 hours of further exposure at 338° F. A third sample gelled after 64 hours of exposure at 338° F alone.

TABLE XII

TEMPERATURE STABILITY OF ALPHA METHYL NAPHTHALENE BASE FERROFLUID

(M = 735 gauss)

Sample No.	Temperature (°F)	Time at Temperature (hr)	Cumulative Heating Time (hr)	Appearance of Fluid
I	194	72	72	No change
	212	24	96	No change
	230	24	120	No change
	248	24	144	No change
	266	96	240	No change
	284	24	264	No change
	302	24	278	No change
	320	24	312	Gelled
II	320	48	48	No change
	338	64	112	Thickened and gelled
III	338	64	64	Thickened and gelled

Flocculation can be considered to occur when the surface concentration of surfactant falls below a minimum value needed to form a stabilizing sheath. The decrease in sol stability with increasing temperature is believed to be due to desorption of the surfactant with increasing temperature, because of increased thermal motion or a reversal of the reaction holding the stabilizing agent to the particle surface. Increasing the concentration of the surfactant in the system tends to result in higher temperature stability, because a higher temperature is needed to decrease the surfactant concentration at the particle surface to below the minimum value needed to form a sheath.

It was observed that it is possible to heat a fluid to a given temperature for a short time without flocculation, whereas prolonged heating at the same temperature will cause flocculation. This is due to the fact that absorption and desorption processes occur at a finite rate. In a short time, insufficient amounts of surfactant desorb to result in flocculation, but this would occur if the system were allowed to reach equilibrium conditions.

These results indicate that the alpha methyl napthalene ferrofluid should not be adversely affected by exposure to a temperature of 160° F. The results also indicate that these ferrofluids would not be decomposed by prolonged exposure to the presence of much higher temperatures, as high as 300° F, as long as precautions were taken to prevent carrier loss by evaporation. This upper limit is 20° F below the minimum temperature at which decomposition was noted.

b. Low Temperature Stability

The effect of very low temperatures on the stability of the fluid is also of interest, since the fluid has to survive exposure to -60° F.

A 15 x 180 mm test tube containing 2 cc of the alpha methyl naphthalene fluid was introduced in a bath of liquid nitrogen for a period of 1 hour. The contents of the tube were solid upon removal from the bath. The sample was examined after it had reached room temperature. There was no apparent change in the properties of the fluid. As the boiling point of liquid nitrogen is -321° F at 1 atmosphere, the sample was exposed to much more severe conditions than the -60° F required.

2. Radiation Effects on Ferromagnetic Fluid

The ferromagnetic liquid consists of three components:

a. Solid particles of magnetic iron oxide, Fe_3O_4.

b. A carrier fluid such as an aliphatic hydrocarbon, e.g., kerosene; a silicone fluid, e.g., dimethyl siloxane; or an aromatic hydrocarbon, e.g., alpha-methyl napthalene.

c. A dispersing agent or surfactant which is physically similar to the carrier fluid, but in addition contains one or more polar functional groups.

Possible effects of radiation on the ferromagnetic liquid include the following:

a. Change of magnetic property of the subdomain particles.

b. Desorption of dispersant from the particle surface, resulting in agglomeration and flocculation. This could conceivably occur through radiation damage to the polar adsorbing group or through a scission of the long chain of the adsorbent species--producing a shorter species, which generally is not as well adsorbed.

c. Polymerization of coated particles, one to the other, because of reaction linkages between the adsorbed layers.

d. Change of viscosity of the ferromagnetic liquid due to a change in the carrier fluid property. This would be harmful because of the direct influence on the damping coefficient of the viscous damper.

Other effects could be postulated as well, but here it is considered that only item d above is the predominant damage mechanism. The crucial check, of course, is testing by experimental irradiation, but this was outside the scope of the program.

The main object of the following is simply to show that negligible viscosity change (item d) is anticipated under the orbital dosage levels of the RAE satellite.

The anticipated dosage is 1.8×10^5 rads (air) of total accumulative radiation.* A rad (or radiation absorbed dose) is such that one rad is required to deposit 100 ergs/gm in any material by any kind of radiation.

As order of magnitude figures, the maximum proton flux (E> 40 Mev) of geocentric space occurs at an altitude of 2000 nautical miles and to latitude of 0-degree; it is 2×10^4 protons/cm^2-sec. At 500 nautical miles, taken as representative of the RAE orbital altitude, the flux is 10^2 protons/cm^2-sec. The worst electron flux (E> 500 Kev), also at a latitude of 0 degrees, is 2×10^8 electrons/cm^2-sec and occurs at altitudes of 5000 and 7000 nautical miles. At 500 nautical miles, the flux is 5×10^4 electrons/cm^2-sec.

*Molloy, K. H., NASA/Goddard Viscous Damper Spec. GCCD-W320-134A, 19 July 1966.

The effect of radiation on the viscosities of various fluids is given in Table XIII.[7]

TABLE XIII

EFFECT OF RADIATION ON THE VISCOSITIES OF VARIOUS FLUIDS
(3 MEV VAN DE GRAAFF GENERATOR)

	Percent Viscosity Increase at 210°F	
Fluid	Dose = 100 megarads	1000 megarads
Aliphatic Hydrocarbon (kersosene)	10	200
Polyphenyl Ethers	5	35
Methyl Phenyl Silicone	3	> 1000

Clearly there is negligible viscosity change due to radiation damage at the less than a megarad dosage specified for the RAE satellite. This is further substantiated by the data of Table XIV, taken from p. 308 of Reference 7.

TABLE XIV

GAMMA RADIATION DOSE REQUIRED TO GEL LINEAR DIMETHYL SILICONE FLUIDS
(COBALT 60 IRRADIATION AT 0.3 mr/hr, 77° F)

Viscosity Before Irradiation	Radiation Dose
1 centistoke	> 1000 megarads
10	300
100	60
1000	20
10, 000	7
100, 000	5

Here it is seen that for one class of fluid carrier, the radiation dosage required to render the material completely useless (as it would be as a gel) is far in excess of the less than a megarad dosage that is anticipated.

The above data are in accord with the general statement of Gunderson and Hart who, summarizing extensive Air Force studies of the early 1950's, find that all mineral and synthetic-based oils are reasonable stable up to

10^7 roentgens of dosage by gamma radiation, but suffer appreciable degradation at 10^8 roentgens. Since a roentgen is defined as 93 ergs per gram of water, or 83 ergs per gram of air, the stability threshold of 10^7 roentgens corresponds to about 10 megarads.

IV. DAMPER ASSEMBLY ENGINEERING STUDIES

A. DAMPING MECHANISM

The damping mechanism consists of a hollow vane partially filled with ferrofluid and a magnet assembly, as shown in Figure 1. Studies of the damping mechanism are discussed in two sections below. The first section describes and evaluates several damping concepts which have been considered and the damping concept selected for the RAE satellite application. The second section describes and evaluates the various magnetic systems which have been considered and then the reference magnetic system selected.

1. Damping Concepts

Viscous damping occurs in the ferrofluid damper when ferrofluid is forced to move with respect to any fixed surface. The ferrofluid is enclosed in a hermitically sealed vane and is captured in a magnetic field between two permanent magnet pole faces, as shown in Figure 1. As the magnet is moved with respect to the vane, the ferrofluid will also move with the magnet, causing relative motion between the ferrofluid and the vane. It is this motion of the ferrofluid with respect to the fixed vane that causes fluid shear and the resulting generation of viscous damping forces.

Several concepts for achieving viscous damping with ferrofluid coupling are discussed below. A configuration of the vane and magnet is considered for each concept.

a. Constant Area Vane

The simplest ferrofluid viscous damping concept to mechanize is one using a constant area ferrofluid cavity and a narrow-angle magnet. (See Figure 21.) Viscous shear forces are developed between the ferrofluid and the vane walls as the body of the fluid is forced to follow the motion of the magnet.

If a magnetic fluid with a maximum magnetic moment of 700 gauss and a magnet with a maximum field strength of 1500 oersteds and a minimum useful strength of 500 oersteds are assumed, the magnetic pressure P_M on the ferrofluid is

$$P_M = \frac{K_1}{4\pi} \int_{1500}^{500} MdH = 0.53 \ lb/in.^2 \qquad (7)$$

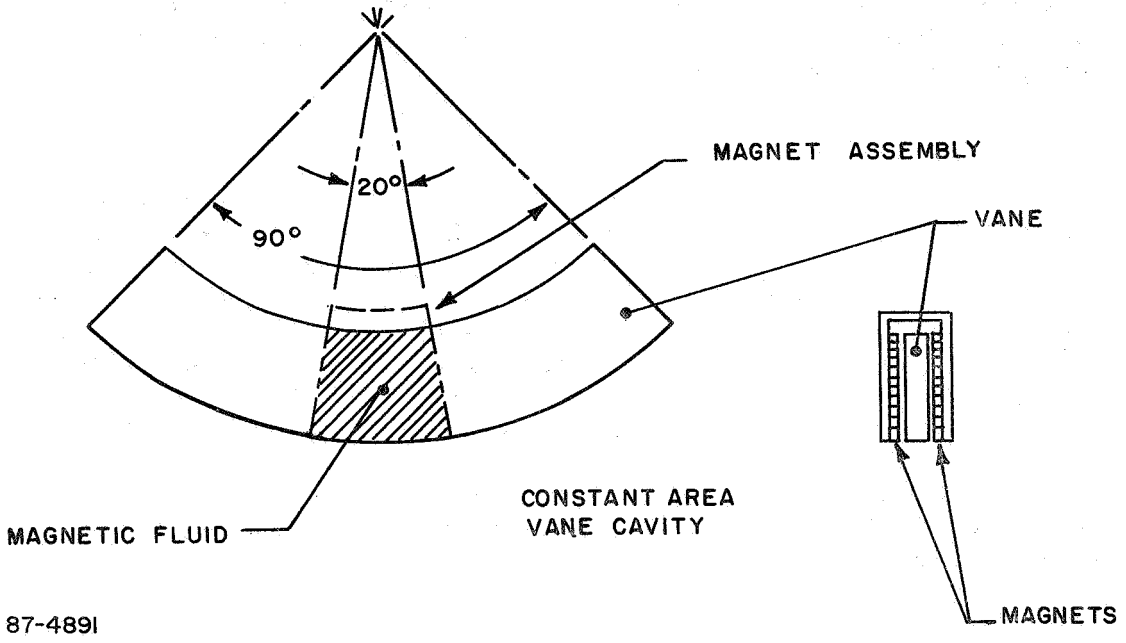

Figure 21 DAMPING CONCEPT: CONSTANT AREA VANE

where

M = ferrofluid magnetic moment, in gauss

dH = rate of change field strength in oersteds

K_1 = unit conversion = 1.46×10^{-5}

Therefore, the fluid cross sectional area is

$$A_V = F/P_m = 0.091 \text{ in.}^2 \quad (8)$$

where F = required magnetic force = 0.048 pound.

(Note: The damper must provide a viscous torque of 0.007 ft-lb to satisfy peak combinations of angular velocity and damping coefficient. The magnetic system is designed to operate with a safety factor of 2, providing 0.014 ft-lb of magnetic torque. These values are used in the following paragraphs, along with a mean damping vane radius of 3.5 inches, to establish typical damping mechanism parameters.)

The radial dimension of the vane cavity has been limited to 2 inches by overall size requirements. Thus, the normal dimension of the cavity must be at least 0.046 inch if equation 8 is to apply. The fluid viscosity required with this size cavity is approximately 5×10^5 centipoise. Ferrofluids with necessary thermal compensation are not available in this viscosity range.

Another alternative which might be considered, in order to reduce the fluid viscosity to an allowable level, is dividing the normal dimension of the cavity by a series of baffles parallel to the magnet pole faces. At best this approach will reduce the required viscosity by a factor of 10, which is still far from acceptable.

One attractive aspect of the constant area vane concept is the size and weight of the magnet assembly required. The magnetic force equation defining the forces developed on the fluid contains no factor regulating the dimension of the magnet in the direction of magnet motion. This magnet dimension is limited only by the shear area required, and shear area, in turn, is limited only by ferrofluid viscosity. Given a high enough fluid viscosity, the magnet assembly dimension in the direction of motion (width) may be as small as is practically feasible. Magnet widths of less than 1 inch are readily conceivable.

A problem can arise in trying to predict the damping ratio for a constant area vane, because of the possibility of fluid circulation in cells within the vane area. Analysis of this problem is covered in Section IV.D.2.C.

The problem can arise if the fluid length in the direction of motion is less than the fluid radial dimension. This problem places a minimum bound on magnet and fluid dimension in the direction of motion.

Although the constant area vane concept has considerable merit and would probably result in the lowest weight configuration, it depends on a high viscosity, thermally compensated ferrofluid which is not yet available, and hence this approach cannot be used at the present time.

b. Vane/Orifice/Wide-Angle Magnet

The simplest way to multiply the viscous forces in a fluid having a predetermined flow rate is to provide a restriction in the path of the flow in the form of a baffle with a circular orifice (see Figure 22). An orifice with reasonable diameter (0.014 inch or larger) and reasonable length (0.1 inch or longer) can multiply the viscous forces by factors as large as 1 million to 1 or more. The characteristics of flow through an orifice are well known, and as long as the Reynolds Number is kept small, laminar flow will result and the viscous forces can be readily predicted.

The only other physical change required to go from the constant area concept to the vane orifice wide-angle magnet concept is the width of the magnet. Since the ferrofluid moves with the magnet, and the magnet rotates through an arc of ± 35 degrees, the magnet width must be at least 70 degrees to keep the ferrofluid body in contact with the orifice at all magnet angular displacements.

The problem then resolves itself to one of determining the combination of magnet and vane parameters which yields a reasonable structure and has minimum weight. This is done in detail in later paragraphs.

Since the magnetic and viscous forces are identical for all concepts, the cross sectional area of fluid required is also identical. As shown in Equation 8, $A_V = 0.091$ in.^{2}. In this concept there is effectively no viscous shear in the large cavity; essentially all of it takes place in the orifice. The equation for the viscous torque developed across the orifice is derived in Section IV.D.2.d. It is restated and used here to illustrate the method of determining the orifice diameter and baffle length.

The viscous torque is:

$$T = \frac{128\ V_V\ \mu\ LA^2\ R}{\pi\ D^4} \qquad (9)$$

where

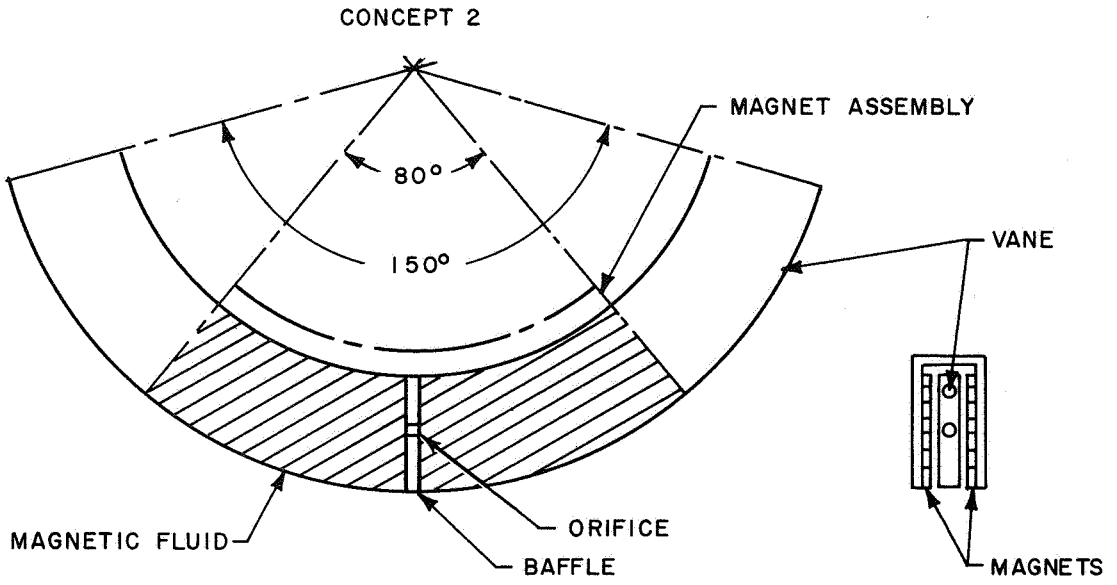

Figure 22 DAMPING CONCEPT: VANE/ORIFICE/WIDE-ANGLE MAGNET

V_V = vane linear velocity at $R = W_V \cdot R$

R = mean vane radius from pivot to cavity centerline

μ = ferrofluid viscosity

L = orifice length

A = cavity cross sectional area

D = orifice diameter

For $T = 0.007$ ft-lb, $\mu = 100$ cp $= 1.46 \times 10^{-5} \frac{lb - sec}{in.^2}$ (10)

$R = 3.5$ in., $A_V = 0.091$ in.^{2}, $W_V = 1.8 \times 10^{-3}$ rad/sec (11)

$$\frac{D^4}{L} = \frac{128 \times 1.8 \times 10^{-3} \times (0.091)^2 \; 1.46 \times 10^{-5} \; (3.5)^2}{\pi \, (0.007) \; 0.024} \quad (12)$$

$$\frac{D^4}{L} = 1.28 \times 10^{-6} \quad (13)$$

For $L = 0.2$ in., $D^4 = 25.6 \times 10^8$ in.^{4} (14)

$D = 0.0225$ inch (15)

This is a reasonable combination of orifice diameter and baffle length.

The vane orifice wide-angle magnet concept showed excellent promise for providing necessary damper performance with low viscosity ferrofluid early in the program. Hence, laboratory experiments were conducted to establish design parameters.

An experimental study of damper performance has been carried out for the vane/orifice/wide-angle magnet concept. Two ferrofluids, one with a magnetic moment of 602 gauss and a viscosity of 57 centipoise, and one with a magnetic moment of 422 gauss and a viscosity of 18 centipoise, have been used with magnet assemblies having field strengths of 1000 and 1400 oersteds. The magnets are mounted rigidly to a test fixture, as shown in Figure 23. The test vane is mounted to a shaft supported by bearings. The shaft is driven by a series of pulleys which allow constant torque to be applied to it in either the clockwise or the counterclockwise direction. The test vane consists of a circular aluminum plate with an annular groove cut in it. The groove is covered by a clear plastic cover so that fluid motions can be monitored.

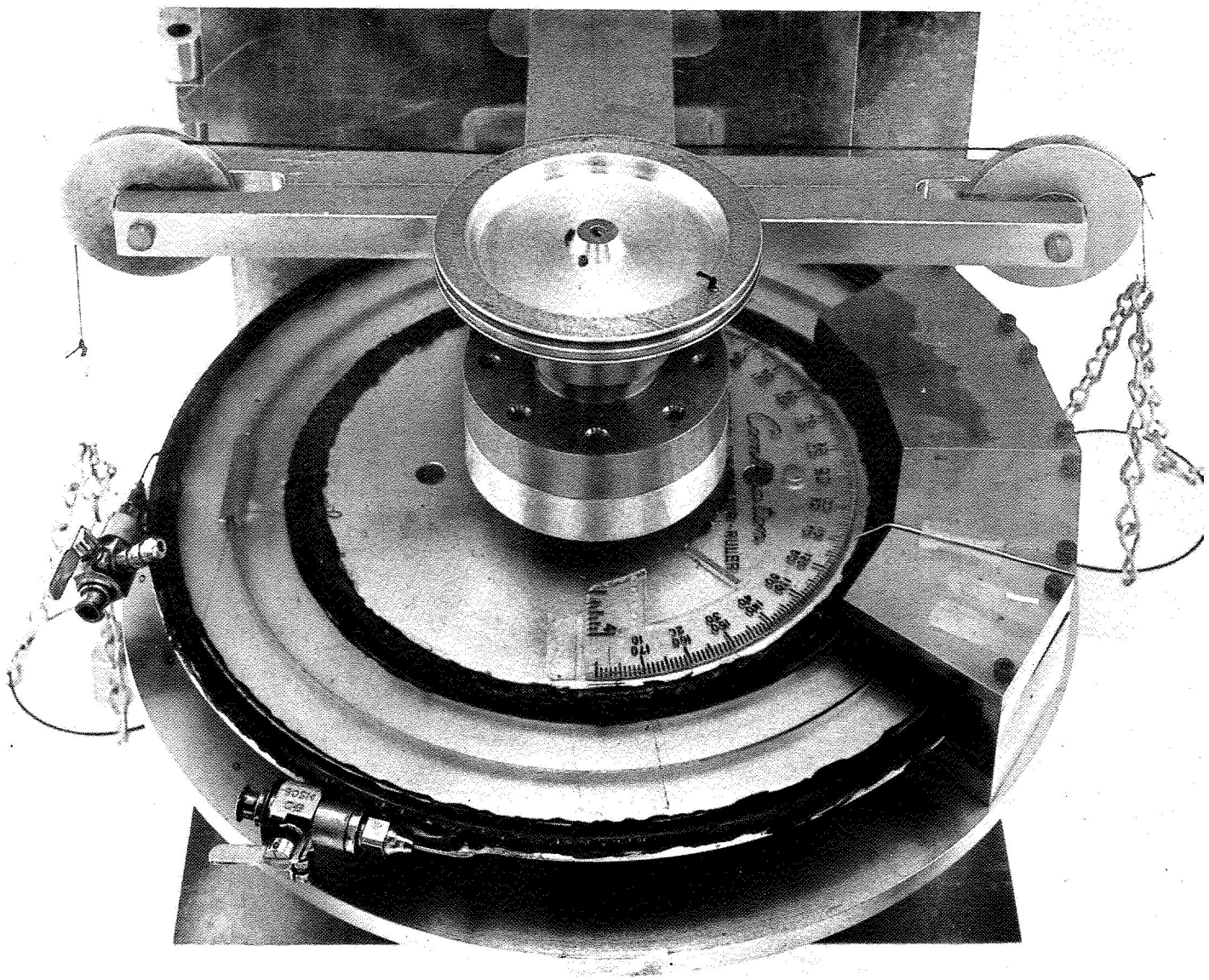

15758A

Figure 23 DAMPING TEST FIXTURE: VANE/ORIFICE/WIDE-ANGLE MAGNET

A baffle having a small hole at its center is placed in the cavity to form the orifice.

Two types of tests have been performed:

1) Damping tests -- to determine the damping coefficient as a function of angle for various applied torques and various test parameters.

2) Magnetic restraint tests -- to determine the vane offset as a function of applied torque.

The results of the damping tests are summarized in Table XV. They show that with ferrofluid filling a vane area which just covers the magnet width, the theoretical and experimental damping coefficients agree to within better than 20 percent in all cases. These cases include two fluid viscosities, two orifice diameters, and several torque loads with either vacuum or atmospheric pressure in the vane. Typical test results are shown in Figures 24a and 24b.

In these tests the damping coefficient is measured every 5 degrees of vane travel, by measuring the time required to travel through that angle. The damping coefficient is computed as follows:

$$C_D = K_2 \frac{\Delta T}{\Delta \theta} \tag{16}$$

where

K_2 = torque applied

ΔT = time elapsed

$\Delta \theta$ = angle covered

From this data it can be concluded that experimental and theoretical results are in good agreement.

Analysis of the data, as a function of the volume of ferrofluid used, points out another conclusion that can be drawn. Figure 25 shows that the damping coefficient is a linear function of the percentage of magnet area covered by the fluid. This result remains unexplained at the present time. Since the volume of fluid used can be controlled quite accurately, the dependence of damping ratio on fluid volume can be ignored in the RAE damper application.

The second type of test, the magnetic restraint test, measures the vane angular displacement for a step torque input. This test is useful

TABLE XV

DAMPING TEST SUMMARY

Test Date	Fluid Viscosity (cp)	Fluid Magnetic Moment (gauss)	Magnet Flux Density (gauss)	Baffle Diameter (in.)	Calculated Damping Ratio (ft-lb-sec)	Measured Damping Ratio (ft-lb-sec)	Vane Area (in.^{2})	Comments
1/7	57	602	1000	0.016	21.4	24.1	0.138	4 tests, 80° fluid; 3 at 0.0051 ft-lb; 1 at 0.0064 ft-lb; 3-4° lag max
1/9	57	602	1000	0.016	21.4	22.5	0.138	2 tests, 80° fluid
1/14	18	422	1400	0.016	6.75	7.8	0.138	84° of fluid, 3 tests at 0.0051 ft-lb; 1 test at 0.0026 ft-lb
1/14	18	422	1400	0.016	6.75	6.2	0.138	78° of fluid, 1 test at 0.0051 ft-lb
1/16	18	422	1400	0.016	6.75	5.1	0.138	70° fluid, 3 tests at 0.0051 ft-lb
1/17	18	422	1400	0.016	6.75	6.7	0.138	80° of fluid, 4 tests at 0.0051 ft-lb
1/17	18	422	1400	0.016	6.75	4.3	0.138	70° of fluid, 4 tests at 0.0051 ft-lb; 2 tests at 0.0026 ft-lb
1/19	18	422	1400	0.022			0.128	80° fluid, new vane; cover area vane: 0.128; 3 tests at 0.005 ft-lb. 3 tests at 0.0026 ft-lb
	18	422	1400	0.022	1.67	1.76		
	18	422	1400	0.022	1.67	1.57		
1/27	18	422	1400	0.016	5.8	6.3	0.128	83° fluid, degassed 1 test, 0.0051 ft-lb
1/27	18	422	1400	0.016	5.8	4.9	0.128	Vane evacuated to 1 mm mercury; 5 runs at 0.0051 ft-lb
1/27	18	422	1400	0.016	5.8	4.6		Atmospheric pressure 1 run
1/27	18	422	1400	0.16	5.8	3.95		Vane evacuated 2 runs
2/1	18	422	1400	0.16	5.8	3.1		Fluid degassed, vane evacuated, 6 runs at 0.0051 ft-lb
2/1	18	422	1400	0.16	5.8	2.8		Vane opened to atmosphere, 2 runs 0.0051 ft-lb approximately 70° fill

in determining the spring constant and the maximum torque capability of the magnetic system. Typical values of spring constant versus load are given in Table XVI, in terms of ratios of spring constant with maximum torque and spring constant at 1/4 maximum torque as the normalizing factors. A typical magnetic spring constant of 0.3 ft-lb/rad can be achieved with torques less than one half the peak magnetic torque. When the peak magnetic torque is exceeded, the fluid no longer moves with the magnet, and damping ceases. The damper is able to recover if lower torques or velocities occur after breakaway. The fluid regathers under the magnet as the magnet moves by it, and normal damping is restored.

TABLE XVI

MAGNETIC SPRING CONSTANT

Torque Ratio (ft-lb/ft-lb max)	Spring Constant Ratio (ft-lb/rad) (ft-lb/rad at 1/4 max torque)
.25	1
.50	.8
.75.	.5
.90	.1

c. Vane/Orifice/Two Narrow-Angle Magnets

Since the major objection to the vane/orifice/wide-angle magnet concept is the weight of the wide magnets, and since magnet length does not determine magnetic force, another damping concept has been considered. The wide-angle magnet is replaced by two narrow-angle magnets whose outer edges cover the same angle as the wide magnet. The vane with baffle and orifice is kept the same. (See Figure 26.)

This concept has a basic flaw. Both magnets attempt to center the magnet fluid symmetrically about their own center line. The only force holding the fluid together is fluid surface tension. Any cavitation of the fluid causes further cavitation. The fluid eventually breaks up into two segments. Fluid flow through the orifice is erratic and may cease entirely when the baffle is midway between the magnets.

Simple tests of this concept show that cavitation occurs almost immediately and satisfactory results cannot be obtained. The concept has been discarded as unworkable.

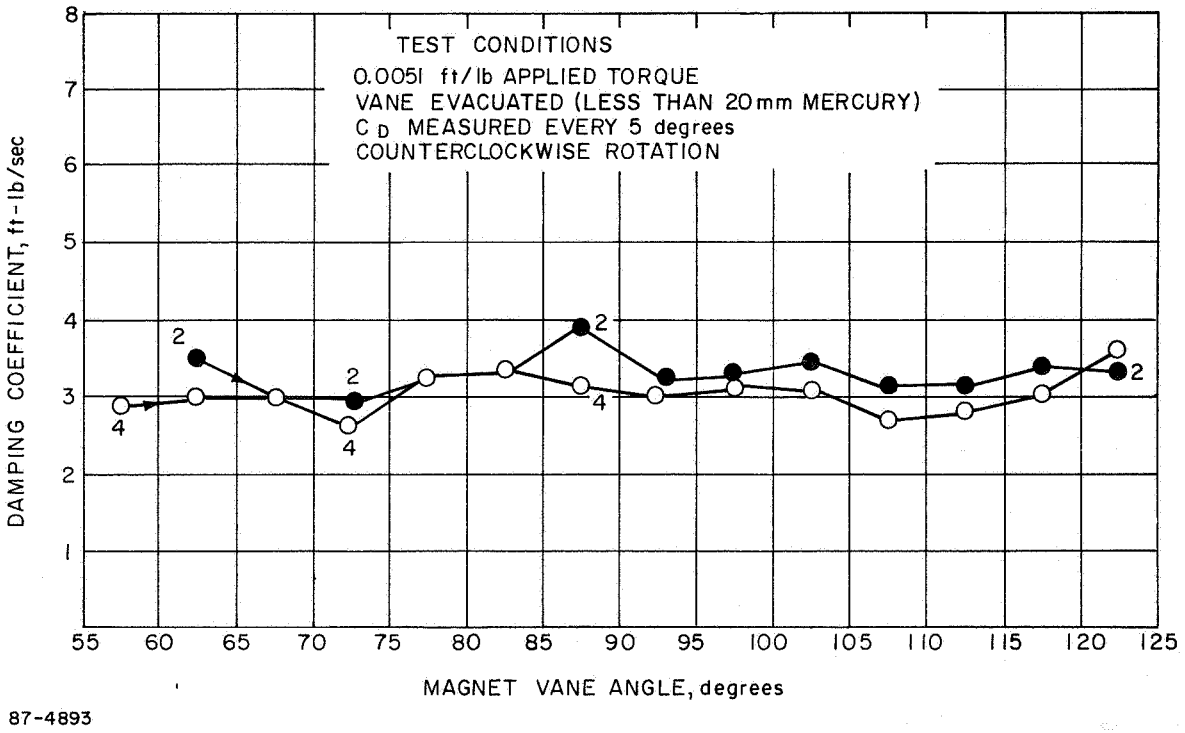

Figure 24a DAMPING TEST No. 1

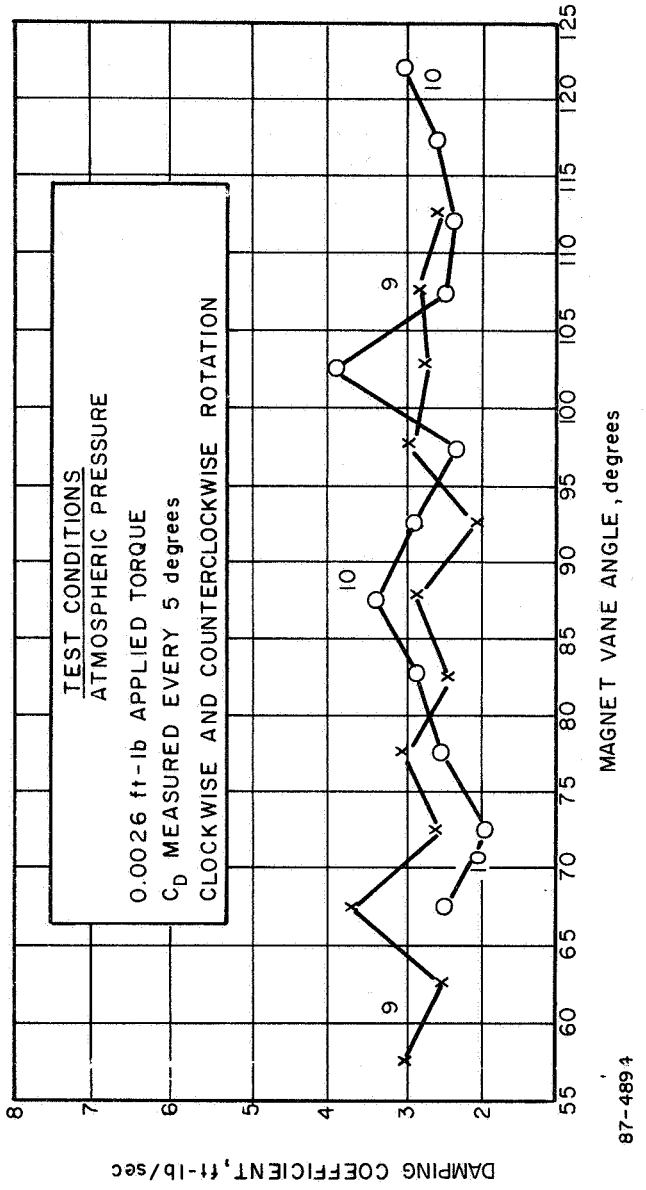

Figure 24b DAMPING TEST NO. 2

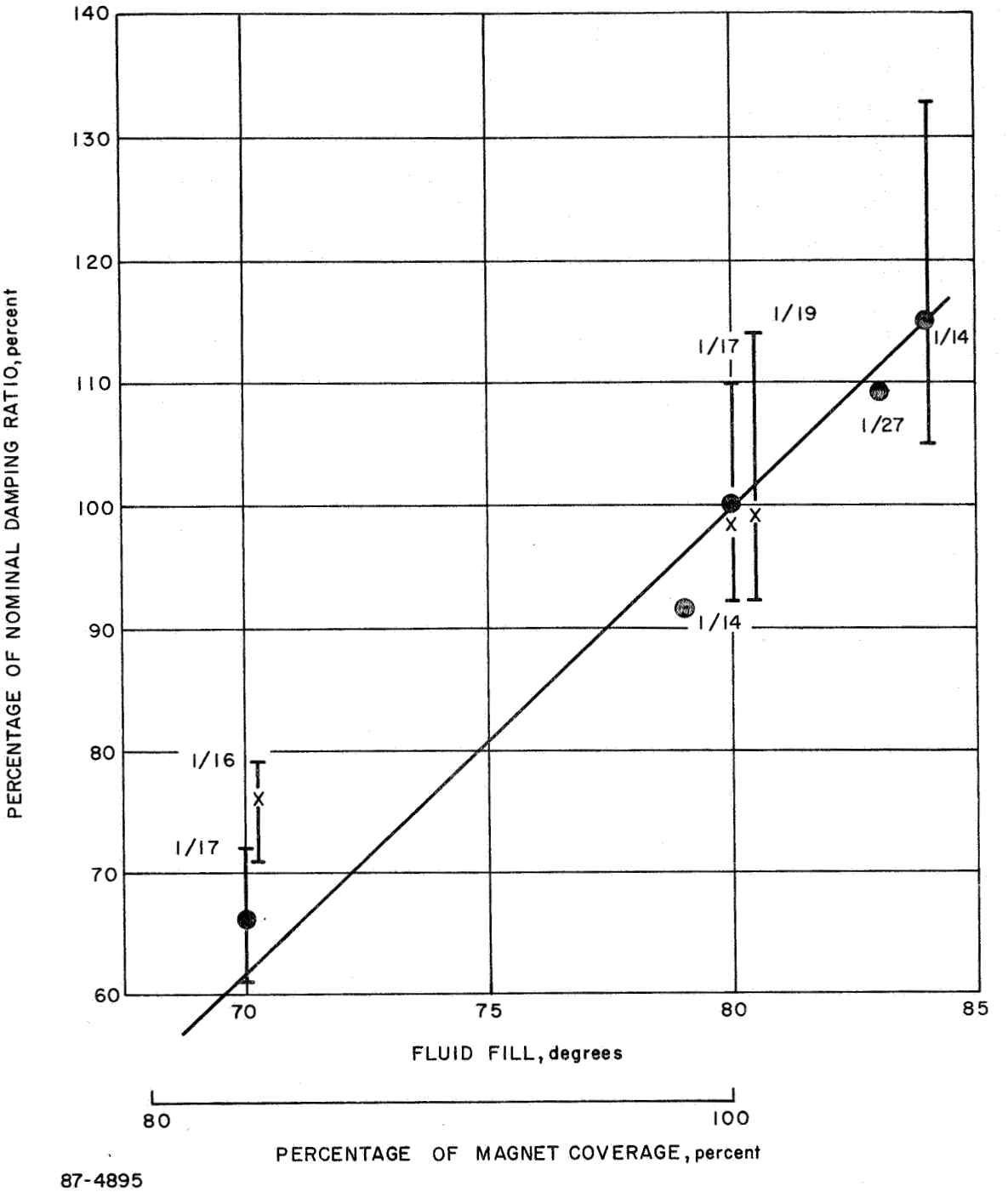

Figure 25 PERCENT OF DAMPING RATIO VERSUS FLUID FILL

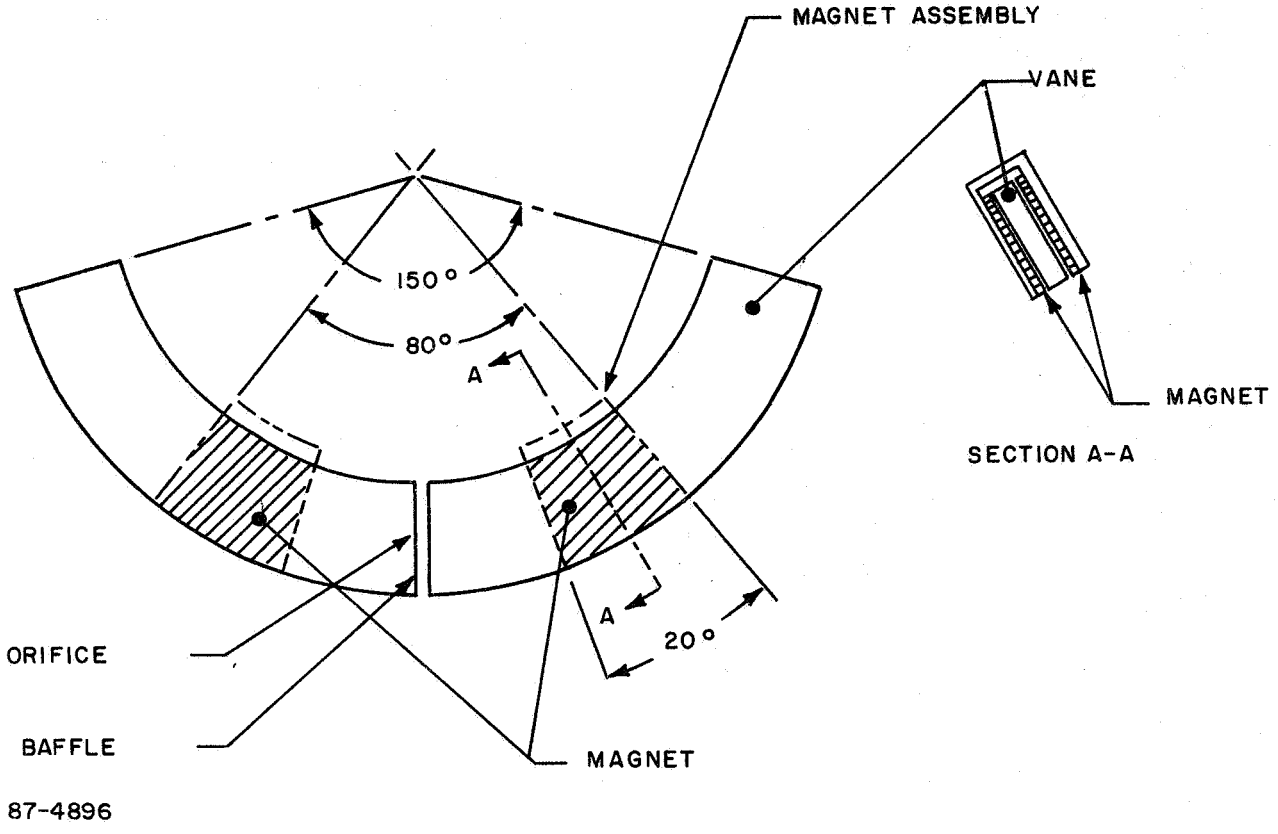

Figure 26 DAMPING CONCEPT: VANE/ORIFICE/TWO NARROW-ANGLE MAGNETS

d. Porous Bed Vane

In place of a single, moderate sized orifice, a packed bed of solid particles provides many orifices of small size and a tortuous path to impede fluid flow. (See Figure 27.) Viscous damping of the required magnitude can be achieved by developing a pressure drop across a short bed length of constant diameter particles. This concept has the additional advantage that more than one magnet can be used to multiply the magnetic force. This is possible because there is a continuous bed of solids through which each magnet sweeps its own body of fluid. The major disadvantages of the concept are as follows:

1) The solids occupy from 50 to 75 percent of the vane volume, requiring either a larger vane area or 2 to 4 times the number of magnets of the same length and field strength as the other concepts.

2) Surface tension forces increase with decreasing particle size. A counter pressure drop is developed which is proportional to fluid surface tension and inversely proportional to particle diameter. This counter pressure tends to keep a portion of the fluid attached to the particles and decreases the effective orifice diameter.

The concept appeared to be promising enough that tests were performed using spherical glass beads to form the packed bed of solids. (See Figure 28.)

The tests were performed in the test fixture shown in Figure 29. The damper vane shown there contains 0.006 inch diameter beads in one half of the experimental vane cavity, and 0.020 inch beads in the other half. Qualitatively, the tests indicate that this method of damping is feasible.

A major disadvantage of using loose glass beads and packing them into the vane is that it is impossible to achieve constant porosity of the proper magnitude. There are several ways available to overcome this difficulty. One is to sinter the glass beads into a porous solid. A sample of sintered glass beads is shown in Figure 30.

Other materials are available which have properties similar to those obtained with sintered glass beads. Various ceramic materials, and also aluminum oxide, can be obtained with a range of porosities. A sample of porous aluminum oxide is shown in Figure 31.

Several other materials were considered for this application. They include metal felt and material cast over rock salt having known dimensions. The rock salt is washed out, leaving a solid with known porosity. Samples of this material are shown in Figure 32.

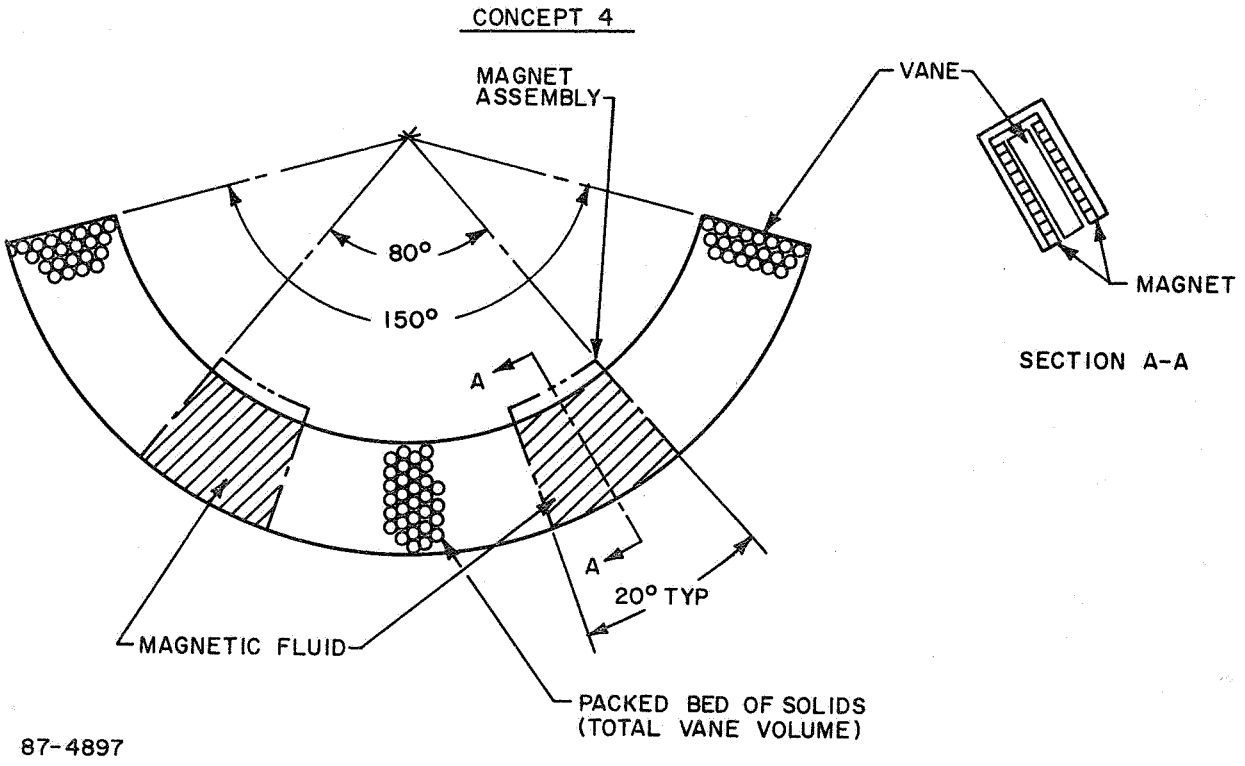

Figure 27 DAMPING CONCEPT: POROUS BED VANE

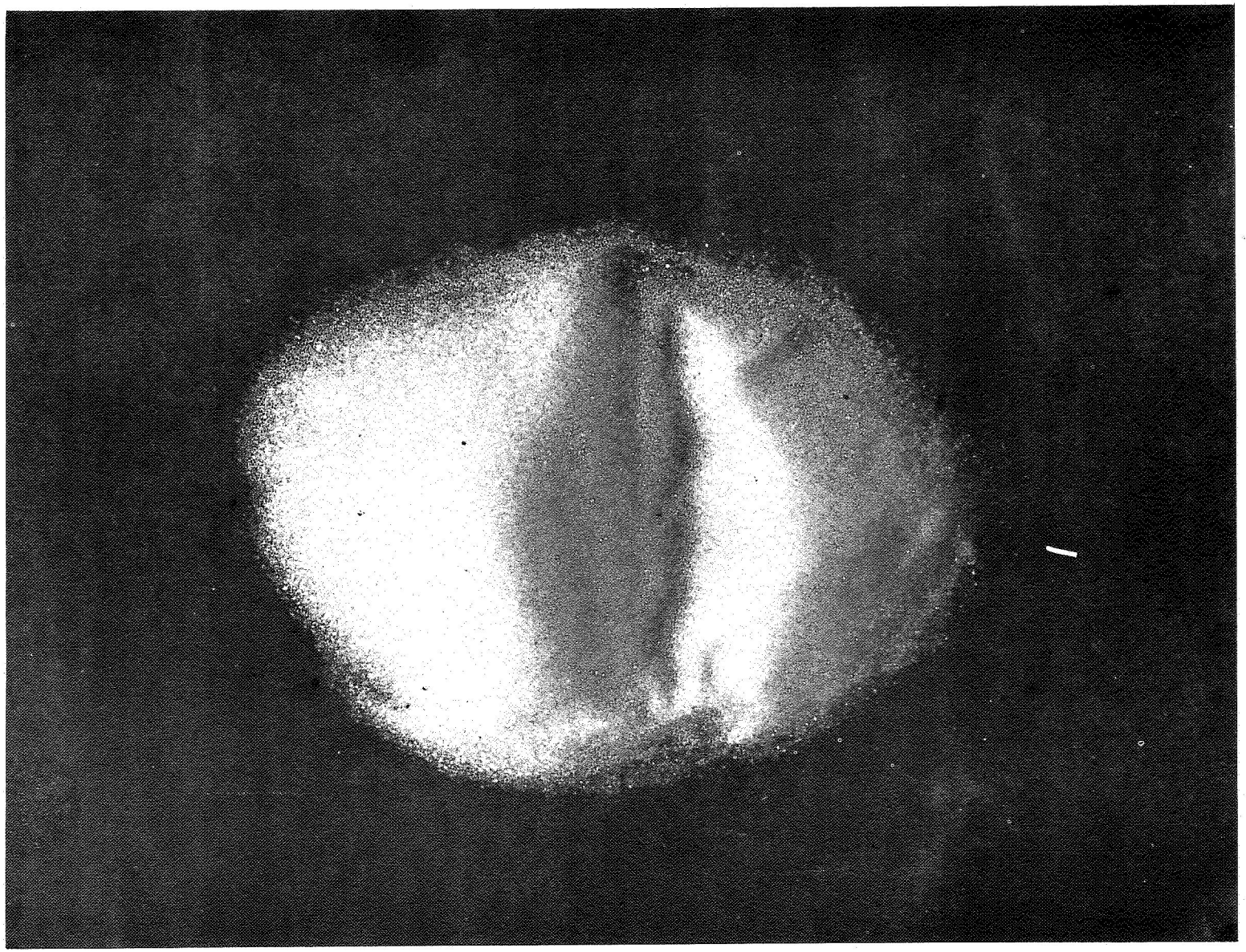

15877C

Figure 28 SPHERICAL GLASS BEADS (0.020 INCH DIAMETER)

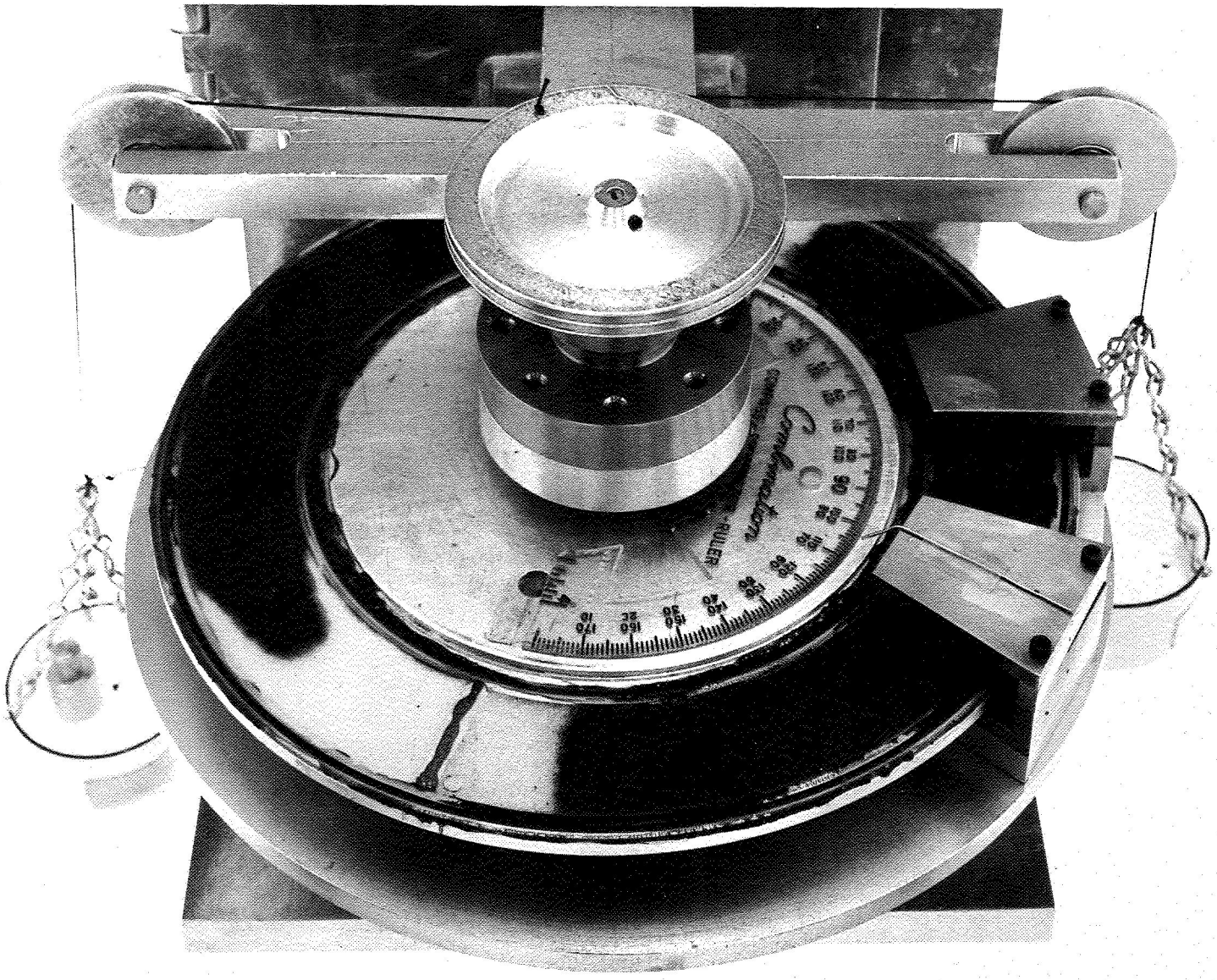

15758B

Figure 29 DAMPING TEST FIXTURE: POROUS BED VANE

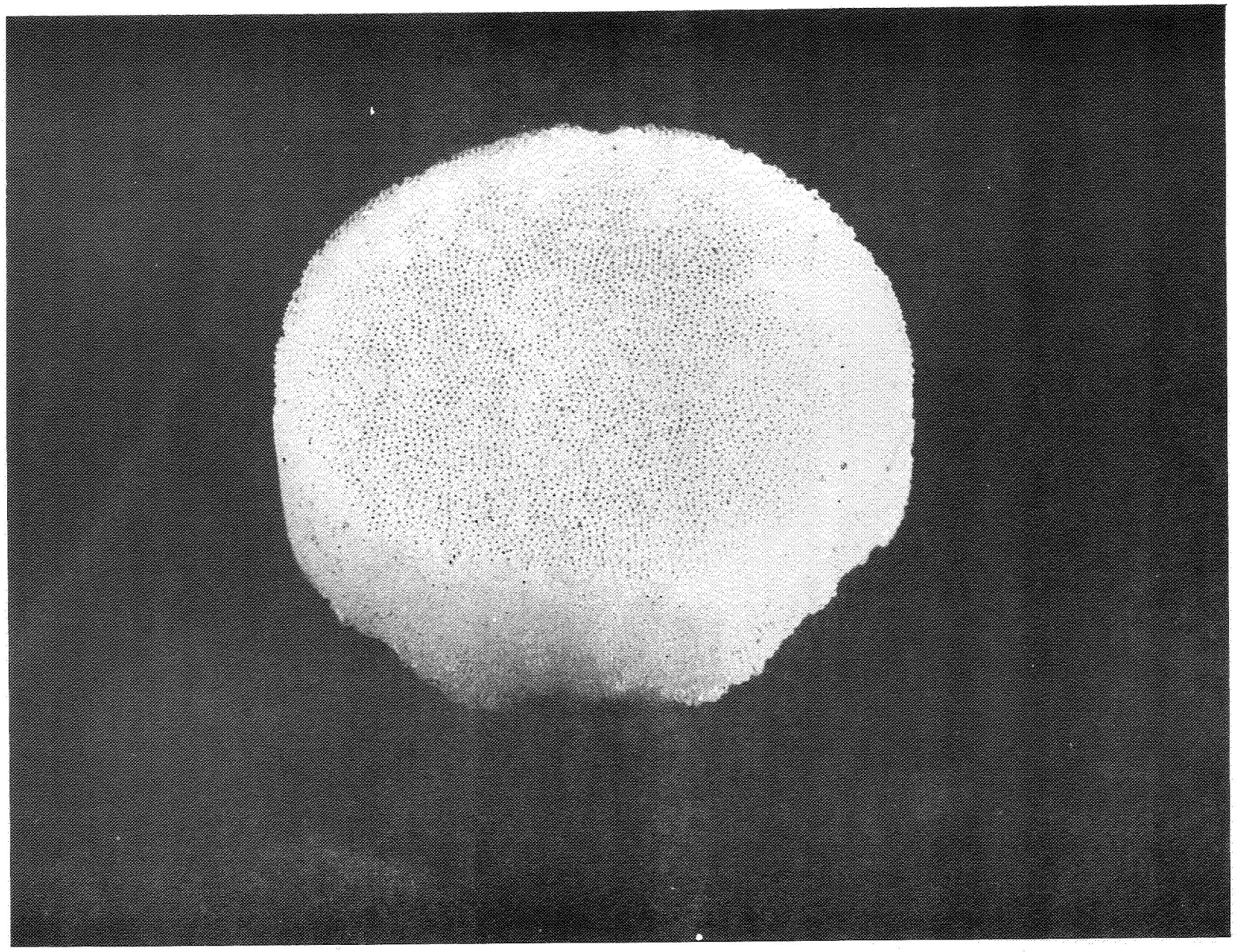

15877A

Figure 30 SINTERED GLASS BEADS

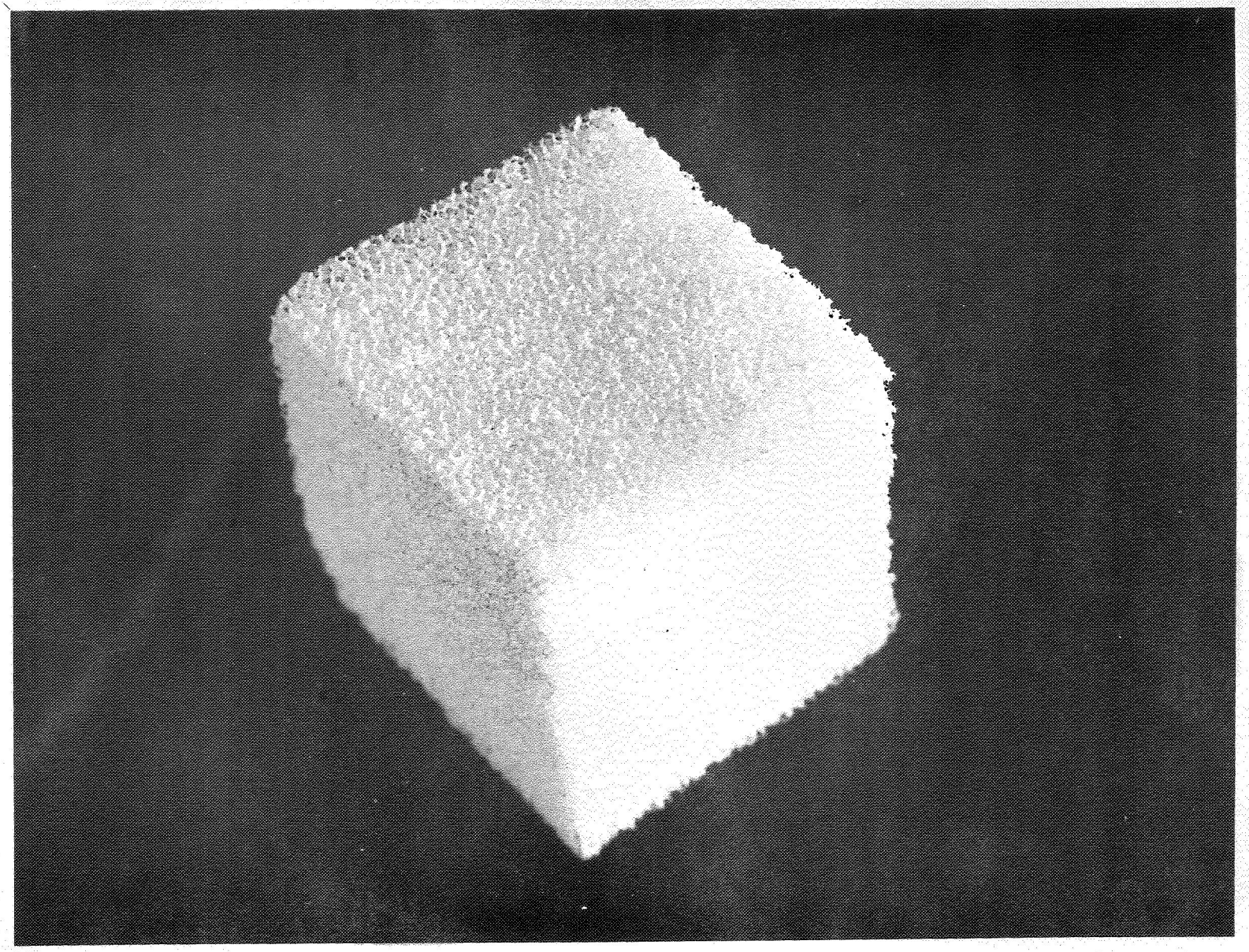

15877B

Figure 31 POROUS ALUMINUM OXIDE

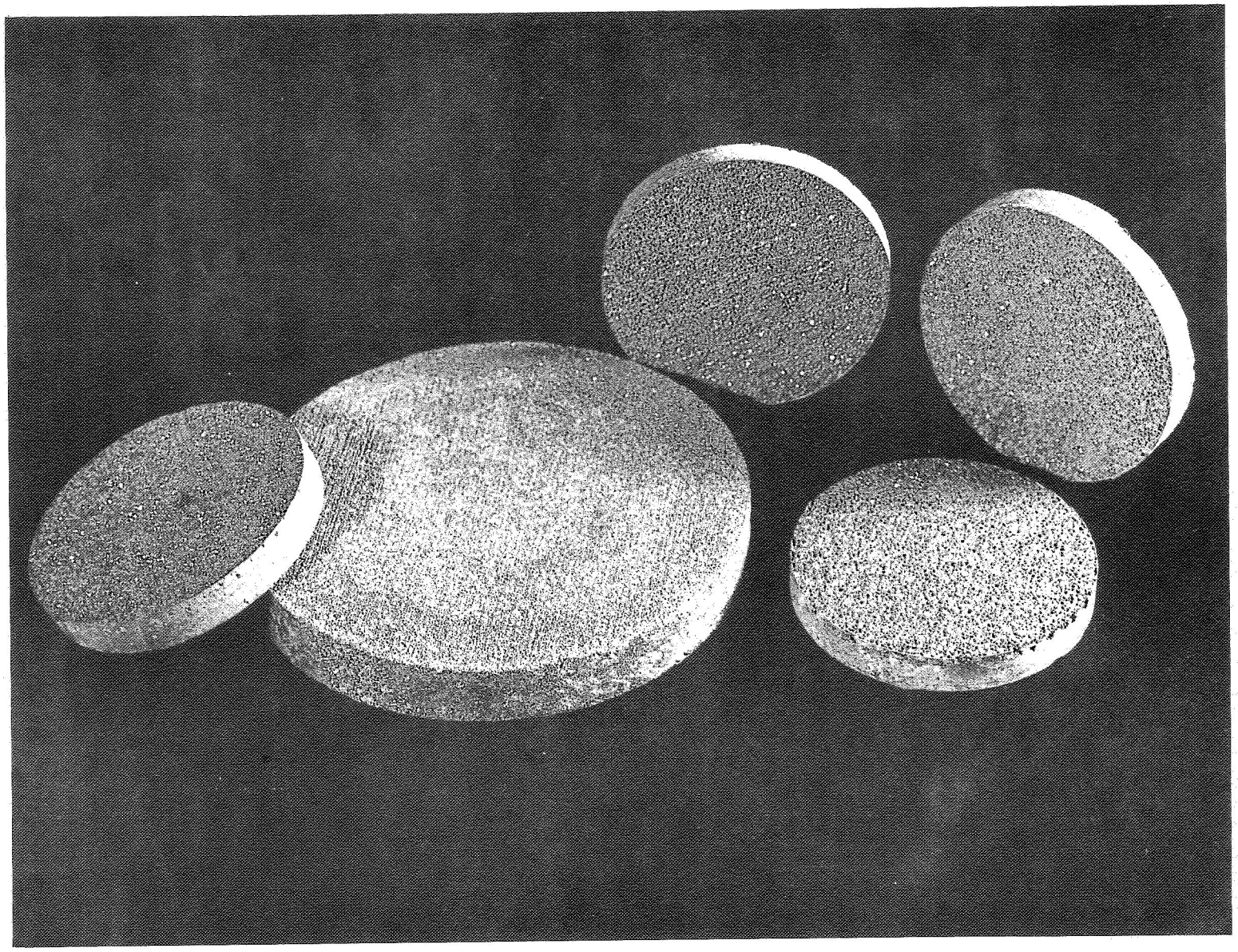

15877R

Figure 32 POROUS MATERIAL OBTAINED AFTER CASTING WITH ROCK SALT

e. Selection of a Damping Concept

Of the many damping concepts described, two can be discarded because they are not practical. The constant area vane concept is a good one because of its simplicity and reliability, but it is not feasible at the present time, because it requires a ferrofluid with a viscosity of several hundred thousand centipoise. Ferrofluid viscosities are more nearly in the 10-200 centipoise range for thermally compensated fluids. The vane/orifice/two narrow-angle magnets concept is completely unworkable because of the unstable condition of the fluid between the magnets. This leaves the vane/orifice/wide-angle magnet concept and the packed bed of solids concept to be compared.

The vane/orifice/wide-angle magnet has the advantage of having well defined mathematical concepts, plus ease in designing and assembling a mechanism that is accurately representable by mathematics. This has been borne out by the experiments performed during the early part of the program. Theoretical damping coefficients and experimental damping coefficients agreed within 20 percent over a wide range of conditions.

A slight disadvantage of this concept is the size and weight of the magnet assembly. The magnet assembly must cover an angle at least as wide as the total relative angle of travel between damper and vane. In spite of the large area which must be covered by the magnet, the magnet assembly can be optimized to a point where its weight is less than 0.6 pound while it still meets the torque requirements of the specification, using available ferrofluids.

The concept of a packed bed of solids appears to offer a weight reduction because it uses narrow magnets. Unfortunately, the packed solids used for packing the vane occupy 50 to 75 percent of the vane cavity volume; so, at best, two magnets are required to produce the torque of one, if the same sized vane is used. The vane cavity cross sectional area cannot be increased without increasing the weight of each magnet. Another difficulty arises in a model using loose solids. The porosity of the bed is not readily controllable, and a 10 percent change in porosity changes the damping constant by more than a factor of 2 to 1. In a production program where a rigid bed can be sintered or cast to size and the porosity can be controlled and measured accurately, this problem will not exist. If ceramic materials are used for the porous material, machining problems exist if the ceramic must be made to fit into a metallic cover. Low porosity ceramics have very low strength, and machining is both costly and difficult.

The vane-orifice damping concept has been selected for the deliverable model of the RAE damper because of its relative simplicity, ease in manufacture, and predictable damping coefficient.

2. Magnetic System Design

a. Material Selection

Two classes of magnet materials, the Alnicos and the barium ferrite ceramics, have been considered for use in the damper mechanism. These materials, as a group, provide the greatest magnetic fields for the least weight. Except for Alnico 7, 8, and 9, which are not readily available, the best of these materials in this respect are Alnico 5 and ceramic Indox 5. Indox 5 is equivalent to ceramic 3 listed in Table XVII.

Alnico 5 and Indox 5 have nearly equal ratios of maximum energy product to density. The ratio is inversely proportional to the weight of the magnet. If the magnet can be operated at its maximum energy product, minimum magnet weight can be achieved. Field strength, magnet area, and length requirements determine whether the magnet can be operated at or near its peak energy product. When a large pole face area and a small gap length are required, and the gap field strength is on the order of 1500 to 2500 gauss, Indox 5 operates more closely to its maximum energy product than does Alnico 5. See Figures 33 and 34 for energy product and demagnetization curves for Alnico 5 and Indox 5.

Alnico 5 magnets are typically of the horseshoe design shown in Figure 35. Since each leg of the horseshoe must take the shape of a sector of an annulus, machining of the magnet would be very expensive. A cast magnet can be made to reduce this problem.

Indox 5 magnet assemblies are of the plate magnet and back iron design shown in Figure 36. Grinding operations are required to form the magnet, but these operations are relatively straightforward.

Indox 5 has a demagnetization force of 2200 oersteds, while Alnico 5 has a demagnetization force of 600 oersteds. Indox 5 is therefore harder to demagnetize, and can be magnetized and will stay magnetized in the short lengths required for the ferrofluid damper.

b. Thermal Effects on Ceramic Magnet Material

Ceramic magnet material is relatively insensitive to temperature, and the effects of temperature are dependent on the operating point of the magnet. The effects are described below for Indox 5 operating at a flux density of 2500 gauss and a field strength of 1250 oersteds -- values representative of the magnet operating conditions in the engineering design of the RAE damper.

TABLE XVII

PERMANENT MAGNET MATERIALS

		CAST ALNICO										SINTERED ALNICO				CERAMIC MAGNETS				DUCTILE
		Alnico 1	Alnico 2	Alnico 3	Alnico 4	Alnico 5	Alnico 5-7	Alnico 6	Alnico 7-S Oriented	Alnico 7-S Unoriented	Alnico 8	Alnico 2	Alnico 4	Alnico 5	Alnico 6	Ceramic 1	Ceramic 2	Ceramic 3	Ceramic 6A	Cunife 1
Magnetic Characteristics																				
Peak energy product, $(B_dH_d)_{max} \times 10^6$		1.4	1.6	1.35	1.3	5.25	7.50	3.5	3.7	2.5	5.0	1.45	1.2	3.5	2.75	1.0	1.65	3.5	2.6	1.3
Residual Induction, B_r (kilogauss)		7.0	7.2	6.9	5.5	12.5	13.40	10.1	8.57	7.54	8.0	6.9	5.2	10.5	8.8	2.2	2.7	3.84	3.3	5.4
Coercive force H_c (oersted)		440	560	470	700	600	730	750	1040	890	1600	520	700	600	800	1825	2250	2200	3000	500
Permeance coefficient, B/H at $(B_dH_d)_{max}$		14.4	13.4	13.7	6.83	20	18.5	12.5	8.0	8.5	5.25	12.7	7.5	17.4	11.0	1.2	1.1	1.05	1.06	12.3
Induction, B_d at $(B_dH_d)_{max}$ (kilogauss)		4.5	4.7	4.3	3.0	10.2	11.8	7.0	5.46	4.5	5.12	4.3	3.0	7.8	5.5	1.1	1.35	1.92	1650	4.0
Mmf per unit length, H_d at $(B_dH_d)_{max}$ (oersteds)		310	350	315	430	512	635	543	680	555	980	340	400	450	500	900	1220	1820	1575	325
Incremental permeability	(Note 1)	6.8	6.4	6.5	4.1	3.8	1.9	5.0	–	–	2.1	6.4	4.1	4.0	5.0	1.1	1.15	1.05	1.06	1.7
Peak magnetizing force required H_p (oersteds)		2000	2000	2000	3000	3000	3000	3000	3500	3500	3000	2000	3000	3000	3000	10,000	10,000	10,000	10,000	2400
Application and Design Factors																				
Ability to withstand demagnetizing *fields*	(Note 2)	G	G	G	E	G	G	E	E	E	Ex	G	E	G	E	S	S	S	S	G
Approx. temp. permanently affecting material (deg F)	(Note 3)	1000	1000	900	1100	1000	1000	1000	1000	1000	1000	900	1100	1000	1000	1800	1800	1800	1800	900
Preferred magnetic orientation	(Note 4)	No	No	No	No	YH	YH	YH	YH	No	YH	No	No	YH	YH	YP	Yes	Yes	Yes	YR
Importance of working at $(B_dH_d)_{max}$	(Note 5)	B	B	B	C	A	A	B	B	B	–	B	C	A	B	D	C	C	C	B
Material Characteristics																				
Weight (lb per cu in.)		0.249	0.256	0.249	0.253	0.265	0.265	0.268	0.265	0.265	0.265	0.243	0.250	0.241	0.241	0.167	.162	0.18	0.162	0.311
Mechanical properties	(Note 6)	HB	HB	HB	HB	HB	HB	HB	HB	HB	HB	H	H	H	HB	HB	HB	HB	HB	D
Critical materials present		Co, Ni	Co, Ni	Ni	Co, Ni	Co, Ni	Co, Ni	Co, Ni	Co, Ni	Co, Ni	Co, Ni	Co, Ni	Co, Ni	Co, Ni	Co, Ni	None	None	None	None	Ni
Relative material cost per unit of energy	(Note 7)	B	B	A	B	A	B	B	D	D	D	C	C	B	B	A	A	A	A	C
Relative processing cost	(Note 7)	B	B	B	B	C	D	C	C	C	D	B	B	C	C	B	B	E	E	D
Electrical resistivity at 25 C (microohm cm)		75	65	60	75	47	47	50	–	–	–	68	68	50	–	10^{12}	–	10^{10}	–	18
Tensile Strength (psi)		4100	3000	12,000	9100	5450	5000	23,000	–	–	–	65,000	60,000	50,000	–	Low	Low	Low	Low	100,000
Transverse modulus of rupture (psi)		13,900	7700	22,500	24,000	10,500	–	45,000	–	–	–	70,000	85,000	–	–	–	–	–	–	–
Coefficient of thermal expansion (per deg C × 10^{-6})		12.6	12.4	13.0	13.1	11.3	–	11.4	–	–	–	12.4	13.1	11.3	–	10	10.3	10	10.3	14.0
Manufacturing Methods and Limitations																				
Method	(Note 8)	C	C	C	C	CM	CM	C	CM	C	C	S	S	SM	SM	S	S	S	S	CR
Shape limitations	(Note 9)	C	C	C	C	C	CB	C	C	C	CB	P	P	P	P	P	P	P	P	Fa
Machinability	(Note 10)	G	G	G	G	G	G	G	G	G	G	G	G	G	G	G	G	G	G	Yes

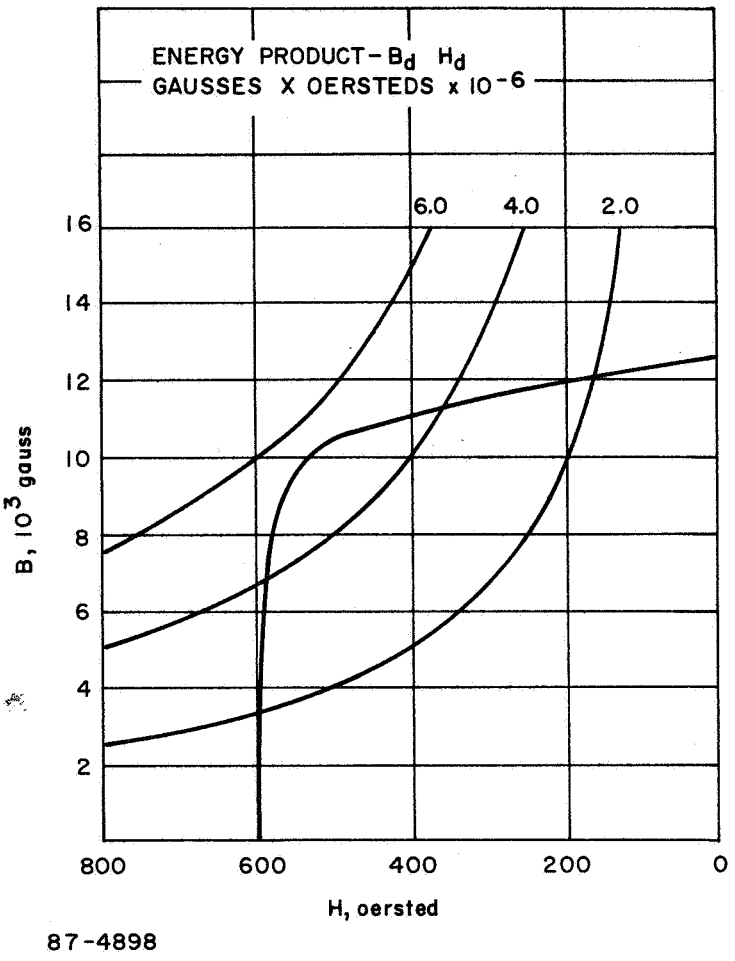

Figure 33 ENERGY PRODUCT AND DEMAGNETIZATION CURVES FOR ALNICO 5

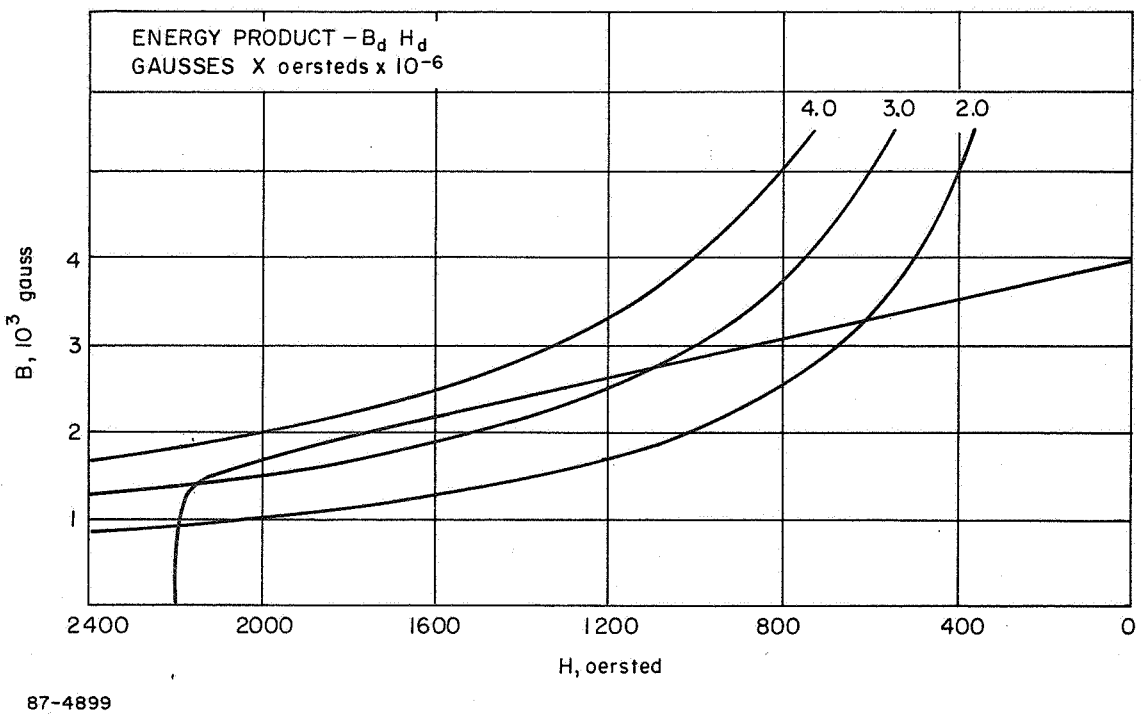

Figure 34 ENERGY PRODUCT AND DEMAGNETIZATION CURVES FOR INDOX 5

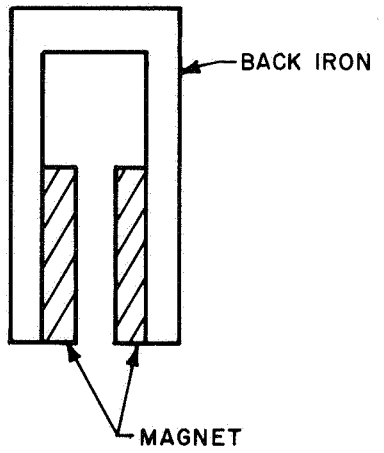

1. PLATE MAGNET WITH CONTINUOUS BACK IRON

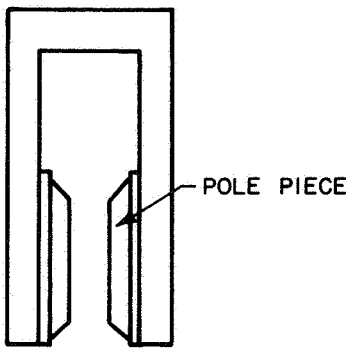

2. PLATE MAGNET WITH CONTINUOUS BACK IRON AND POLE PIECES

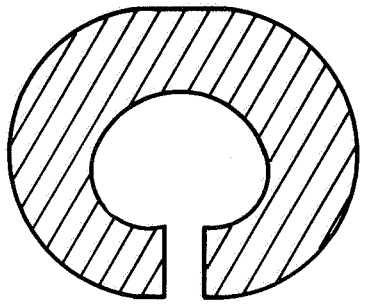

3. HORSESHOE MAGNET

87-4900

Figure 35 MAGNET CONFIGURATIONS

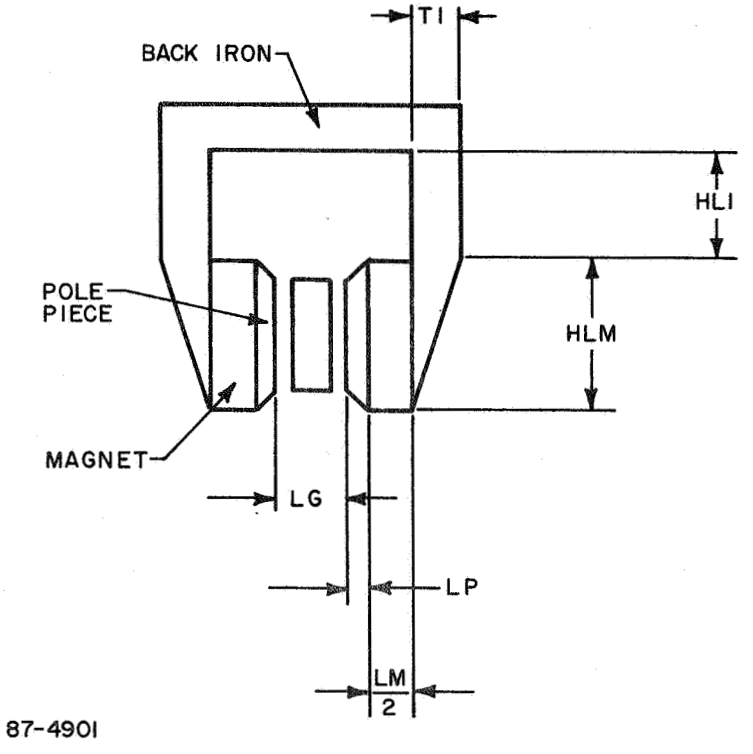

Figure 36 MAGNET ASSEMBLY CROSS SECTION

When the magnet is stored at -50° F for long periods, the flux density increases permanently by 4 percent and the field strength by 8 percent. These changes are in the right direction, increasing the magnet effective strength.

At elevated temperatures of 160° F, the flux density decreases 10 percent and the field strength decreases 8 percent. This change is made insignificant by providing an adequate safety margin in the magnetic design.

c. Radiation Effects on Ceramic Magnet Material

The expected radiation dose seen by the damper is 0.18 megarad. The heating effect of 0.18 megarad is 2.39 cal/gm (Reference 8). The heat capacity of barium ferrite, the magnet material, is 0.2 (cal/gm)° C, (Reference 9). Therefore, the temperature rise is 12° C, or 22° F. This temperature rise has an insignificant effect on magnet parameters.

Ceramic magnet materials have been subjected to very high neutron flux densities (Reference 10), up to 10^{18} N.V.T., with less than 4 percent decrease in field strength. Ceramic magnets are in general more resistant to radiation than other magnet material. Radiation effects other than heating effects are considered negligible (Reference 8). Indox 5 ceramic magnet material has been selected for use in the RAE damper because its magnetic and mechanical properties most closely meet the requirements of the damper.

d. Magnet Design Equations

The theoretical equations governing magnet design are well known. They relate flux densities of the magnet and its air gap and field strengths within the magnet and in its air gap. These equations must be modified to account for practical considerations which modify magnet performance markedly. They are flux leakage and path reluctance. The practical equations are developed in the next paragraphs. These equations assume values of flux leakage and reluctance and then provide a method of checking the design for the proper flux leakage constant. The reluctance constant is a function of materials used and material joint separation. This factor is typically 1.2 to 1.5 and can best be checked experimentally. A conservative value of 1.5 is used throughout the study.

In an ideal magnet, the area A_m and the length of the magnet L_m can be related as follows:

$$\phi = B_m A_m = B_g A_g, \; H_m L_m = H_g L_g \tag{17}$$

where

ϕ = flux

B = flux density

H = field strength

L = length

A = area

g = gap subscript

m = magnet subscript

In the practical magnet there is flux leakage, and a flux leakage factor F is used to calculate the required magnet area:

$$A_m = F \frac{B_g A_g}{B_m} \tag{18}$$

If the permeability of the gap is unity, $B_g = H_g$ and

$$A_m = F \frac{H_g A_g}{B_m} \tag{19}$$

The flux leakage factor can be as high as 10 or more, depending on magnet assembly configuration. With care this factor can be kept below 2. Graphical and analytical methods of evaluating this factor, for a given design, are presented by Crucible Steel[11] and Thomas and Skinner [12] in their magnet design handbooks. The analytical method provided by Thomas and Skinner was used in evaluating the F factor of several magnet assemblies, including that of the reference design.

The practical magnet also has finite path reluctance, resulting from iron reluctance and gaps between material joints. A reluctance factor f is used to provide adequate magnet length with reluctance:

$$L_m = \frac{f H_g L_g}{H_m} \tag{20}$$

Typical values of f lie between 1.2 and 1.5. A value of $f = 1.5$ was used throughout the parametric studies to provide a conservative design. The magnet area and length equations can now be combined to determine magnet volume; when this is multiplied by magnet density ρ_m, magnet weight W_m becomes

$$W_m = \rho_m A_m L_m = \rho_m \frac{f F H_g^2 L_g H_g}{H_m B_m} \quad (21)$$

The magnet material properties are ρ_m, H_m, and B_m. The larger $H_m B_m/\rho_m$, the smaller the magnet weight. If the magnet assembly consists of magnet, plus back iron, plus pole pieces, then the weight of these pieces must also be considered.

In this configuration the cross section of the back iron is tapered from zero width at the base of the magnet to a width TI, at the top of the magnet, which is great enough to provide adequate iron area in the return circuit. The formula used to compute the iron weight is:

$$WI = 0.28\ LI\ AI \quad (22)$$

where

0.28 = iron density

AI = iron area

LI = iron length

The iron area is determined from

$$AI = (AM)\ (BM)\ BI \quad (23)$$

where BI is the flux density in the iron. The length of the iron LI is

$$LI = 2\ (HLI + LP + TI) + HLM + LG + LM \quad (24)$$

where HLI, LP, TI, HLM, LM, and LG are defined in Figure 36.

The weight of the pole pieces is defined as

$$WTP = 0.28\ (AM + AG)\ LP \quad (25)$$

where 0.28 is the iron density, $\frac{AM + AG}{2}$ = average pole area.

$2\,LP$ = the length of the poles

The total weight WT is equal to

$$WT = WTI + WTM + WTP \quad (26)$$

The flux leakage factor is computed, using Thomas and Skinner's formula:

$$FCC = 1 + \frac{(LG)\ (CX)}{1.75\ AG}\left[\frac{3\ LP}{LP + LG} + \frac{1.5\ LM}{0.65\ LM + 2LG + 4LP} + \frac{2\ LG}{2M}\right] \quad (27)$$

where CX is the perimeter of the pole piece. When no pole pieces are used, CX is the perimeter of the magnet and $LP = 0$.

Equations 19 through 27 are used in a digital computer program to compute the weight of the magnet assembly.

An initial guess is made of the value of F, labeled FC in the program. The computed value FCC is then used to re-estimate FC. The process converges on an approximate solution of magnet and iron weight and dimension.

e. Magnet Configuration

Three magnet configurations have been considered for the damper. These configurations are shown schematically in Figure 35. Configuration 1 uses plate magnets, magnetized in the direction normal to their faces and back iron to complete the magnetic circuit. Configuration 2 differs from configuration 1 only in that the magnet area does not match the required gap area, so that pole pieces are required. Configuration 3 is the standard horseshoe magnet which uses no soft iron, either in the back circuit or as pole pieces. Configurations 1 and 3 require magnet materials with specific properties, because the lack of pole pieces requires that the magnet area match the gap area. It follows directly that

$$B_m = FH_g \quad (28)$$

The operating flux of the magnet B_m must equal the flux leakage factor F times the gap field strength H_g. Assuming that $F = 2$ and $H_g = 1500$, then $B_m = 3000$. If Alnico 5 is used, the energy product is approximately 1.75, far below the peak value of 5.3. The field strength in the magnet H_M is 610 oersted and

$$L_m = \frac{f(H_g L_g)}{H_m} = \frac{(1.5)(1500)\ L_g}{610} \quad (29)$$

$$L_m = 3.8\ L_g$$

For a gap length L_g of 0.2 inch, the magnet length is 0.76 inch. Alnico 5 is not used effectively with this configuration.

Indox 5 with B_m = 3000 has an energy product of 2.5 and a magnet field strength of 900 oersteds. The length of the Indox 5 magnet required is only 0.5 inch. This is no problem with ceramic magnets, because of their higher demagnetization force.

If the horseshoe configuration is used, approximately a 3 inch minimum magnet length is required, and with f = 1.5,

$$L_g = 0.21, \; H_g = 1500 \tag{30}$$

then:

$$H_m = 1.5 \; (1500) \; \frac{0.2}{3} = 150 \text{ oersteds} \tag{31}$$

If Alnico 5 is used, the energy product is approximately 1.7 and the magnet field strength is 12,000 gauss. If the flux leakage factor is still 2, the magnet area is only

$$A_m = 2 \; \frac{1500}{12{,}000} \; A_g = 0.25 \, A_g \tag{32}$$

In actual practice it is impossible to keep F below 4 or 5 for this configuration, so it might be possible to match magnet and gap areas without pole pieces. The magnet cross sectional area must be maintained around the entire loop. Since Alnico 5 and iron have the same density, and iron can carry a higher flux density, 15,000 to 20,000 gauss, a magnet assembly with back iron will weigh less than an equivalent horseshoe magnet.

Typical values of field strength, gap length, and flux leakage factors, matching the requirements of the RAE damper, have been used to illustrate why Indox 5 is a superior material for this application. The parametric analysis of damping vane and magnet which follows illustrates how these values were selected.

f. Magnet-Vane Parametric Study

A computer program has been written which takes a list of inputs including torque, ferrofluid magnetic moment, and desired magnet field strength and computes the vane cross sectional area and the magnet operating characteristics, dimensions, and weight. This program makes use of the equations developed in paragraphs IV.A.2.d and IV.D.2.a. The inputs to the program are listed in Table XVIII. The outputs of the program are listed in Table XIX. The program is listed in Figure 37.

TABLE XVIII

INPUTS TO MAGNET AND VANE COMPUTATION PROGRAM

1. *T* = magnetic trapping torque (ft-lb)
2. *MMX* = maximum magnetic moment of magnetic fluid (gauss)
3. *ANG* = angular extent of magnet (degrees)
4. *TW* = vane wall thickness (in.)
5. *TA* = air gap length between vane and magnet (in.)
6. *BI* = flux density in back iron (gauss)
7. *RV* = vane radius (in.)
8. *HGX* = field strength in gap (oersteds)

   HGN = field strength in fringe field (oersteds)
9. *BLG* = fluid depth normal to pole faces (in.)
10. *FC* = flux leakage constant
11. *FL* = reluctance constant
12. *BD* = flux density in magnet (gauss)
13. *MAG* = magnet material (Alnico 5 to Indox 5)
14. *HLI* = back iron radial extension past magnet (in.)
15. *LP* = length of pole pieces (in.)

TABLE XIX

OUTPUTS FROM MAGNET AND VANE COMPUTATION PROGRAM

FM = magnetic trapping force (lb)

AV = vane cross sectional area (in.^{2})

MS = fluid magnetic moment (gauss)

HLG = radial fluid length (in.)

LTM = magnet arc length (in.)

AG = gap area (in.^{2})

BDP = magnet flux density required for equal magnet and vane areas (gauss)

AM = magnet area (in.^{2})

HLM = radial magnet length (in.)

HD = magnet coercive force (oersteds)

LG = air gap length (in.)

LM = magnet length (in.)

WTM = magnet weight (lb)

WTI = back iron weight (lb)

WTP = pole piece weight (lb)

WT = weight of magnet, back iron, and pole piece (lb)

AI = iron cross sectional area (in.^{2})

TI = thickness of iron (in.)

FCC = computed flux leakage constant

MSH = integral of $M\,dH$

```
1.0 DEMAND STP
1.01 TO STEP STP
1.1 DEMAND T, ANG, TW, TA,BI
1.101 DEMAND MMX
1.11 DEMAND RV
1.12 TYPE "HGX MUST BE BETWEEN 1000 AND 2500"
1.13 TYPE "HGN MUST BE BETWEEN 300 AND 1000"
1.14 DEMAND HGX, HGN
1.15 HG =HGX
1.2 FM =T*12/RV
1.21 TYPE FM
1.3 MSH = MMX*(4.76*10↑-5*HGX↑2 +.616*HGX-2.2*10↑-4*HGN↑2-.268*HGN-175)
1.31 TYPE MSH
1.32 AV =FM*4*$PI/(MSH*1.42*10↑-5)
1.391 TYPE AV
1.40 DEMAND BLG
1.5 HLG=AV/BLG
1.51 TYPE HLG
1.6 LTM=$PI*RV*ANG/180
1.61 TYPE LTM
1.7 AG=LTM*HLG
1.71 TYPE AG
1.8TO PART 2

2.0 DEMAND FC,FL
2.1BDP=FC*HG
2.11 TYPE BDP
2.2 DEMAND BD,MAG
2.3AM= FC*HG*AG/BD
2.31 TYPE AM
2.4 HLM= AM/LTM
2.41 TYPE HLM
2.5 TO PART 3 IF MAG=1
2.6 DO PART 4 IF MAG=2
2.8 TYPE HD
2.801 DEMAND HLI,LP
2.81 LG=BLG +2*(TW+TA)
2.82LM=FL*HG*LG/HD
2.83 WTM=RHM*AM*LM
2.831 TYPE LG,LM,WTM
2.84 AI=AM*BD/BI
2.85TI= AI/LTM
2.86 LI= 2*(HLI+HLM+LP+TI) +LG+LM
2.861 TYPE AI, TI, LI
2.87 WTI=.28*AI*(LI-HLM)
2.88 WTP = .28*(AM +AG)*LP
2.89WT=WTI+WTP+WTM
2.891 TYPE WTI, WTP, WTM, WT
2.9 CX=2*(HLM+LTM)
2.91FCD=LG*CX*(3*LP/(LP+LG)+(1.5*LM)/(.65*LM+2*LG+4*LP)+2*LG/LM)
2.92 FCC = 1 +FCD/(1.75*AG)
2.921TYPE FCC
2.93 TO PART 1.0

3.0 RHM= .18
3.1TO STEP 3.3 IF BD<1850
3.2 HD=-.89*BD+3475
3.21 TO STEP 2.8
3.3 DEMAND HD
3.4 TO STEP 2.8

4.0 RHM =.27
4.1 TO STEP 4.5 IF BD> 10400
4.2 TO STEP 4.4 IF BD <8600
4.3 HD =-.0375*BD +894
4.31 TO STEP 4.6
4.4 HD=-.003*BD+600
4.41 TO STEP 4.6
4.5 DEMAND HD
4.501 TYPE HD
4.6TYPE HD
4.7 TO STEP 2.8


DUMPED
```

87-4902

Figure 37 MAGNET AND VANE COMPUTATION PROGRAM

Parametric studies have been performed with Alnico 5 and Indox 5 as the magnet materials. The results of these studies are listed in Tables XX and XXI. They are discussed in the following two subsections.

1) Alnico 5 Magnet Configurations -- A series of Alnico 5 configurations has been computed for a magnetic pull torque capability of 0.009 ft-lb. The initial configurations, runs 2 and 5 listed in Table XX, are of the second type of magnet structure shown in Figure 35, using iron pole pieces to match the magnet and gap areas. These configurations use the Alnico at its peak $B_m H_m$. Excessive iron weight is required.

Run 22 in Table XX is typical of the horseshoe configuration. The value of L_m is only half of that required to achieve a complete horseshoe. In addition, the flux leakage factor FCC computed for this configuration is high, and larger than the one used in the computation. The actual magnet weight required is more than twice that indicated in the table.

Another configuration is evaluated in Run 31 of Table XX. This configuration is identical to that of type 1 in Figure 35. Here again the magnet assembly weight is excessive.

2) Ceramic Magnet Configurations -- The only configuration evaluated for the ceramic magnet is the one shown as type 1 in Figure 35. Short slabs of magnet on either side of the gap are connected by back iron. Table XXI shows the dependence of magnet assembly weight on several factors.

a) Flux Leakage Factor R -- Run 26 and 27 differ only in that for run 27, a smaller factor is used in the computation, and yet the weight is reduced 25 percent. This factor is still conservative, as indicated by the smaller FCC obtained after determining a reasonable configuration.

b) Vane Radius -- Inputs for runs 27 and 28 are identical, except for the mean radius of the magnet assembly. A 15 percent smaller radius increases the weight less than 6 percent.

c) Fluid Magnetic Moment -- Inputs for runs 43 and 46 are identical, except for the fluid magnetic moment. The indicated weight reductions for that obtained in run 27 are not entirely achievable, becuase of the increase in flux leakage factor. The increase in FCC results from the decreased ratio of gap length to gap area.

d) Effect of Torque -- Runs 51 and 57, when compared with run 27, show the effect of increased torque capability and of increased fluid magnetic moment on weight. The weight increases almost linearly with torque.

TABLE XX

ALNICO 5 MAGNET DESIGN

	Run Number			
Outputs	2	5	22	31
AV	.22	.16	.023	.061
HLG	1.19	.92	.20	.77
AG	5.82	5.82	.96	3.22
LM	.77	.77	2.31	.82
WTM	.29	.22	.60	.77
WTI	1.03	.97	0	.83
WTP	.40	.40	0	0
WT	1.72	1.59	.60	1.60
FCC	1.81	1.96	3.4	1.51
Inputs				
T	.009	.009	.009	.009
MMX	500	500	500	500
RV	3.5	4.5	3.5	3.0
HG	1000	1000	1000	2000
BLG	.18	.18	.12	.08
GC	2.5	2.5	2.5	2.5
FL	1.5	1.5	1.5	
BD	10,400	10,400	10,000	5,000
MAG	Alnico	Alnico	Alnico	Alnico
HLI	.6	.7	.3	.3
LP	.2	.2	0	0

TABLE XXI

INDOX 5 MAGNET DESIGN

Outputs	Run Number						
	26	27	28	43	46	51	57
W	.128	.128	.15	.085	.064	.256	.171
WLG	1.07	1.07	1.25	.71	.53	2.13	1.42
AG	5.22	5.22	5.22	3.48	2.61	10.44	6.96
AM	5.22	5.22	5.22	3.48	2.61	10.44	6.96
LM	.24	.18	.18	.18	.18	.143	.177
WLM	1.07	1.07	1.25	.71	.53	2.13	1.42
WTM	.23	.17	.17	.11	.08	.27	.22
WTI	.61	.45	.50	.25	.16	1.03	.72
WTP	0	0	0	.00	0	0	0
WT	.84	.62	.67	.36	.24	1.30	.94
FCC	1.6	1.72	1.66	2.0	2.3	1.50	1.57
Inputs							
T	.006	.006	.006	.006	.006	.012	.012
MMX	500	500	500	750	1000	500	750
RV	3.5	3.5	3.0	3.5	3.5	3.5	3.5
HGX	1000	1000	1000	1000	1000	1000	1000
HGN	500	500	500	500	500	500	500
BLG	.12	.12	.12	.12	.12	.12	.12
FC	2.5	2.0	2.0	2.0	2.0	1.5	1.5
FL	1.5	1.5	1.5	1.5	1.5	1.5	1.5
BD	2500	2000	2000	2000	2000	1500	2000
MAG	Indox	Indox	Indox	Indox	Indox	Indox	Indox
HLI	.3	.3	.3	.3	.3	.3	.3
LP	0	0	0	0	0	0	0

TABLE XXI (Concl'd)

	Run Number				
Outputs	62	64	65	67	68
AV	.127	.106	.091	.091	.064
HLG	1.06	.884	.758	.910	.637
AG	5.18	4.32	3.70	4.44	3.111
AM	5.18	4.32	3.70	4.44	3.111
LM	.336	.373	.373	.275	.336
HLM	1.06	.884	.758	.910	.637
WTM	.313	.290	.25	.220	.188
WTI	.68	.56	.45	.49	.35
WT	.99	.85	.70	.71	.53
FCC	7.54	1.6	1.67	1.56	1.71
AI	.83	.73	.63	.667	.53
TI	.17	.15	1.28	.136	.108
Inputs					
T	.014	.014	.014	.014	.014
MMX	500	600	700	700	1000
RV	3.5	3.5	3.5	3.5	3.5
HGX	1500	1500	1500	1500	1500
HM	500	500	500	500	500
BLG	.12	.12	.12	.10	.10
FC	1.6	1.7	1.7	1.5	1.7
FL	1.5	1.5	1.5	1.5	1.5
BD	2400	2550	2250	2250	2550
MAG	Indox	Indox	Indox	Indox	Indox
HLI	.5	.5	.5	.5	.5
LP	0	0	0	0	0

e) Effects of Magnetic Moment and Field Strength -- Runs 62, 64, and 65 again show the influence of magnetic fluid moment on weight and also show the effect of increased field strength in the gap. With the field strength increased to 1500 oersteds, the magnet assembly weight is decreased further.

The results of the magnet-vane parametric study are summarized in Figures 38, 39, and 40.

In Figure 38, magnet assembly weight is plotted versus maximum damping torque for several values of ferrofluid magnetic moment M_s, and maximum magnetic field HGX. The importance of using a ferrofluid with a magnetic moment of 700 or more is obvious. The importance of using a magnet field strength of at least 1500 oersteds is also clearly noted. Significant weight increases result if either parameter value is decreased.

Figure 39 is a plot of magnet assembly weight versus ferrofluid magnetic moment. This plot shows that with a magnetic field of 1500 oersteds, the reduction in weight achieved by increasing the ferrofluid magnetic moment is linear until 700 gauss. Above 700 gauss there is less than linear reduction in weight.

Figure 40 shows plots of radial vane dimension versus fluid magnetic moment for two values of vane normal dimension b. This relationship is linear throughout.

The magnet and vane parameters computed in run 65 have been selected for use in the reference design.

B. SUSPENSION MECHANISM

This section of the report presents a detailed analysis of several possible types of damper suspension mechanisms. The following suspension techniques have been considered:

1. Flexural pivots
2. Jewel pivots

3. Ball bearings

4. Sleeve bearings

5. Torsion wire

The analysis includes:

1. Parametric studies of load versus size and weight for each type of suspension

2. An evaluation of environmental sensitivities

3. Effects of dynamic loading

4. Lubrication requirements

5. Evaluation of materials

6. Parts availability and manufacturability

With this background information available, a tradeoff study is performed to integrate the most promising components into the overall design. Damper loading and location of the damper with respect to the satellite axes are defined in Figure 41.

1. Flexural Pivot Suspension

a. Design Features

Flexural pivots have been used for many years as a frictionless bearing of limited angular travel, requiring no lubrication. In this report any reference to "pivot" implies use of the Bendix Free Flex Pivot.

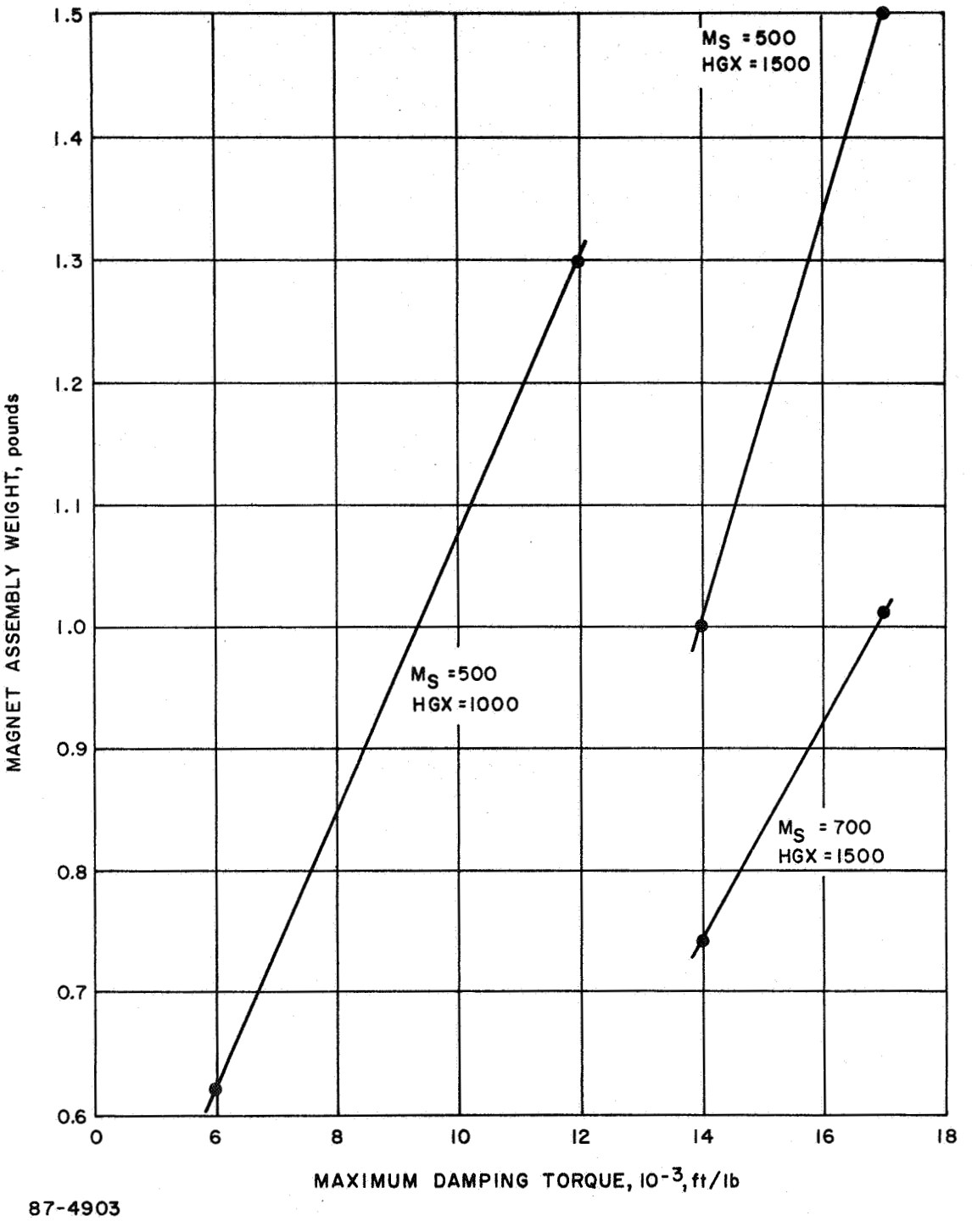

Figure 38 MAGNET ASSEMBLY WEIGHT VERSUS MAXIMUM DAMPING TORQUE

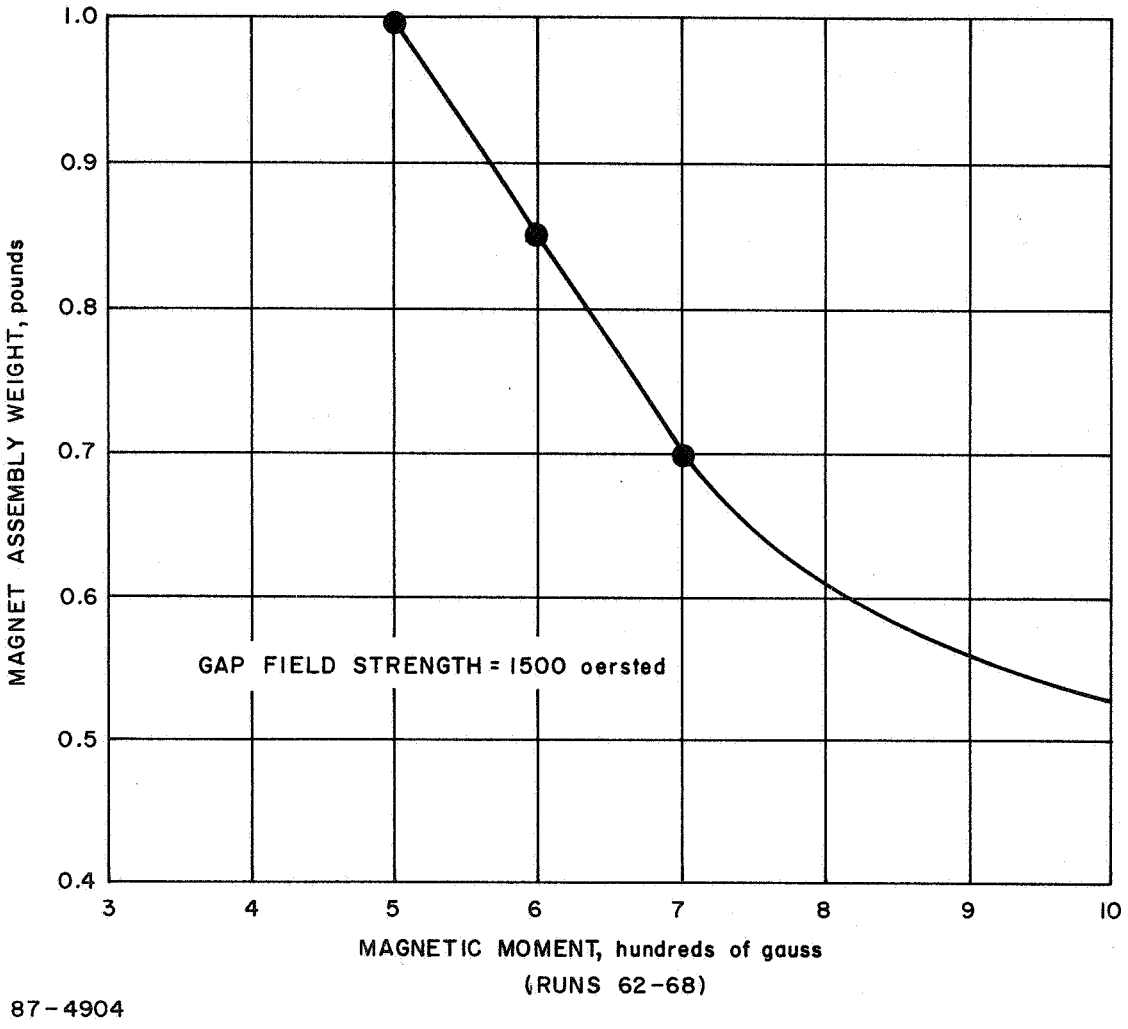

Figure 39 MAGNET ASSEMBLY WEIGHT VERSUS FLUID MAGNETIC MOMENT

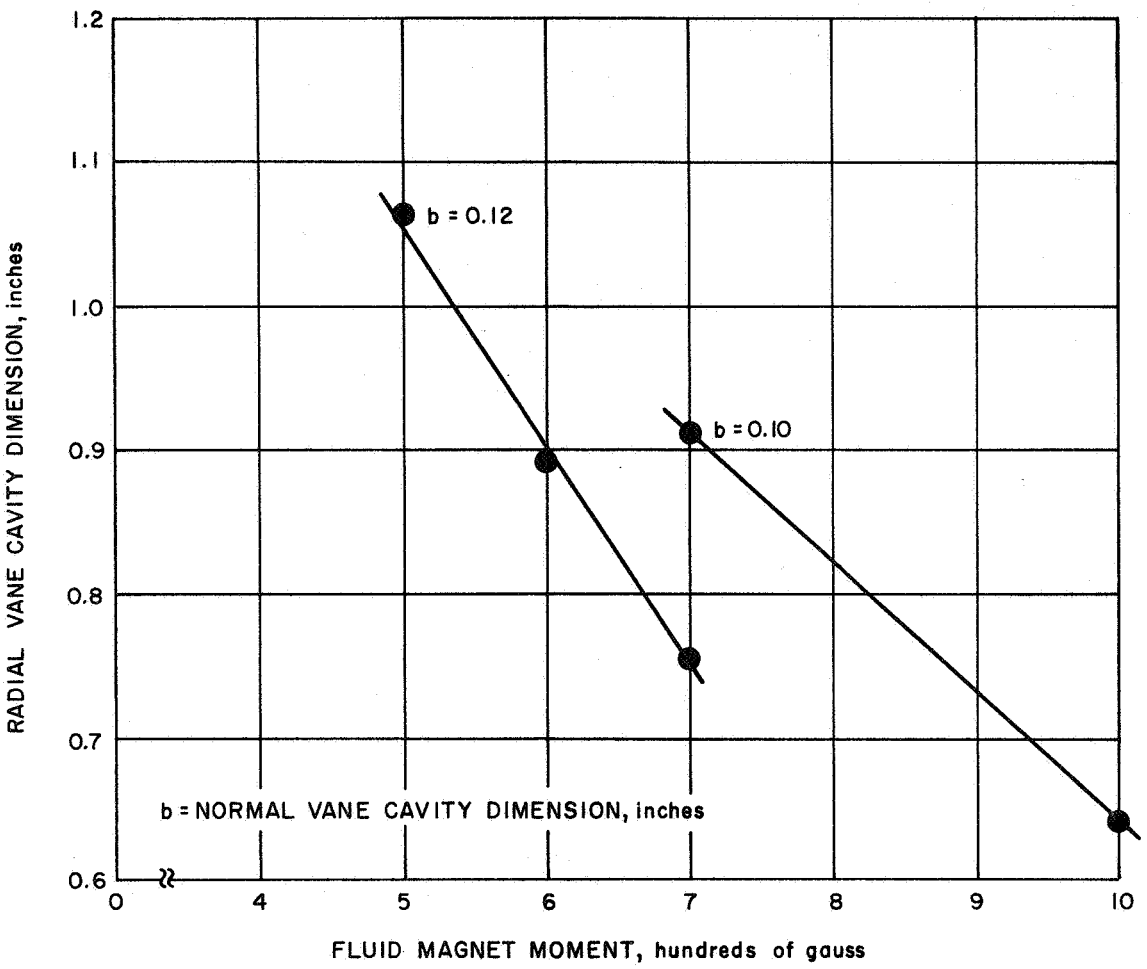

Figure 40 VANE RADIAL DIMENSION VERSUS FLUID MAGNETIC MOMENT

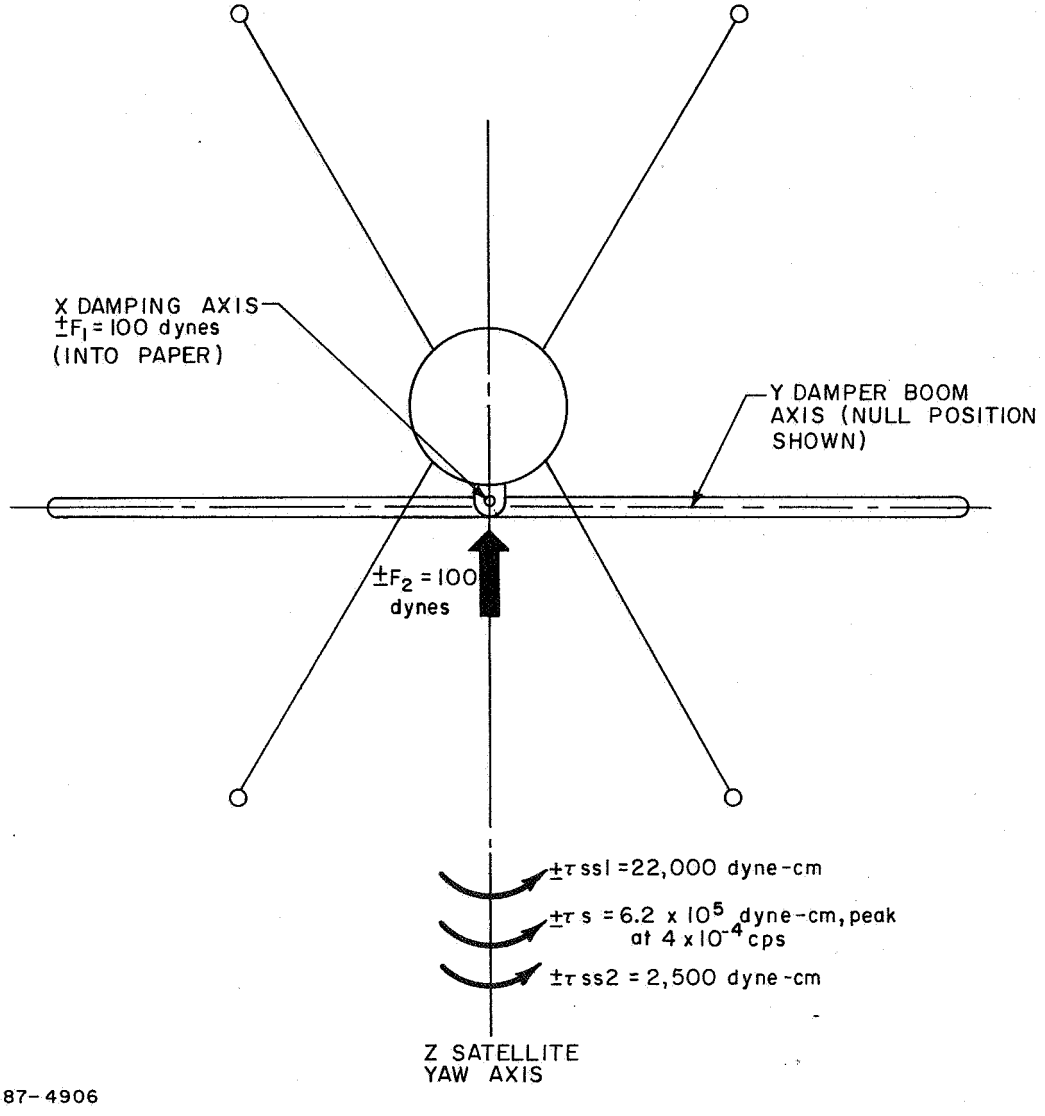

Figure 41 RAE DAMPER SUSPENSION LOADING

The pivot is made of pairs of flat crossed springs supporting rotating sleeves and is designed to be a simple package which is compact, integrated, and easy to install. It can be manufactured from various materials, depending upon the application and operation requirements. (See Figure 42).

The primary factors to be considered in pivot selection are life (total number of reverse cycles), applied loads, angular travel, spring rate, and in some cases linearity, hysteresis, and center shift.

The flexural pivot can perform its function without any sort of lubrication and does so with the complete absence of material rolling or rubbing. Thus the "space welding" phenomenon, lubrication, evaporation, and other problems associated with vacuum environment are eliminated.

Other design and performance features include:

1) No internal fretting corrosion, because there are no rolling or sliding parts.

2) Substantially stable performance over wide temperature ranges with various materials.

3) Suitability for miniaturization because of the compact design. Pivots are available down to 1/8 inch in diameter.

4) The absence of such variables as lubrication, wear, and backlash, resulting in predictable performance throughout the life of the pivot.

5) High linearity up to 15 degrees (deflection proportional to torque applied).

6) Hysteresis ordinarily negligible for low deflection angles and predictable for higher angles.

7) Insensitivity to dirt.

b. Application to RAE Damper Suspension

Shown in Figure 43 is the proposed suspension system for the RAE damper boom. This suspension system using flexural pivots will be analyzed, and design or application changes will be recommended as required.

The angular travel required of the suspension system has been defined as $\theta_s = \pm$ 35 degrees, with a torsional restraint of

$$8.6 \times 10^{-3} \leqq K_s \leqq 12.5 \times 10^{-3} \quad \frac{ft - lb}{rad}$$

or

$$0.103 \leqq K_s \leqq 0.15 \quad \frac{in - lb}{rad}$$

Referring to Figure 44, the system restraint is determined as follows:

$$K_s = \frac{K_1 K_2}{K_1 + K_2} + \frac{K_3 K_4}{K_3 + K_4} \tag{33}$$

Since $K_1 = K_2 = K_3 = K_4$,

$$K_s = \frac{K^2}{2K} + \frac{K^2}{2K} = \frac{2K^2}{2K} \tag{34}$$

or $K_s = K$ (the system restraint is equal to the individual restraints). In addition it is evident that $X_s = 2X$ (the system deflection is equal to twice the individual spring deflection), or for rotational motion:

$$\theta_s = 2\theta \tag{35}$$

Bendix Cantilever Flexure Pivot 5008-800 has the following characteristics, which make it suitable for this application:

Diameter = D = 0.250 inch

Maximum Deflection = θ_{max} = 30 degrees

Nominal Spring Constant = K = 0.102 in.-lb/rad

Load Capacity in Compression = V_c = 4.2 lb

Load Capacity in Tension = V_t = 14 lb

Material of Construction = AISI 410 or AISI 420 corrosion resistance steel for pivot body; AISI 420 corrosion resistant steel for the flexing elements

Hence this particular pivot would be deflected through 17.5 degrees/30 degrees or about 58 percent of its range. It should also be noted that the nominal spring constant is at the low end of the specified requirement, but this problem can be alleviated in either of two ways: either by selection from a large lot or by slight modifications of the standard design by the manufacturer.

WHERE A V_t CONDITION EXISTS, A V_C CONDITION MAY BE OBTAINED BY ROTATING THE PIVOT 180 degrees, CONVERSELY, A V_t MAY BE OBTAINED FROM A V_C LOADING BY ROTATING THE PIVOT 180 degrees WITHIN THE FIXED MOUNT

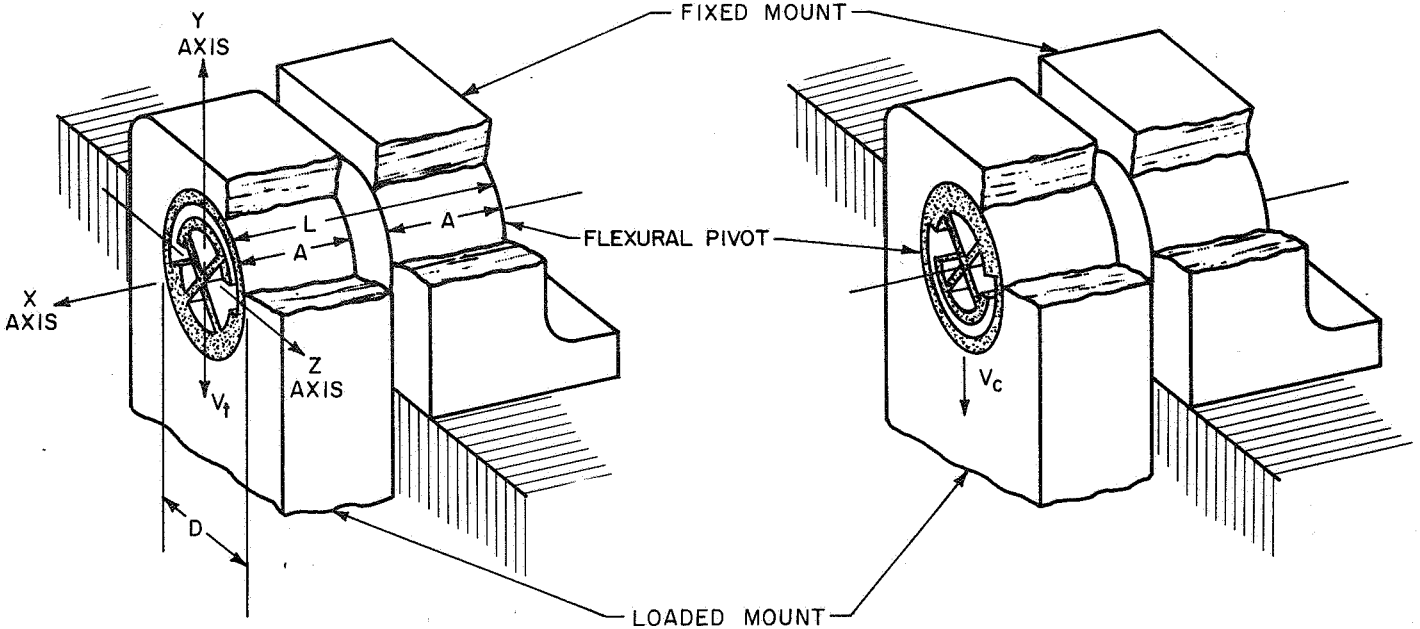

Figure 42 CANTILEVER PIVOTS

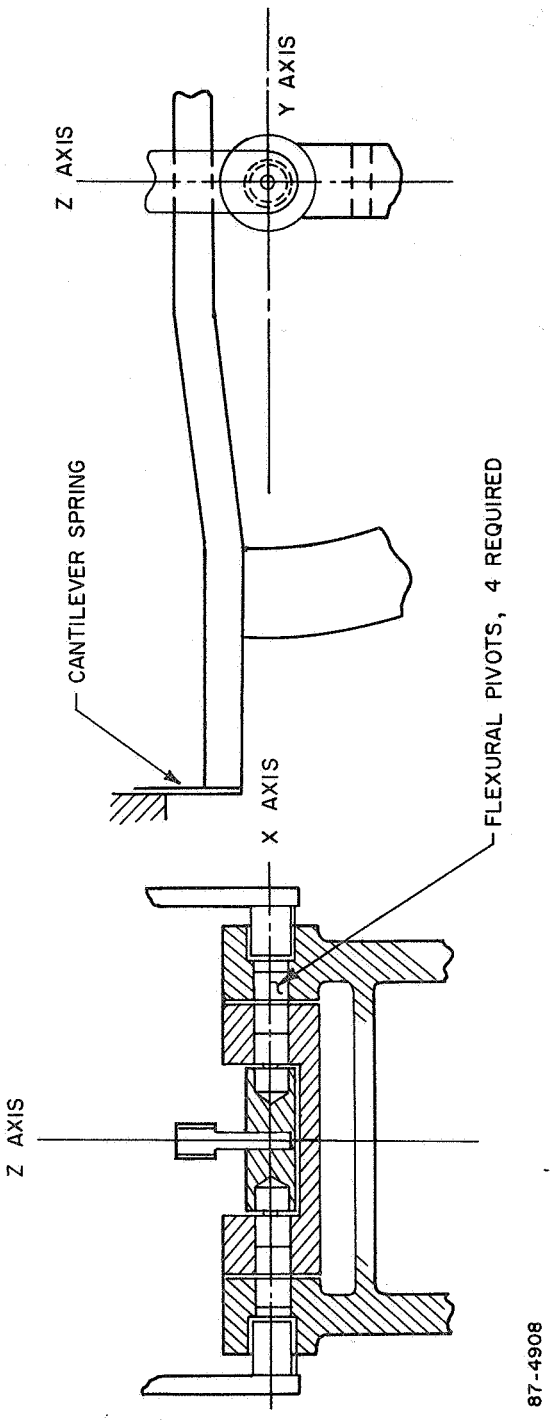

Figure 43 PROPOSED SUSPENSION SYSTEM FOR RAE DAMPER

The "worst case" system loading is depicted in Figure 45. The maximum radial load on a cantilever pivot is approximately 0.5 lb. This value is well below the maximum recommended load in compression or tension. Suspension system radial load V is plotted in Figure 46 for one complete orbit.

The effect of radial loading on pivot spring constant is shown in Figure 47. It is evident that spring constant is a function of orbital position. Spring constant K is plotted as a function of orbital position in Figure 48.

The spring constant is found to vary from 0.092 to 1.22 in.-lb/rad; hence the lower values are out of specification. Figure 49 illustrates how these spring constants compare with the range allowed in the specification.

It is therefore evident that a higher nominal spring constant is required in the flight models.

c. Pivot Life

The dominant factors affecting the life of the pivots are the number of reversal cycles and the radial load.

According to curves published by the manufacturer,[13] the expected pivot life with a constant compression load would be 220,000 cycles. Similar curves are given for tension loading. They again indicate that the expected pivot life would be 220,000 cycles.

Life tests were performed on pivots mounted in the configuration to be used in the reference design. The pivots were subjected to 40,000 cycles of ±35 degrees with a constant 1 lb radial load. Figure 50 shows that there was no significant change in spring constant for the combined pivot assembly over the total length of the test. This performance far exceeds specification requirements.

d. Deflection Angle of Pivots Under Maximum Orbital Load Conditions

Cantilevered flexural pivots deflect as follows:

(at midpoint of cantilever) with a 1 lb V_c load $y = 0.20 \times 10^{-3}$ in.

with a 1 lb V_t load $y = 0.22 \times 10^{-3}$ in.

with V_c max = 0.47 lb, deflection at midpoint is 9.42×10^{-5} in.

with V_t max = 0.43 lb, deflection at midpoint is 9.56×10^{-5} in.

The analogous system is shown in Figure 51a.

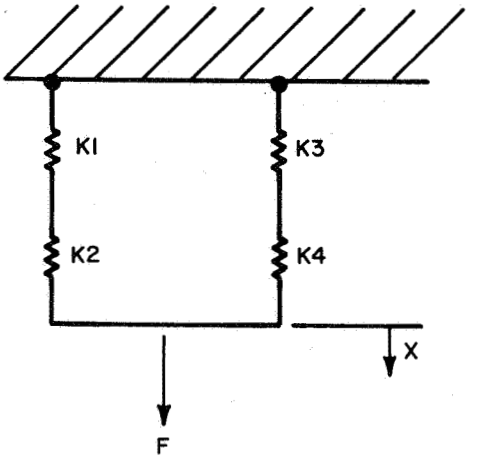

Figure 44 ANALOGOUS SPRING SYSTEM

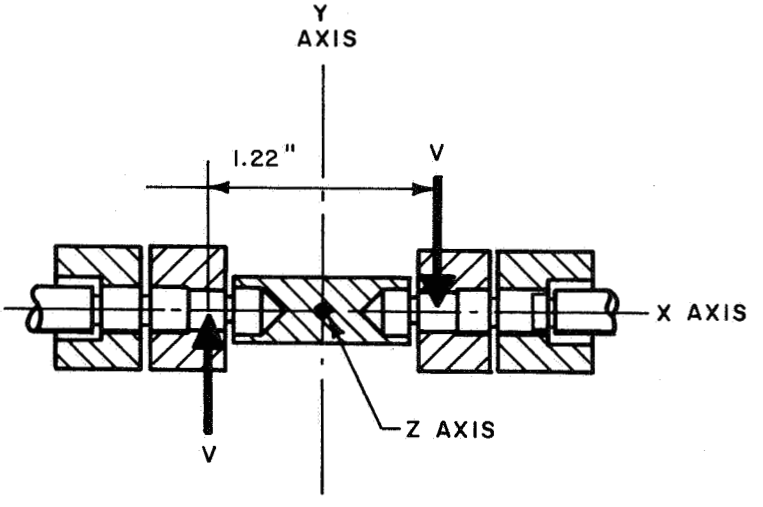

87-4910

Figure 45 SYSTEM LOADING ABOUT Z AXIS

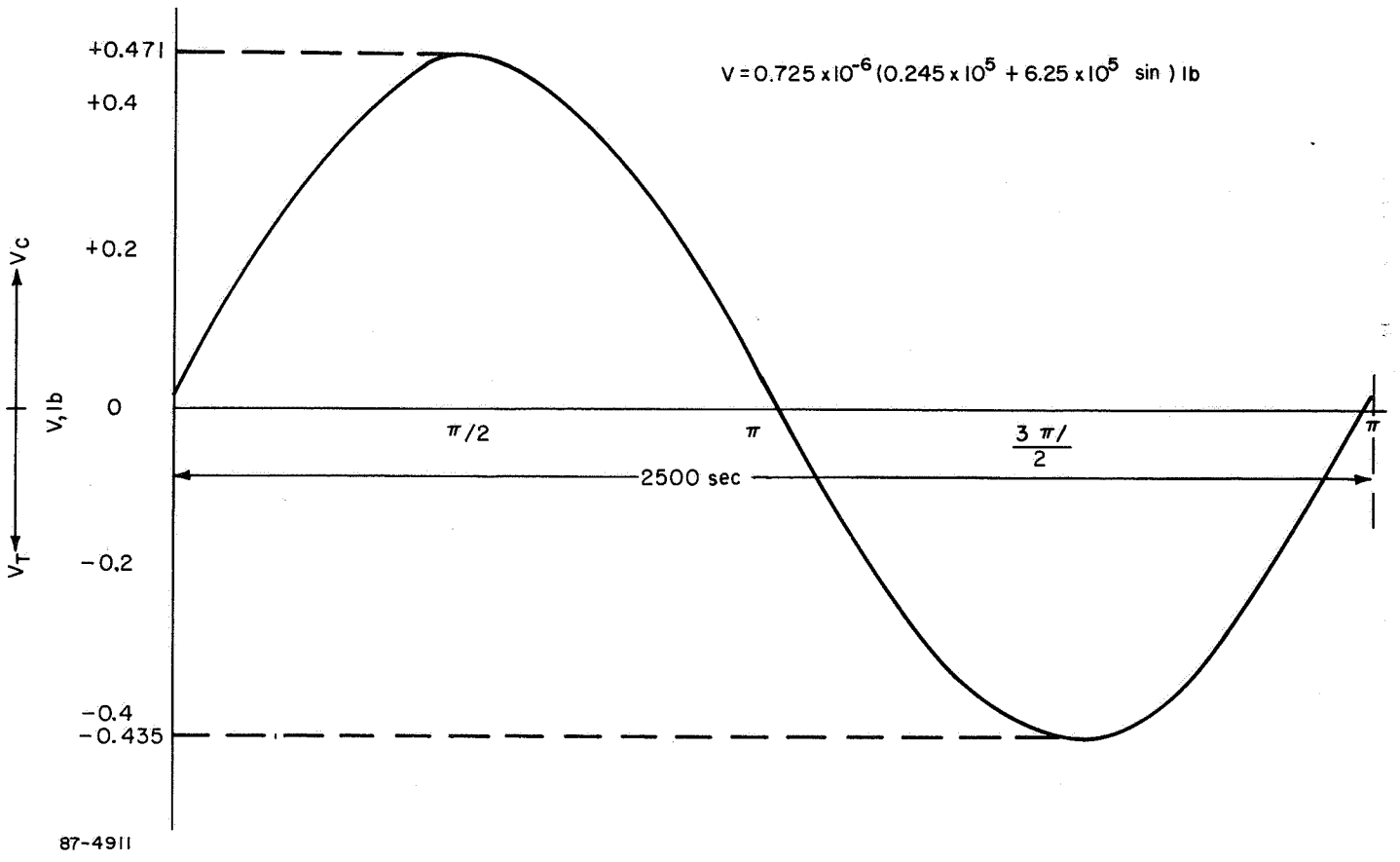

Figure 46 SUSPENSION SYSTEM RADIAL LOAD VERSUS ORBIT ANGLE

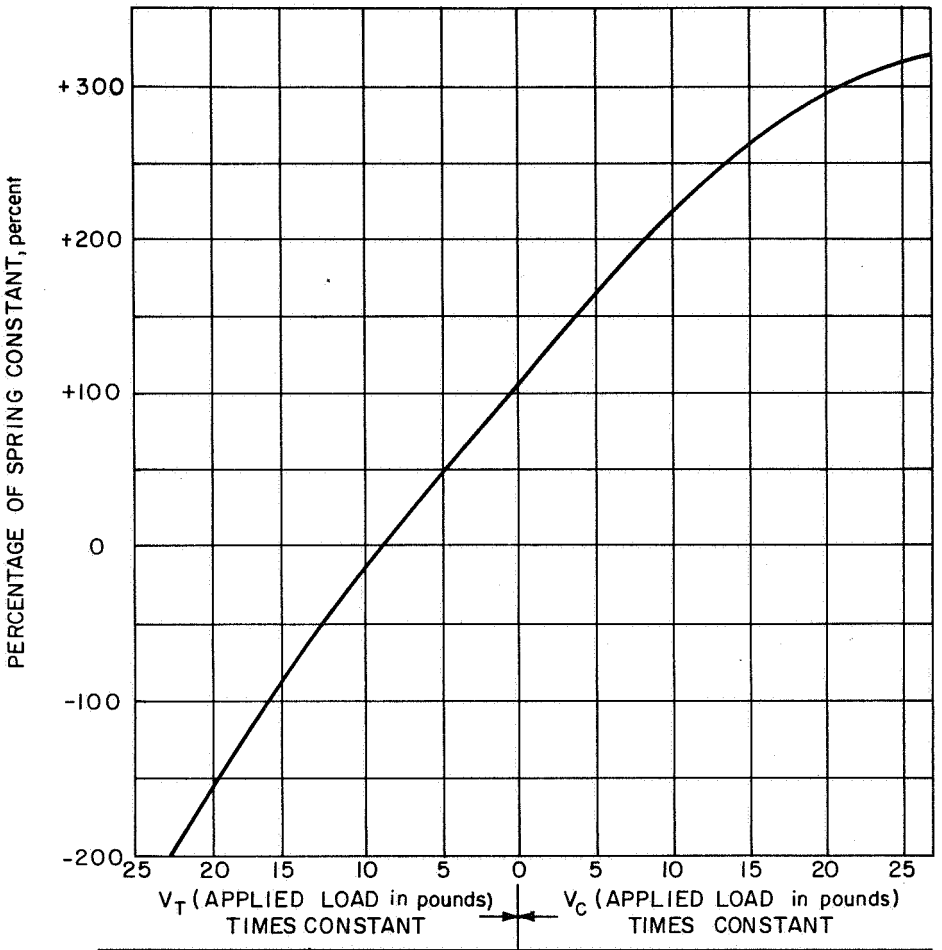

	TABLE OF CONSTANTS		
*PIVOT DIA	FOR ± 30° * *	FOR ±15° * *	FOR ± 71/2° * *
0.1250	11.51	1.2850	0.1601
0.1562	6.41	0.0016	0.1002
0.1875	4.71	0.5885	0.0709
0.2500	2.57	0.3213	0.0402
0.3125	1.60	0.2002	0.0256
0.3750	1.19	0.1437	0.01796
0.5000	0.65	0.0813	0.01016
0.6250	0.40	0.0512	0.00640
0.7500	0.29	0.0359	0.00449
0.8750	0.22	0.0265	0.00331
1.0000	0.16	0.0203	0.00254

* In inches.

**Represents maximum angle of pivot type. Used angle can be less. Curve valid for only standard pivots as defined herein.

87-4912

Figure 47 EFFECT OF RADIAL LOAD ON SPRING RATE

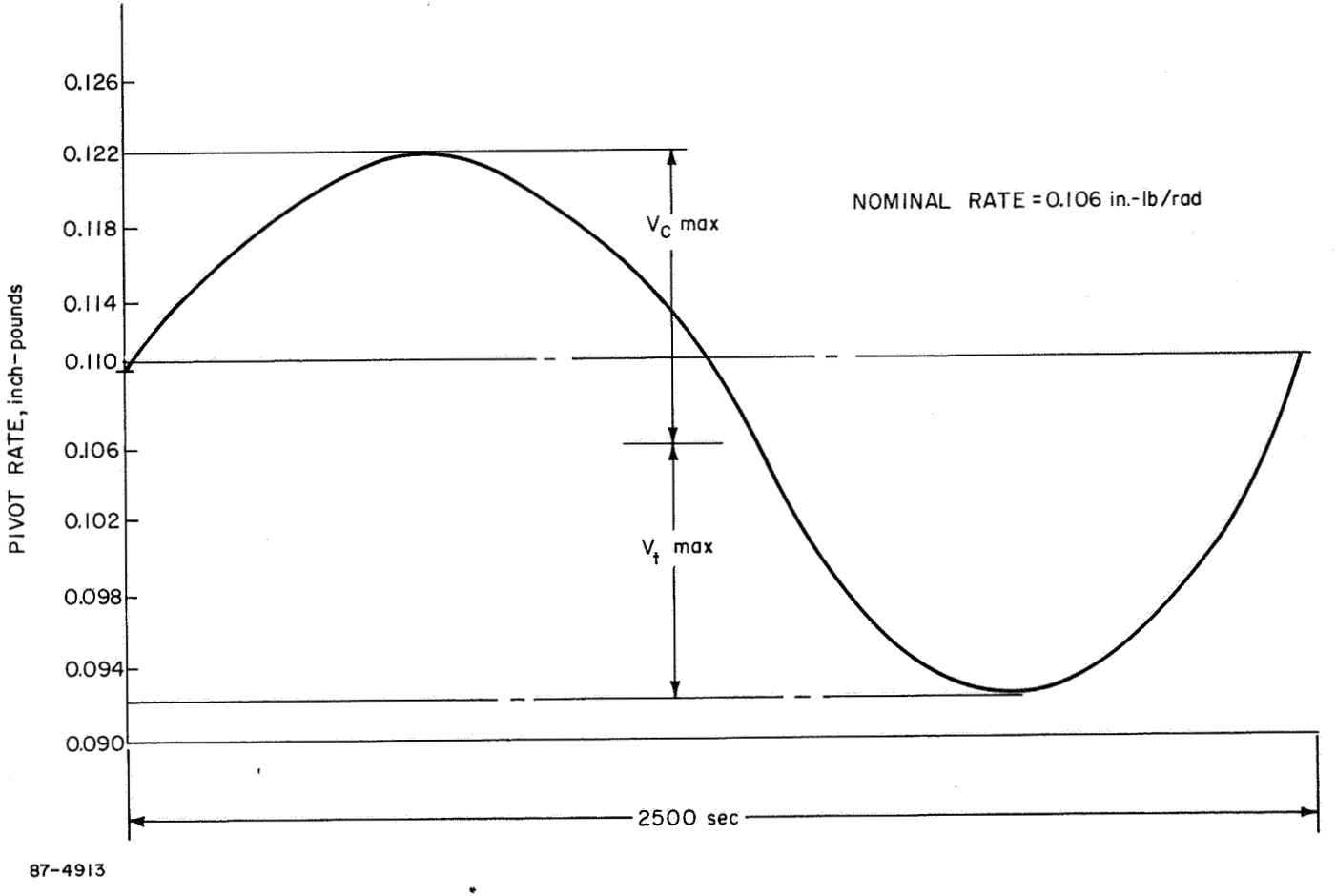

Figure 48 PIVOT SPRING CONSTANT VERSUS ϕ

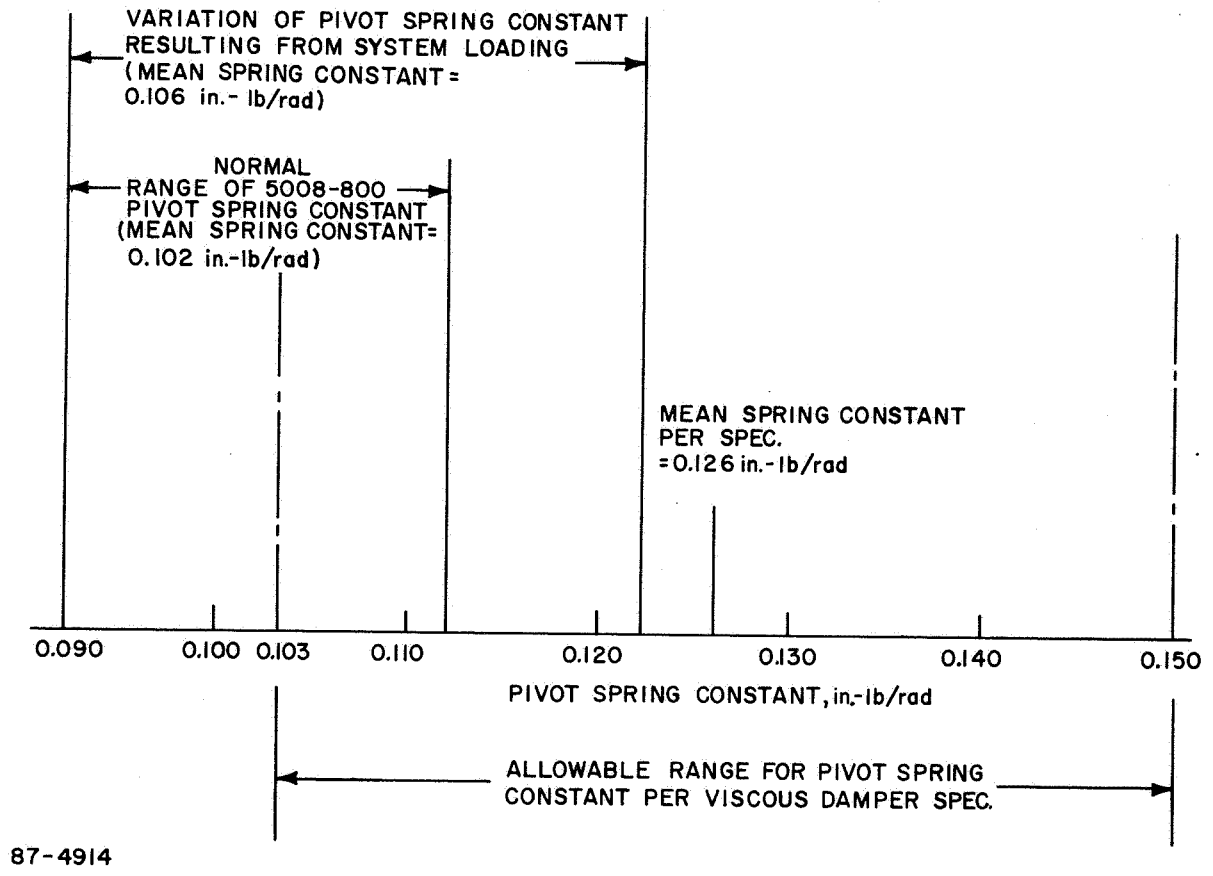

Figure 49 PIVOT SPRING CONSTANT RANGE

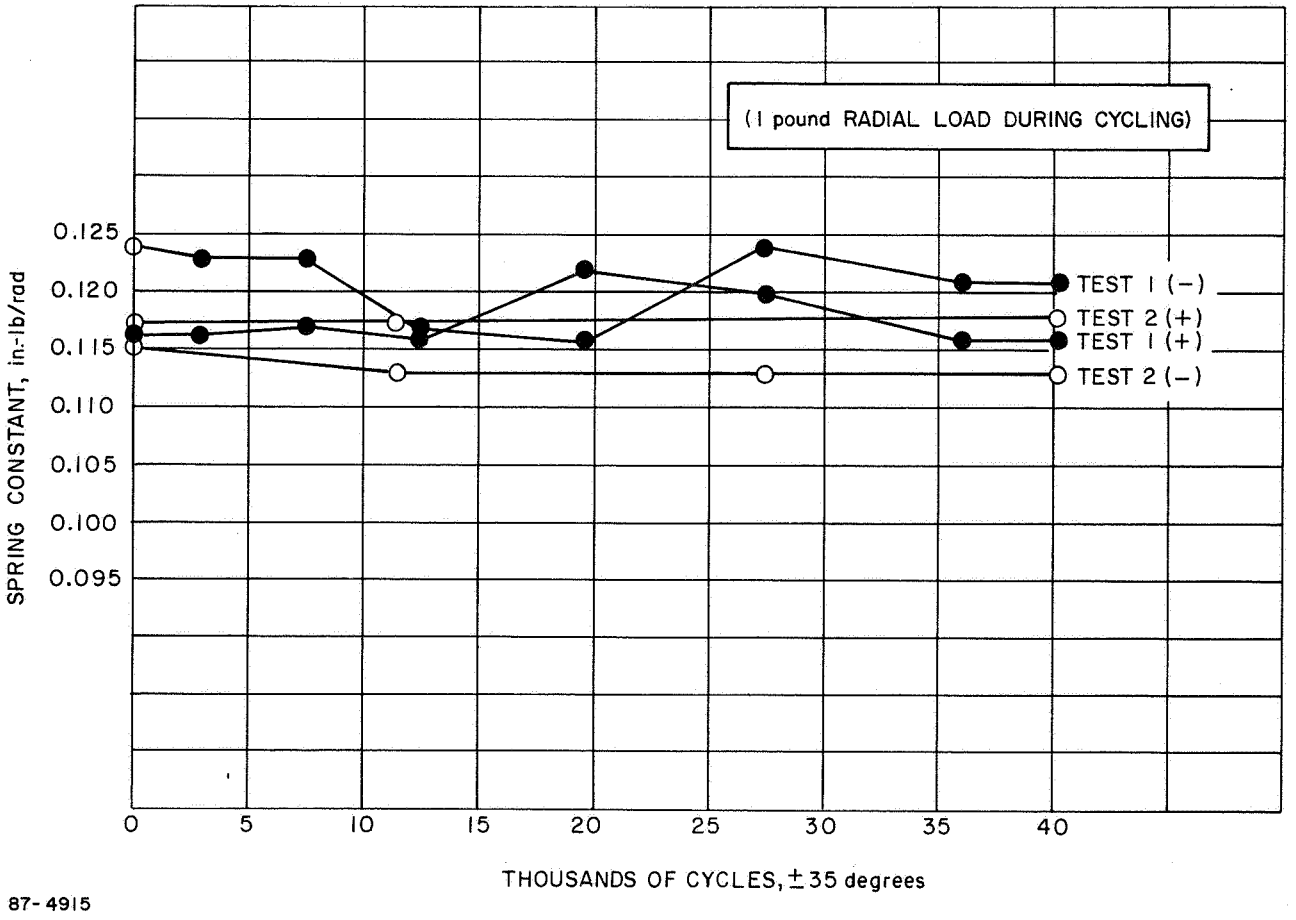

Figure 50 FLEX PIVOT LIFE TEST

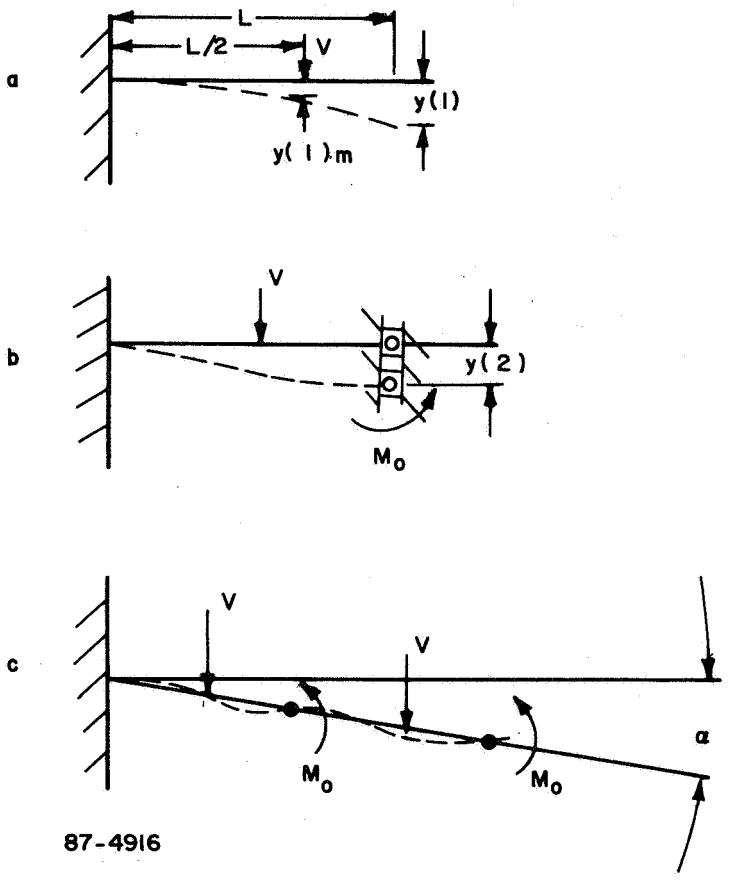

Figure 51 DEFLECTION ANGLE OF PIVOTS UNDER MAXIMUM LOAD CONDITIONS

In the RAE application, however, a moment is applied to the free end, restricting its rotational deflection. The analogous system in this case is shown in Figure 51b.

Comparing midpoint deflections:

$$y\,(1) = \frac{5}{48}\ \frac{VL^3}{EI} \quad for\ (1) \tag{36}$$

$$y\,(2) = \frac{5}{48}\ \frac{VL^3}{EI} - \frac{M_o L^3}{2\,E\,I} \quad for\ (2) \tag{37}$$

$$\text{or} \quad y\,(2) = \left(1 - \frac{24}{5}\ \frac{M_o}{V}\right)\ y\,(1) \tag{38}$$

Letting $V = 0.435\ lb$

and $y\,(1)\,m\ at\ midpoint = \frac{VL^3}{24\,EI}$

$$\text{or} \quad y\,(1) = \frac{5}{2}\ y\,(1)\,m = \frac{5}{2} \times 0.956 \times 10^{-4} = 2.38 \times 10^{-4}\ in.,$$

then,

$$y\,(2) = \left(1 - \frac{24 \times 0.01}{5 \times 0.435}\right)\ (2.38 \times 10^{-4})\ in. \tag{39}$$

$$y\,(2) = 2.12 \times 10^{-4}\ in.$$

where M_o = 0.01 in.-lb (minimum realistic value),

For two cantilever pivots in series, the moments and deflections are shown in Figure 51c:

$$\tan \alpha = \frac{2\,y(2)}{2L}$$

$$\tan \alpha = \frac{2(2.12 \times 10^{-4})}{2\,(0.21)} = 0.001\ rad \tag{41}$$

The maximum allowable angular displacement is 2 degrees according to the viscous damper specification, hence this requirement is satisfied.

e. Recommended Mounting Techniques

Figure 42 shows the orientation of the pivots for optimum performance. The recommended methods of mounting the pivots are shown in Figure 52. In the first method, dowel pins are used and the mounting hole diameters are 0.0005 to 0.0015 inch larger than the pivot diameter. The dowel pin holes are drilled and reamed at the time of assembly.

The second mounting method uses a mounting hole 0.001 to 0.003 inch larger than the pivot diameter. The larger clearances are applicable to the larger pivots only. Screw length must be controlled to prevent interference with flexures.

The third mounting method uses mounting hole diameters 0.005 to 0.0015 inch larger than the pivot diameter. The set screw locks into a drill point with a 120 degree included angle.

f. Effect of Cantilever Spring

The cantilever suspension of the damping mechanism is shown in Figure 53; the dimensions and applied forces are also shown in this figure. In this case F_P is applied normal to V_c or V_t, where F_P is the reaction force on the flexural pivots due to the caging load. A maximum recommended value for F_P is 0.50 lb. (Note from Figure 43 that the load is split between the two pivots in parallel.)

Then:

$$F_s = 10.7\ F_P = 10.7\ (0.5) = 5.35\ lb\ max \qquad (42)$$

Note that $F_s = K_s X_s$, where X_s is the spring deflection determined from the system geometry.

g. Linearity and Hysteresis

Both linearity and hysteresis are secondary factors in this application. They are inherent characteristics of a selected pivot. The linearity for a Bendix 5008-800 (0.250 inch diameter) flexural pivot is:

15 degree deflection -- 2 percent max

20 degree deflection -- 3 percent max

The hysteresis of a typical cantilevered flexural pivot is approximately ± 0.5 percent.

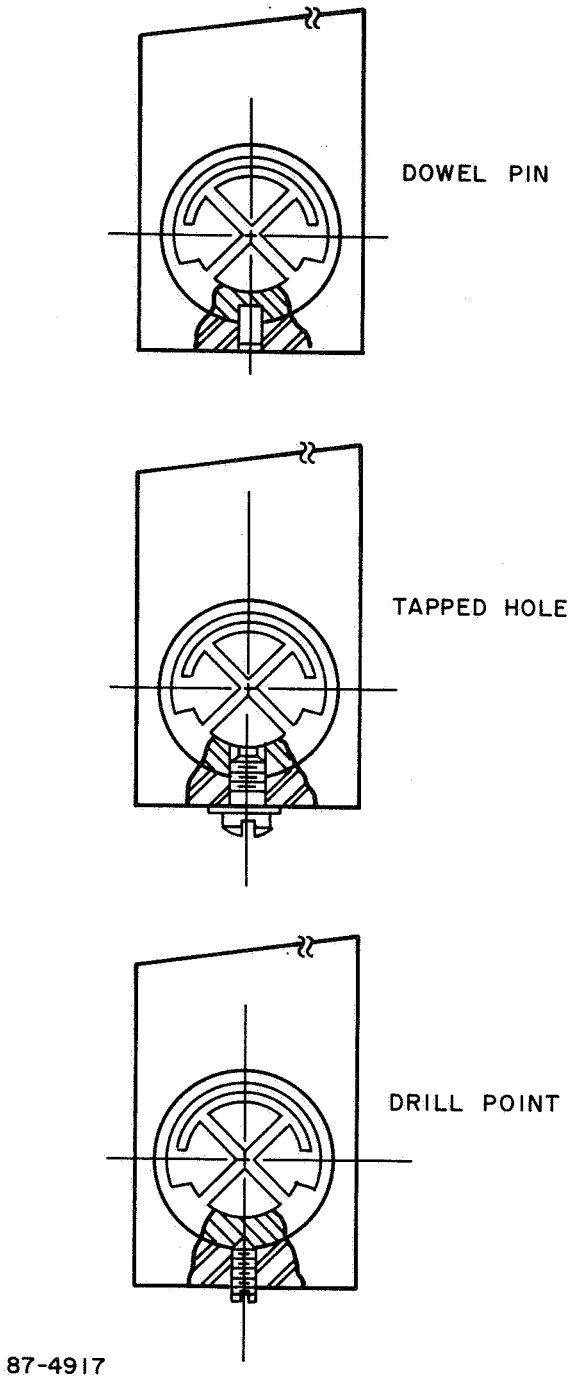

Figure 52 PIVOT MOUNTING TECHNIQUES

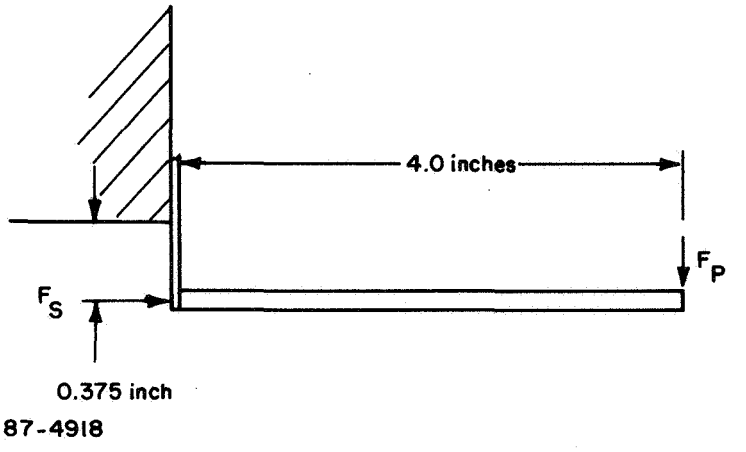

Figure 53 CANTILEVER SUSPENSION SCHEMATIC

2. Jewel-Pivot Suspension

Hollow, cylindrical jewels, and spherical metal pivots are commonly used as floated gyro suspensions where insignificant loads are carried by the suspension. This type of suspension requires very close machining tolerances and complex adjustment mechanisms for alignment. Because of the small load carrying capability of jewel pivots and the complicated mounting mechanism required, this type of suspension is not recommended for the damper suspension.

3. Ball Bearing Suspension

The application of miniature precision bearings as the support for the viscous damper is highly practical, since the torsional restraint of the system is of much greater magnitude than the frictional torque level. The major drawback for use on this application is the bearing lubrication in a space vacuum of 10^{-10} torr or less. State-of-the-art space lubrication methods will be discussed in this portion of the report.

a. Effect of Bearing Friction Torque

The system torsional restraint is given as

$$11.9 \times 104 \leqq K_s \leqq 17.2 \times 10^4 \quad \frac{dyne\text{-}cm}{rad} \tag{43}$$

Assume that a 10^{-2} radian uncertainty is acceptable. The allowable bearing frictional torque is then $r_f \leqq 1190$ dyne-cm.

b. Selection of Single or Double Bearing Suspension

The maximum operational radial torque on the suspension support is

$$r_Z = 22{,}000 + 625{,}000 + 2{,}500 = 6.5 \times 10^5 \ dyne\text{-}cm \tag{44}$$

Other loading is negligible.

Figure 54 depicts loading in a single bearing suspension application. It is seen that this couple of 6.5×10^5 dyne-cm is similar to an axial preload, and it will be treated as such for this analysis.

A single Barden RO deep groove bearing is used for analysis purposes. This bearing, the smallest available in the miniature instrument bearing range, has static load ratings of

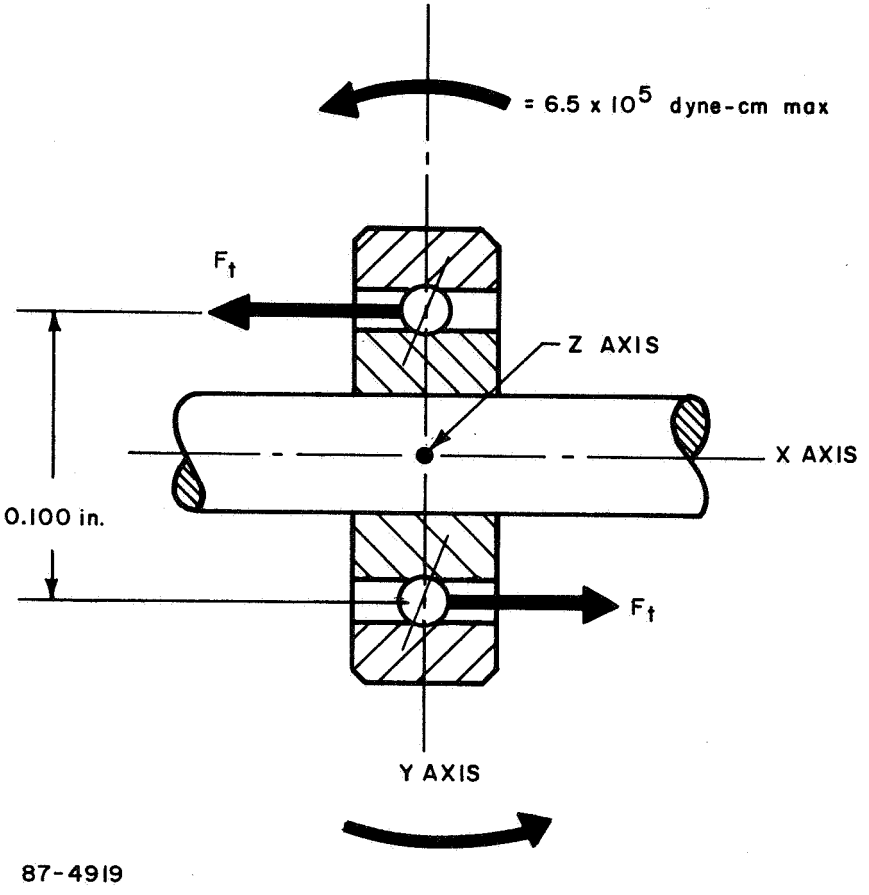

Figure 54 SINGLE BEARING SUSPENSION

T_o = *Thrust* = *12 lb*

C_o = *Radial* = *7 lb*

The torque r_Z is equivalent to

$$r_Z = 0.1\ F_t \tag{45}$$

$$F_t = \frac{6.5 \times 10^5\ \text{dyne-cm}}{0.1\ \text{in.} \times 2.54\ \text{cm/in.}} = 25.6 \times 10^5\ \text{dynes}$$

where F_t = an axial preload of 5.7 lb.

This axial preload is considered high for this type of bearing even though it is below the static load ratings. If a single bearing is used as the suspension, the R144 size is recommended:

OD = 0.250 inch

ID = 0.125 inch

Ball Circle = 0.211 inch

r_Z = 0.211 inch

$$F_t = \frac{6.5 \times 10^{-5}\ \text{dyne-cm}}{0.211 \times 2.54} = 1.22 \times 10^6\ \text{dynes} = 2.73\ \text{lb}$$

Static Thrust Load Rating = 22 lb

Static Radial Load Rating = 13 lb

If a pair of bearings is used, the Barden RO size will be adequate. According to Figure 55, r_Z imparts a radial load on the bearings:

$$F_r = \frac{r_Z}{2.54} \tag{46}$$

$$F_r = \frac{6.5 \times 10^5\ \text{dyne-cm}}{2.54} = 2.56 \times 10^5\ \text{dynes} = 0.576\ \text{lb}$$

Running torques are given in Figure 56 as a function of radial or thrust load under normal environmental operating conditions with light oil lubrication.

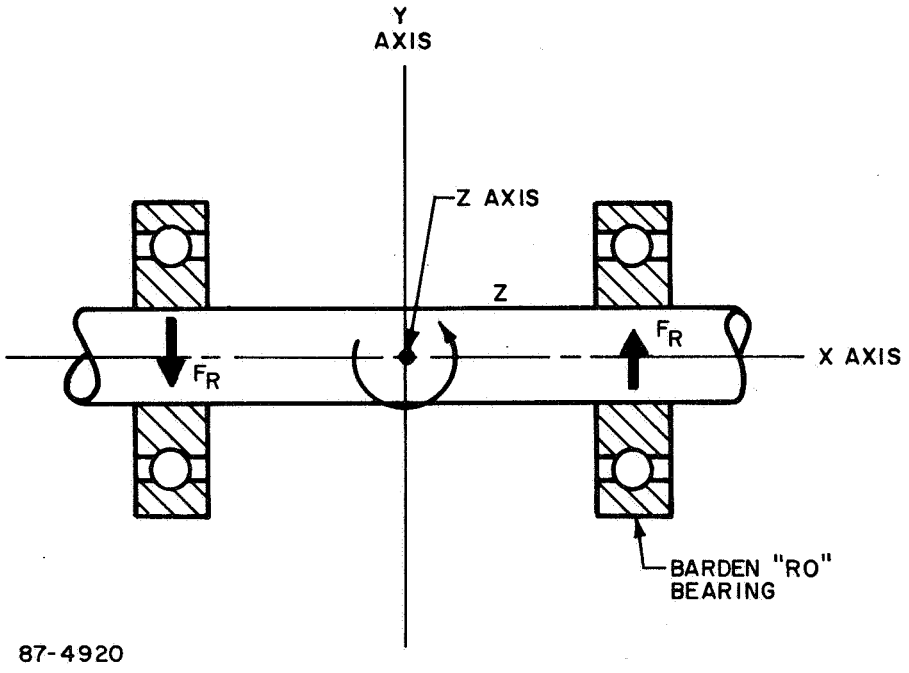

Figure 55 DOUBLE BEARING SUSPENSION

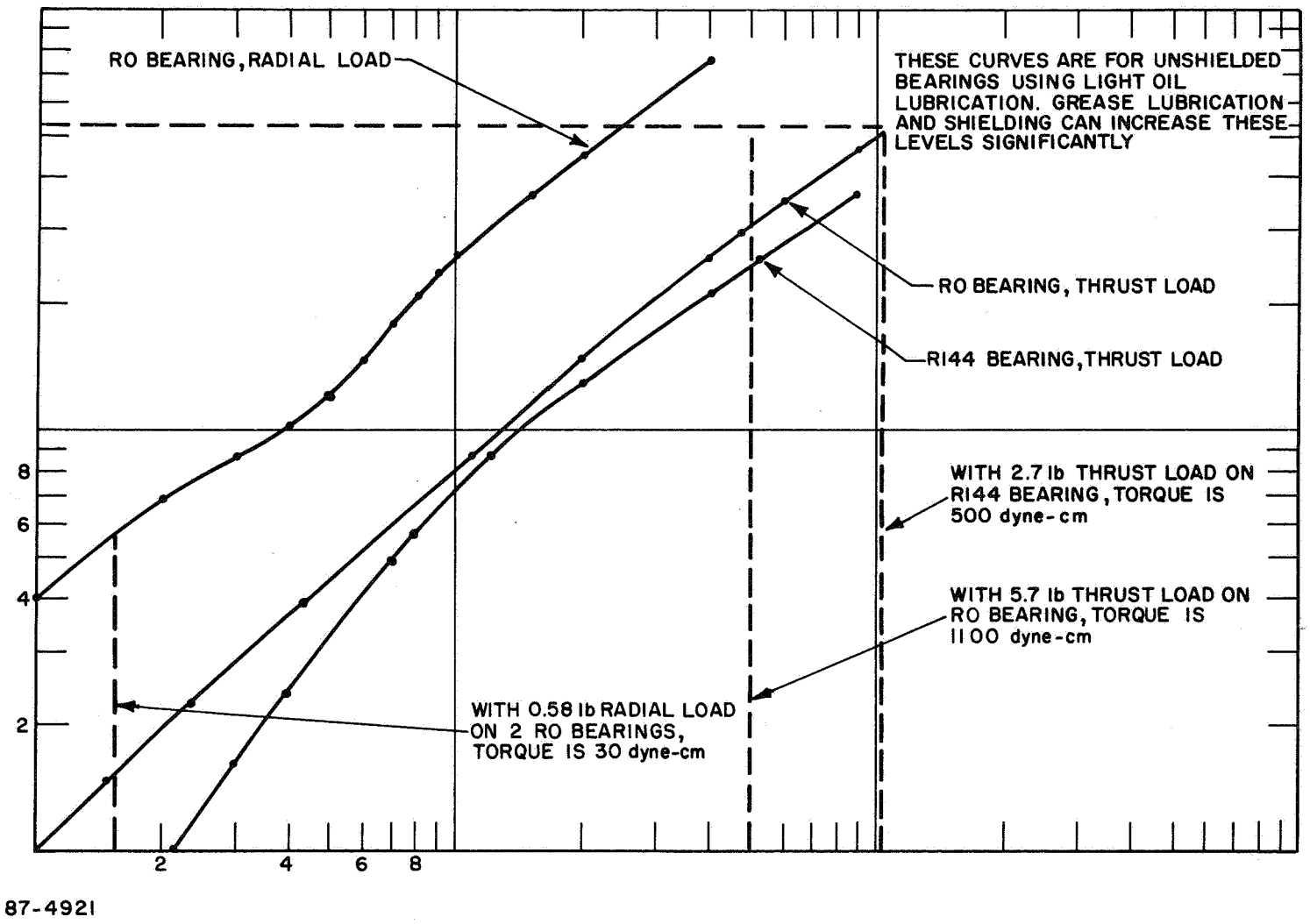

Figure 56 RUNNING TORQUES

c. Effect of Space Environment

The high vacuum of space will tend to degrade the bearing lubrication (i.e., increase the bearing frictional torque) because of evaporation of the lubricant. The difficulties in providing lubrication can be met in several ways. The effects of vacuum, for instance, can be overcome by sealing the bearing in a hermetic unit, or forced feed lubrication can be used to replenish the bearing periodically. However, weight and complexity restrict the use of these means -- especially in this case, where the damper boom is exposed to space and a flexible seal would be required.

Since the damper will be subjected to a one-year orbital environment plus the additional time accumulated during operational tests and checks, reduction of wear is a prime objective along with minimizing frictional torque.

Of the available lubricants, either Versilube 6-300 grease or Aeroshell 15 grease (Mil-G-25013, 27343) will do an adequate job in the specified environment, providing the bearing has double metal shields. Also applicable is Versilube F-50 oil, which is vacuum impregnated into a phenolic retainer, and the bearing is double shielded. The conditions of use of the above recommended lubricants are as follows:

Temperature: -65° F to 225° F

Speed: to 8000 rpm

Size: 2 inches OD or less

Pressure: Ambient to 10^{-9} torr

Operating Life: 1 year of continuous operation

Radiation: 1×10^{6} rads

The F-50 oil gives very low starting torques at low temperatures. Providing that adequate lubrication is supplied to the bearing throughout its life cycle, the frictional torque values at extremely low pressures should approximate those at normal environmental conditions.

4. Sleeve Bearing Suspension

a. Bearing Lubricants

A number of dry solid lubricants provide low frictional torques under light loading. These solid lubricants, such as molybdenum disulfide and Teflon, do not lose their lubricity in a hard vacuum and normally are not affected by radiation. (They can be rubbed into hard metal surfaces or reinforced plastics, i.e., phenolics.)

In addition, Teflon, which has the lowest friction coefficient of any solid, has recently been strengthened by the incorporation of fillers and the addition of MoS_2 for about 10 times better wear resistance. (MoS_2 has the second lowest friction coefficient of any solid.) Kinetic friction coefficients of 0.03 have been observed for this reinforced Teflon; however, a friction coefficient of 0.05 is more realistic.

A variety of these reinforced Teflon compositions are available commercially from different manufacturers. These include Bartemp (Duroid 5813) from Barden Corporation and Rulon C from Dixon Corporation. These dry lubricants provide satisfactory operation for one-year orbits at 500 to 600 mile altitudes, as discussed in Reference 15.

b. Frictional Torque Levels

The maximum frictional torque level acceptable for a 10^{-2} radian (1/2 degree) uncertainty is f = 1190 dyne-cm.

Given a shaft diameter of 0.125 inch, a spacing between sleeve bearings of 2 inches, and a coefficient of kinetic friction of 0.05, the torque would be

$$\tau_Z = 6.5 \times 10^5 \text{ dyne-cm} \tag{47}$$

$$F_{SB} = \frac{6.5 \times 10^5}{2 \times 2.54} = 1.28 \times 105 \text{ dynes} = 0.288 \text{ lb} \tag{48}$$

$$\tau_{SB} = 0.125\ (0.05)\ (0.288) = 18 \times 10^{-4} \text{ lb-in.} \tag{49}$$

$$= 2070 \text{ dyne-cm}$$

This value exceeds the maximum allowable by about 2 to 1, so either the shaft diameter must be halved or the bearing spacing must be doubled.

5. Torsion Wire Suspension

The damper boom can be suspended from the satellite by means of torsion wires. With an initial tension on the wires, the damper boom is suspended and is restricted from rotating more than a specified angle (± 2 degrees) about the Z axis.

The rotational stiffness of the torsion wires depends on the length and diameter of the wire used.

a. Determination of Wire Torsional Stress

The basic formulas are as follows:

T = twisting moment

L = length of the wire

r = radius of the wire

J = polar moment of inertia of the section

S_s = shear stress

θ = angle of twist (radians)

G = modulus of rigidity of the material

Then,

$$\theta = \frac{TL}{JG} \tag{50}$$

$$S_s = \theta\, Gr/L \tag{51}$$

b. Determination of Wire Tensile Stress

Figure 57 is a loading diagram about the Z axis. From this diagram:

$$\Sigma\, \tau_A = 0 = \tau_Z - 2\,[T_2\,(L_1 + R_1)(\sin\phi)] \tag{52}$$

$$T_2 = \frac{\tau_Z}{2(L_1 + R_1)\sin\phi} = S_{T_2} A \tag{53}$$

$$S_{T_2} = \frac{\tau_Z}{2A(L_1 + R_1)\sin\phi} \tag{54}$$

where $R_1 \sin\alpha = \tan\phi\,(L_1 + R_1(1 - \cos\alpha))$

$$\tan\phi = \frac{R_1 \sin\alpha}{L_1 + R_1(1 - \cos\alpha)}$$

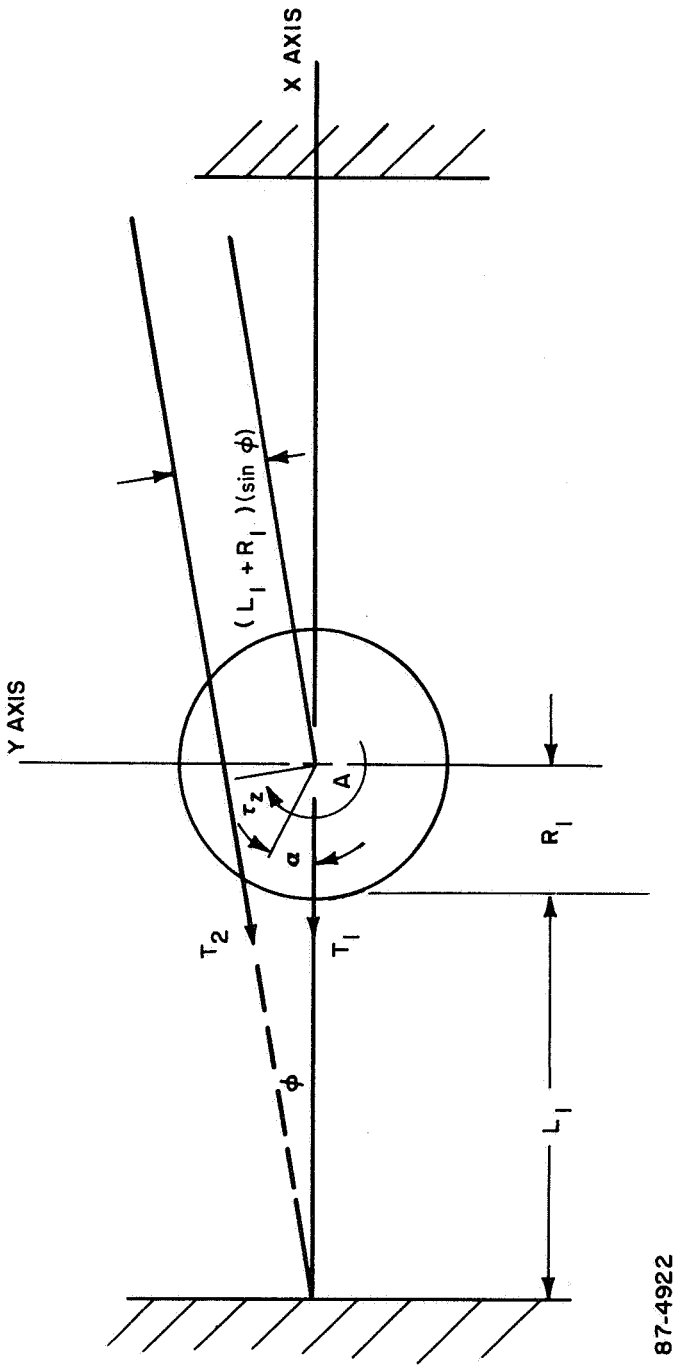

Figure 57 TORSION WIRE LOADING DIAGRAM

$\tan \phi \approx \sin \phi$ *for small* ϕ

Hence

$$S_{T_2} = \frac{r_Z \left[L_1 + R_1 (1 - \cos a)\right]}{2A (L_1 + R_1) R_1 \sin a} \qquad (55)$$

The total wire tensile stress is

$$S_T = S_{T_1} + S_{T_2}$$

S_{T_1} = Initial tensile stress prior to rotation about the Z axis

S_{T_2} = Tensile stress resulting from damper rotation about the Z axis

c. Determination of Wire Length and Diameter

Torsional restraint = $K = \frac{JG}{L} = 63.5 \times 10^{-3}$ in.-lb/rad (per wire) for steel of $G = 12 \times 10^6$ psi, $L = 2.96 \times 10^8 \, r^4$. Figure 58 plots L versus r, where L = the length of the wire and r = the radius of the wire, both in inches.

For this application, music wire is recommended. This is a high grade spring wire extensively used for small springs subjected to high stresses. Music wire is more expensive than ordinary hard-drawn wire, but it can be subjected to higher stresses. Wire length versus wire diameter for standard gage sizes of music wire are shown in Figure 58. The tensile strength is about 250,000 psi.

The torsional stress for wire gages 3, 4, 6, 7, and 8 is given in Table XXII, where $S_s = \frac{\theta G r}{L}$.

TABLE XXII

TORSIONAL STRESSES FOR TORSION WIRES

S_s (psi)	Gage No.	Length (inches)
97.5×10^3	3	0.45
68.0	4	0.75
48.7	6	1.20
35.5	7	1.85
25.2	8	2.90

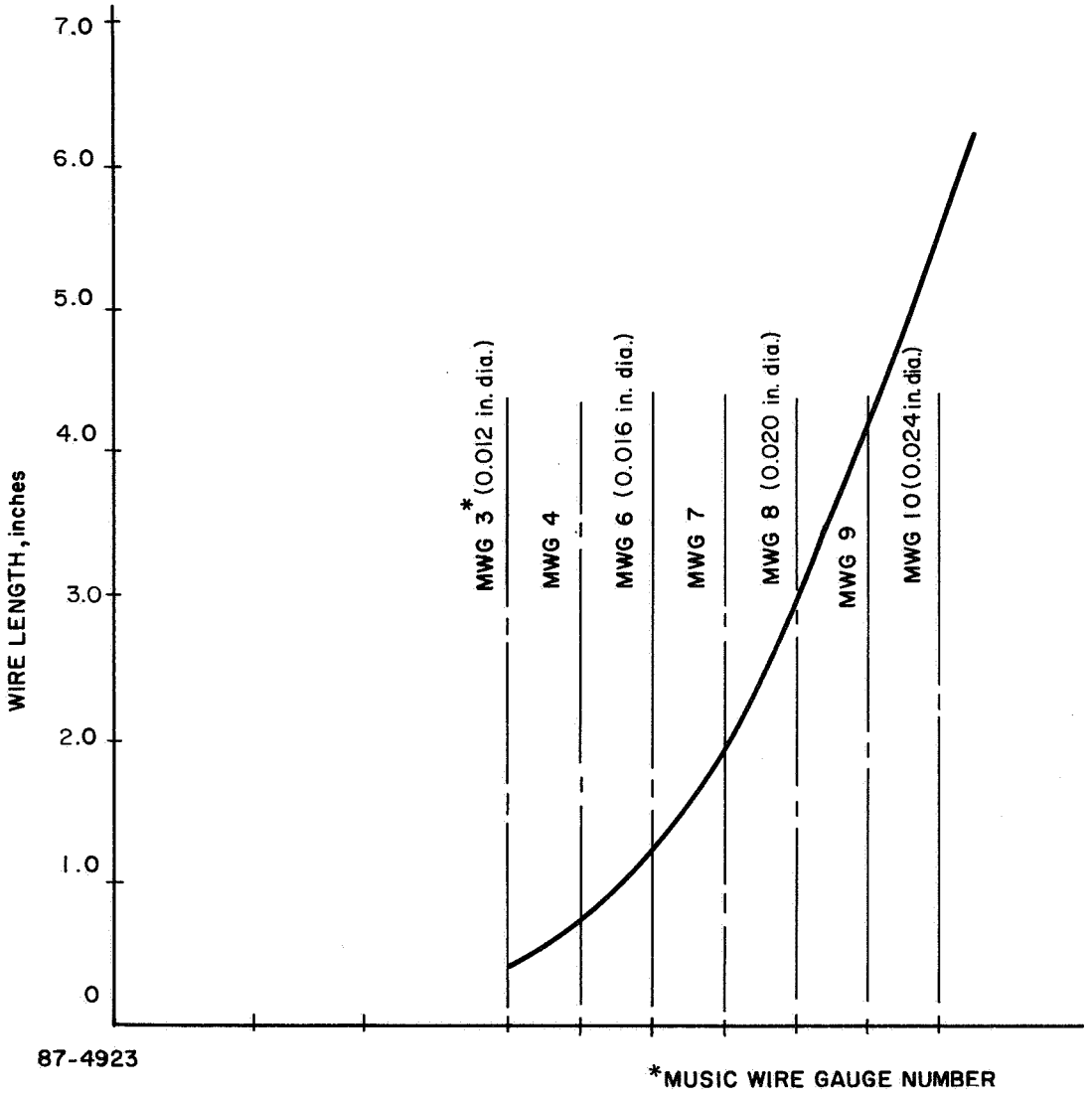

Figure 58 WIRE LENGTH VERSUS WIRE DIAMETER

The wire tensile stress is given below where

$\frac{r_Z}{2}$ = 0.36 in.-lb

L_1 = (See Table XXII)

R_1 = 1.5 inches (design requirements)

A = πr^2 (See Table XXII)

a = 2 degrees, $\cos a = 1$, $\sin a = 0.035$

$$S_{T_2} = \frac{2.18\ L_1}{(L_1 + 0.5)\ r^2}$$

Table XXIII lists the tensile stresses S_{T_2} for the previously denoted wire sizes.

TABLE XXIII

TENSILE STRESSES FOR TORSION WIRES

S_{T_2}(psi)	Gage No.	Length (inches)
28.7×10^3	3	0.45
26.7	4	0.75
24.1	6	1.20
21.2	7	1.85
18.6	8	2.90

An initial preload tension on the wires is required for support and for preventing a rotation of 2 degrees during the orbital dynamic loading. This preload tensile stress should not exceed 10,000 psi for the wire size used in this report.

The critical stress points are those on the outer surface of the wire. Combining the torsional and axial stresses yields the principal tensile stress:

$$S = \frac{S_{T_1} + S_{T_2}}{2} + \sqrt{\left(\frac{S_{T_1} + S_{T_2}}{2}\right)^2 + S_s^2} \qquad (56)$$

Principal tensile stress plus safety margins are given below for various wire gages and lengths:

Wire Diameter (inches)	Wire Length (inches)	Principal Tensile Stress (psi)	Ultimate Strength (psi)
0.012	0.45	119,450	250,000
0.014	0.75	91,135	250,000
0.016	1.20	71,395	250,000
0.018	1.85	54,400	250,000
0.020	2.90	43,300	250,000

d. Fatigue Life of Torsion Wires

The torsion wire fatigue life is difficult to analyze unless some basic assumptions are made. This conservative "worst case" analysis takes the following points into consideration:

1) The torsional shear stress and the tensile stress in the wire are both cyclic, at two different frequencies. Hence for a "worst case" assumption, let the torsional shear stress be in phase with the applied torque about the Z axis (τ_Z).

2) The applied torque about the Z axis:

$$\tau_Z = \tau_{ss1} + \tau_{ss2} \pm \tau_s \tag{57}$$

$$= 22 \times 10^7 + 2.5 \times 10^7 \pm 6.2 \times 10^5 \sin 2\pi ft$$

$$= 0.245 \times 10^5 \pm 6.2 \times 10^5 \sin 2\pi ft$$

$$\tau_{Z\,max} = + 6.445 \times 10^5 \text{ dyne-cm} \tag{58}$$

$$\tau_{Z\,min} = -5.955 \times 10^5 \text{ dyne-dm} \tag{59}$$

Since the difference is less than 10 percent assume a torque amplitude of $\tau_Z = 6.445 \times 105 \sin 2\pi ft$. From (1) and (2) it is evident that the principal tensile stresses correspond to those given for the various wire sizes.

Since the frequency of the applied torque about the Z axis is 4×10^{-4} cps, the wire is subjected to the following number of principal tensile stress reversals:

$$N = 126 \times 10^2 = 1.26 \times 10^4 \text{ cycles/year} \quad (60)$$

The appropriate S-N curve is shown in Figure 59.

Since F_F= 119, 450 psi, none of the wires in D will fail in fatigue.

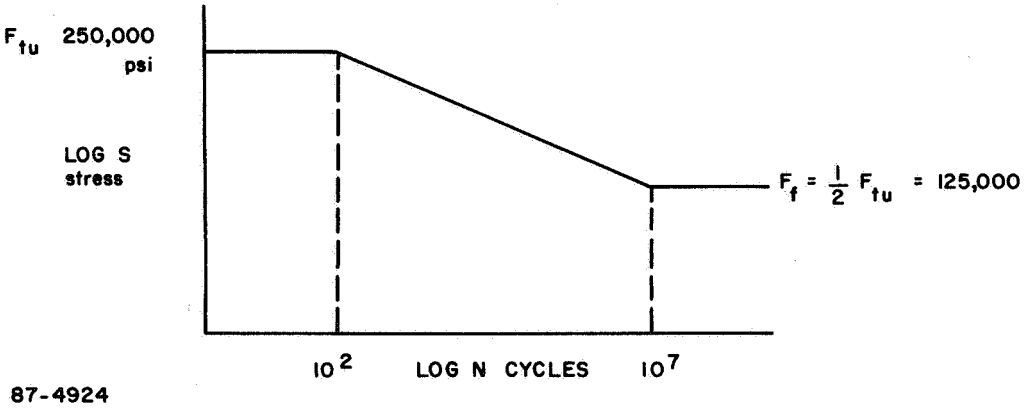

Figure 59 TORSION WIRE STRESS VERSUS TEST CYCLE

6. Suspension Tradeoff Studies

The most significant features of each of the five suspension mechanisms are compared below, and one mechanism is selected for the reference design. The design features are listed in Table XXIV for convenient reference.

a. Ball Bearings

A ball bearing suspension system could be easily integrated into a suspension design along with a spiral torsional spring. The smallest available instrument bearings are satisfactory for this application, since the dynamic loading effects are relatively small. The main disadvantage is the possible loss of lubrication in a hard vacuum. Sufficient data regarding space lubrication is not yet available, and hence the reliability of a ball bearing suspension would be questionable. The loss of lubrication not only could seriously affect bearing life, but also could increase frictional torque to an unacceptable level during orbital operation.

TABLE XXIV

SUSPENSION DESIGN FEATURES

Suspension Mechanism	Design Description	Size	Material	Weight	Availability and Cost	Caging	Design Implementation	Lubrication	Frictional Levels	Life	Hysteresis and Linearity	Rotational Stiffness About Z Axis
Ball Bearings	Miniature instrument bearings, low torque, low speed, deep groove, pressed steel retainers, oil lubrication, double shielded, either single or double bearing suspension applicable, spring required	For single bearing suspension, use R144 size (0.125 bore, 0.250 OD); for double bearing suspension, use RO size (0.0469 bore, 0.156 OD)	Rings and ball: corrosion resistant A151440C stainless steel; Retainers: hardened pressed stainless steel	RO at 0.0003 lb R144 at 0.0007 lb	2 week delivery, $2.50 per bearing for large quantities	Required during launch and powered flight	Easily implemented into a suspension design	Versilube 6-300 grease, Aeroshell 15 grease (MIL-G-25013), Versilube F-50 oil	With oil lubrication: R144, 500 dyne-cm; RO, 30 dyne-cm (grease lubrication and shields can more than double these values)	1 year orbital life if lubrication is retained	Depends on type of spring used	Excellent
Sleeve Bearings	Fabricated from solid lubricants such as MoS_2 and/or Teflon, spring required, two required for suspension mechanism	0.125 inch inside sleeve bearing diameter, space 4 inches apart	Stainless steel Bartemp (Duroid 5813), Rulon C (these are Teflons with MoS_2 fillers)	Density = 0.074 $lb/in.^3$	Bartemp available from Barden Corp. (6-8 weeks delivery); Rulon available from Dixon Corp. (same delivery)	Required during launch and powered flight	Easily implemented into a suspension design	Do not loose lubricity in a hard vacuum and normally are not affected by radiation	About 1000 dyne-cm for sleeve bearing sizes stated	1 year orbital life with little or no loss of lubricity	Depends on type of spring used	Excellent
Jewel Pivots	Because of dynamic loading effects, brittleness of jewels, complexity of mounting structure, and frictional torques expected, jewel pivots are not recommended for this application.											
Flexural Pivots	Pivot is made of parts of flat crossing springs supporting rotating sleeves in a simple compact package; four required for suspension mechanism; different size combinations can be used to obtain desired torsional restraint	Any of the following combinations gives the desired torsional restraint: two 1/4 inch diameter pivots, with two 5/16 inch diameter pivots; four pivots of the diameter required to give the desired rate	Corrosion resistant steel is standard; however, other materials are available	1 gram per 1/4 inch diameter pivot	1/4 inch pivots: $7.95 for 1 to 300 units off the shelf; 5/16 inch pivots: $16.74 for 1 to 300 units off the shelf; special pivot prices available on request	Required during launch and power flight	Requires accurate dimensional control of pivot support structure to prevent preloads	None Required	None	40,000 cycles for 1/4 inch diameter pivots used with 5/16 inch diameter pivots; 220,000 cycles if 4 1/4 inch diameter pivots are used	Less than ± 1% hysteresis; Linearity: 1% to 50% defl. 3% to 67% defl. 5% to 75% defl.	Excellent (less than 0.1°)
Torsion Wires	Two wires required for suspension system, several wire lengths and diameters applicable	The following wire sizes are applicable: Length / Dia. 0.45" / 0.012" 0.75 / 0.014 1.20 / 0.016 1.85 / 0.018 2.90 / 0.020	Music wire (high grade steel spring)	Wire itself is negligible; however, wire mounting and clamping structure weight can be significant	Off the shelf	Required during launch and powered flight	Difficult to mount and control wire tensions	None Required	None	Indefinite life if stress levels are not exceeded	Highly linear, negligible hysteresis	Depends on initial wire tension; less than 2° is within stress limitations

b. Sleeve Bearings

Sleeve bearings made from MoS_2 reinforced Teflon would be more reliable in vacuum operation than ball bearings. However, the frictional torque levels can become excessive. A spiral spring would be necessary to obtain the torsional restraint.

c. Jewel Bearings

Because of the brittleness of jewels, these bearings are used only under extremely light loading conditions. In addition, a complex pivot mounting structure is required to protect the jewels. A suspension mechanism of this type is not recommended in this application.

d. Flexural Pivots

From a performance standpoint, flexural pivots would be excellent for this application. Flexural pivots exhibit a high rotational stiffness about the cross axes to normal rotation, and since they are frictionless bearings, no lubrication is required; hence corrosion, wear, and backlash are non-existent.

e. Torsion Wires

Theoretically, torsion wires should provide a good suspension system. The performance characteristics are analytically predictable, and provided that adequate control of wire stresses is maintained, the wire will theoretically have an infinite life. Several wire sizes (lengths and diameters) are applicable. Like flexural pivots, they are frictionless, and hence lubrication is not a problem.

However, experience has shown that torsion wires are extremely difficult to mount, and regardless of any precautions taken in the system design, the system performance is dependent on precise assembly techniques. An assembly error could induce high initial wire tensions, and since the stress levels are usually marginal to begin with, excessive stress levels could result in structural fatigue after a limited number of cycles. In short, the reliability of a torsion wire suspension system is questionable.

Considering performance and reliability as prime factors in this design tradeoff, the results of the suspension study indicate that a flexural pivot system is the prime candidate for this application.

C. MECHANICAL DESIGN CONSIDERATIONS

This section discusses the study of the RAE viscous damper mechanical configuration. The study includes consideration of

1) Vibration

2) Shock

3) Acceleration

4) Thermal characteristics

5) Vacuum operation

6) Radiation

7) Humidity

8) Magnetic field intensity

The design is shown schematically in Figure 1.

1. Summary and Conclusions

a. Vibration

The damper mechanism is essentially a three-degree-of-freedom system; however, caging eliminates one of the degrees of freedom. Vibration along the two critical axes -- the Z and the Y (see Figure 41) -- has been analyzed. The natural frequencies are ω_{1z} = 780 cps, ω_{2z} = 3360 cps, ω_{1y} = 925 cps, ω_{2y} = 3380 cps.

The critical components during vibration are the flex-pivots. The loads on the pivots are given as

Random Vibration Input:	0.65 Q lb at 780 cps
	0.16 Q lb at 3360
Sinusoidal Vibration Input:	0.56 Q lb at 780 cps
	0.28 Q lb at 3360 cps

where Q is the peak system transmissibility, which would be determined by model testing. The design precaution taken at this stage has been to stagger the natural frequencies to avoid amplification at resonant frequencies.

b. Shock

The magnitudes of shock loading during launch and powered flight are similar to the random vibration levels; hence separate analysis is not

required. However, a shock is introduced into the system by the deployment of the damper boom package in orbit, and the magnitude of this shock was calculated to produce a stress of 94,500 lb/in.^{2} The structure is capable of absorbing this stress wave, but the only damping available is from internal hysteresis and impact energy loss; these magnitudes could be determined by testing the model. If required, a shock absorbing material could be added to the system.

c. Acceleration

Of primary concern during acceleration is the flex pivot loading. This load plus the load on the pivots resulting from caging are additive; the total was determined to be 1.1 lb, which is not critical.

d. Thermal Considerations

The mechanism has been designed so as to operate satisfactorily within the temperature limits stipulated by the specification. This has been accomplished by proper selection of materials and by proper coefficient of thermal expansion matching.

e. Vacuum

The 10^{-10} mm Hg vacuum expected in orbit will not affect the structural materials. Because of evaporation, however, magnesium could pose a problem for long term orbital operation unless a proper coating were used. Hence, all magnesium parts are coated with silicon monoxide.

f. Radiation

The levels of penetrating radiation and particle bombardment flux which will be encountered naturally in space are too low to cause any damage to to the damper mechanism.

g. Humidity

Corrosion resistant steels are used to minimize humidity effects.

h. Magnetic Field Intensity

The only magnetic components are the extension spring, the cantilever spring, and the flex pivots. These will create a very minimal magnetic field about the vane-magnet assembly.

The important factors denoted in this report are as follows:

- All materials and material coatings have been successfully used in similar satellite applications.

- The vane will contact the magnets during launch and powered flight due to vibration inputs. Further thought will be given to the possibility of caging the vane during this portion of operation, by using a material which is normally solid but sublimates when exposed to the vacuum environments.

- A weight breakdown of the laboratory model and a computed weight for a flight test model resulted in the following weights:

  Laboratory Model Weight -- 1.082 lb

  Flight Test Model 0.835 lb

  The basic difference is that aluminum is the major structural material in the laboratory model, whereas magnesium and titanium replace aluminum in the flight test model. In addition, a lighter magnet assembly would be used on the flight test model. It is believed that a final weight of 0.75 lb could be achieved with a more intensive design effort.

2. Installation and Operation

The installation and functional operation of the damper mechanism are described as follows:

a. The interface bracket is mounted to the satellite structure.

b. The damper boom package is attached to the boom package damper interface spacer.

c. The damper boom package is rigidly attached to the satellite structure, deflecting the damper extension spring through about 0.25 inch.

d. The extension spring in turn deflects the cantilever spring, and the structure is loaded against the adjustable stops. This completes the caging operation.

e. The mechanism is then subjected to dynamic loads during launch and powered flight in the caged position.

f. When the satellite has achieved its orbit, the damper boom package is released from the satellite, whereupon the extension spring raises the boom package until the guide rods are seated.

g. The cantilever spring lifts the entire structure off the stops and is the the sole support of the damper boom and damping mechanism during orbital operation.

h. The flex pivot suspension system provides support of the damping structure and torsional compliance about the rotation axis.

i. The vane is fixed with relation to the satellite and oscillates with respect to the magnet assembly and damper boom.

j. Damping is achieved by passing the ferromagnetic fluid through an orifice in the vane.

3. Determination of Cantilever Spring Size

The cantilever spring is designed to provide support for the entire RAE damper mechanism in orbit. It is very stiff in torsion and bending, yet its location with reference to the flex pivots prohibits excessive loading of the pivots. Its flexibility permits caging and its high torsional stiffness minimizes deflection about the Z axis during orbital loading.

The size of the cantilever spring was determined as follows (see Figure 60).

$$FL = F_s L_s \tag{61}$$

$$F = \frac{F_s L_s}{L} \tag{62}$$

$$K = \frac{K_s \delta_s L_s}{L Z} = \text{equivalent stiffness through the X axis} \tag{63}$$

Let us define K as K_4 and Z as Z_3.

Then

$$\sin \theta = \frac{Z_3}{L} \tag{64}$$

or $\sin \theta \sim \theta$ for small displacements.

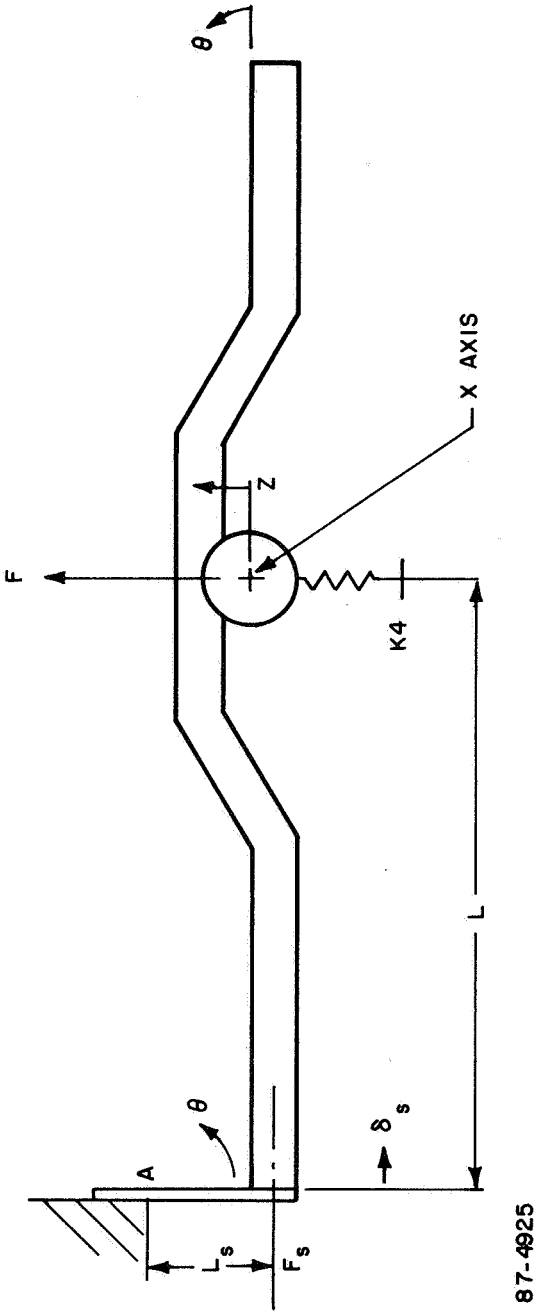

Figure 60 CANTILEVER SPRING -- VANE SUPPORT YOKE LOADING DIAGRAM

$$\therefore \quad \theta = \frac{Z_3}{L} \tag{65}$$

For an end loaded cantilever

$$\theta = \frac{F_s L_s^2}{2 E_s I_s} \tag{66}$$

$$\therefore \frac{F_s L_s^2}{2 E_s I_s} = \frac{Z_3}{L} \tag{67}$$

And since $F = K_4 Z_3$,

$$K_4 = \frac{2 E_s I_s}{L^2 L^S} \tag{68}$$

where

$$I_s = \frac{2a(2b)^3}{12} = \frac{4}{3} \quad ab^3$$

Then

$$K_4 = \frac{8 E_s \, ab^3}{3 L^2 L_s} \tag{69}$$

In addition, the spring is loaded in torsion during orbital operation by a torque about the Z axis. The problem is depicted below (see Figure 61).

$$\phi = \frac{TL_s}{KG_s} \tag{70}$$

where

T = τ_Z = orbital torque

L_s = free length of cantilever spring

K = torsional spring constant

G_s = modulus of rigidity

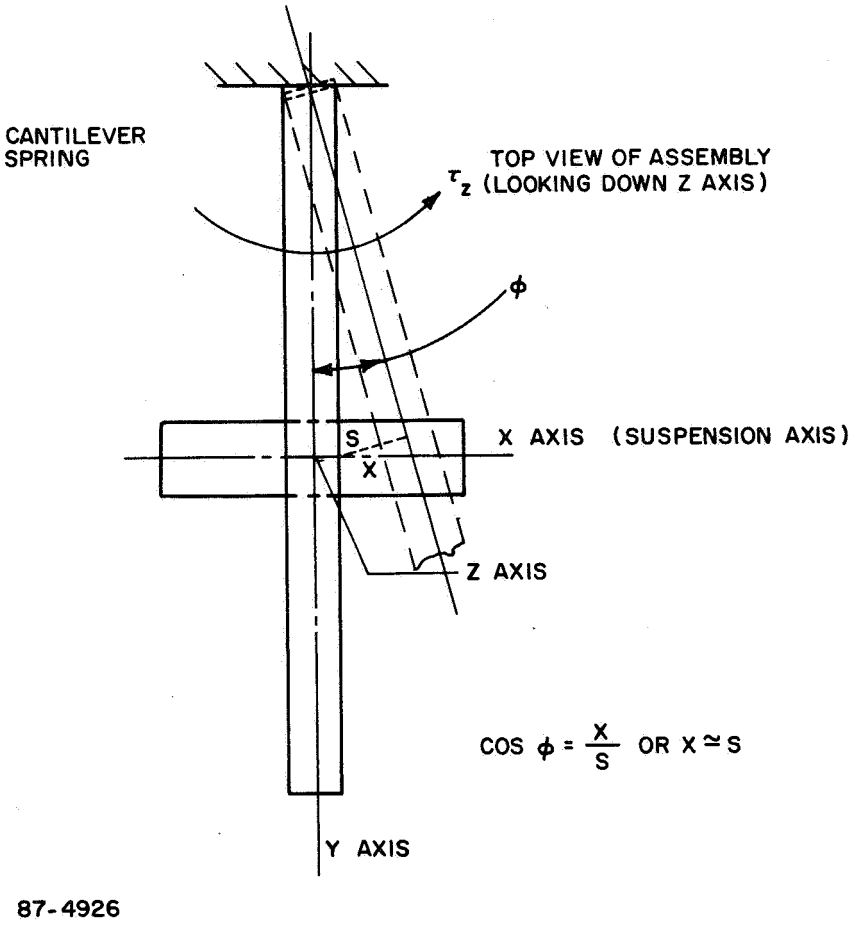

Figure 61 ORBITAL LOADING DIAGRAM

$$K = ab^3 \left[\frac{16}{3} - 3.36 \frac{b}{a} \frac{(1 - b^4)}{12 a^4} \right] \tag{71}$$

$$\therefore \phi = \frac{\tau_Z L_s}{ab^3 \left[\frac{16}{3} - 3.36 \frac{b}{a} \frac{(1 - b^4)}{12 a^4} G_s \right] G_s} \tag{72}$$

Also,

$$\sin \phi = \frac{x}{L} \quad \text{or} \quad x = \phi L \text{ for small } \phi\text{'s} \tag{73}$$

Then

$$x = \frac{L \tau_Z L_s}{ab^3 \left[\frac{16}{3} - 3.36 \frac{b}{a} \frac{(1 - b^4)}{12 a^4} \right] G_s} \tag{74}$$

Given

L_s = 0.593 inch (from layout)

E_s = 30×10^6 psi (steel)

L = 4.5 inch (from layout)

G_s = 11.6×10^6 psi (steel)

τ_Z = 6.45×10^5 dyne-cm = 0.572 in.-lb

For x = 0.005 inch (arbitrarily chosen; it corresponds to 0.06 degree, letting ϕ = rotation about the z axis),

a = 0.156

Solving for b,

$$5.34\, b^3 - 21.7 b^4 + 0.306 \times 10^{-4} b^8 = 169 \times 10^{-6}$$

By approximation,

$$5.34 b^3 >> -21.7 b^4 + 0.306 \times 10^{-4} b^8$$

Then

b = 0.032 inch

Actually, $(0.12)(5.34b^3) \simeq 21.7b^4$. Then $0.88\ (5.34)\ (b^3) = 169 \times 10^{-6}$, or $b = 0.033$ inch and $2b$ = cantilever spring thickness = 0.066 inch.

Summarizing the cantilever spring dimensions:

Thickness = 0.066 inch

Width = 0.312 inch

Active length = 0.593 inch

Then solving for K_4:

$$K_4 = \frac{8\,E_s\,ab^3}{3L^2\,L_s}$$

$$= \frac{8\,(30 \times 10^6)\,(0.156)\,(0.033)^3}{3\,(4.5)^2\,\,(0.593)}$$

$$K_4 = 37.5\ lb/in.$$

This value of the equvalent spring constant is used later in the dynamic analysis portion of this report.

4. Radiation Effects

The levels of penetrating radiation and particle bombardment flux which will be encountered naturally in space are too low to cause any significant damage to the metals used on the RAE damper mechanism.

Radiation effects on the ferromagnetic fluid are covered in another portion of this report.

5. Vibration Effects

The RAE damper mechanism after caging is a two-degree-of-freedom system. Vibration along the two critical axes, the Z and the Y, is analyzed when the system is caged.

The mechanical analog of the system is shown in Figure 62.

M_1 = Mass of structure assembly

M_2 = Mass of pivot support yoke

M_3 = Mass of damper vane pivot arm and fixed rotor shaft

K_1 = Stiffness of extension spring

K_3, K_2 = Stiffness of flexural pivots

K_4 = Equivalent stiffness of cantilever lever spring

Z_3 = Deflection of M_3

Z_2 = Deflection of M_2

Z_1 = Deflection of M_1 (zero when caged)

During launch and powered flight the system will vibrate in response to the sinusoidal and random vibration loads. Natural frequencies and amplitudes are determined from the free body diagram (see Figure 62).

Then

$$M_3 \ddot{Z}_3 = -K_4 Z_3 - 2K_3 (Z_3 - Z_2) \tag{75}$$

$$M_2 \ddot{Z}_2 = 2K_2 Z_2 - 2K_3 (Z_2 - Z_3) \tag{76}$$

Assume that motion is periodic and composed of harmonic motions of various amplitudes and frequencies. Let one of these components be

$$Z_2 = A \sin(\omega t + \phi)$$

$$Z_3 = B \sin(\omega t + \phi)$$

where A, B, and ϕ are arbitrary constants and ω is one of the system natural frequencies. Then:

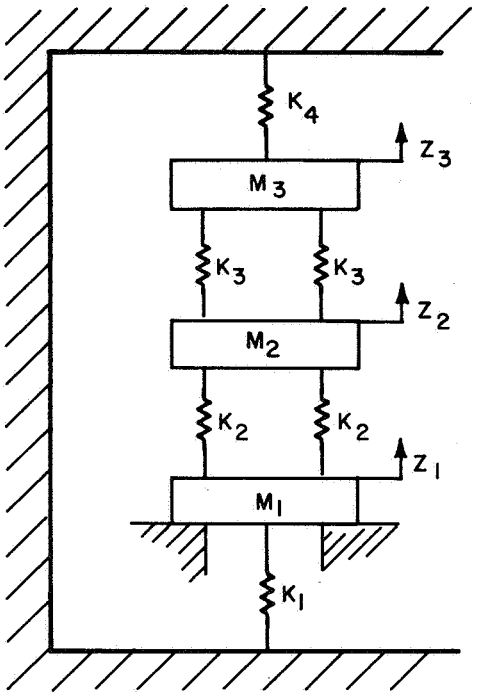

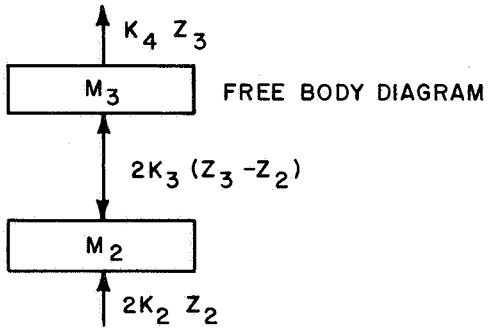

87-4927

Figure 62 MECHANICAL ANALOG OF RAE DAMPER SYSTEM

$$\dot{Z}_2 = A\omega \cos(\omega t + \phi) \tag{77}$$

$$\ddot{Z}_2 = -A\omega^2 \sin(\omega t + \phi) \tag{78}$$

$$\ddot{Z}_3 = B\omega^2 \sin(\omega t + \phi) \tag{79}$$

Substituting:

$$-M_3 B\omega^2 \sin(\omega t + \phi) + (K_4 + 2K_3) B \sin(\omega t + \phi) - 2K_3 A \sin(\omega t + \phi) = 0 \tag{80}$$

$$-m_2 \omega^2 \sin(\omega t + \phi) + (2K_2 + 2K_3) A \sin(\omega t + \phi) - 2K_3 B \sin(\omega t + \phi) = 0 \tag{81}$$

and

$$-m_3 B \omega^2 + (K_4 + 2K_3) - 2K_3 = 0 \tag{82}$$

$$-m_2 A \omega^2 + (2K_2 + 2K_3) A - 2K_3 B = 0 \tag{83}$$

Solving:

$$\omega^4 (M_2 M_3) + \omega^2 (-2M_2K_3 - 2K_2M_3 - M_2K_4 - 2K_3M_3) + (2K_2K_4 + 4K_2K_3 + 2K_3K_4) = 0$$

$$\omega = \sqrt{-\frac{b \pm \sqrt{b^2 - 4ac}}{2a}} \tag{85}$$

where

$$b = -2M_2K_3 - 2K_2M_3 - M_2K_4 - 2K_3M_3$$

$$a = M_2M_3$$

$$c = 2K_2K_4 + 4K_2K_3 + 2K_3K_4$$

given

$$M_2 = 4.8 \times 10^{-5} \quad \frac{lb\text{-}sec^2}{in.}$$

$$M_3 = 1.92 \times 10^{-4} \quad \frac{lb\text{-}sec^2}{in.}$$

$$K_2 = K_3 = 5000 \ lb/in.$$

$$K_4 = 37.5 \ lb/in.$$

then

$$b = -4.32 \quad \frac{lb^2\text{-}sec^2}{in.^2}$$

$$a = 9.22 \times 10^{-9} \quad \frac{lb^2\text{-}sec^4}{in.^2}$$

$$c = 1 \times 10^{8} \quad \frac{lb^2}{in.^2}$$

Solving for ω:

$$\omega_1 = 780 \ cps$$

$$\omega_2 = 3360 \ cps$$

Since $\omega_1 << \omega_2$, the amplifications at resonance will not be multiplied significantly.

The vibration levels at these resonant frequencies are:

$$|A|_{random} = 0.045 \ g^2/cps \ (at \ 3000 \ cps) = 8.75 \ g_{rms}$$

$$|A|_{sine} = 10 \ g, \ 15 \ g \ (at \ 3000 \ cps)$$

$$|A|_{random} = 0.045 \ g^2/cps \ (at \ 780 \ cps) = 8.75 \ g_{rms}$$

$$|A|_{sine} = 5 \ g, \ 7.5 \ g \ (at \ 780 \ cps)$$

The force levels at which the flex pivots could be subjected at the resonant frequencies are

Random: at 780 cps

$$\left(\frac{1.189\ oz.}{16}\right)\ (8.75\ g)\ Q\ =\ 0.65\ Q\ lb$$

at 3360 cps

$$\left(\frac{0.297\ oz.}{16}\right)\ (8.75\ g)\ Q\ =\ 0.16\ Q\ lb$$

Sinusoidal:

at 780 cps

$$\left(\frac{1.189\ oz.}{16}\right)\ (7.5\ g)\ Q\ =\ 0.56\ Q\ lb$$

at 3360 cps

$$\left(\frac{0.277\ oz.}{16}\right)\ (15\ g)\ Q\ =\ 0.28\ Q\ lb$$

Hence it is evident that the greatest damage potential occurs at the lowest resonant frequency during random vibration.

Vibration in the Y axis is similar to Z axis vibration, the only basic difference being that K_s replaces K_4. Hence

$$\omega^4 (M_2 M_3) + \omega^2 (-2M_2K_3 - 2K_2M_3 - M_2K_s - 2K_3M_3) \qquad (88)$$

$$+ (2K_2K_s + 4K_2K_3 + 2K_3K_s) = 0$$

$$a = M_2 M_3\ ,\quad b = -2M_2K_3 - M_2K_s - 2K_3M_3\ ,\quad c = 2K_2K_s + 4K_2K_3 + 2K_3K_s$$

$$\omega = \sqrt{\frac{-b \pm \sqrt{b^2 - 4ac}}{2a}}$$

Given

$$M_2 = 4.8 \times 10^{-5} \quad \frac{lb\text{-}sec^2}{in.}$$

$$M_3 = 1.92 \times 10^{-4} \quad \frac{lb\text{-}sec^2}{in.}$$

$$K_2 = K_3 = 5000 \ lb/in.$$

For cantilevers,

$$P = \frac{3EI\,\delta}{L^3}$$

$$K_s = \frac{3\,E_s\,I_s}{L_s^{\,3}}$$

$$I_s = \frac{4}{3}\,ab^3$$

$$K_s = \frac{4\,ab^3\,E_s}{L_s^{\,3}}$$

where

$$a = 0.156 \ in.$$

$$b = 0.033 \ in.$$

$$E_s = 30 \times 10^6 \ psi$$

$$L_s = 0.593 \ in.$$

$$K_s = 32 \times 10^2 \ lb/in.$$

and

$$a = 9.22 \times 10^{-9} \quad \frac{lb^2\text{-}sec^4}{in.^2}$$

$$b = -4.47 \quad \frac{lb^2\text{-}sec^2}{in.^2}$$

$$c = 1.416 \times 10^8 \ lb^2/in.^2$$

Solving for ω:

$$\omega_1 = 925 \ cps \tag{90}$$

$$\omega_2 = 3380 \ cps \tag{91}$$

Hence, dynamic loading of the same magnitude can be expected along both axes.

A more detailed analysis of the system should be undertaken before final flight model design. Of prime importance is the determination of Q, since $M \simeq Q$ at resonance. Using the Q obtained, accurate pivot loads can be determined. At this stage of the design the precaution has been taken to stagger the natural frequencies to minimize any amplifying effects of the coupled resonator.

6. Thermal Considerations

Proper thermal design of the RAE damper mechanism is attained by geometrical design and the selection of materials with the required thermophysical properties.

The ferromagnetic fluid is expected to operate at 0° F to 70° F, and is temperature compensated.

However, the design could provide for more precise damping control during temperature variations by utilizing a baffle material which would expand or contract in inverse proportion to the change in ferromagnetic fluid viscosity.

The proposed thermally compensated baffle is depicted in Figure 63.

Prior to final flight model design, a more extensive thermal analysis of the damper mechanism is required, to predict adequately the operating temperatures expected throughout the structure, and to aid in the material and finish selection. Proper design will minimize thermal strains, fatigue failures, and other temperature induced damage.

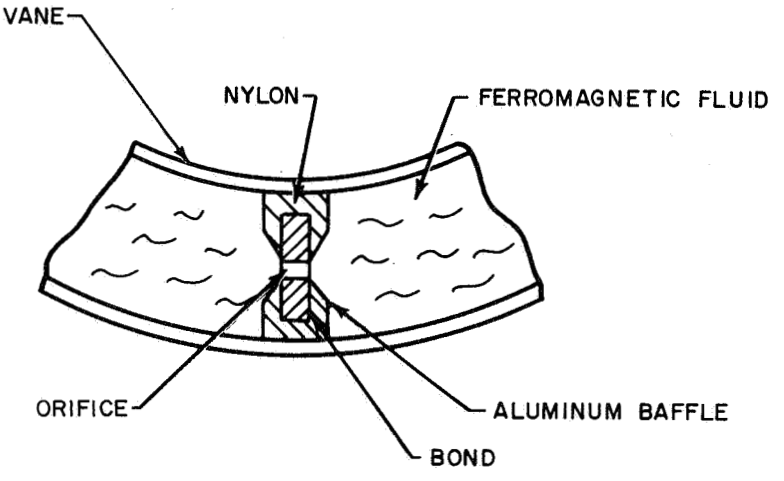

87-4928

Figure 63 PROPOSED THERMALLY COMPENSATED BAFFLE

7. Material Selection

Several primary requirements were considered in the material selection:

a. Materials will not vaporize at an appreciable rate when subjected to the high vacuum of outer space.

b. Materials must exhibit high strength/weight ratios.

c. Material interfaces will not corrode in a corrosive atmosphere.

d. The total contribution of the structural materials to background magnetic fields must be minimized.

Table XXV is a complete list of all RAE viscous damper parts, with the proposed materials of construction and finishes.

The proposed materials and finishes have been successfully used on numerous satellites to date, for example:

a. Silicon monoxide on exterior magnesium surfaces--Vanguard 2
--Vanguard 3
--Midas II

b. Silicon monoxide on aluminum surface--Vanguard 1

c. Titanium alloy fasteners--NAV SAT3
--NAV SAT7A

d. Corrosion resistant steels -- many satellite applications.

8. Vacuum Operation

The high vacuum of outer space (expected to be about 10^{-10} mm Hg) will cause metals such as magnesium to vaporize at an appreciable rate unless precautions are taken. All the magnesium parts of the RAE structure will be coated with silicon monoxide, eliminating this evaporation problem. The titanium and aluminum parts do not pose any evaporation problems in the vacuum environment.

The vane assembly will be hermetically sealed (soldered) to prevent any loss of ferromagnetic fluid in the vacuum.

The flex pivots used for the damper suspension mechanism have no rubbing surfaces; hence corrosion, space "welding," lubrication, etc., are not problems in the vacuum environment.

TABLE XXV

LIST OF RAE DAMPER PARTS

Part	Material and Finish
1. Flex Pivots	AISI 420 Corrosion Resistant Steel
2. Extension Spring	ASTM A227 Steel, Black Oxide Finish
3. Cantiliver Leaf Spring	SAE 1074 Steel, Black Oxide Finish
4. Vane Support	Magnesium-Silicon Monoxide Finish
5. Magnet Assembly	Indox V Ceramic Magnet Material, Magnetic Ingot Iron (High Purity, Black Oxide Finish
6. Vane Assembly	Aluminum, Copper Flashed, Soldered, Silicon Monoxide Finish
7. Pivot Support Yoke	Titanium
8. Guide Rod	Titanium
9. Spring Yoke	Magnesium-Silicon Monoxide Finish
10. Bracket	Magnesium-Silicon Monoxide Finish
11. Adjustable Stop	Magnesium-Silicon Monoxide Finish
12. Shaft--Fixed	Titanium
13. Dowel Pins	AISI 420 Corrosion Resistant Steel
14. Structure	Magnesium-Silicon Monoxide Finish
15. Interface Bracket	Magnesium-Silicon Monoxide Finish
16. Cantilever Spring Bracket	Magnesium-Silicon Monoxide Finish
17. Fasteners	Titanium
18. Spacer	Titanium

9. Acceleration Effects

During powered flight the RAE damper mechanism will be subjected to a 23 G acceleration load. This load on the flex pivots must be added to the load for caging.

The problem is similar to the case of a displacement loading, but the mass x G forces must be taken into account. The basic equations are

$$\Sigma F_{M_3} = 0 = K_4 Z_3 + 2 K_3 Z_3 - 2K_3 Z_2 - M_3 G \tag{92}$$

$$\Sigma F_{M_2} = 0 = 2K_2 Z_2 + 2K_3 Z_2 - 2K_3 Z_3 - M_2 G \tag{93}$$

Solving for $K_2 Z_2 = F_P$,

$$F_{P_a} = \frac{(M_3 + M_2) G - K_4 Z_3}{2} \tag{94}$$

or

$$2 K_2 Z_2 = (M_3 + M_2) G - K_4 Z_3$$

$$Z_2 = 1.07 \times 10^{-4} \text{ in.}$$

$$F_{P_a} = 5000 (1.07 \times 10^{-4}) = 0.535 \text{ lb}$$

10. Caging

Of primary concern in caging is the flex pivot loading. The magnitudes of these loads are determined as follows (the mechanical analog is shown in Figure 64):

K_4 = Stiffness of equivalent cantilever spring

$K_3 = K_2$ = Stiffness of flex pivots

M_2 = Mass of pivot support yoke

M_3 = Mass of damper vane pivot arm and fixed shaft

Z_3 = Deflection of M_3 upon caging

Z = Caging displacement ($Z = Z_2 + Z_3$)

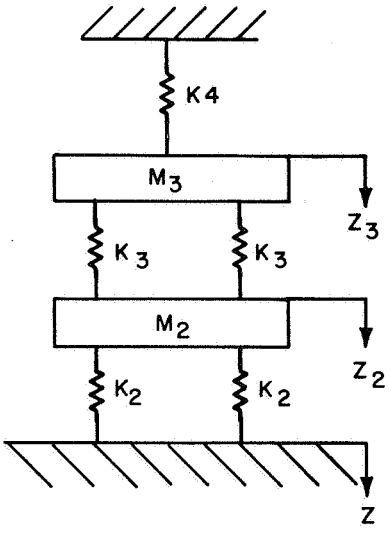

MECHANICAL ANALOG

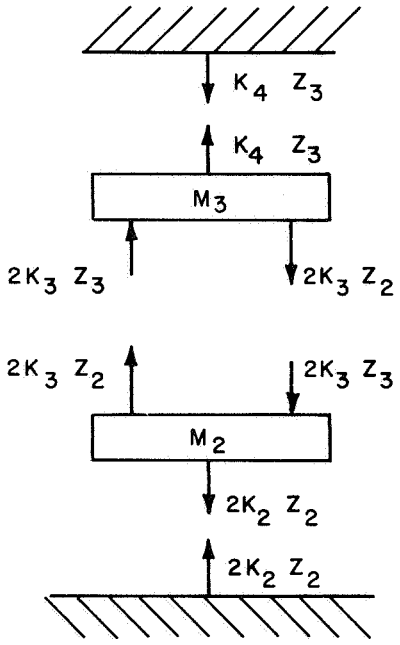

FREE BODY DIAGRAM

87-4929

Figure 64 CAGING LOAD

The free body diagram is shown in Figure 64.

$$\Sigma F_{M_3} = 0 = K_4 Z_3 + 2 K_3 (Z_3 - Z_2) \tag{95}$$

$$\Sigma F_{M_2} = 0 = 2 K_2 Z_2 + 2 K_3 (Z_3 - Z_2) \tag{96}$$

Solving:

$$K_4 Z_3 = 2 K_2 Z_2$$

For $Z = 0.030$ inch,

$$K_4 = 37.5 \ lb/in.$$

$$K_2 = 5000 \ lb/in.$$

$$37.5 Z_3 = 2 (5000) Z_2$$

$$Z_3 = 267 Z_2$$

$$Z_3 + Z_2 = 0.030$$

Thus

$$F_{p_c} = \text{pivot load} = 5000 \ (1.12 \times 10^{-4}) \tag{97}$$

$$= 0.56 \text{ lb}$$

This load is acceptable.

The total pivot load resulting from acceleration and caging:

$$F_{p_c} + F_{p_a} = 0.56 \ lb + 0.535 \ lb \tag{98}$$

$$= 1.1 \ lb$$

This load is not critical.

In determining the extension spring size, acceleration and vibration induced forces were considered. During the powered portion of the flight an acceleration level of 23G's is expected. This acceleration load must be overcome by the extension spring to prevent the structure from being lifted off the mechanical stops and damaging the flexural pivots.

The spring rate was determined as follows (see Figure 64):

$$K_1 Z_o > (M_1 + M_2 + M_3) G + K_4 Z_3 \tag{99}$$

where

K_4 = 37.5 lb/in.

Z_3 = 0.0299 in.

$(M_1 + M_2 = M_3)$ = 0.812 lb

Z_o = Caging Distance = 0.22 in.

Hence for K_1 > 90 lb/inch, acceleration loads are overcome by the extension spring force.

The extension spring used on the flight model will have a spring rate of 100 lb/inch, with an initial tension of 0 to 10 lb.

At resonance, the structure will be subjected to vibration induced loads, the magnitude of which depends on the system Q. These loads are not expected to approach the magnitude of the acceleration loads, and hence are of secondary concern in the extension spring design.

11. Vane Dynamics

During the launch and powered flight, the damper vane will be subjected to sinusoidal and random vibration at the levels specified. The following analysis defines the vane excursion during these environments (see Figure 65):

$$\delta_A = \frac{W R_o^3 K_\delta}{E_{AL} I} \tag{100}$$

where

$$K_\delta = \frac{1}{2} \alpha (1 - \cos \alpha)^2 + C (\alpha - \sin \alpha)^2$$

$$C = \frac{EI}{JG}$$

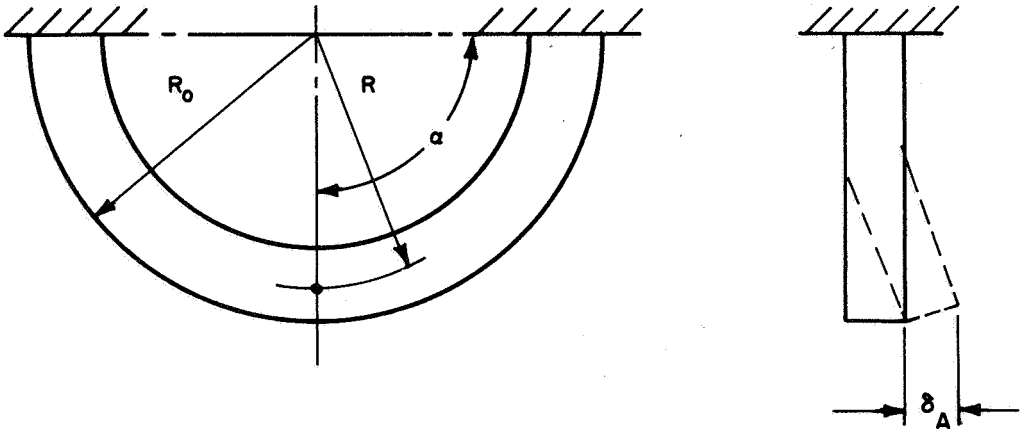

87-4930

Figure 65 DAMPER VANE DIAGRAM

$$a = \frac{170^\circ}{2} = 85^\circ = 1.48 \text{ radians}$$

$E_{al} = 10 \times 10^6$ psi

$G_{al} = 3.6 \times 10^6$ psi

$W = wRa, \quad w = lb/in.$

$$\delta_A = \frac{\omega R a R_o^3}{EI} \quad \frac{a}{2} \left[(1 - \cos a)^2 + \frac{EI}{JG} (a - \sin a)^2 \right] \tag{101}$$

$$W = W_{vane} + W_{fluid} = 0.32 + 0.23 \text{ oz.} = 0.034 \text{ lb}$$

$$I = \frac{b h^3 - b_1 h_1^3}{12}$$

$$J = \frac{b h^3 + h b^3 - b_1 h_1^3 - h_1 b_1^3}{12} = \text{polar moment of inertia}$$

For $h = 0.160$ in.

$h_1 = 0.120$ in.

$b = 0.820$ in.

$b_1 = 0.780$ in.

$I = 0.17 \times 10^{-3}$ in.^{4}

$J = 2.8 \times 10^3$ in.^{4}

$$\frac{I}{J} = 0.0607$$

$$\frac{E}{G} = 2.78$$

$$K = \frac{1}{2}(1.48)\left[(1-0.088)^2 + (2.78)(0.0607)(1.48-0.996)^2\right] = 0.643$$

$$\delta_A = \frac{W R^3}{EI} K_\delta = \frac{(0.034)(3.5)^3 (0.643)}{(10 \times 10^6)(0.17 \times 10^{-3})} \tag{102}$$

$= 0.55 \times 10^{-3}$ in. static deflection

$$\omega_n = \sqrt{\frac{g}{\delta_A}} = \sqrt{\frac{32.2 \times 12}{0.55 \times 10^{-3}\ in.}} = 840\ rad/sec$$

= 133 cps

Sinusoidal vibration level at 133 cps = 10 G's:

$$\delta_{10} = 0.55 \times 10^{-3} (10) = 0.0055 \tag{103}$$

Since the allowable vane excursion is 0.020 inch, a 0.020/0.0055 = 3.6 magnification factor is permitted before contact with the magnet. Since a magnification factor of at least 20 to 30 is expected, contact is inevitable.

In the flight model design, vane caging should be considered. This can be accomplished by filling the 0.020 inch gaps between the vane and magnet by a material which would sublimate when exposed to the vacuum of space. A similar approach was successfully used on the Nav Sat 7A satellite (15 November 1961), where the damping spring was encapsulated in biphenyl and was actuated in space by the evaporation of the biphenyl. The optimum material for the RAE application would be carefully selected after a survey of potential volatile solids with specific evaporation rates. A sketch of this caging method is shown in Figure 66.

Evaporation of the caging material is a potential problem unless certain design precautions are taken. (Reference here is to optical or electronic components whose performance could be degraded if the evaporated caging material deposited on them.) Since the evaporating atoms will travel in straight lines at the air pressure encountered in space, they should deposit only on colder surfaces in an optical line of sight. Proper design can eliminate this problem.

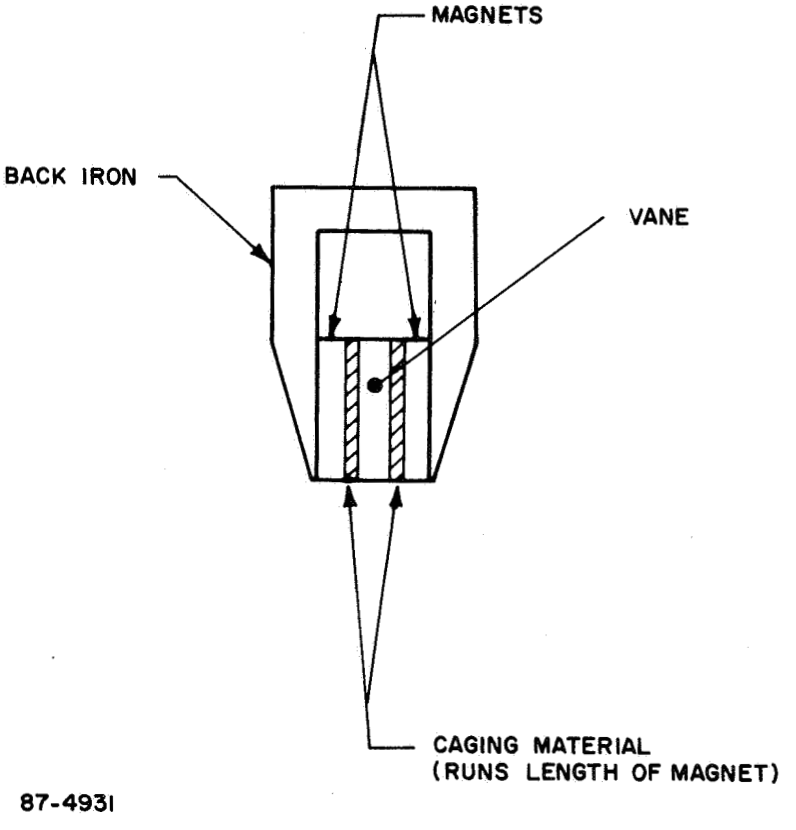

Figure 66 VANE CAGING

12. Uncaging Dynamics

After the RAE satellite has achieved orbit, the damper boom package and damper mechanism are deployed. This deployment is accomplished by first releasing the marman clamp securing the boom package to the satellite and then allowing the four negator springs to drive the entire mechanism outside the satellite, exposing it to the space environment. The dynamics of this uncaging operation are discussed in this section.

Energy of negator springs = kinetic energy of boom package
+ potential cantilever spring energy
+ potential extension spring energy

$$\text{or} \quad E_{NS} = \left(\frac{1}{2} MV^2\right)_{BP} + \left(\frac{1}{2} KZ^2\right)_{CS} + \left(\frac{1}{2} KZ^2\right)_{ES} \tag{104}$$

but $\left(\frac{1}{2} KZ^2\right)_{CS} \ll \left(\frac{1}{2} KZ^2\right)_{ES}$ and can be disregarded.

Of interest is the intensity of the tensile stress wave which is propagated when the damping structure is suddenly stopped and the spring yoke pivot impacts the damper structure as a result of the momentum of the boom package. This stress wave is propagated through the guide rods, and then back to the adjustable stops and into the satellite structure.

The maximum stress produced in the guide rods is given by

$$S_{max} = \frac{v}{V} (E) \left(1 + \sqrt{\mu + 2/3}\right) \tag{105}$$

where

v = velocity of the boom package on impact = $\sqrt{\left(E_{NS} - \frac{K_2^2}{2}\right)\frac{2}{M_{BP}}}$

V = velocity of the propagated stress wave = $\sqrt{\frac{386.4\,E}{\delta}}$

$\mu = \frac{\text{mass of boom}}{\text{mass of guide rods}}$

E = modulus of elasticity of guide rods

Thus

$$v = \sqrt{\frac{2\left(4\ ft\text{-}lb - 90\frac{lb}{in.}\ \frac{(0.312)^2}{24}\ ft\text{-}lb\right)}{20\ lb/32.2}} \tag{106}$$

$$= 3.4\ ft/sec$$

$$v = \frac{1}{12}\sqrt{\frac{386.4\,(16\times 10^6)}{0.16}}\ \frac{ft}{sec}$$

$$v = 1.64\times 10^4$$

$$\mu = \frac{20}{0.0116} = 1.73\times 10^3$$

$$S_{max} = \frac{3.4}{165}(16\times 10^6)(1.73\times 10^3)^{1/2} \tag{107}$$

$$= 94{,}500\ lb/in.^2$$

Since titanium (alloyed) has a tensile strength of 150, 000 psi, this dynamic stress does not overstress the guide rod.

This maximum stress is only approximate since initial conditions assume that the guide rods are perfectly elastic, the damper boom package is rigid, and the spring yoke simultaneously contacts the structure at all points. The damping of the initial stress waves by elastic hysteresis in the guide rod and the cushioning effect of the non rigid damper boom package would tend to reduce the expected stress level. Because of the relatively low velocities encountered in this application, impact loading should cause no problems.

This generated tensile stress wave is then transmitted through the structure back to the adjustable stops and into the satellite structure.

The question then arises as to the magnitude of the system damping which would serve to eliminate the vibrations caused by uncaging in a transient manner. There are only two means by which energy can be dissipated in the proposed system: by internal hysteresis of the structural materials, and by continued impact between structural components. Since internal friction is principally of thermal origin, dissipation of this generated heat in the vacuum environment is questionable; hence the effectiveness of the hysteresis damping is also questionable. Magnesium is used as the structural material, since it has a relatively high hysteresis damping capacity. The magnitude of the impact energy loss is also undefined at this point in the design. The recommendation is to determine the system Q after the initial flight test model has been built.

An energy absorbing material such as a synthetic rubber (Buna-N) could then be easily added to the design if deemed necessary to provide required system damping.

13. Weight

A weight breakdown of the laboratory model and of a flight test model is given in Table XXVI. The laboratory model weight is 1.082 lb*, whereas the flight model, utilizing magnesium and titanium in place of aluminum, is expected to weigh about 0.835 lb*. With a more intensive structural design effort, it is believed that 0.75 lb could be achieved.

14. Stray Magnetic Fields

The problems of minimizing stray magnetic fields has been considered. The specification requires that the maximum field 12 inches from any edge of the mechanism must not exceed 135 gammas after the mechanism has been subjected to a magnetized field of 25 oersteds.

The first measure taken to minimize stray fields was to build all parts of the mechanism, wherever possible, of nonmagnetic materials. It is therefore impossible to induce any remanence in these materials when they are subjected to magnetizing fields. The second measure was to design the magnet assembly with a tightly closed path, to use the very best soft iron available, and to achieve the narrowest practicable air gap. This design criterion not only minimized stray fields but at the same time contributes to an efficient and lightweight design.

* The damper-satellite interface bracket is considered part of the satellite and its weight is not included here.

TABLE XXVI

WEIGHT OF LABORATORY MODEL AND FLIGHT TEST MODEL

	Lab Model (lb)	Flight Test Model (lb)
1. Structure	0.070	0.047
2. Yoke-Vane Support	.049	.033
3. Shaft--Fixed	.011	.018
4. Stops (2)	.002	.0013
5. Yoke Pivot Support	.009	.015
6. Guide Rod (2)	.012	.020
7. Stop Bracket (2)	.020	.017
8. Spring Yoke	.008	.005
9. Cantilever Spring	.005	.005
10. Extension Spring	.051	.051
11. Spacer Guide Rod	.008	.005
12. Magnet Assembly	.739	.520
13. Vane Assembly	.067	.067
14. Pivots	.009	.009
15. Magnetic Fluid	.022	.022
	1.082	0.835

In order to see how effective these design measures had been, measurements were made in out laboratory to map the strength of the stray fields about 12 inches from the mechanism. Since these measurements were performed in the earth's field, special precautions were taken and only difference techniques used. The measuring probe was faced with respect to the earth and the earth's field was electronically bucked out with the nulling controls of the gaussmeter.

By moving the mechanism in circles with a 12 inch radius from the gaussmeter probe and turning the mechanism simultaneously end over end, it was possible to determine that the maximum change in field was approximately 1400 gammas for the worst orientation conditions.

Consequently the maximum intensity of the stray field was deduced to be about 700 gammas. Moreover, if the changes due only to the oscillations of the magnet through its full travel of ± 35 degrees were measured, the readings were only of the order of 200 gammas. Since the magnet being used for the model is stronger than the one required for future models, by a factor of about 1.5, it would appear that the magnetic interference problem is not serious.

Several shield materials, such as Numetal or Moly Permolloy, could be used effectively to attenuate the stray fields substantially. Even though a completely enclosed box cannot be placed around the assembly, very thin sheets of this material could be placed at appropriate locations to minimize the fields, particularly those directed toward the spacecraft.

Future designs of the mechanism will investigate the advisability of fixing the magnet assembly rigidly to the spacecraft and allowing the vane to move -- as opposed to the present design, which was designed with a moving magnet for convenience.

D. DAMPING FLUID DYNAMICS STUDIES

Damping fluid dynamics studies provide the analytical basis for predicting the performance of a ferrofluid viscous damper. They relate the parameters of the fluid, the damper cavity, and the magnet field strength to the viscous and magnetic forces imposed on the fluid.

Three related studies were performed. First the models of the fluid were developed which described the forces on the fluid in a magnetic field. Then the dynamic performance of the fluid was analyzed while the fluid was exposed to design magnetic influence. Finally the dynamic performance was extended parametrically to cover a range of damper and magnetic field strengths.

1. Models of Ferrofluid in a Magnetic Field

The following two subsections develop the fundamental relationships governing the forces exerted upon a ferrofluid by an applied magnetic field. The first subsection describes the body force theory; the second describes the surface stress theory. The latter theory, recently developed, satisfies some anomalous situations which could not be explained by the body force theory. In the RAE damper applications, both theories yield the same resultant force.

a. Body Force Model

Classical electromagnetic theory has been used to derive the relationship between ferrofluid magnetization M, a field of magnetic intensity H, and the magnetic force F_m, developed on ferrofluid. The relationship and its effect on the body are described in this subsection. The detailed mathematics is derived in Section IV.D. 2. a.

The theory establishes the magnetic fluid force as a body force, one which is experienced throughout a unit volume of the fluid by each molecule of the fluid, independent of the boundary conditions of the molecule. In ordinary fluids the only body forces that arise are those due to gravitational force and accelerations of the fluid body. Ordinary fluids are also acted upon by forces resulting from boundary conditions, such as differential pressures on the fluid surfaces. A unit volume of the ferrofluid can have a combination of gravitational acceleration body forces, magnetic body forces, and pressure gradient forces acting upon it. These are shown schematically in Figure 67.

The magnetic body force acting on any unit volume of fluid is proportional to the ferrofluid magnetization, times the rate of change of field strength, in the direction of the force. The magnetic body force acting on the total volume of the fluid is proportional to the integral of the ferrofluid magnetization, times the rate of change of field strength, integrated from maximum field strength to the field strength at the edges of the fluid. The field strength and rate of change of field strength are shown for a dipole magnet in Figure 68. If no forces are acting on the fluid other than the magnetic body force, the edges of the fluid will take the shape of an equipotential surface. If the source of the magnetic field is a dipole magnet with a symmetrical force field in the plane of the centerline between the poles, the ferrofluid will center itself equally along either side of the centerline. As other forces are applied in the plane of the centerline, the fluid moves farther into the fringing field.

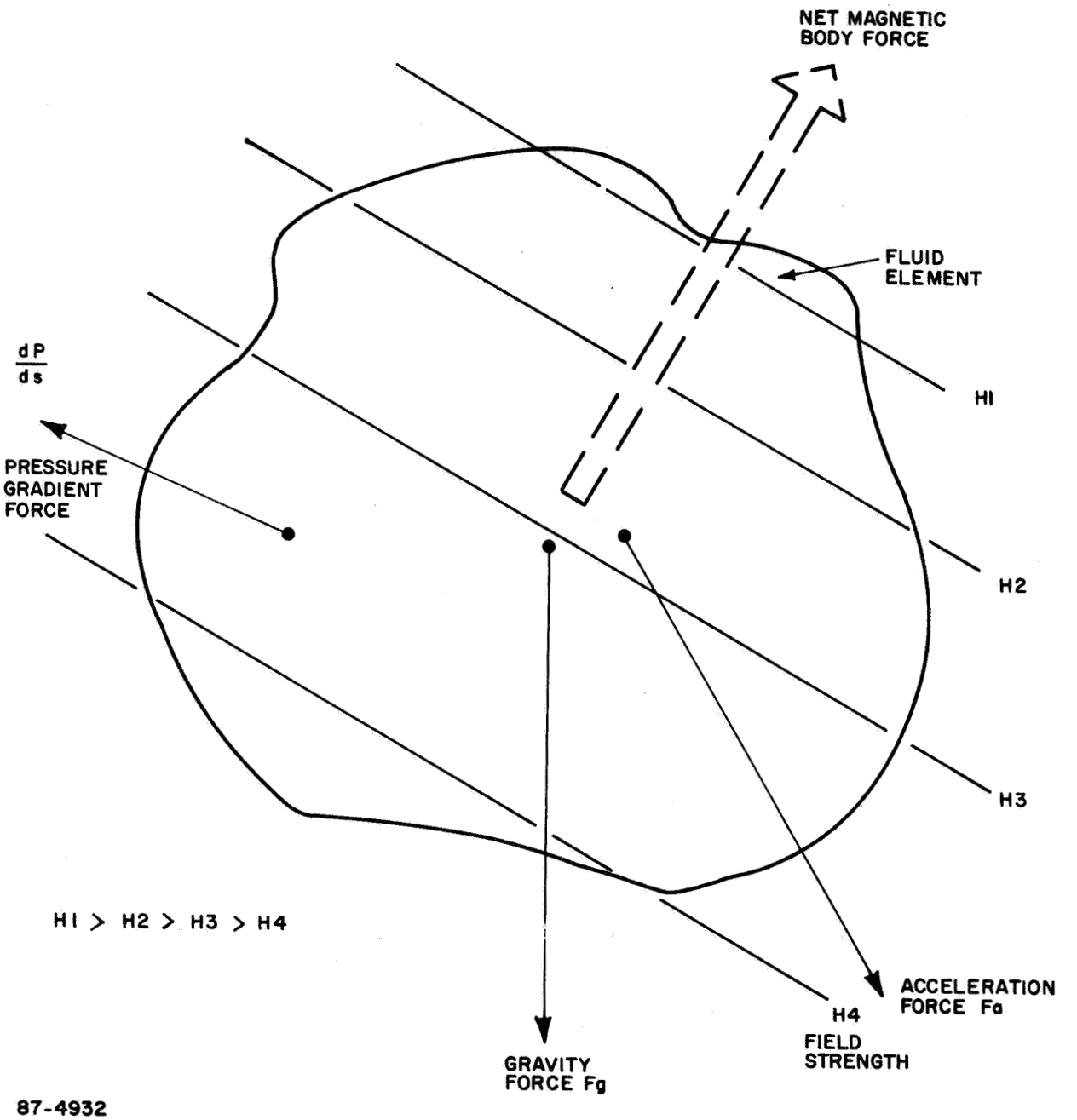

Figure 67 FLUID ELEMENT BODY FORCE MODEL

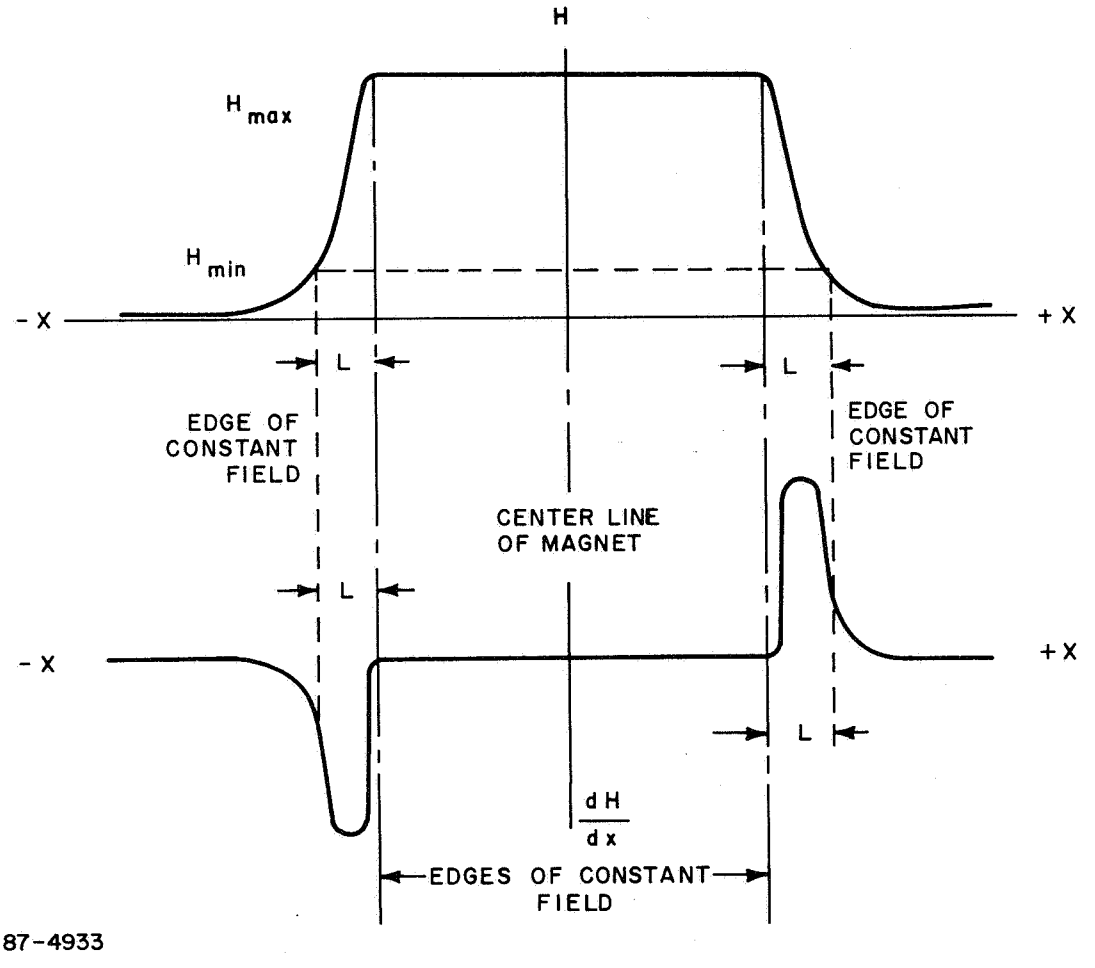

Figure 68 FIELD STRENGTH AND RATE OF CHANGE OF FIELD STRENGTH FOR A DIPOLE MAGNET

The magnetic body force magnitude increases in the area along the leading edge in the fringing field and decreases in the area along the trailing edge which is moving out of the fringing field. Since these forces are in opposite directions, there is a net magnetic body force acting to oppose the other forces acting on the body. This force is dependent on the distance the ferrofluid moves into the magnetic fringing field and the magnitude and rate of change of the magnetic field. The effect is to have a nonlinear spring restraint acting on the fluid. These cases are shown in Figures 69a, 69b, and 69c. In the first case, Figure 69a, the ferrofluid extends across the full length of the constant magnetic field. In the second case, Figure 69b, there is less fluid, and the body of the fluid must move through a distance X before any magnetic force acts. In the third case, Figure 69c, the fluid extends a distance X beyond the constant field in both directions. Again the fluid must move a distance X before any net magnetic force can act on the body of the fluid.

b. Surface Stress Model

There is experimental evidence that surface stress of a magnetic origin is present in a ferromagnetic fluid exposed to a magnetizing field. Consider, for example, Figure 70. A pool of ferromagnetic liquid held by a watch glass is positioned over the poles of a horseshoe permanent magnet. The fluid is collected into a rounded glob whose surface in certain regions has the appearance of a porcupine. Now the lines of force of the applied field arch from one pole to the other, and it is seen that perturbation of the surface occurs at the two ends where the field intersects the surface with an appreciable normal component. Between these regions the field is oriented parallel to the surface, and the surface remains smooth. This photograph illustrates a rather complex physical situation, since the field varies in all spatial directions, in both magnitude and direction.

The phenomenon is demonstrated under simpler conditions in the photograph in Figure 71. Here the applied field, parallel and uniform, is oriented normal to the undisturbed fluid surface, which is initially smooth and flat under the influence of gravity in the absence of the magnetic field. As the field is increased to finite values, there is no change initially, except for an effect on the meniscus at the rim which is unimportant for this discussion. At a critical value of the field, the smooth surface suddenly undergoes a transition to the perturbed state and a regular spacing appears. In Figure 71 the applied field is much larger than the critical value. The liquid cones are grown to such a size that the container bottom in now dry. Removal of the field is accompanied by a nearly instantaneous return to the original state as a liquid pool. The fluid element undergoing magnetic surface stresses is shown in Figure 72.

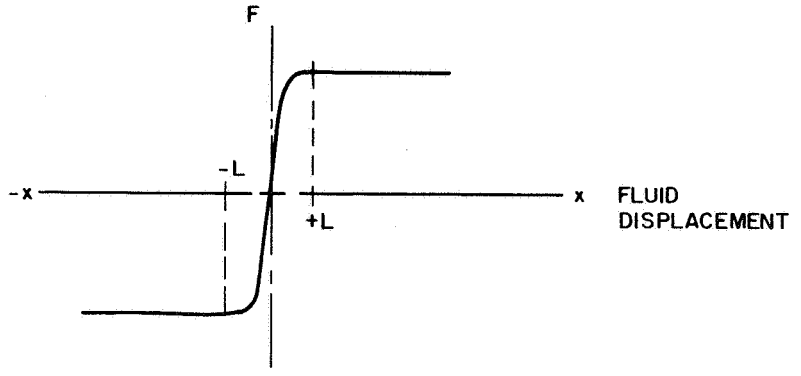

A. FLUID WIDTH EQUAL TO WIDTH OF CONSTANT FIELD

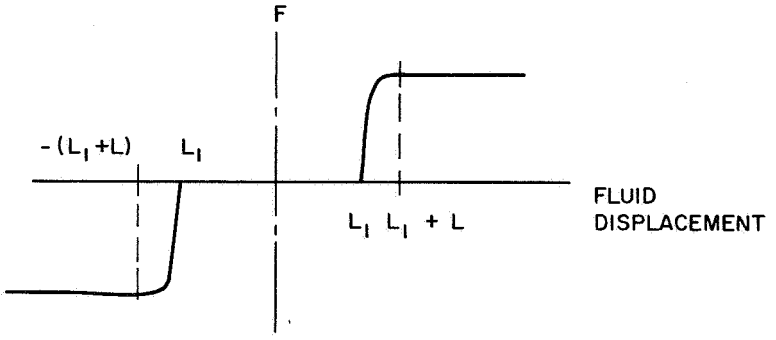

B. FLUID WIDTH LESS THAN WIDTH OF CONSTANT FIELD

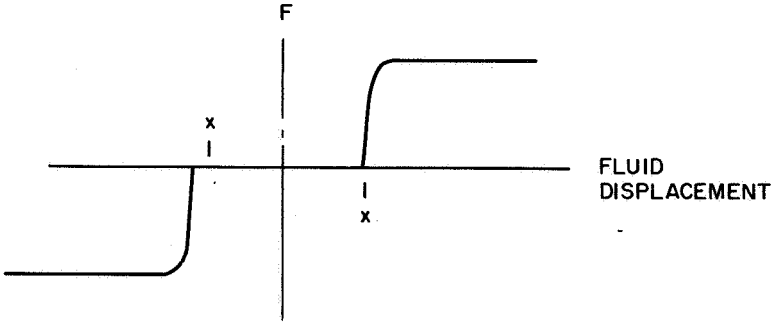

C. FLUID WIDTH GREATER THAN WIDTH OF CONSTANT FIELD

87-4934

Figure 69 MAGNETIC FORCE VERSUS FLUID DISPLACEMENT

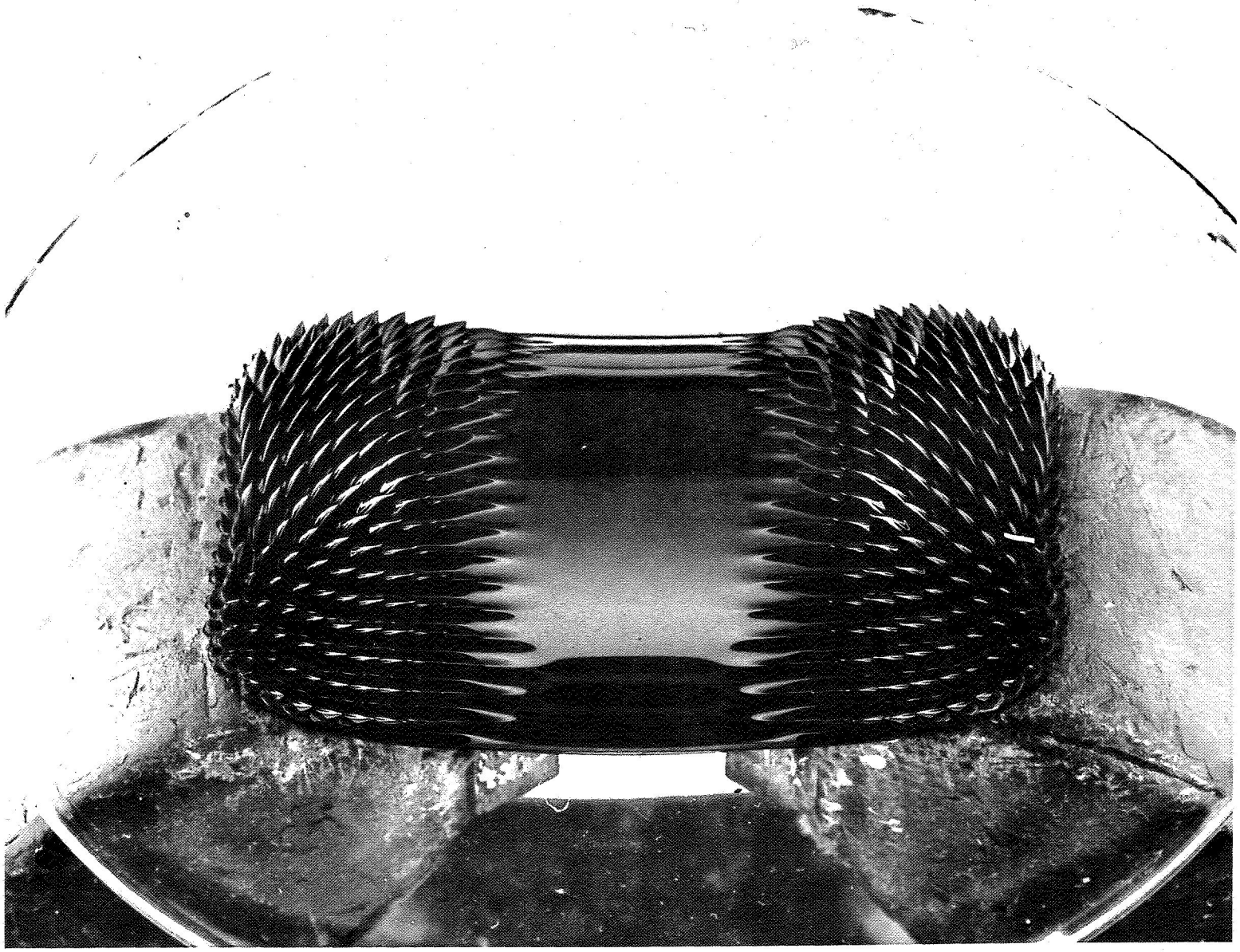

14156A

Figure 70 FERROFLUID EXHIBITING SURFACE STRESS (A)

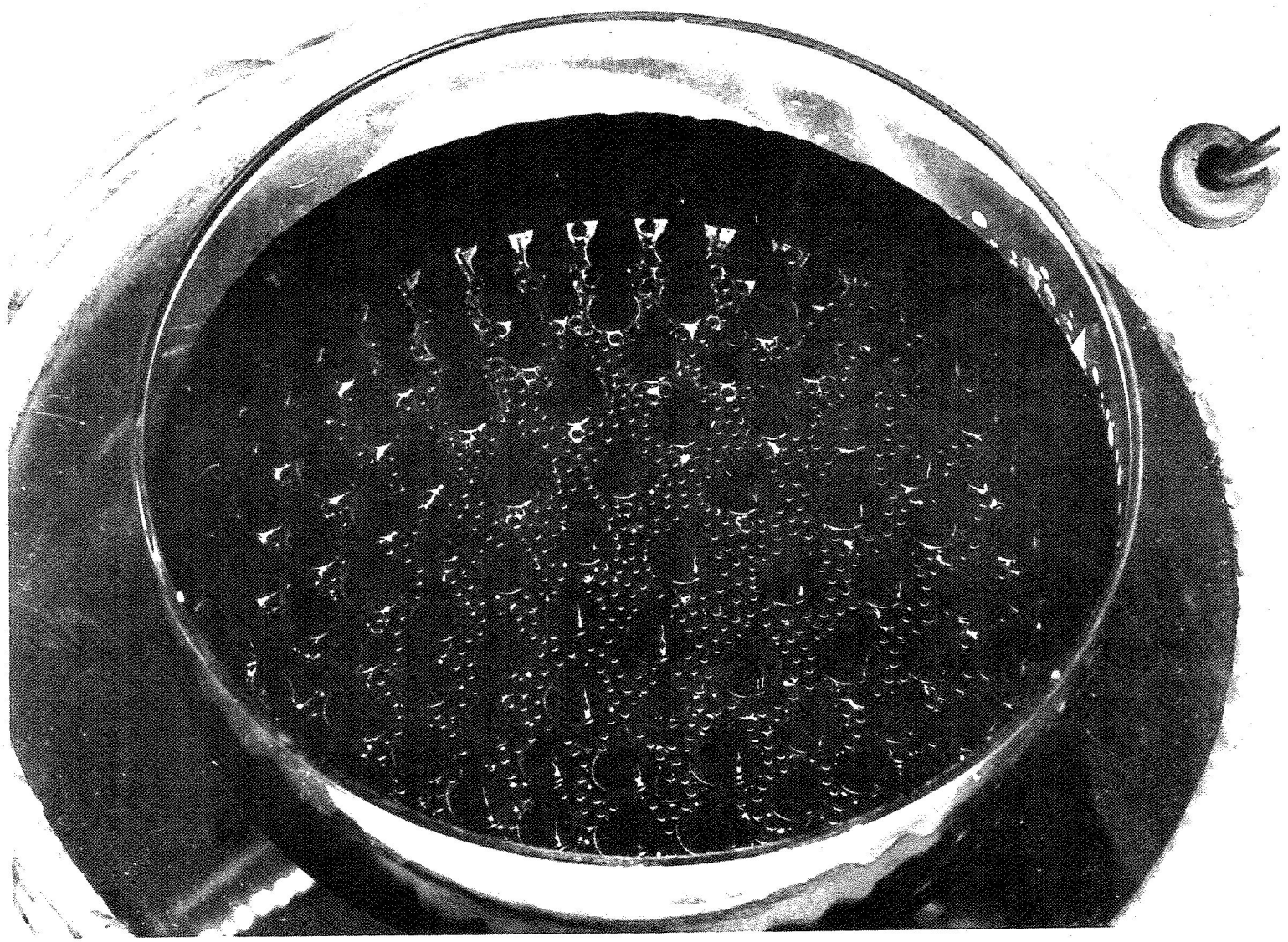

14746D

Figure 71 FERROFLUID EXHIBITING SURFACE STRESS (B)

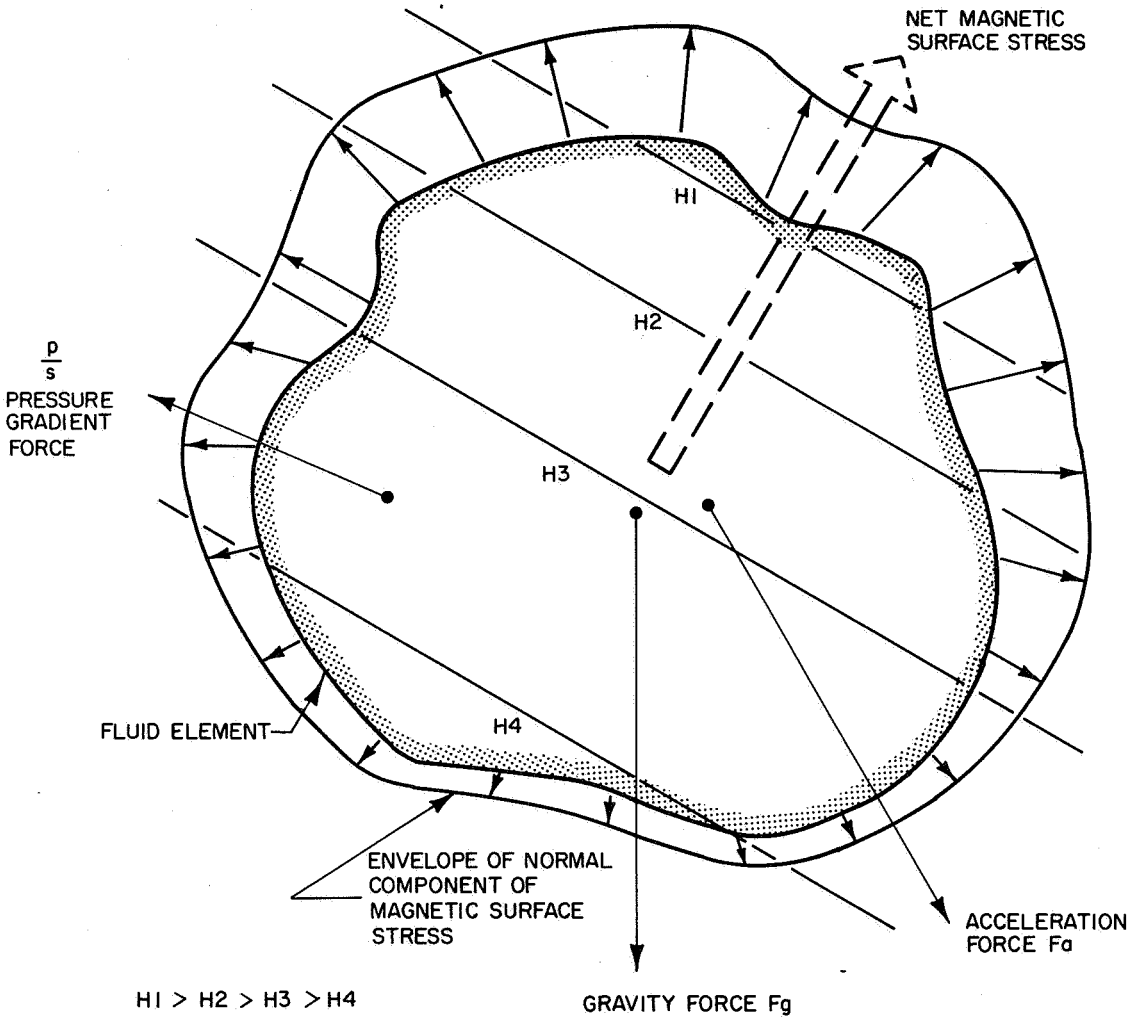

Figure 72 FLUID ELEMENT SURFACE STRESS MODEL

From classical physics the total force on a ferromagnetic body is given by

$$\underline{F} = \int_V (\underline{M} \cdot \text{grad}) \underline{H}_o \, dV \tag{108}$$

where $\underline{H}_o$ is the applied field. When $\underline{H}_o$ is uniform and parallel, the total force vanishes. However, there remains the possibility that a stress system may exist within the material, and the photographs are evidence of the reality of such stresses. Section IV.D.2.b develops the stress tensor.

Cowley and Rosensweig[32] have developed a theory for the critical field and spacing of the pattern which is supported by experimental observations over a wide range of variables. The mathematical treatment gives a result which can be interpreted as follows. The applied magnetic field having magnitude B_o is perturbed by a surface disturbance, to yield at the interface a perturbation field of magnitude $B_o + b$. Then the restoring forces of gravity and surface tension are countered by an effective surface stress which is normal and possesses magnitude $\mu_o M_o b$, where μ_o is the magnetization of unperturbed fluid. It is found that the minimum value of the magnetization which can support a neutrally stable perturbation of the interface is given by (MKS system)

$$\mu_o M_o^2{}_{crit} \Big/ \left(1 + \frac{1}{r}\right) = 2\sqrt{g \Delta\rho T} \tag{109}$$

$$r^2 = \left(\frac{1}{\mu_o^2 H} \frac{\partial B}{\partial H}\right) \tag{110}$$

while the critical spacing between peaks is given by

$$\ell_{crit} = \frac{4\pi}{\sqrt{3}} \sqrt{\frac{g \Delta\rho}{T}} \tag{111}$$

where g is the acceleration of gravity, $\Delta\rho$ is the density difference across the interface, T is the interfacial tension, and r is a composite permeability whose details are evaluated from the magnetization curve.

The surface stress model yields the same results in the RAE magnetic damper application, because an equivalent body force can be derived which is identical to that obtained from the initial approach. The importance of this surface stress model is that it more completely describes the action of the fluid under all conditions.

2. Ferrofluid Performance While Exposed to Design Magnetic Influence

Ferrofluid performance equations are derived for the cases when the fluid is exposed to design magnetic influence. The forces resulting from the magnetic influence are derived in subsections a and b below. The dynamics of flow in a constant area vane are derived in subsection d.

a. Magnetic Body Force Derivation

The magnetic body force can be developed from the classical electromagnetic theory, where the force per unit volume, in CGS units, on a piece of magnetized material of magnetization M, in a field of magnetic intensity H, is given by $(\underline{M} \cdot \text{grad})\ \underline{H}$. If the direction of magnetization of a fluid element is always in the direction of the local magnetic field, then

$$(\underline{M} \cdot grad)\ \underline{H} = (M/H)(\underline{H} \cdot grad)\ \underline{H} \tag{112}$$

Using a vector identity:

$$(\underline{H} \cdot grad)\ \underline{H} = \frac{1}{2}\ grad\ (\underline{H} \cdot \underline{H}) - curl\ \underline{H} \tag{113}$$

If the fluid is nonconducting and the displacement current is negligible so that curl $\underline{H} = 0$, one obtains

$$(\underline{M} \cdot grad)\ \underline{H} = M\ del\ \underline{H} \tag{114}$$

This result is valid when $\underline{M}$ is parallel to $\underline{H}$ -- a good approximation for the flow of ferrofluid particles, which are mechanically free to align with the field at all times.

If it is assumed that the field varies only in the direction of x, the magnetic body force can be expressed simply as:

$$dF_m = KM \left(\frac{dH}{dx}\right) dx \tag{115}$$

where

F_m is the differential force

K a constant proportional to area

$\frac{dH}{dx}$ the rate of change of field strength in the X direction

dx the differential displacement

The total force obtained by displacing the fluid through a distance L, over which the fluid strength has gone, from H_{max} to some value H_{min}, is then

$$F_M = K \int_0^L M \frac{dH}{dx} dx = K \int_{H_{max}}^{H_{min}} MdH \tag{116}$$

The product MH has the units of pressure, so K is a constant with the units of area. For a force F_m in pounds, an area A_v in square inches, a field strength H in oersteds, and a magnetization M in gauss:

$$F_m = \frac{1.42 \times 10^{-5}}{4\pi} A_v \int_{H_{max}}^{H_{min}} MdH \tag{117}$$

The cross sectional area of fluid required can be determined once the values of H_g, M, and F_m have been selected.

The magnetization M is a function of the magnitude of H, as shown in Figure 73. The integration can be carried out numerically over the regions of H between H_{max} and H_{min}. This process is carried out for each evaluation of the fluid area required for the RAE damper.

b. Surface Stress Derivation

A general stress tensor is developed to describe the fundamental relationships governing the forces exerted upon a ferro magnetic fluid by an applied magnetic field. This stress tensor is then applied to the problem of the design of the RAE viscous damper.

1) Derivation of the Stress Tensor for a Nonlinear Magnetizable Fluid -- The stress tensor in linear fluids is derived in several textbooks. This derivation for a nonlinear material is modeled on the linear analysis of Landau and Lifschitz (1960) but incorporates a few simplifications. For the purpose of illustrating essentials and obtaining the result used in the subsequent design work, this derivation omits the compressibility effect (striction). It then proves possible to eliminate thermodynamic arguments.

As another simplification, superconductors are postulated to carry the currents which serve as the sources of magnetic field. Since the flux enclosed by a superconductor remains constant, no electrical work can be exchanged with an external circuit, and thus any mechanical work performed by the magnetic stress, during a displacement,

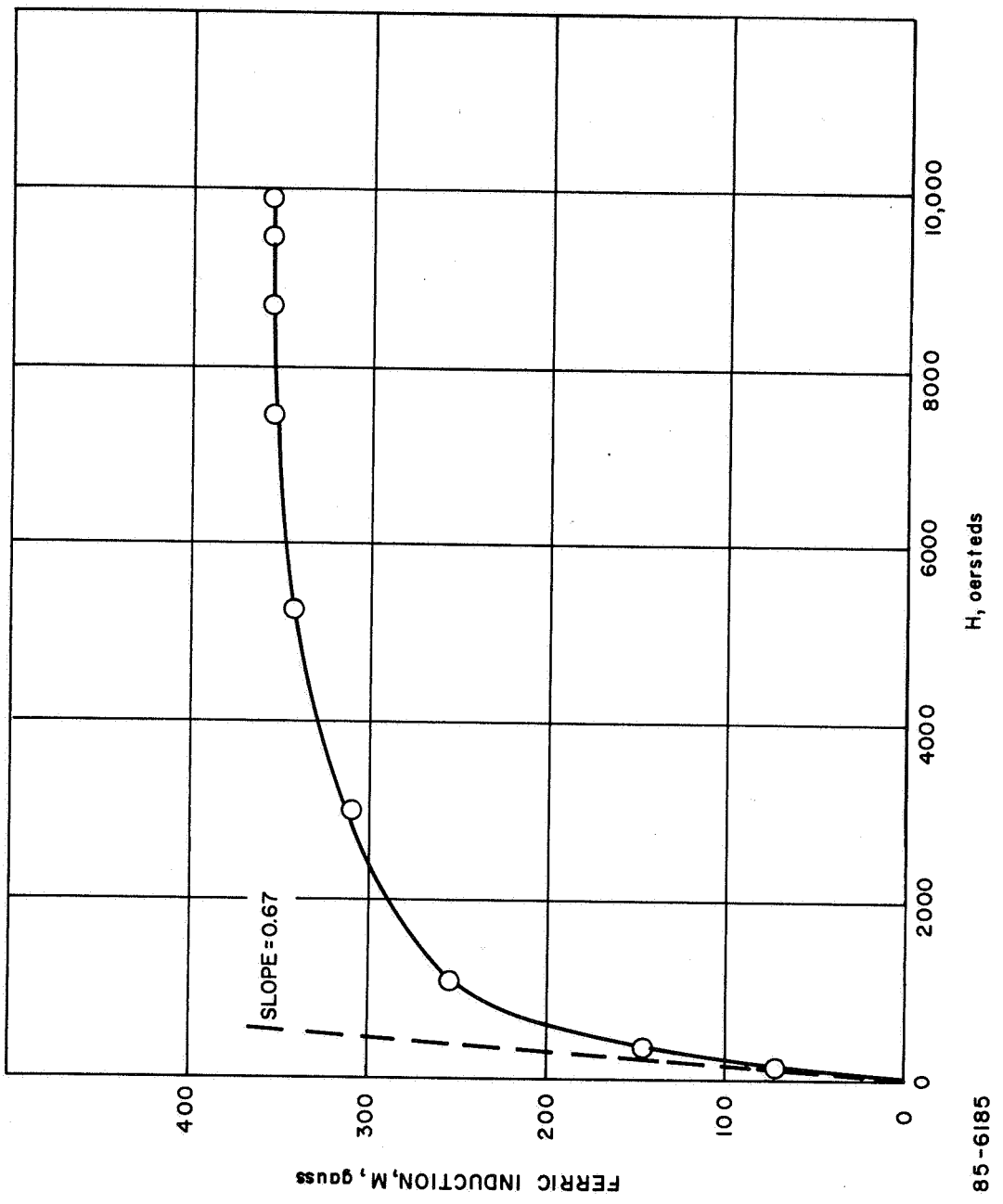

Figure 73 FERROFLUID MAGNETIZATION VERSUS FIELD STRENGTH

is accompanied by a change of field energy. The system consists of ferromagnetic fluid between parallel planes separated by distance h. A uniform field B is impressed throughout the fluid by elementary current loops, making an angle θ with the planes, and the entire system is surrounded by a medium of zero reluctance. The system of current loops combines to yield a current sheet in each plane.

Considering a unit projected area, the volume of fluid is $h \times 1$ and the field energy is $h \int_0^B HdB$. If the upper plane with unit normal $\underline{n}$ is displaced by an arbitrary differential $\underline{\xi}$, an incremental amount of fluid enters from a field-free reservoir, and mechanical work $\sigma_{ij}\, \xi_j\, \eta_i$ is performed on the fluid between the planes as the result of the stress σ_{ij} acting on the moving boundary.

$$\sigma_{ij}\, \xi_j\, \eta_i = - P_o\, \delta h + \delta \left\{ h \int_0^B HdB \right\} \tag{118}$$

$$= - P_o\, \delta h + \delta h \times \int_0^B HdB + h\delta \int_0^B HdB$$

Here P_o is fluid pressure in the absence of a magnetic field. In general, since $B = B(h, \theta)$ the variation of the integral gives

$$\delta \int_0^B HdB = H \left(\frac{\partial B}{\partial h} \right)_\theta \delta h + H \left(\frac{\partial B}{\partial \theta} \right)_h \delta\theta \tag{119}$$

Explicitly, from geometry, $B = \frac{\phi}{h} \sin\theta$, so the partial derivatives are

$$\left(\frac{\partial B}{\partial h} \right)_\theta = - \frac{B}{h} \quad , \quad \left(\frac{\partial B}{\partial \theta} \right)_h = B \cot\theta \tag{120}$$

Combining the equations above,

$$\sigma_{ij}\,\xi_j\,\eta_i = \left\{ -P_o - \int_0^H B\,dH \right\} dH + hH \left(\frac{\partial B}{\partial \theta}\right)_h \delta\theta \tag{121}$$

Additional geometrical relationships may be written for $\delta\theta$ and δh :

$$\delta\theta = \frac{\underline{\xi} \cdot \underline{B}}{hB} \sin\theta, \quad \delta h = \underset{\sim}{\xi} \cdot \underline{\eta} \tag{122}$$

Then, from (121) and (122), the work may be written

$$\sigma_{ij}\,\xi_j\,\eta_i = -\left\{ P_o + \int_0^H B\,dH \right\} \underline{\xi} \cdot \underline{\eta} + H\cos\theta\,\underline{\xi} \cdot \underline{B} \tag{123}$$

But $H\cos\theta = \underline{H} \cdot \underline{\eta} = H_i\,\eta_i$, $\underline{\xi}\,\underline{B} = \xi_j\,B_j$, and $\underline{\xi} \cdot \underline{\eta} = \xi_j\,\eta_i\,\delta_{ij}$

Substituting these into (123) and dividing by the common factor $\xi_j \eta_i$ gives the final expression for the stress tensor:

$$\sigma_{ij} = -\left\{ P_o + \mu_o \int_0^H M\,dH + \frac{\mu_o}{2} H^2 \right\} \delta_{ij} + H_i\,B_j \tag{124}$$

Here $M = \frac{B}{\mu_o} - H$ and when $B = \mu H$, with μ constant, this reduces, as it must, to

$$\sigma_{ij} = -\left\{ P_o + \frac{\mu}{2} H^2 \right\} \delta_{ij} + \mu\,H_i\,H_j \tag{125}$$

which is the standard Korteweg-Helmholtz result for a linear medium in the absence of striction, corresponding to the condition $\frac{\partial \mu}{\partial \rho} = 0$, where ρ is the mass density. Additionally, when applied to field in a vacuum, where accordingly $P_o = 0$ and $\mu = \mu_o$ one obtains from (125) the better known Maxwell stress tensor:

$$\sigma_{ij} = -\frac{\mu_o}{2} H^2\,\delta_{ij} + \mu_o\,H_i\,H_j \tag{126}$$

The body force corresponding to a stress tensor is given by the divergence of the tensor:

$$f_i = \frac{\partial \sigma_{ij}}{\partial x_j} \tag{127}$$

Applied to the terms of (124), this gives

$$\frac{\partial}{\partial x_j}\left\{p_o + \mu_o \int_0^H M dH + \frac{\mu_o}{2} H^2\right\}\delta_{ij} = \frac{\partial}{\partial x_i}\left\{\quad\right\} \tag{127a}$$

and

$$\frac{\partial H_i B_j}{\partial x_j} = H_i \frac{\partial B_j}{\partial x_j} + B_j \frac{\partial H_i}{\partial x_j} = B_j \frac{\partial H_i}{\partial x_j} \tag{127b}$$

since div $B = 0$. Thus

$$\underline{f} = -\,grad\left\{p_o + \mu_o \int_0^H M dH + \frac{\mu_o}{2} H^2\right\} + (\underline{B} \cdot grad)\,\underline{H} \tag{128}$$

Now in the fluid, $\underline{B}$ is parallel with $\underline{H}$, so that

$$(\underline{B} \cdot grad)\,\underline{H} = \frac{B}{H}(\underline{H} \cdot grad)\,\underline{H} = \frac{B}{H}\left\{H\,grad\,H - \underline{H} \times (curl\,\underline{H})\right\} \tag{128a}$$

where the second equality follows from a well known vector identity. Then, since there is no current flow -- the fluid being a nonconductor -- curl $H = 0$, so that $(B \cdot grad)\,H = B\,grad\,H$. Substituting into (128), expanding $B\,grad\,H = \mu_o H\,grad\,H + \mu_o \bar{M}\,grad\,H$, and combining terms gives simply, if $M = M(H)$,

$$\underline{f} = -\,grad\,p_o \tag{129}$$

With no other forces present, e.g., gravity or viscous shear, and when any fluid element in the medium is in equilibrium, i.e., free of acceleration so that $f = 0$, it follows that p_o is constant throughout the medium. Therefore, according to this formulation the effective magnetic stresses are purely surface stresses. The formulation is applied to the viscous damper problem in the next section.

2) Application to Viscous Damper -- The fluid arrangement in the viscous damper is shown schematically in Figure 74, where the nomenclature is also identified. The magnetic field is uniform over the fluid region, except at the ends in the vicinity of an interface, and there $H = (0,\ H_2(X_1)\ 0)$. The interface separates a gas or vapor region from the fluid region.

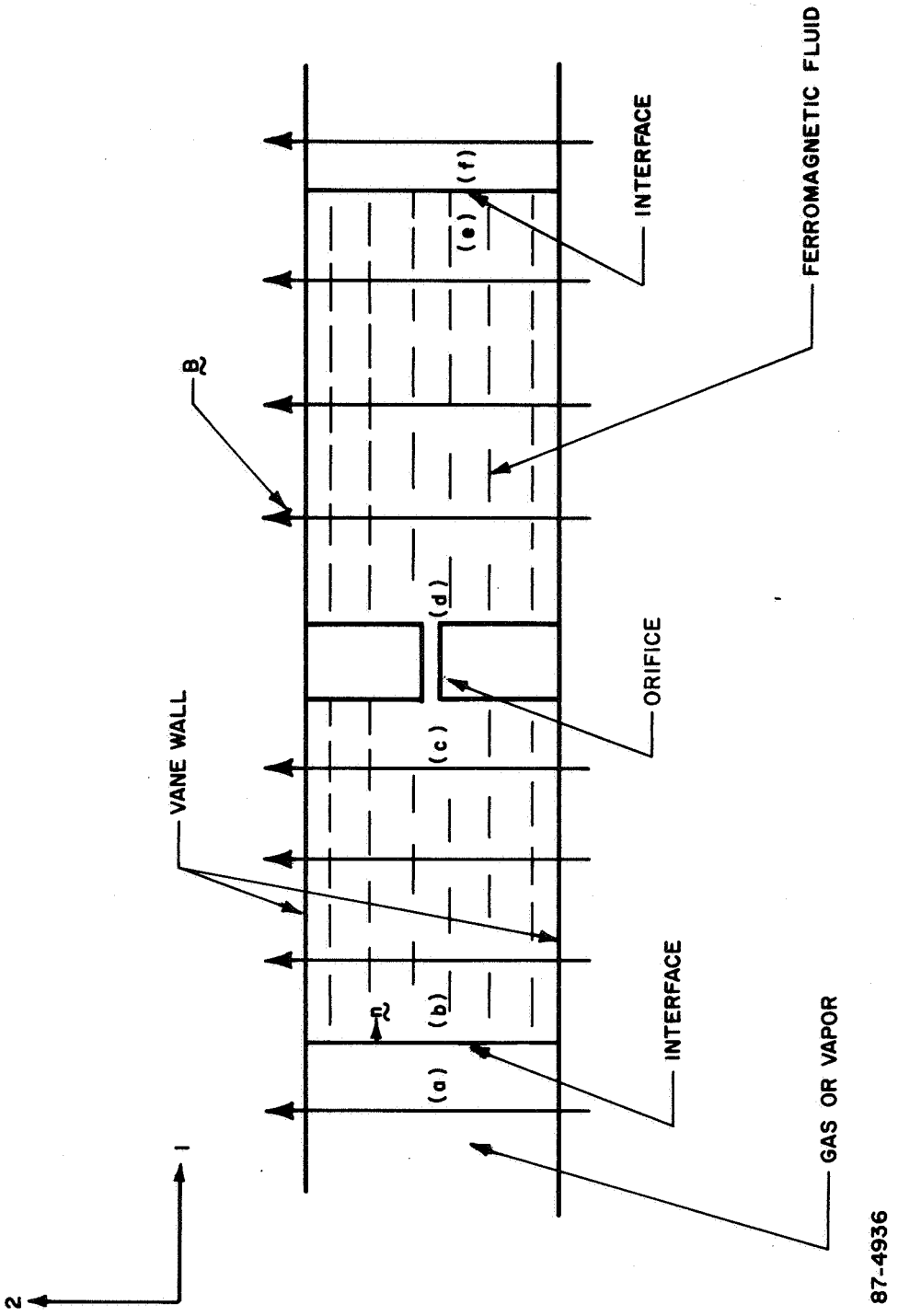

Figure 74 DIAGRAM TO ILLUSTRATE MAGNETIC FLUID DYNAMICS

It may be imagined that the magnet is moved to the right with regard to a frame of reference attached to the vane. The purpose of the analysis, then, is to determine an expression for the pressure difference $\Delta p = p^{(c)} - p^{(d)}$ which accompanies flow through the orifice tube.

As shown in the preceding section, the fluid pressure even in the presence of magnetic fields is constant under certain conditions. Since in this flow system the only significant viscous forces appear within the orifice tube and since gravity forces are assumed absent, it may be concluded that

$$p^{(b)} = p^{(c)} \text{ and } p^{(d)} = p^{(e)}$$

so that the pressure difference is also given by

$$\Delta p = p^{(b)} - p^{(e)} \tag{130}$$

which reduces the problem to the determination of $p^{(b)}$ and $p^{(e)}$.

Neglecting any effects of ordinary surface tension, the condition of equilibrium of the interface is

$$[\sigma_{ij}\,\eta_j] = 0 \tag{131}$$

where brackets indicate the difference of the quantity across the interface. For the coordinate system indicated in the diagram, the unit normal vector is $\underline{n} = (1, 0, 0)$ when the normal is directed toward the medium from the gas or vapor space. Equation 124 gives the stress tensor,

$$\boxed{\sigma} = \begin{bmatrix} -p^* - \frac{\mu_o}{2} H_2^2 & 0 & 0 \\ 0 & -p^* - \frac{\mu_o}{2} H_2^2 + H_2 B_2 & 0 \\ 0 & 0 & -p^* - \frac{\mu_o}{2} H_2^2 \end{bmatrix}$$

since $\underline{H}$ and $\underline{B}$ are assumed to be oriented along the 2-direction. In this p^* is defined:

$$p^* = p_o + \mu_o \int_0^H M\,dH$$

Hence for a surface in the medium at b oriented normal to the positive x_i direction, the stress is

$$(\sigma_{ij}\ \eta_j)_{i=1} = \sigma_{11}^{(b)} = -p_o^{(b)} - \mu_o \int_0^H M\,dH - \frac{\mu_o}{2}\ {H_2}^{2\,(b)}$$

while for a similar surface just outside the medium at (a),

$$\sigma_{11}^{(a)} = -p_o^{(a)} - \frac{\mu_o}{2}\ {H_2}^{2\,(a)}$$

since the surrounding gas or vapor is presumed void of magnetic moment. Thus from (131),

$$p_o^{(b)} = p_o^{(a)} - \mu_o \int_0^{H^{(b)}} M\,dH \tag{132}$$

since $[H_2] = 0$, because the tangential component of H is continuous across an interface. The same procedure followed through for the remaining interface gives

$$p_o^{(e)} = p_o^{(f)} - \mu_o \int_0^{H^{(e)}} M\,dH \tag{133}$$

In the damper, the vapor spaces communicate so that $p_o^{(a)} = p_o^{(f)}$, and accordingly subtraction of (133) from (132) gives

$$\Delta p = p_o^{(c)} - p_o^{(d)} = p_o^{(b)} - p_o^{(e)} \tag{134}$$

$$= \int_b^e M\,dH = \int_a^f M\,dH$$

This result is appropriate for use as a design equation. Then the volumetric flow rate for well developed laminar flow through the orifice tube is given by

$$Q = \frac{\pi}{128} \frac{\Delta p\, d^4}{\mu \ell} = \frac{\pi}{128} \frac{d^4}{\mu \ell} \int_a^f M\, dH \qquad (135)$$

3) Cavitation -- It is noted from (132) or (133) that the magnetic quantity $\int_0^H M\, dH$ in this system acts as an interfacial stress directed away from the magnetic medium and so causes a reduction of the pressure in the fluid below the pressure of the ambient. Hence, nowhere in this system is the ferromagnetic fluid under an increased pressure; rather, the fluid is everywhere acted upon by a reduced pressure and this of course, is a condition that favors cavitation.

As a final note, the assumption that $H = (0, H_2, 0)$ with H_2 a function only of position along the x_1 axis is, strictly speaking, incompatible with the condition $curl\ \underline{H} = 0$. However, the objection is not an important one and does not lead to any real difficulties. For example, the objection may be overcome by consideration of a cylindrically symmetric magnetic field.

c. Cellular Flow in a Constant Area Vane

For the constant area vane configuration we may define boundary conditions of an idealized flow, although one of some complexity, which may adequately predict the flow and drag characteristics. Referring to Figure 75 the boundary conditions are

1) $u = 0 \quad \frac{\partial v}{\partial x} = 0 \quad on \quad X = 0,\ L$

2) $v = 0 \quad on \quad y = 0,\ H$

3) $u = const.\ only = H$

4) $u_y = 0 \quad on \quad y = 0$

The solution of a closely related problem is available from the work of Weiss and Florsheim. Approximate solutions were obtained for the flow fields in rectangular cavities by neglecting the convection of vorticity. These solutions yield multicell recirculation regions for high aspect ratio cavities. Water tank experiments at a Reynolds Number of 150 confirmed the prediction of double-celled cavity flow and show good agreement with the theoretical cell dimensions. It was inferred that zero Reynolds Number solutions have an extensive range of validity in flows with closed streamlines.

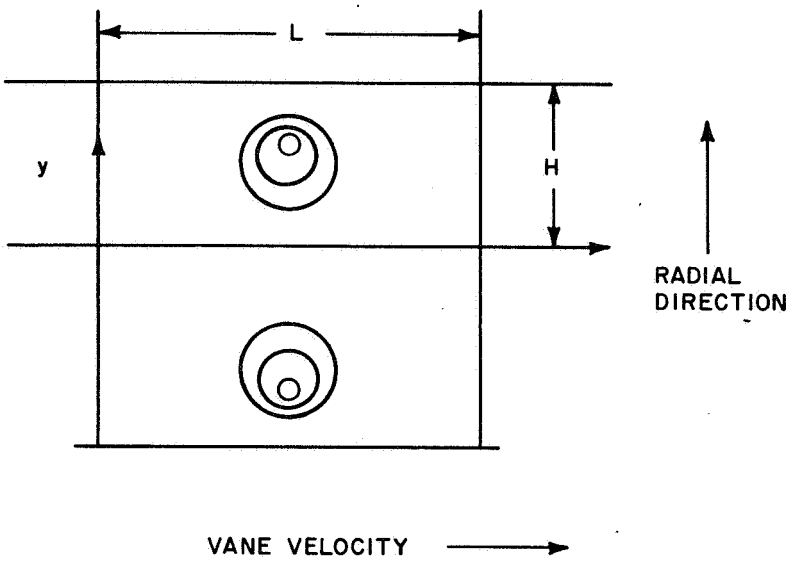

87-4937

Figure 75 CELLULAR FLOW WITHIN A CAVITY

Referring to Figure 75 again, the problem considered was defined by the following boundary conditions:

1) $u = v = 0 \quad on \quad X = 0, \; L$

2) $v = 0 \quad on \quad y = 0, \; H$

3) $[u]_{\pm} = [\tau]_{\pm} = [p]_{\pm} = 0 \; on \; y = H$

4) $u_y = 0 \quad on \quad y = 0$

where brackets denote the difference of the quantity evaluated on each side of a surface, and a subscript denotes differentiation with respect to the indicated variable. At $y = H$ the velocity component v was taken as a function of x having a maximum value of $x = L/2$. With ψ the stream function such that $u = \psi y$ and $v = -\psi x$, the Navier-Stokes equation for the incompressible medium reduces to

$$\nabla^4 \psi = 0$$

Considering the problem by variational principles it may be shown that the square of the vorticity in the region is minimized. The first order approximation to the solution is

$$\psi^{(1)} = \frac{3^{1/4}}{2\pi} \frac{u(x, H)_{max} L}{2\pi\Gamma} \sin^2 \frac{\pi X}{L} \left\{ \cos h(by) \sin(ay) - \frac{\tan(aH)}{\tan h(bH)} \sin h(by) \cos(ay) \right\} \tag{136}$$

where Γ, a, and b are complex functions of the geometry.

$$\begin{aligned} \Gamma = {} & \sin(1/2 \tan^{-1}\sqrt{2}) \cos h(bH) \cos aH \\ & + \cos(1/2 \tan^{-1}\sqrt{2}) \sin h(bH) \sin(aH) \\ & - \frac{\tan aH}{\tan h(bH)} \left[\cos(1/2 \tan^{-1}\sqrt{2}) \cos h(bH) \cos(aH) \right. \\ & \left. - \sin(1/2 \tan^{-1}\sqrt{2}) \sin h(bH) \sin(aH) \right] \end{aligned} \tag{137}$$

and

$$a = \frac{2\pi}{3^{1/4} L} \sin(\tan^{-1}\sqrt{2})$$

$$b = \frac{-2\pi}{3^{1/4} L} \cos(\tan^{-1}\sqrt{2}) \qquad (138)$$

The solution reveals the presence of a core or a point of zero velocity within the recirculation region. As a most important result it is found that more than one core and hence more than one cell may be found, depending on the aspect ratio of the cavity.

The following tabulation illustrates the nature of the solution, showing the number of cells on either side of the centerline of the cavity as a function of the aspect ratio:

Aspect Ratio	Cell Structure
$0 < H/L < 1$ to 2	one cell
1 to $2 < H/L < 4$	two cells
$H/L = 4$	three cells

Experiments with aqueous glycerin solutions confirmed the existence of two cells at H/L = 3.0, while the core centers were within 19 percent of the predicted value.

For the constant area vane configuration, the damper is characterized by cavities in which the aspect ratio follows the inequality.

$$0 < H/L < 4$$

Hence it may be concluded that with the constant area vane concept with higher aspect ratios, the calculated damping factor might be in error by a factor of 2 to 1.

d. Incompressible Flow of a Viscous Fluid Through an Orifice

An analytical description of fluid motion including the effects of viscosity is given by the equations of Navier-Stokes. These equations, when expressed in cylindrical coordinates, describe the velocity of the the viscous fluid through an orifice, in terms of the pressure gradient and the body forces acting on the fluid.

For cylindrical flow, the Navier-Stokes force equation is:

$$\rho \left(\frac{\partial V_z}{\partial t} + V_r \frac{\partial V_z}{\partial r} + V_\phi \frac{\partial V_z}{\partial \phi} + V_z \frac{\partial V_z}{\partial z} \right) = \tag{139}$$

$$F - \frac{\partial P}{\partial z} + \mu \left(\frac{\partial^2 V_z}{\partial r^2} + \frac{1}{r} \frac{\partial V_z}{\partial r} + \frac{1}{r^2} \frac{\partial^2 V_z}{\partial \phi^2} + \frac{\partial^2 V_z}{\partial^2 z^2} \right)$$

where

P = Pressure

ρ = Fluid Density

V = Velocity

z = Axial direction

r = Radial direction

ϕ = Azimuthal direction

F_z = Body force

For steady horizontal flow along z :

$$\frac{\partial V_z}{\partial t} = 0, \quad V_\phi = 0, \quad V_r = 0, \quad \frac{\partial V_z}{\partial z} = 0 \tag{140}$$

Therefore

$$\frac{dP}{dz} = \mu \left(\frac{d^2 V_z}{dr^2} + \frac{1}{r} \frac{dV_z}{dr} \right) \tag{141}$$

Pressure P can only be a function of z , and $\frac{dP}{dz} \left(\frac{1}{\mu} \right)$ must equal a constant K.

Attempting a solution of the form $V_z = A r^n + b$,

$$\dot{V}_z = n A_r^{n-1} \tag{142}$$

$$\ddot{V}_z = n(n-1) A_r^{(n-2)}$$

Substituting,

$$K = A\,\eta\,(n-1)\,r^{n-2} + \frac{A}{r}\,n\,r^{n-1} \tag{143}$$

Therefore for K = constant, n must equal 2.

$$V_z = A\,r^2 + b \tag{144}$$

Substituting $\frac{\dot{V}}{r} = 2A$, $\ddot{V} = 2A$ in Equation 141:

$$A = \frac{1}{4}\,\frac{dP}{dz}\,\frac{1}{\mu} \tag{145}$$

Substituting in Equation 143 for A,

$$V_z = \frac{1}{4}\,\frac{dP}{d}\,\frac{1}{\mu}\,r^2 + b \tag{146}$$

Since $V_z = 0$ at $r = R$,

$$b = -1/4\,\frac{dP}{dz}\,\frac{1}{\mu}\,R^2 \tag{147}$$

Therefore,

$$V_z = \frac{1}{4\mu}\,\frac{dP}{dz}\,(r^2 - R^2) \tag{148}$$

The velocity distribution in the orifice is parabolic with zero velocity at the outer diamter and maximum velocity at the centerline. The mean velocity is 1/2 the maximum velocity.

$$\bar{V}_z = \frac{R^2}{8\mu}\left(-\frac{dP}{dx}\right) \tag{149}$$

The volume rate of flow is

$$Q = \pi\,R^2\,\bar{V}_z \tag{150}$$

Therefore, the pressure drop is equal to

$$\frac{dP}{dx} = \frac{-V_z\,8\mu}{R^2} = -\frac{Q\,8\,\mu}{\pi\,R^4} \tag{151}$$

For entry and exit areas A and orifice length L

$$F = -A\ dP = A\ (P_1 - P_2) = \frac{Q\ 8\ \mu\ L\ A}{\pi\ R^4} \tag{152}$$

For a vane velocity flow V_v in area A_v:

$$F = \frac{V_v\ 8\ \mu\ LA_v^2}{\pi\ R^4} = \frac{128\ V_v\ \mu\ LA_v^2}{\pi\ D^4} \tag{153}$$

The viscous torque T exhibited by the damper is just $F\ R_v$:

$$T = \frac{128\ V_v\ \mu\ LA^2\ R}{\pi\ D^4} \tag{154}$$

This value of torque is identical to that computed by more elementary methods in the section relating baffle and orifice design.

3. Parametric Study of Damper Cavities

Several damper concepts are considered for use in the RAE damper application in Section IV. A. 1. In the following subsections a basis for comparison is made in terms of damper parameters for each of the concepts. The first three subsections describe the relationships between the viscous parameters and the vane parameters. The fourth subsection relates the magnetic force parameters and the vane parameters.

a) Constant Area Vane

In a constant area vane similar to the one shown in Figure 21, the fluid midway between the walls moves at the velocity of the magnet assembly, while the fluid at the walls has zero relative velocity with respect to the walls. The fluid velocity increases linearly between the walls and the centerline, with the flow being laminar and parallel to the walls.

A viscous shear stress S_s is developed which is proportional to the viscosity of the fluid μ, and the rate of shear strain dv/dy:

$$S_s = \mu\ \frac{dv}{dy} \tag{155}$$

where v is the velocity of the fluid at a distance y from the centerline of the vane. The shear stress is equal to the ratio of viscous force F_S to shear area A_S:

$$S_s = F_S / A_S \tag{156}$$

The viscous torque T_S is equal to

$$T_S = R_V F_S = R \mu \frac{dv}{dy} A_S \tag{157}$$

The mean fluid velocity $\bar{v}$ is one-half the peak fluid velocity, and the velocity gradient occurs over one-half the normal dimension of the vane b/2, so the torque reduces to

$$T_S = R \mu \frac{2v}{b/2} A_S \tag{158}$$

The shear area is the length of the fluid times twice the radial dimensions of the vane, since two shear areas are involved; therefore:

$$A_S = 2 L h \tag{159}$$

The shear torque equals

$$T_S = \frac{R \mu \bar{V} h L}{b/2} = \frac{8 R \mu \bar{V} L h}{b} \tag{160}$$

Since $\bar{v}$ equals the angular velocity ω times the mean radius R, the viscous torque equals

$$T_S = 8 R^2 \frac{\mu \omega L h}{b} \tag{161}$$

The damping coefficient C_D is equal to $\frac{T}{\mu}$, so:

$$C_D = \frac{8 R^2 \mu L h}{b} \tag{162}$$

For C_D = ft -lb-sec, L, h, b, R = inches, and μ = centipoise,

$$C_D = 9.7 \times \frac{10^{-8} R^2 \mu L h}{b} \tag{163}$$

Figure 76 gives the parametric plot of μ versus R for several values of C_D. The following values are used:

$L = 2.5$

$h = 1$

$b = .1$

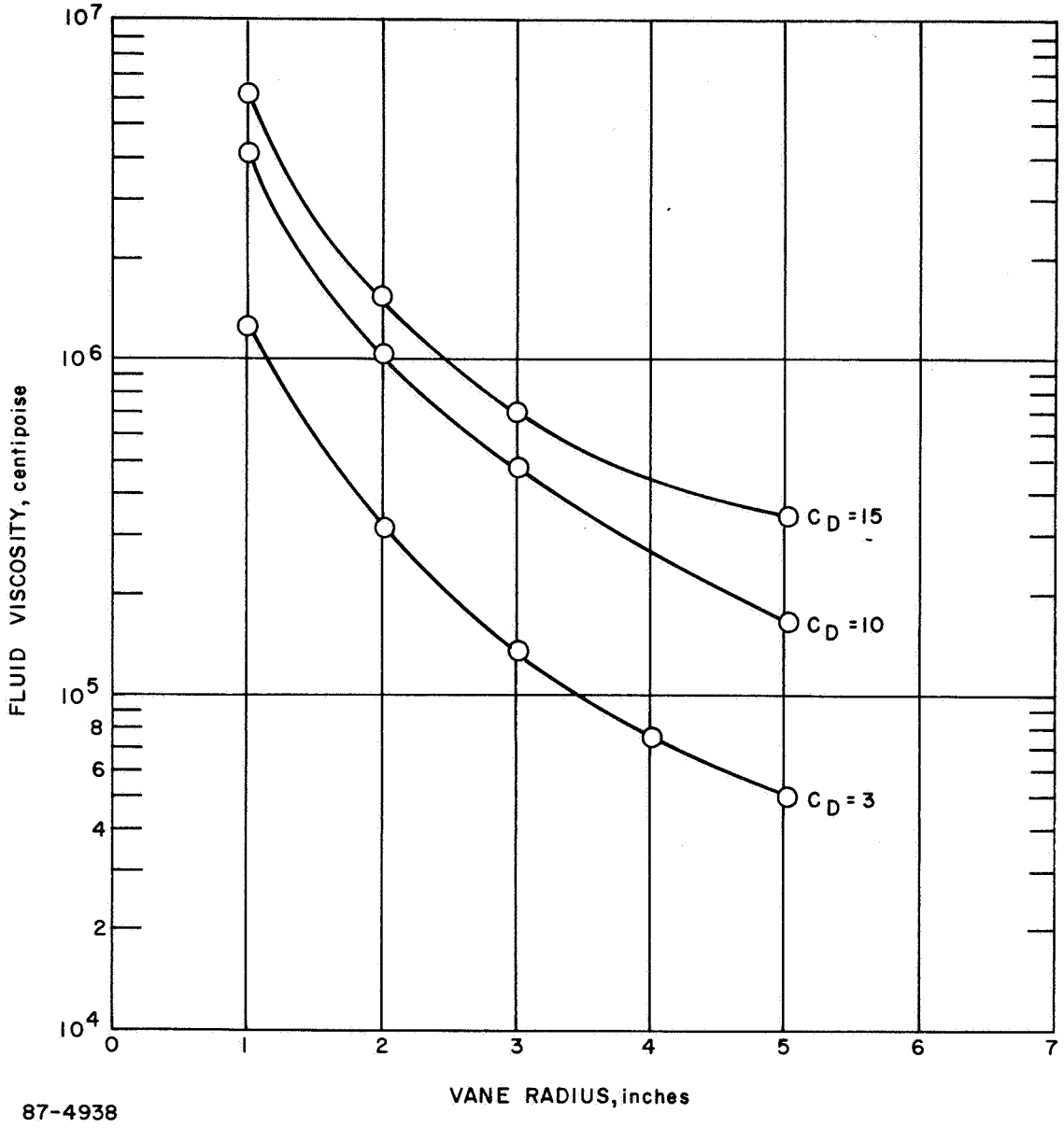

Figure 76 CONSTANT AREA VANE FERROFLUID VISCOSITY VERSUS DAMPER RADIUS

The curves are a plot of

$$\mu = 4.14 \times 10^5 \, C_D / R^2 \tag{164}$$

b. Vane/Orifice

Large viscous forces can be obtained with relatively low viscosity fluids by placing a baffle with a small orifice in the path of the fluid. A pressure drop is generated in the orifice which is proportional to the length of the orifice. This pressure drop times the total vane area equals the viscous force developed.

The viscous shear force F is equal to the shear stress S_s times the shear area $2\pi y L$, where y is the radial distance from the centerline of the orifice:

$$F = S_s \, 2\pi y L = (P_1 - P_2) \pi y^2 \tag{165}$$

The shear stress S_s is equal to

$$S_s = \mu \frac{dv}{dy} \tag{166}$$

Therefore the rate of shear strain $\frac{dv}{dy}$ is

$$\frac{dv}{dy} = - \frac{\Delta p \, y}{2 \mu L} \tag{167}$$

The velocity at any radius y is

$$V = - \frac{\Delta p y}{2 \mu L} + C \tag{168}$$

Since at

$$C = \frac{\Delta p}{4 \mu L} \, (D^2/4) \tag{169}$$

and

$$V = \frac{\Delta p}{4 \mu L} \, (D^2/4 - y^2) \tag{170}$$

The maximum velocity occurs at the centerline of the orifice:

$$V_{max} = \frac{\Delta p\, D^2}{16\, \mu\, L} \tag{171}$$

The volume of fluid flow Q is

$$Q = \int_0^{D/2} 2\pi\, \gamma\, V\, dV = \frac{\pi\, \Delta p\, D^4}{128\, \mu\, L} \tag{172}$$

The mean velocity of the fluid in the orifice $\bar{v}_o$ is

$$\bar{V}_o = \frac{Q}{A_o} = \frac{\Delta P\, D^2}{32\, \mu\, L} \tag{173}$$

Therefore, the pressure drop is

$$p = \bar{V}_o \frac{32\, \mu\, L}{D^2} \tag{174}$$

The total force:

$$F = \Delta p\, A_v \tag{175}$$

If $\bar{V}_v$ is the velocity of the fluid in the vane,

$$\bar{V}_o = \frac{A_v}{\pi\, D^2/4}\, \bar{V}_v \tag{176}$$

Then the viscous force is

$$F = \frac{32\, \mu L\, A_v^2}{D^2(\pi D^2/4)}\, \bar{V}_v \tag{177}$$

The viscous torque is

$$T = F R_v = \frac{128\, A_v^2\, L \mu\, \bar{V}_v\, R_v}{\pi\, D^4} \tag{178}$$

The orifice length is equal to

$$L = \frac{T\, \pi\, D^4}{128\, A_v^2\, V_v\, R_v} \tag{179}$$

$$L = C_D \frac{\pi D^4/\mu}{128 A_v^2 R_v^2} \tag{180}$$

For C_D = ft-lb-sec, D = inches, μ = centipoise, A_v = inches squared, R_v = inches, and L = inches,

$$D^4 = \frac{4.29 \times 10^{-7} A_v^2 R_v^2 \mu L}{C_D} \tag{181}$$

For C_D = 4.0 ft-lb-sec, R_v = 3.5 inches, A_v = 0.128 in.^{2}, $L = 10^7 C_D D^4/\mu$, and $L = 4 \times 10^7 D^4/\mu$. See Figure 77 for a plot of orifice diameter versus orifice length.

It is desirable to have fairly large length to diameter ratios, approaching 10/1, to minimize entry losses. It is also desirable to have orifice diameters which exeed 0.0135 inch, so that standard drills can be used. In smaller diameters, drilled lengths rarely exceed 5 times the diameter. A 0.200 inch long orifice will provide reasonable diameters and length to diameter ratios for fluids with viscosities from 10 to 100 cp. It is expected that the magnet fluid will have a viscosity between 10 and 200 cp at 70° F. Since this temperature is near the maximum seen by the damper in space, the damping coefficient selected for the computation is near the minimum specified.

c. Porous Bed Vane

Damping can be achieved in the RAE damper vane by creating a pressure drop across magnetic fluid trapped in a bed of packed spheres.

The pressure drop for a fluid flowing through a packed bed of spheres is proportional to the fluid viscosity μ, the bed length (or fluid length in the bed) L, and the fluid velocity v. The pressure drop is inversely proportional to the square of the diameter of the spheres. The pressure drop is also a function of the porosity e, where

$$e = \frac{\textit{void volume}}{\textit{total volume}}$$

The pressure drop Δp is equal to

$$\Delta p = \frac{K' V (\mu)(1-e)^2 L}{D^2 e^3} \tag{182}$$

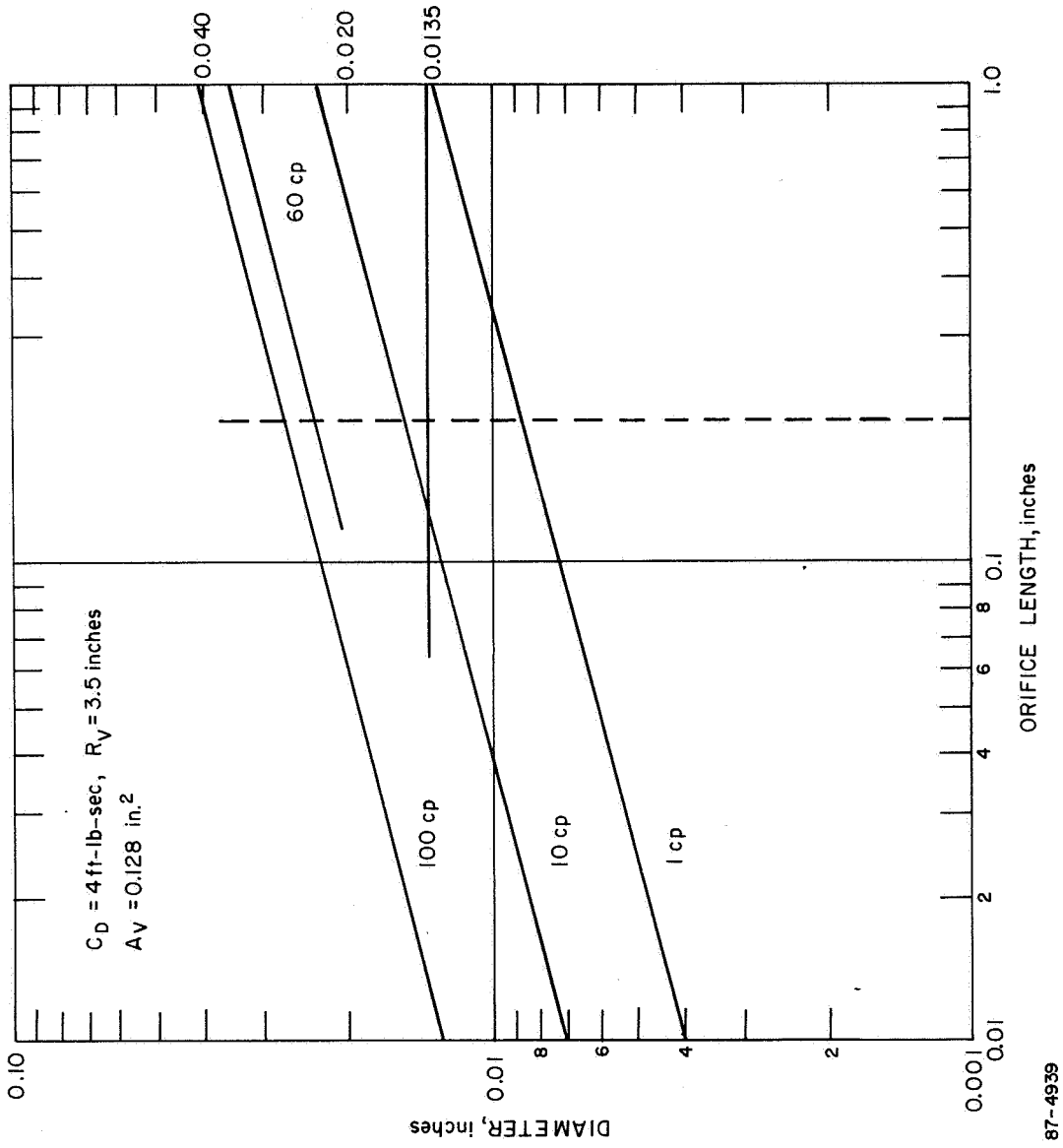

Figure 77 ORIFICE DIAMETER VERSUS ORIFICE LENGTH

$K' = 200$ (Perry's Chemical Handbook) for any consistent set of units. Putting μ = centipoise, D = inches, L = inches, V = inches/sec, and Δp = lb/in.^{2}

To convert $\mu\,(cp)$ to $\mu \frac{lb\text{-}sec}{in.^2}$, multiply $\mu\,(cp)$ by 1.45×10^7. Then the pressure drop achieved is equal to

$$\Delta p_A = \frac{2.9 \times 10^{-5}\, V\,(\mu)\,(1-e)^2\, L}{D^2\, e^3} \tag{183}$$

The pressure drop required is

$$\Delta p_R = \frac{T_{MAX}}{R_v\, A_v\, e}$$

To simplify the calculations and make the pressure drop required independent of porosity, multiply both Δp equations above by e. The pressure drop achieved is then

$$\Delta p_A = \frac{2.9 \times 10^{-5}\, V\,(\mu)\,(1-e)^2\, L}{D^2\, e^2} \tag{184}$$

The pressure drop required is then

$$\Delta p_R = \frac{T_{MAX}}{R_v\, A_v} \tag{185}$$

Multiplying the Δp equations by $R_v\, A_v$ and dividing by w yields C_D.

$$C_D = \frac{2.9 \times 10^{-5}\,(\mu)\,(1-e)^2}{D^2\, e^2}\; L\, R_v\, A_v \tag{186}$$

If a typical vane has a radius of 3.5 inches and an area of 0.2 inch, then

$$C_D = 7.1 \times 10^{-5}\,(\mu)\, \frac{(1-e)^2}{e^2}\, \frac{L}{D^2} \tag{187}$$

Rearranging:

$$D^2/L = 7.1 \times 10^{-5}\, \frac{(\mu)}{C_D}\, \frac{(1-e)^2}{e^2} \tag{188}$$

Plots of D^2/L versus e for $\frac{\mu}{C_D}$= 25, 10, and 4 are given in Figure 78. They are plots of

$$D^2/L = 1.73 \times 10^{-3} \frac{(1-e)^2}{e^2} \tag{189}$$

and

$$D^2/L = 7.1 \times 10^{-4} \frac{(1-e)^2}{e^2}$$

and

$$D^2/L = 2.9 \times 10^{-4} \frac{(1-e)^2}{e^2}$$

d. Vane Area as a Function of Magnetic Force

The magnetic force developed between the ferrofluid and an applied magnetic field is proportional to the cross sectional area of the fluid in the fringing field. The expression for the force was derived earlier and is restated below:

$$F_m = \frac{1.42 \times 10^5}{4\pi} A_V \int_{H_{max}}^{H_{min}} M \, dH \tag{190}$$

The magnetic torque is proportional to the mean vane radius R_v, where A_v is the vane cross-sectional area, M is the ferrofluid magnetic field moment, and H is the magnetic field strength.

Figure 73 shows that M is a function of H, so that an integration of the curve under the region between H_{max} and H_{min} is required prior to a solution for the vane area A_v. A computer program was written to perform this computation, and the other computations required to design the vane and magnet. The program is described in Section IV. A. 2. d.

Three linear approximations to the M-H curve have been used, one in the region between 0 and 300 oersteds, one between 300 and 1000 oersteds, and the third between 1000 and 2500 oersteds. Higher fields have not been considered, because of excessive magnet weight.

The minimum field strength H_{min} has been selected arbitrarily as 500 oersteds. Maximum field strengths of 1000, 1500, 2000, and 2500 oersteds have been considered, with maximum ferrofluid magnet moments of 500, 600, 700, and 1000 gauss. Parametric plots of vane area versus fluid magnetic moment are shown in Figure 79 for peak

torque of 0.024 ft/lb. The area is directly proportional to the torque, so the area can be determined for any other torque by multiplying the value on the curve by the ratio of the torque values.

The area is inversely proportional to the vane radius, so a similar operation can be carried out for other radii.

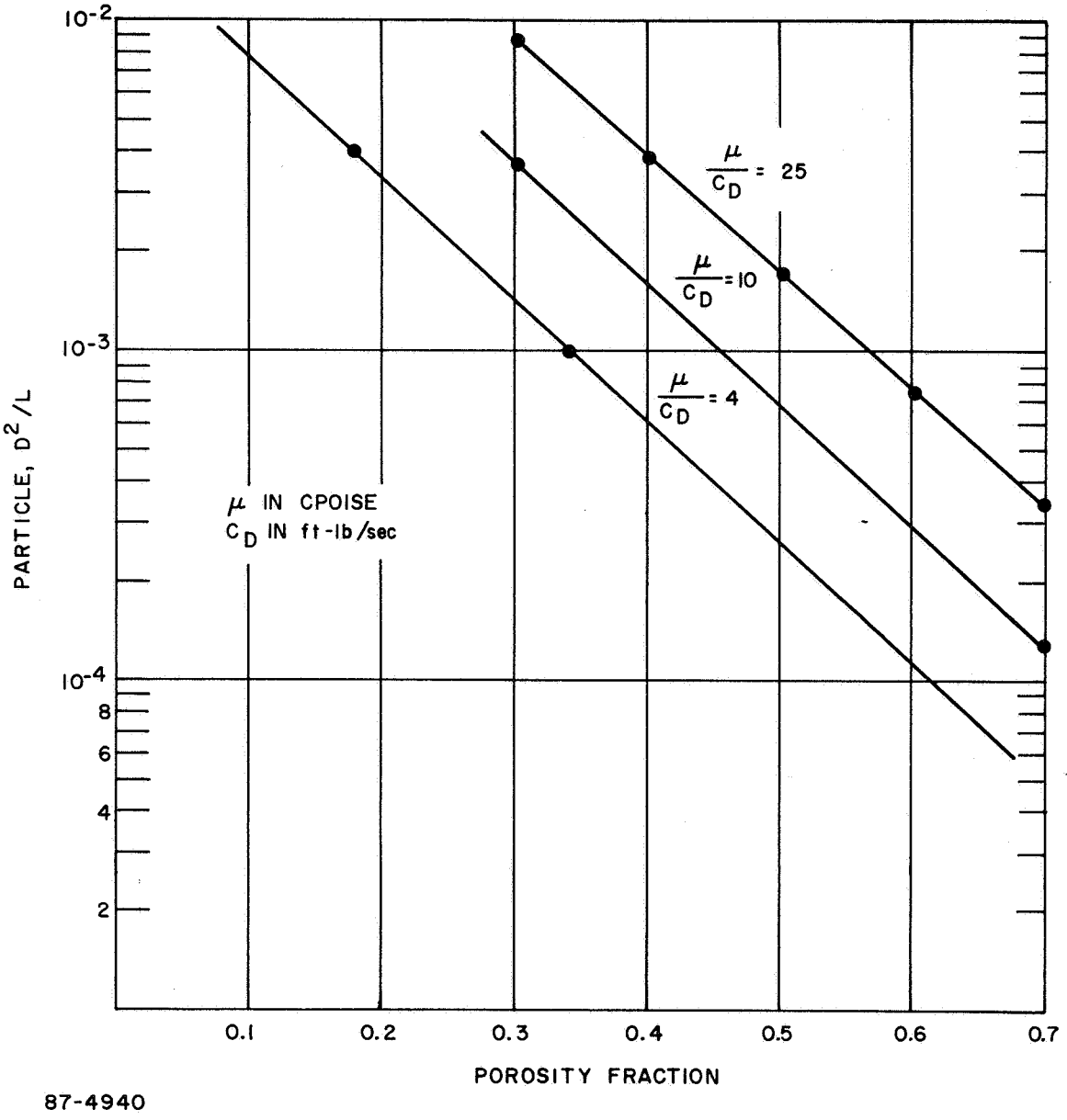

Figure 78 PARTICLE BED PARAMETERS -- VANE WITH PACKED BED OF SOLIDS

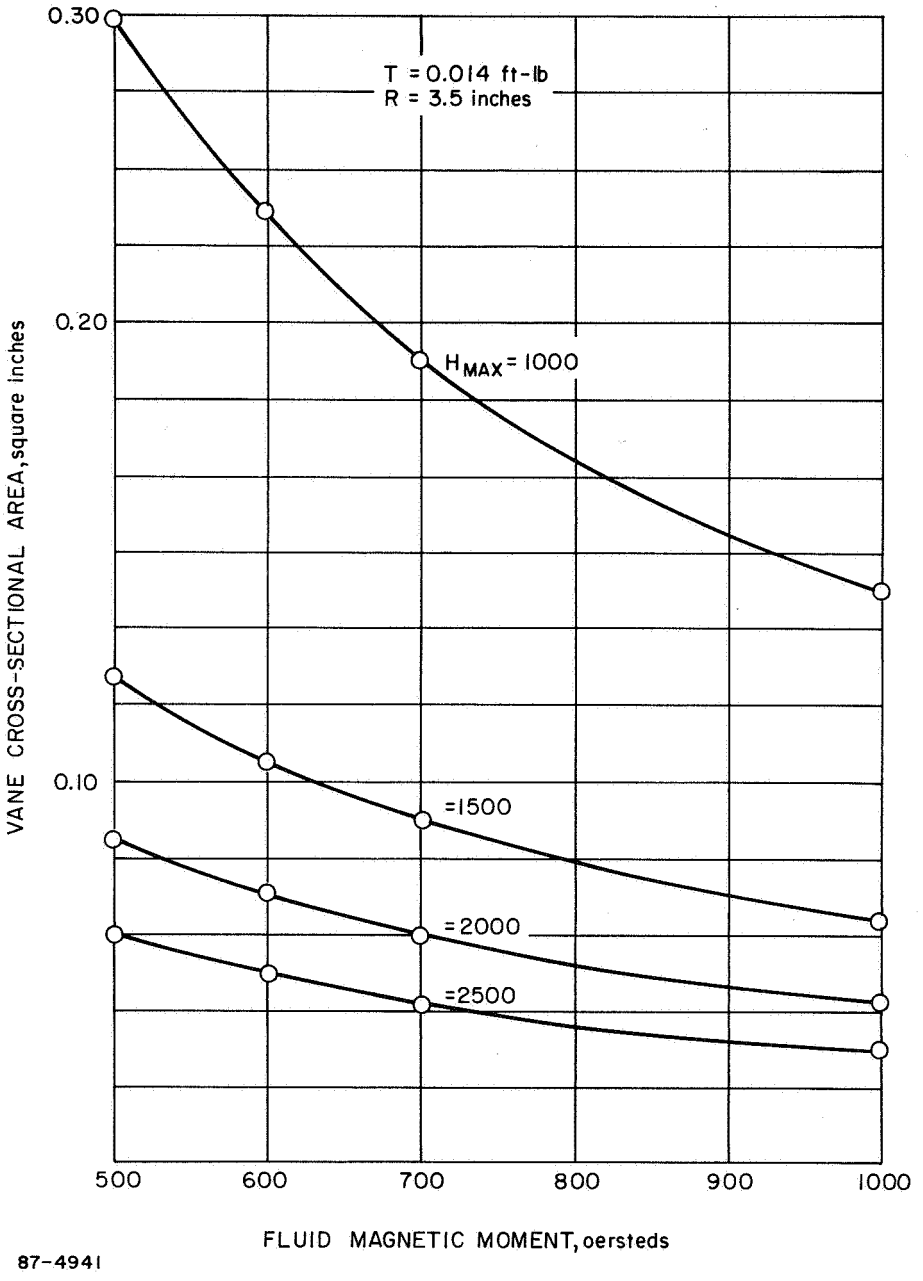

Figure 79 VANE AREA VERSUS MAGNETIC MOMENT

V. CONCLUSIONS AND RECOMMENDATIONS

A. CONCLUSIONS

1. The ferrofluid viscous damper will meet the requirements of the Radio Astronomy Explorer Satellite over the specified operating temperature range (0^{o} F to 70^{o} F).

2. Development of a damping mechanism using low viscosity hydrocarbon ferrofluid was shown to be feasible both in study results and by test.

3. While development of a high viscosity silicone fluid was not successful during this study, positive results were obtained in producing a low viscosity silicone fluid stabilized by a silicone surfactant. The low viscosity hydrocarbon damping mechanism discussed in 2 above does, however, eliminate immediate need for a silicone ferrofluid. The objectives of the program were met through development of a suitable, thermally compensated hydrocarbon ferrofluid.

4. Mechanical and magnetic design considerations for the ferrofluid damper showed that the damper can be made reliably at a weight far below that normally associated with viscous dampers of comparable performance. The study showed a damper weight of 0.84 pound exclusive of any satellite interface bracket requirements.

5. A pivot type suspension was shown to provide the best suspension means for the ferrofluid viscous damper.

6. Consideration of environmental exposure showed the damper well able to meet requirements, as discussed in Section IV.C of this report.

B. RECOMMENDATIONS

In view of the performance advantages of the ferrofluid viscous damper for Radio Astronomy Explorer satellite application, it is recommended that the present program be extended to include development of a prototype model for application on future satellite launchings.

VI. BIBLIOGRAPHY

1. Rosensweig, R. E., and Resler, E. L., AIAA Journal 2, 1418 - 1422 (1964).

2. Papell, S. S., USP 3215572, November 2, 1965.

3. Rosensweig, R. E., Nestor, J. W., and Timmins, R. S., A.I. Ch.E I., Chem E., Symposium Series, No. 5, 114 - 118 (London, 1965).

4. Lifschitz, E. N., Soviet Physics, JETP 2, 78-83 (1956).

5. Dintenfass, L., Kolloid. Z. 155, 121 (1957).

6. Rosenweig, R. E., and Kaiser, R., Research in the Synthesis and Characterization of Magnetic Ferrofluids, Final Report, Contract NASW 1219, Avco Research and Technology Laboratories, Wilmington, Massachusetts (February 1967).

7. Synthetic Lubricants, Edited by R. C. Gunderson and A. W. Hart, Reinhold Publishing Corp., New York (1962); see Figure 5.8, p. 202.

8. Kircher, J., and Bowman, R. E., Effects of Radiation on Materials and Components, Reinhold, New York (1964).

9. Smit, Wein, Ferrites, Wiley(1964).

10. Radiation Damage Thresholds for Permanent Magnets, NOLTR-61-45, U. S. Naval Ordance Laboratory, White Oak, Maryland.

11. Permanent Magnet Design Handbook, Crucible Steel Company, Inc.

12. Permanent Magnet Design, Bulletin M303, Thomas and Skinner, Inc.

13. Flexural Pivot Technical Literature, Bendix Corporation, Utica Division, Utica, New York.

14. Barden Precision Bearings, Engineering Catalog G-3, The Barden Corporation, Danbury, Connecticut.

15. Roark, R. J., Formulas for Stress and Strain, Fourth Edition, McGraw-Hill Book Company.

16. " Design and Application of Metallic Flexures for Equipment With Specific Life Requirements, " ASME Paper 871A.

17. Goetzel, Rittenhouse, and Singletory, Space Materials Handbook, Lockheed Missiles and Space Company.

18. Molloy, K. H., Progress in Design and Development of the RAE Viscous Damper, 1 January 1966 - 1 August 1966, Avco Space Systems Division.

19. Molly, K. H., NASA Goddard Viscous Damper Specification, GCCD-W320-134A, Avco Space Systems Division.

20. A Proposal for a Magnetic Fluid Viscous Damper for the Radio Astronomy Explorer Satellite, AVSSD-D613-216, Avco Space Systems Division.

21. Crede, C. E., Vibration and Shock Isolation, John Wiley and Sons, Inc. New York.

22. Lindon, "Aerospace Electronic Materials," Electro-Technology (December 1961).

23. Ray, K. A., Sublimation of Materials in a Vacuum, NASA Contract NASw-6, Jet Propulsion Laboratory, California Institute of Technology.

24. Bolton, A., "Effects of Radiation Environment on Structural Materials," Electro-Technology (June 1958).

25. Bushness, D., and Kraus, A. D., "Thermal Equilibrium of Space Vehicles", Sperry Engineering Review (December 1960).

26. "Hermetic Seals," Electromechanical Designing, Volume 4 (October 1960).

27. Stambler, I., "Agena Structure Makes Wide Use of Magnesium," Space/Aeronautics, Volume 34 (July 1960).

28. Neuringer, J. L., and Rosenweig, R. E., "Ferrohydrodynamics," The Physics of Fluids, Volume 7, No. 12 (December 1964).

29. Landau, L. D., and Lifschitz, E. M. Electrodynamics of Continuous Media, Oxford: Permagon Press (1960).

30. Weiss, R. F., and Florsheim, B. H., "Flow in a Cavity at Low Reynolds Number," The Physics of Fluids, Volume 8, No. 9 (September 1965).

31. Schlichting, H., Boundary Layer Theory, McGraw-Hill (1955).

32. Prandtl, L., and Tietjens, O. G., Applied Hydro and Aeromechanics, Dover (1934).

33. Scheidegger, A. E., The Physics of Flow through Porous Media, MacMillan Company (1957).

34. Cowley, M. D., and Rosensweig, R. E., "The Interfacial Stability of a Ferromagnetic Fluid," paper to be submitted for publication.

VII. GLOSSARY

Section I

None

Section II

C_D = viscous damping coefficient

P = pitch axis

R = roll axis

Y = yaw axis

Section III

Ferrofluid Development Terminology

A = characteristic constant

E = energy

e = Naperian base

K = viscosity temperature coefficient

M = magnetization of ferrofluid

M_s = saturation magnetization of ferrofluid

R = gas constant

r = sphere radius

T = absolute temperature

δ = thickness of stabilizing layer

ϵ = volume fraction of solids in suspension

N_o = absolute viscosity of ferrofluid

N_s = absolute viscosity of carrier fluid

μ = microns

ϕ = volumetric concentration of coated particles

ϕ_c = critical concentration of suspended matter at which suspension becomes rigid

Section IV

Damping Terminology

A_v = vane cavity cross section

b = normal dimension of vane cavity

C_D = damping coefficient

D = orifice diameter

F_M = magnetic force

H = field strength in the gap

h = radial dimension of vane cavity

K = torque applied

L = fluid body length, orifice length

M = ferrofluid magnetic moment

M_s = ferrofluid magnetic moment

P_M = magnetic pressure

R = mean vane radius

T = torque

ΔT = time elapsed

$\Delta \theta$ = angle covered

μ = fluid viscosity

Magnetic System Terminology

A = area

B = flux density

F = flux leakage constant

f = reluctance factor

H = field strength

L = length

W = weight

p = density

ϕ = flux

$( )_g$ = gap subscript

$( )_I$ = iron subscript

$( )_M$ = magnet subscript

Computer Notation

FC = assumed flux leakage factor

FCC = computed flux leakage factor

$( )G$ = gap parameter

$( )I$ = iron parameter

$( )M$ = magnetic parameter

$( )P$ = pole parameter

Magnet - Vane Parametric Study Input Variables

ANG = angular extent of magnet

BD = flux density in magnet

BI = flux density in back iron

Magnet - Vane Parametric Study Input Variables (Cont'd)

BLG = fluid depth normal to pole faces

FC = flux leakage constant

FL = reluctance constant

HGN = field strength in fringe field

HGX = field strength in gap

HLI = back iron radial extension past magnet

LP = length of pole pieces

MAG = magnet material (Alnico 5 or Indox 5)

MMX = maximum magnetic moment of magnetic fluid

RV = vane radius

T = magnetic trapping torque

TA = air gap length between vane and magnet

TW = vane wall thickness

Magnet - Vane Parametric Study Output Variables

AG = gap area

AI = iron cross sectional area

AM = magnet area

AV = vane cross sectional area

BDP = magnet flux density required for equal magnet and vane areas

FCC = computed flux leakage constant

FM = magnetic trapping force

HD = magnet coercive force

HLG = radial fluid length

Magnet - Vane Parametric Study Output Variables (Cont'd)

HLM = radial magnet length

LG = air gap length

LM = magnet length

LTM = magnet arc length

MS = fluid magnetic moment

MSH = integral of MdH

TI = thickness of iron

WT = weight of magnet, back iron, and pole piece

WTI = back iron weight

WTM = magnet weight

WTP = pole piece weight

Suspension Parameters

C_o = radial load

D = diameter

F_f = reaction force

F_s = pivot system force

F_{SB} = force, sleeve bearing

F_T = axial preload

F_{tu} = ultimate tensile stress

F_ϕ = radial load

G = modulus of rigidity

J = polar moment of inertia

K = spring constant

Suspension Parameters (Cont'd)

L = length of wire

M_o = moment

MS = margin of safety

N = number of cycles

P = pressure

r = radius of wire

S = stress

S_s = shear stress

S_T = tensile stress

S_{T_z} = tensile stress due to torque about Z axis

T = twisting moment

T_o = thrust load

T_{ssl} = steady state torque about Z axis

T_{ss} = steady state torque

V = load

V_c = compression load

V_T = tensile

X = damping axis

Y = damper boom axis

y = deflection

Z = satellite yaw axis

α = system rotation angle about Z axis

θ = deflection, angle of twist of torsion wire

Suspension Parameters (Cont'd)

r_F = friction torque

r_S = sinusoidal torque about Z axis

r_{SB} = torque, sleeve bearing

r_Z = torque about Z axis

ϕ = wire rotation angle about Z axis

Damping Fluid Dynamics

A = constant

A_o = orifice area

A_s = shear area

A_v = vane area

a = complex function of damper geometry

B_o = applied magnetic field

b = complex function of damper geometry, constant

C = constant of integration

C_D = damping coefficient

D = orifice diameter, solid diameter

d = orifice diameter

e = porosity = void volume / total volume

F = force

$\underline{F}$ = force vector

F_M = magnetic force

F_s = viscous force

f_i = divergence of stress tensor

Damping Fluid Dynamics (Cont'd)

H = magnetic field strength

$\underline{H_o}$ = magnetic field vector

h = fluid dimension in direction of motion, radial fluid dimension

K = constant

K' = constant

L = orifice length

$\underline{M}$ = fluid magnetic moment

$\underline{n}$ = unit normal

P = pressure

P_o = pressure

Q = volume of fluid flow

R = orifice radius

R_v = mean vane radius

r = composite permeability, radial dimension

S_s = shear stress

T = interfacial tension, viscous torque

T_s = viscous torque

U = constant

$\underline{V}$ = volume

$\bar{V}_o$ = mean fluid velocity in orifice

V_v = velocity of fluid in vane

Damping Fluid Dynamics (Concl'd)

v = velocity, fluid velocity

X = direction of motion

y = radial dimension

$curl$ = cross product of an operator with a vector

del = differential operator

$grad$ = gradient operator

$\Delta\rho$ = density difference

Δp = pressure drop

δ = differential operator

θ = angle between current loops and plane of ferromagnetic fluid

Γ = complex functions of damper geometry

μ = viscosity

μ_o = magnetization of unperturbed fluid

ξ = differential

σ_{ij} = stress tensor

ϕ = azimuth angle

$\sigma_{ij}\,\xi_j\,\eta_i$ = mechanical work

ψ = stream function

$()Z$ = axial direction

$()_r$ = radial direction

$()\phi$ = azimuthal direction